1999 thesis. SIgned copy at University of Minnesota, Twin Cities

Thesis · June 1999

DOI: 10.13140/RG.2.2.32782.77127

1 author:

Paul James Pilarski
Minnesota Deptartment of Transportation
4 PUBLICATIONS **62** CITATIONS

SEE PROFILE

EFFECT OF WELDED STIFFENERS ON CRACK GROWTH RATE

A THESIS
SUBMITTED TO THE FACULTY OF THE GRADUATE SCHOOL
OF THE UNIVERSITY OF MINNESOTA
BY

PAUL PILARSKI

IN PARTIAL FULFILLMENT OF THE REQUIREMENTS
FOR THE DEGREE OF
MASTER OF SCIENCE

JUNE 1999

UNIVERSITY OF MINNESOTA

This is to certify that I have examined this copy of a master's thesis by

Paul James Pilarski

and have found it complete and satisfactory in all respects,
and that any and all revisions required by the final
examining committee have been made.

_____

Name of Faculty Advisor

_____

Signature of Faculty Advisor

_____

Date

GRADUATE SCHOOL

Abstract

Effect of Welded Stiffeners on Crack Growth Rate

by Paul Pilarski

Chairperson of the Supervisory Committee: Professor Robert Dexter

Department of Civil Engineering

Fatigue crack growth is studied in welded, stiffened panels through the use of analytical, numerical, and experimental means. Full scale testing is conducted by integrating welded, stiffened panels into a box girder configuration subjected to cyclic fatigue loading. Analytical modeling is performed based on of superposition of linear elastic fracture mechanics, assuming a worst-case residual stress field representation. Numerical modeling is performed using finite element models, with temperature gradients simulating residual stresses, to calculate the J-Integral around the crack tip at different stages of crack development, and transforming the results into a propagation rate prediction. An initial crack is introduced and crack propagation behavior is observed, noting variations due to interaction with the inherent residual stress field of welded stiffeners. The two modeling techniques are compared in their ability to predict worst-case crack growth rates and correlated with experimental results.

TABLE OF CONTENTS

LIST OF TABLES

LIST OF FIGURES

ACKNOWLEDGMENTS

This research was conducted at the Department of Civil Engineering at the University of Minnesota, Twin Cities. The study was conducted under the support of the U.S. Coast Guard and the Ship Structure Committee, and would not have been possible without the generous support of the Project Technical Committee. The committee members ideally represented project interests, giving sound advice while granting considerable leeway for research direction. Robert Sedat was especially responsible for the smooth operation of the project on the administrative front.

The author wishes to thank his advisor, Prof. Robert Dexter, for his constant guidance, practical advice, friendship and technical assistance. Dr. Dexter is an accomplished engineer who never loses sight of practicality in assessing problems of variable nature. He has been a source of inspiration and has always reaffirmed my interest in becoming a practicing engineer.

I would also like to thank those who made the experimentation phase of the project a success despite overwhelming roadblocks along the way. In particular, Paul Bergson, the Civil Engineering Department's Research Engineer, has devoted a tremendous amount of time, support and mentoring to the author and this project. I thank the undergraduate research assistants and laboratory personnel who have been instrumental in the maintenance of the experiments.

The development of the prediction models was greatly assisted by the advice of Alain Nussbaumer and the staff at the Minnesota Supercomputing Institute (MSI). Without the top-notch staff at MSI the F.E. modeling would not have been completed.

Most importantly, I would like to thank my parents, family and loved ones. My family has been supporting a ghost for too many years, and I only hope they realize how much they

mean to me. My fiancée, Jessica Collin, has been a well of hope and encouragement. I am forever indebted to her for her patience, love and understanding.

1 INTRODUCTION

1.1 PROBLEM STATEMENT

Structural elements subjected to fluctuating loads of significant amplitude are susceptible to fatigue cracking [98, 33]. The primary variables influencing the possibility of fatigue cracking in welded steel structural elements are the severity of the stress concentration of the particular design detail and the nominal stress range, i.e. the algebraic difference between the maximum nominal stress and the minimum nominal stress. Ship structure is subjected to significant stress ranges from wave loading in rough seas as well as vibration from slamming or impact of waves, and therefore fatigue cracking is a potential problem with ships.

Classification societies have recently developed rigorous fatigue design criteria that should substantially reduce the incidence of fatigue cracking in ships [5, 30]. However, most ships in service today were not explicitly designed for fatigue, and consequently many of these ships are exhibiting frequent cracking [97, 2]. Fatigue cracking in modern ships is a serviceability problem rather than a structural integrity problem [118]. Fatigue cracks cause leaks and are a nuisance to repair. A large tanker may have hundreds or even thousands of fatigue cracks discovered during inspection [2, 97, 118, 149-151]. Yet these cracks are not an immediate threat to the structural integrity of the ship. The tolerance of ships to these cracks is attributable to the notch toughness of the steel and the overall structural redundancy.

Fatigue design is usually performed using the S-N approach, where structural details are grouped into categories sharing a common S-N curve. The S-N curve gives the number of cycles before the element develops a through-thickness crack, given the stress range for those cycles. This approach is suitable for design. However, the number of cycles to develop a through-thickness crack represents only a small fraction of the total fatigue life in

redundant structures. In ships, cracks may propagate to lengths as great as eight meters before structural safety is compromised. Therefore, for assessment of existing ships and other structures, particularly if there are existing through-thickness cracks, a method is needed for predicting the safe propagation life of long, through-thickness cracks. The research involved in this report is focused on developing fatigue crack propagation models for predicting worst-case crack growth rates in welded stiffened panels, a common structural element in ship structure.

Although crack growth in plates and riveted stiffened panels (for airframes) has been studied extensively, an investigation of crack propagation in a panel with multiple welded stiffeners has never been performed. Welded stiffeners affect crack growth in a unique way because of residual stresses present from the welding process. Furthermore, in contrast to riveted stiffeners, cracks may propagate into and sever integral welded stiffeners.

In addition to calculating the crack growth rate, it is also essential to determine a safe critical crack size. Current fracture models are based on brittle fracture and predict unreasonably conservative critical crack lengths on the order of 400-mm [129]. Field observations have consistently shown that crack lengths can greatly exceed the brittle fracture model predictions without a complete fracture occurring. For example, a crack 150-mm long was noticed in a military frigate and that this crack propagated to 8 meters in length during a severe 36-hour storm involving about 10,000 stress reversals. More recently, a 15-meter crack was reported in the deck of the 744-foot Ro-Ro (Roll-on, roll-off vehicle carrier) "Great Land" without complete brittle fracture of the section [102]. Such tolerance illustrates the fracture resistance of typical ship steel and the need for improved models to take advantage of the residual strength found in the redundant structure.

Prior to 1940, steel ships were riveted. Riveted construction was good for structural integrity because a crack in one structural element could not propagate into adjoining structural elements. If a crack propagated in the shell, the intact structural elements, such as stiffeners, limited the crack opening and often arrested the crack growth. A corresponding

increase in the amount of force carried by the stiffeners resulted from providing displacement control to the crack opening. This effect is known as load shedding.

During World War II, all-welded construction was introduced, perhaps most noted in the construction of Liberty Ships. A combination of steel with low notch toughness, poor weld processes, and high stress concentrating details contributed to brittle fracture in many of these ships [18]. In addition, welding creates tensile residual stresses near stiffeners, which tend to accelerate crack growth. The investigation of these fractures led to the founding of the Ship Structure Committee. These early investigations led to notch toughness requirements for ship steel, as well as improved welding methods and design details. The adoption of these provisions substantially reduced the incidence of brittle fracture.

The advent of high-strength steel in the 1970's allowed ship designers to design for a higher allowable stress. Unfortunately, the stress ranges increase in magnitude if the allowable stress is increased, because the scantlings are typically reduced relative to what they would be if low-strength steel were used. Although the yield and ultimate tensile strength of the steel had increased, the resistance to fatigue cracking of welded details is independent of the strength level and the type of steel [33, 34, 98, 52, 54, 69, 70]. Therefore, the higher stress ranges have translated to an increase in the incidence of cracking. Fortunately, the notch toughness of the steel and weld metal allows the cracks to grow in a stable manner.

The number of cracks observed in tankships has become markedly increased in recent years, including those of the Trans-Alaska Pipeline Service (TAPS) [97]. As a result, visual inspections are routinely essential. A formal documentation plan known as NVIC 15-91 has been prepared by the U.S. Coast Guard regarding the tracking of various structural failures [163]. The guidelines describe three categories of "failures" that are related to the impact the failures could have on service structural performance. Ship owners submit the documentation, known as critical area inspection plans (CAIP's), as a method of monitoring the performance of repairs and a means of identifying areas of recurring failure.

Inspection procedures have been the subject of numerous investigations in terms of their quality and reliability as a fracture control procedure. A study by Kim et al. [84] concluded that cracks greater than 200 mm in length could be detected 70% of the time, while a study by Demsetz estimated only a 50% probability of detecting a crack less than 300-mm [32]. These reports, in combination with the number of cracks surfacing in the aging tankships, has stimulated interest in understanding the behavior of cracks propagating through welded, stiffened panels.

There is a need to estimate the time before any crack can grow to a critical length, or length at which the ship's integrity is susceptible. Such estimates severely affect the profitability of ship transport, as any time out of service represents a substantial loss in revenue. At the same time, any risk of failure is a financial gamble as well. Better prediction models developed in this research will advance the assessment of safety and economic considerations.

1.2 OBJECTIVES OF THE PRESENT RESEARCH

One of the primary goals of this research is to recreate and observe fatigue crack propagation in a panel with multiple, welded stiffeners. Although fatigue cracks have been observed in the field, never before has load-controlled fatigue crack growth been recorded through multiple welded stiffeners.

The second objective is to investigate the load shedding effects of crack propagation through stiffening elements. The experimental setup attempts to simulate the cellular, redundant structure of tanker vessels. The growth of long fatigue cracks in a redundant system will allow observation of the interplay between crack growth parameters and structural performance.

A third objective is to gauge the significance of residual stresses on the rate of crack growth. Welding creates tensile residual stresses, on the order of the yield stress of the steel in the vicinity of the stiffeners, and lower level compressive stresses in the plating between the stiffeners. These stresses increase crack growth rates near stiffeners, and decrease (or arrest) it between stiffeners. It is necessary to identify worst-case scenarios for crack growth rates to correctly estimate the time for a crack to propagate from the detectable size to the critical length.

Developing both analytical and finite element methods of predicting crack growth is the final goal of the research. These models of crack growth will facilitate successful use of these research results in the industry. Worst-case models of crack growth rates are compared with experimental results, bridging the gap between predictions and actual behavior. These models will prove essential tools for fatigue life predictions, inspection interval rationale, and fitness for service qualifications for vessels containing the particular configurations tested.

2 BACKGROUND

2.1 FRACTURE MECHANICS

Fundamental principles of fracture mechanics are required to predict fatigue crack propagation. Linear Elastic Fracture Mechanics (LEFM) can be used under conditions where there is relatively little plastic deformation around the crack tip. LEFM is applicable to high-cycle fatigue crack growth, which typically occurs when applied stresses are well below the yield stress of the steel. LEFM is also usually applicable to brittle fracture, which often occurs at applied stress levels less than the yield stress.

Elastic-Plastic Fracture Mechanics (EPFM) considers limited amounts of plastic deformation during fracture. Both fields of Fracture Mechanics deal with fracture as a function of crack size, applied stress or displacement, and material toughness. There are many available texts that review the principles of both LEFM and EPFM [6, 15, 22]. Reemsnyder presented a review of fatigue and fracture principles relevant to ship structures [126]. The application of ductile fracture models is explained in a recent Ship Structure Committee report SSC-393 [35]. Therefore, only a brief review will be presented here.

The root of LEFM is the stress-intensity factor, K, which describes the magnitude of the stress field at the crack tip by relating it to the applied gross-section stress acting remotely from the crack plane and the crack length. The stress-intensity factor has units of MPa-$m^{1/2}$ in S.I. units and ksi-$in^{1/2}$ in English units, although ASTM has recently changed the English unit to the *Irwin*. Solutions have been obtained for the stress-intensity factor for various geometrical configurations and loadings, many of which can be found in handbooks [104, 131, 145]. Alternately, the stress intensity factor can be determined from finite-element analysis or other numerical methods.

The solution for the stress-intensity factor for a through-thickness crack in an infinite panel with an applied tensile stress is discussed here for example. The through thickness crack in an infinite plate is also referred to as the center-cracked tension (CCT) panel. This solution forms the basis for most crack models for stiffened panels.

The relation is:

$$K = \sigma * \sqrt{\pi * a} \qquad \text{Eqn. 2-1}$$

where "σ" is the remotely applied nominal gross-section tensile stress and "a" is the crack half-length, as described in Figure 2-1.

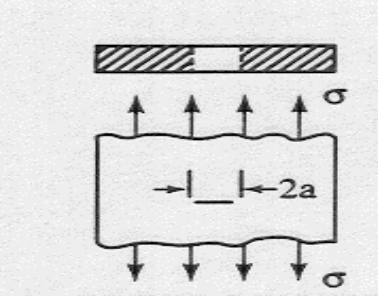

Figure 2-1: Through thickness crack in infinite plate under tension.

To predict the onset of fracture using LEFM, the material's fracture toughness is measured in terms of a critical stress-intensity factor, K_{Ic}. K_{Ic} may vary with constraint, loading rate, and temperature. In order to maintain linear elastic conditions, K_{Ic} must be measured with very large thick specimens to get valid results. For relatively thin plates (< 26 mm), it is impossible to get valid K_{Ic} values. Therefore, the fracture toughness is often estimated from correlations to "notch toughness", i.e. the results of the inexpensive Charpy V-Notch test (CVN) [22].

For ship structures, the loading rate is usually moderate and an appropriate K_c correlation to the CVN test is made by:

1) Obtain dynamic fracture toughness K_d from CVN through the relation:

$$K_d = 11.5 * \sqrt{CVN} \qquad \text{Eqn. 2-2}$$

where CVN is in Joules and K_d in MPa-$m^{1/2}$

2) Shifting the K_d curve -38 degrees Celsius to obtain an estimate of the fracture toughness appropriate for intermediate loading rates.

Elastic-Plastic Fracture Mechanics characterizes crack tip stress and strain fields through the J integral or the Crack-Tip Opening Displacement (CTOD) rather than the stress-intensity factor.

For linear elastic conditions, the J integral can be directly related to K. For plane-stress conditions:

$K = \sqrt{J * E}$ where E is the modulus of elasticity. Eqn. 2-3

The crack-tip opening displacement (CTOD) is directly proportional to the J integral and therefore is really no different. However, the CTOD is the preferred EPFM parameter in some industries [33, 129].

To predict the onset of fracture in EPFM, the material's fracture toughness is measured in terms of a critical value of the J integral or CTOD. Similar to K_c, the critical J or CTOD may vary with constraint, loading rate, and temperature. However, the requirements for specimen size and thickness are not nearly as stringent using these EPFM parameters.

The applied J-integral is often calculated using finite-element analysis. Dexter and Xiao [169] discussed issues involved in calculating J integral values for stiffened panels in typical ship structure. These issues are also discussed in SSC-393 [35]. A comparison with the methodology and full-scale testing of structural components is made, and observations in J-integral behavior have led to a simple bilinear approximation equation for ductile fracture

applied J-integrals. Stenseng has also shown the use of this procedure applied to a plate with a single, coped stiffener and a crack emerging underneath [141].

EPFM is really only valid for limited amounts of plasticity. As explained in SSC-393 [35], the conditions of fracture in typical relatively thin (less than 26 mm thick) ship plate with notch toughness (CVN test) requirements involve extensive plasticity. This extensive plasticity invalidates the EPFM procedures. SSC-393 concludes that maximum load capacity of a cracked section in such relatively thin notch tough plate can be predicted accurately in terms of the plastic limit load for the net section.

The failure analysis diagram (FAD) is a convenient way of representing the interaction between fracture and net-section collapse. FADs are explained in detail in the paper by Reemsnyder [126] and in SSC-393 [35]. The FAD is also the basis of the procedures in PD-6493 [23]. PD6493 has very well documented step-by-step procedures for assessing fatigue crack growth and fracture from weld flaws. SSC-393 discusses ways that PD-6493 can be applied to larger cracks typical in ship structure.

Just as the range in stress governs the fatigue life of details, fatigue crack growth is governed by the range in stress-intensity factor, or ΔK. Paris noted that the rate of crack growth could be described by fitting a power law, which is known as the Paris Law [117].

The Paris law is expressed as:

$$\frac{da}{dN} = C * (\Delta K)^m \qquad \text{Eqn. 2-4}$$

where a = half crack length

N = number of cycles

C = an experimentally determined coefficient

ΔK = stress intensity factor range

m = material constant

The Paris Law is a relatively simple model that has proven to predict crack growth in a variety of situations with good success. Experimentally determined da/dN verses ΔK data typically exhibit a sigmoidal shape as shown in Figure 2-2.

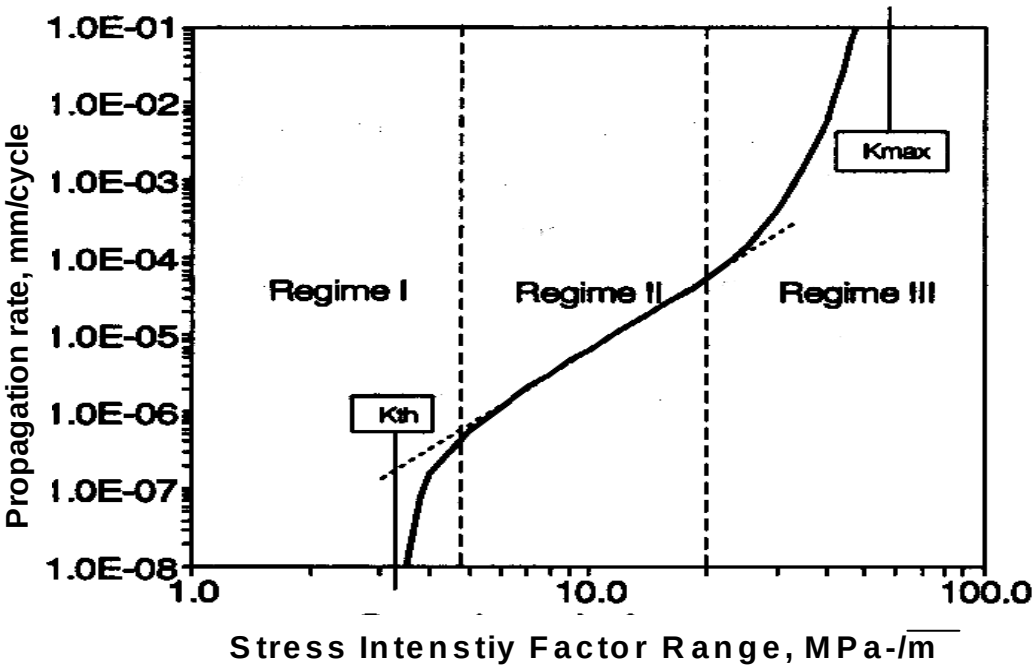

Figure 2-2: Typical plot of fatigue life [109].

The Paris Law is fit to the middle range of ΔK, from 5-20 MPa-$m^{1/2}$. Regime 1 indicates that there is a ΔK threshold, ΔK_{th}. For steel, the threshold value of ΔK is can be conservatively taken as 3 MPa-$m^{1/2}$. For values of ΔK greater than this threshold, fatigue crack growth obeys the Paris Law. Region 3 shows an acceleration of crack growth rate as ΔK approaches fracture toughness, K_{IC}. In region 3 fatigue crack growth is accompanied by some ductile tearing or brittle fracture in each cycle.

The environment often influences crack propagation rates. The effects of seawater on crack growth in steel have been reported in SSC-326 and SSC-335 [25, 37]. A saltwater environment increases crack growth rates in ΔK_{eff} ranges higher than the material threshold. As ΔK_{eff} increases above the threshold crack growth is accelerated proportionally. In contrast, crack growth occurring under a ΔK_{eff} near the threshold exhibits decreased

propagation rates. Such a phenomenon is explained by the corrosive effects of saltwater—at low stress intensity factor ranges, corrosion at the crack tip may actually retard crack growth by increasing crack closure and blunting. As the stress intensity factor range increases, however, corrosion is less likely to cyclically accumulate at the crack tip, and instead assists crack growth by degrading the crack tip material in each cycle. The environmental effects can often be included in the Paris Law by slightly changing the coefficients C and m.

The value of m, the exponent in the Paris Law, is typically is equal to 3.0 for steel in air. Careful experimentation shows this value of m to range from 2.8 to 3.2. As with any statistical fit to experimental data, misleading results can sometimes be obtained. Values of m as low as 2 and as high as 5 have been reported in the literature. However, it is our opinion, and the opinion of most other researchers working in fatigue, that the value of m should be 3.0, and the other reported values are actually due to error rather than actual variance in the slope of the data on the log-log plot.

Variance in the crack growth rate is usually expressed by variance in the coefficient C. Most researchers agree that all C-Mn steel has similar crack growth rates, and that the variance observed is just the typical material variation. In other words, there is not a real difference in the crack growth rates among various types of C-Mn steels, there is only scatter. The scatter can be substantial, on the order of a factor of 10 difference between the minimum crack growth rates and the maximum crack growth rates. Therefore, most reported values of C are intended to represent a conservative upper bound to the data.

Barsom and Rolfe [15] established an upper bound for a variety of ferritic steels where C was 6.8×10^{-12} for units of MPa and meters. However, the British Standard Institute PD6493 [31] recommend an upper bound of 9.5×10^{-12} for C. (Both of these sources agree that m is equal to 3 for steel). A recent study of HSLA-80 steel [53] showed that the upper bound crack growth rate was close to 9.0×10^{-12}, which is close to the upper bound recommended by PD6493. Therefore, it appears Barsom and Rolfe's upper bound is not sufficiently conservative.

Taking the slope m equal to 3, the Paris Law may be integrated to get an expression for N as a function of S_r and a:

$$N = \frac{k}{S_r^3}\left(\frac{1}{\sqrt{a_i}} - \frac{1}{\sqrt{a_f}}\right) \qquad \text{Eqn. 2-5}$$

where k is a constant, S_r is the stress range, and a_i and a_f are the initial and final crack length, respectively. The constant k is equal to $2/(C\pi^{1.5})$.

Figure 2-2 illustrates a typical S-N curve. The S-N curve is a design curve for characterizing the susceptibility of specific structural details to fatigue.

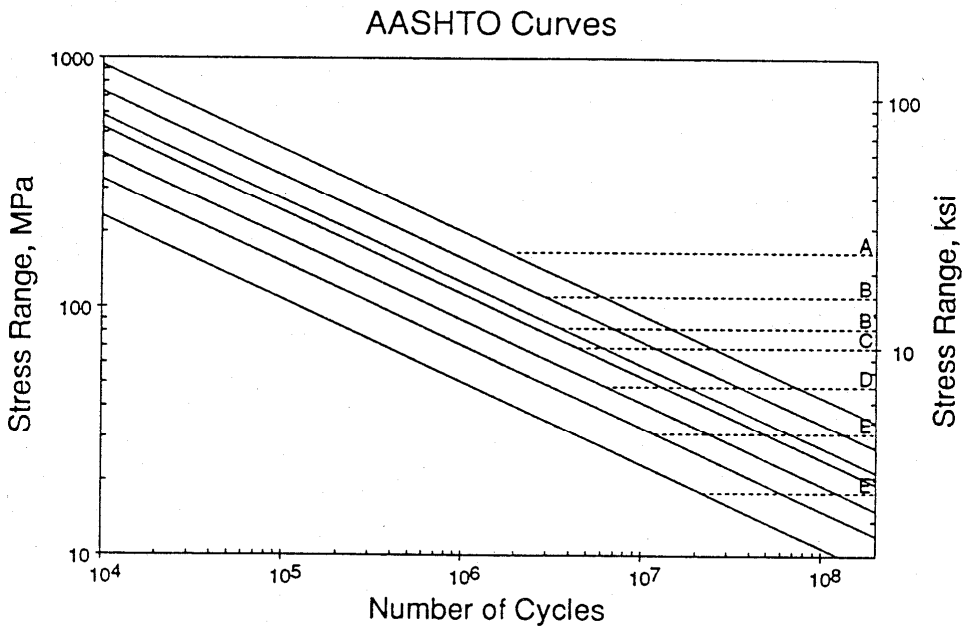

Figure 2-2: Typical S-N curve for fatigue design.

The integrated form of the Paris Law has the same form as the S-N curve, thus the two approaches to modeling fatigue are interrelated. The S-N curve, developed from full-scale test data, has built into it some initial and final crack lengths. If these crack sizes can be accurately characterized, the Paris Law allows them to be explicitly included in the analysis. Note that the exponent of 3 in the Paris law is the same as the inverse slope of the S-N

curves. All S-N curves in the design codes, such as AASHTO, AWS, BS7608, DnV, and ABS Safehull [5] use a constant inverse slope of 3.

Fatigue tests are often described by their applied stress intensity factor range, or load ratio. The load ratio, or R-ratio, is expressed as:

$$R = \frac{\sigma_{min}}{\sigma_{max}} = \frac{K_{min}}{K_{max}} \qquad \text{Eqn. 2-6}$$

where σ_{max} and σ_{min} are applied stresses, and K_{max} and K_{min} are applied stress intensity factors.

Several definitions of ΔK exist which characterize the effectiveness of a loading cycle on crack growth. When tensile loading is applied, plasticity forms in the region surrounding the crack. This region has been stretched to occupy more area than previously occupied by the same material. Upon removing the tensile load, the plastic region remains permanently deformed, creating compressive forces around the plastic zone when the surrounding region unloads elastically. As the crack grows, a plastic zone path is left in the wake of the crack. These plastic zones can be seen in Figure 2-3.

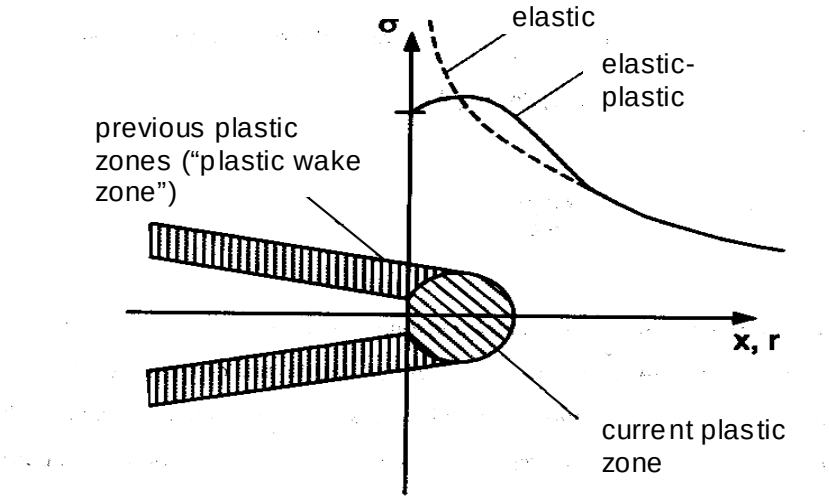

Figure 2-3: Plastic zones formed in crack growth [109].

Elber [45] theorized that this wake, and the compressive forces ahead the current plastic zone, have the tendency to keep the crack closed under limited amounts of applied tension. This phenomenon is known as crack closure.

A crack will only grow when it is opened fully at the tip. Therefore, a portion of the tensile loading may not contribute to new crack growth and only serves to open the crack. Elber defined the effective tensile loading as:

$$\Delta\sigma_{eff} = \sigma_{\max} - \sigma_{op} \qquad \text{Eqn. 2-7}$$

where σ_{op} represents the amount of load necessary to open the crack up to the tip.

A ratio describing the effectiveness of an applied cycle was also defined:

$$U = \frac{\Delta\sigma_{eff}}{\Delta\sigma} = \frac{\sigma_{\max} - \sigma_{op}}{\sigma_{\max} - \sigma_{\min}} = \frac{\Delta K_{eff}}{\Delta K_{applied}} \qquad \text{Eqn. 2-8}$$

where $\Delta K_{eff} = K_{max} - K_{op}$

K_{op} is defined as the amount of stress intensity factor necessary for the crack front to open. This includes all the effects of internal forces—namely, that of residual stress and plasticity effects. De Koning has presented an approach when plasticity effects are to be considered [88]. In the case of most fatigue crack growth, however, plasticity effects are assumed to be negligible because the majority of fatigue cycling occurs at stresses well below the material yield stress. The effective stress intensity factor for opening the crack can be determined by procedure outlined in Figure 2-4.

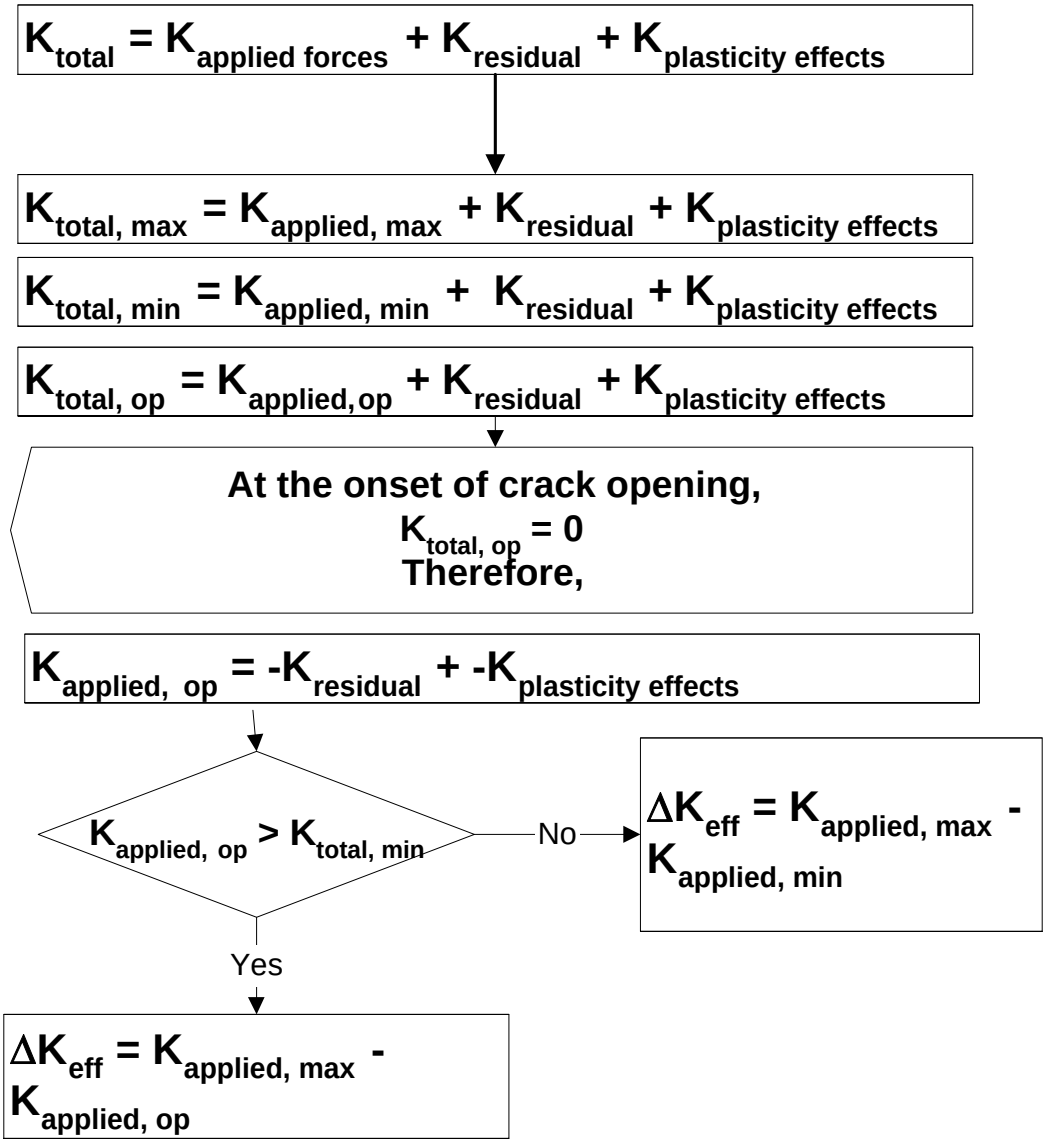

Figure 2-4: Procedure for determining effective stress intensity factor range [109].

In regions of compressive residual stress (for which the K-factor solution will be discussed later), K_{op} can be quite large and possibly consume most of the applied stress intensity factor. When the effective stress intensity factor is low, crack growth may slow down. If the effective ΔK decreases below the ΔK_{eff} threshold, the crack will arrest. Definitions of these various stress intensity factor ranges can be seen graphically in Figure 2-5.

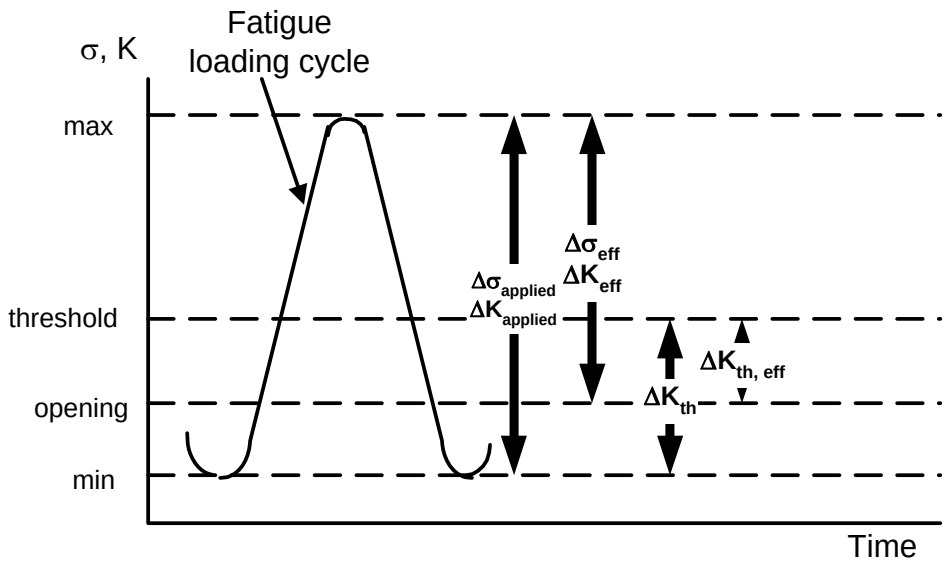

Figure 2-5: Definitions of K-factor ranges.

A great number of references are available to discuss the Paris Law and various modifications suggested to account for factors such as residual stress [22, 6]. A comprehensive guide to fatigue crack growth can be found in Ellyin's recent work [46].

2.2 SHIP DESIGN AND ASSESSMENT GUIDELINES FOR FATIGUE AND FRACTURE

Many papers have addressed the problem of cracking and crack propagation in ship structures, giving guidelines on a wide range of issues from design to maintenance to repair. A good overview of fatigue crack growth in ship structure is presented by Francis et al. [58]. The Ship Structure Committee has published a series of reports addressing various aspects of design, maintenance and assessment [43, 80, 81, 99, 100, 128, 130]. Specifically, SSC-244 established toughness requirements for ship structural steel. Minimum toughness requirements were specified in terms of both the 5/8-inch ductile tear test and Charpy V-notch test.

Prof. Stanley T. Rolfe of the University of Kansas significantly influenced the SSC-224 report. His 1974 paper [128] summarized the application of fracture mechanics to ship hull design and fracture performance. Rolfe identified the key factors to insure ductile failure modes, and discussed the interaction among them. Primary factors in crack growth were the stress level, flaw size and material toughness, while secondary factors included temperature, residual stress and loading rate. To assure ductile behavior, a minimum value of 339 Joules was recommended based on the 16 mm ductile tear test conducted at room temperature. A coupled criterion was that the ratio of the fracture toughness to the yield stress was at least 1.5, where fracture toughness is in units of $ksi*in^{1/2}$ and yield stress is in ksi. (Fracture toughness to yield strength ratio must be greater than 0.24, where fracture toughness is measured in $MPa*m^{1/2}$ and the yield stress in MPa.) These conditions were considered conservative because they were based on the assumption of dynamic loading in the ships, while in reality the loading rate is tending toward static more so than dynamic.

Specific ship structural steels were studied in 1973 by Kinoshita et al. in Japan [85]. Large plate specimens of mild and high strength steel were tested, verifying their fatigue behavior could be predicted using the Paris Law. In addition, a ship hull corner detail with an edge notch was tested and modeled with finite element analysis (FEA). Both a constant

amplitude loading and a two-step loading was performed, the results of which suggested the Paris Law in conjunction with FEA K-values could be successfully applied to ship hull crack propagation.

Jordan et al. [80, 81] documented fatigue sensitive details in older ship structures. Cracking in tanker ships is documented in a series of reports from the Tanker Structure Cooperative Forum [149-151].

In 1993, Rolfe et al. directly addressed the high incidence of cracking in TAPS trade tankers [129]. Critical details were identified, where the cutouts near master butt welds and hull plates near drainage holes presented the most critical concern. A characteristic material fracture toughness was determined from typical TAPS service tankers in terms of CTOD, with minimum values found in the base metal of .061 mm (.024 in). This toughness value was converted to an approximate value of K using the LEFM relation:

$$K_{Ic} = \sqrt{m * \delta_c * \sigma_{FL} * E} = 101.6 MPa * \sqrt{m} \qquad \text{Eqn. 2-9}$$

where K_{Ic} = critical stress intensity factor, MPa*$m^{1/2}$

$m \approx 1.7$ based on research studies of structural grade steels

δ_c = CTOD value in m., in base metal of TAPS trade tankers = $6.1*10^{-5}$ m

E = modulus of elasticity, $206.9*10^3$ MPa

σ_{FL} = flow stress (Average of yield and ultimate tensile strength), MPa

$$\frac{379MPa + 586MPa}{2} = 482.5MPa$$

This results in a K_{IC} value of:

$$K_{Ic} = \sqrt{1.7 * (6.1*10^{-5}) * (482.5MPa) * (206.9*10^3)}$$

$$K_{Ic} = 101.6 * MPa * \sqrt{m} = 92.5 * Irwins$$

This value was rounded up to 110 MPa-$m^{1/2}$ to obtain a reasonable estimate of the critical crack size. Using LEFM, Rolfe calculated a critical crack size for the material based on the stress intensity factor for the through-thickness crack in an infinite plate under uniform

tension. A coefficient of 0.6 was used to account for the crack opening constraint, or crack growth retardation, provided by several stiffeners. The final relation is as follows:

$$K_{Ic} = (RF_{MS})\sigma_{\max}\sqrt{\pi * a_{CR}} \qquad \text{Eqn. 2-10}$$

where a_{CR} = Critical crack size half length, in m.

RF_{MS}= Reduction factor for multiple stiffeners, approximately 0.6

σ_{MAX} = Maximum working stress, given as $2/3\sigma_{ys}$ = 234.4 MPa

Solving for the critical crack size,

$$2 * a_{CR} = \frac{2}{\pi} * \left(\frac{K_{Ic}}{0.6 * \sigma_{MAX}} \right)$$

$$2 * a_{CR} = \frac{2}{\pi} * \left(\frac{109.9MPa}{0.6 * 234.4MPa} \right) \approx 0.38meters = 15inches \qquad \text{Eqn. 2-11}$$

This LEFM approach is very conservative despite the omission of residual stress effects on crack growth, since an applied stress of 234 MPa would induce significant plasticity at the crack tip. Plasticity at the crack tip is not accounted for in an LEFM analysis, which treats the ductile steel as a brittle material. (Note LEFM *can* be applied to fatigue crack growth, however, because the vast majority of fatigue crack propagation occurs at applied stresses well below the yield stress of the material, thereby creating only a negligible amount of plasticity at the crack tip).

Rolfe's paper [129] went further to outline a method for extrapolating constant stress fatigue life predictions to variable amplitude loading. In concluding, it was recommended that a two year inspection interval could be deemed appropriate if cracks no larger than a 50-mm surface crack were allowed. If a 75-mm crack was to be the maximum allowed, then the recommended inspection interval was reduced to one year. Finally, it was noted that the actual reduction factor due to multiple stiffeners may be even lower than 0.6, although residual stresses were not taken into account, and suggested experimental determination of the actual effects.

Rolfe's calculation for a critical stress-intensity factor conservatively underestimates the critical crack size, based on service observations, i.e. cracks up to 8-m in length reported without catastrophic fracture as indicated in the introduction. In SSC-393 [35], Dexter and Gentilcore illustrated that ships constructed with the minimum toughness materials would fail by net section collapse, in most cases, rather than brittle fracture. Garwood et al. [61] have corroborated this phenomena, outlining the assessment procedure provided by BSI PD6493 for structural collapse. However, Bacci and Ligaro [12] assert that brittle fracture can occur in any material given the right conditions. They present an evaluation procedure illustrating the transition between brittle fracture and ductile fracture.

The toughness of weld metal usually exceeds the base metal toughness, allowing the crack to propagate in a stable manner in most cases. In the heat-affected zone (HAZ) adjacent to the weld, many steels develop local brittle zones which may induce limited brittle fracture or "pop-in" fracture. Pisarski and Slatcher [121] have noted that these pop-in fractures will be limited in structurally redundant systems. Peak loading conditions, minimum design temperature and flaw location in the most brittle portion of the HAZ would need to be coincident for an extensive fracture to occur. In addition, these local fractures usually propagate into the higher toughness base metal where they are arrested.

2.3 FATIGUE CRACK PROPAGATION IN STIFFENED PANELS

A great amount of research has been performed in the past on the solution for the stress intensity factor for cracked, stiffened panels. Much of the research addresses crack growth in aircraft, and appropriately the studies are made on aluminum materials with either riveted or adhesive connections. These types of attachments limit crack growth in that a crack progressing in a shell will not propagate up into the stiffener. This presents the beneficial effect of load shedding, as the load originally placed on both the shell plate and the stiffeners is transferred to the intact stiffeners. In such a case, the crack may only grow to a limited length because the intact stiffeners constrain the crack opening displacement, thereby removing the driving force of the crack. The development of fracture mechanics analysis of stiffened panels sought to explain this behavior quantitatively.

As early as 1959, Sanders studied the case of an integral stiffener centrally located on a thin, orthotropic sheet with a symmetric transverse crack [135]. He made the simplification that the sheet was extendible only in the longitudinal direction, giving a solution independent of Poisson's ratio. Grief and Sanders [64] later revisited this assumption in 1965, developing a plane stress solution as well as the solution for a non-symmetric crack case. Arin continued the study to multiple stiffeners [8]. Isida [74] studied the effect of bending stresses in this problem in 1970, but for most stiffened plates in ships the effect can be neglected. Isida later developed a solution for a center-cracked panel with stiffened edges, once again incorporating the effects of bending stresses [76].

As mentioned previously, the driving force in fracture research of stiffened panels was their use in aircraft. Consequently, much research was devoted toward developing stress-intensity factor solutions for riveted, stiffened panels. Bloom and Sanders [21] first modeled the effect of a riveted stiffener on the stress intensity factor for both a symmetric and non-symmetric crack in 1966. Cartwright et al. [26] adapted the riveted stringer methodology to Dugdale's strip yield model [44] in 1978.

Mansoor Ghassem [62] developed the fracture diagram as a design aid to stiffened panels in 1980. The fracture diagram is a plot of the transition between brittle fracture and gross section yield, using LEFM to evaluate the stress intensity factor. An extension was made for crack tip plasticity by manipulating Dugdale's strip yield model [44] into a stress intensity factor. The fracture diagram assumed stable crack growth occurred up to the line denoting the failure surface. Furthermore, a computer code was written as a means of predicting the number of cycles to failure based on LEFM analytical K solutions. The concept seems to have merit, although the assumptions within the development of the computer code necessitate further study in stiffened panel application. Also, the approach did not take into account residual stresses and was compared to a limited amount of test data for stiffened panels.

In 1971, Poe studied fatigue crack growth rates in aluminum panels with both riveted and integral stiffeners [122-23]. He used the Paris Law in conjunction with LEFM stress intensity factors to predict fatigue crack growth. Crack growth predictions were backed by full scale testing of aluminum stiffened panels with varied rivet spacing and stiffening ratios.

In order to predict the crack growth rate according to the Paris Law, a stress intensity factor range is required to characterize the crack driving force. Closed form solutions for stress intensity factors for different loading conditions and geometries have been developed for years [104, 145, 131]. Poe combined the known solutions for a center through-thickness crack with remote, uniformly applied stress, symmetric point forces, and crack face pressure distributions. This procedure, known as superposition, was also demonstrated by Vlieger in 1973 [164].

Superposition, as well as LEFM, is valid only in cases of linear elastic behavior. However, since the vast majority of service stresses are well below the yield strength of the material, these principles may be applied to fatigue crack propagation. An illustration of his use of superposition in the case of riveted stiffeners is shown in Figure 2-6.

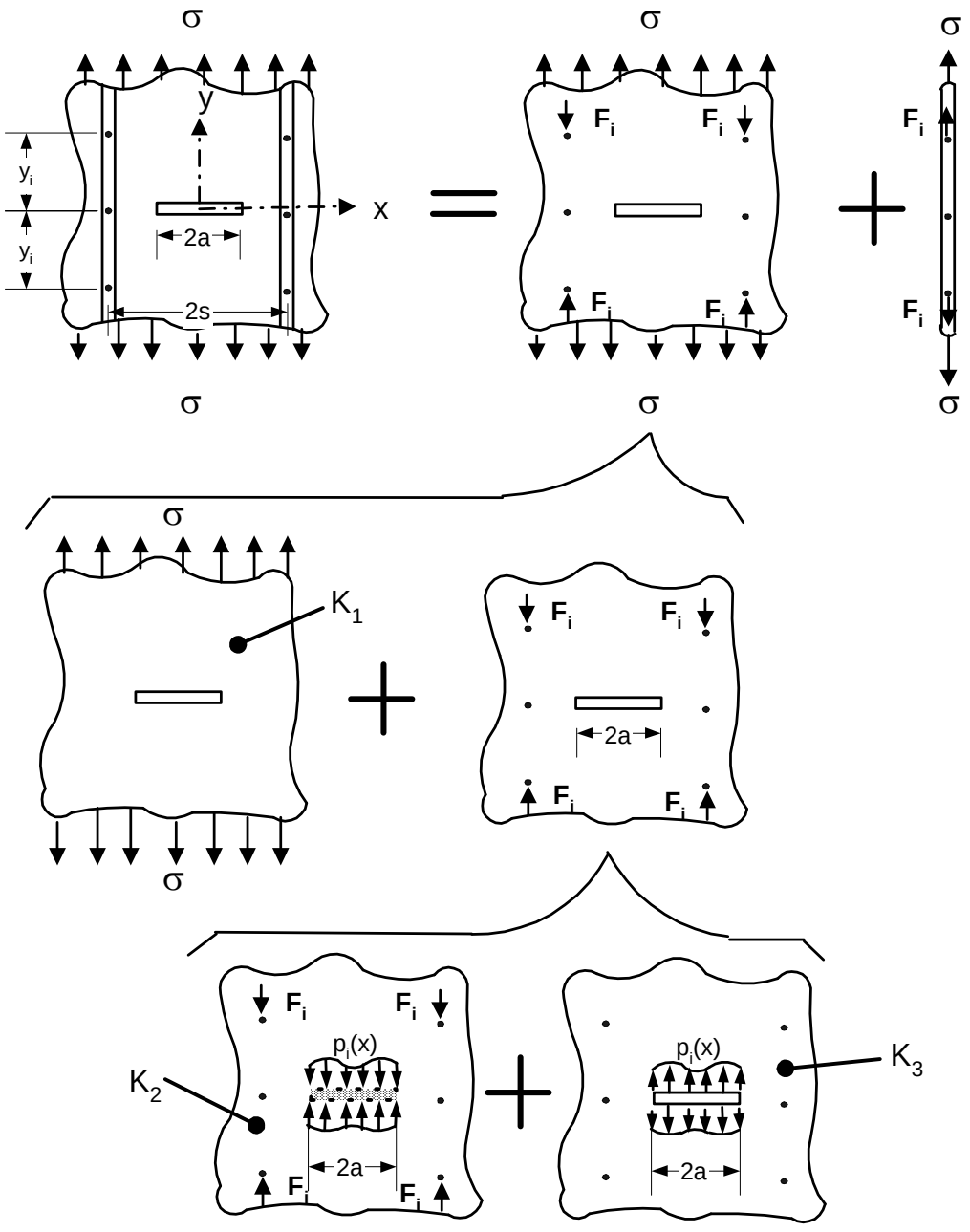

Figure 2-6: Use of superposition to develop analytical solution total stress intensity factor.

The stress intensity factor for the case of a plate with riveted stringers will now be explained. The stiffened panel can be subdivided into several contributions. First, the geometry is separated into two parts:

1. A plate subjected to uniform axial stress and stiffener connection forces
2. A separate stringer with reaction forces

The stiffener with reaction forces serves only as a means to determine the connection forces and does not contribute to the total K-factor. The connection forces are determined through displacement compatibility and force equilibrium between the stiffener and the plate, and the interested reader is referred to Poe's original work for the methodology (The connection forces will be determined through another means in this paper, as developed by Nussbaumer [109]).

Next, the plate is subdivided into two components:

1. A plate subjected to uniform axial stress, for which Equation 2-1 applies. For convenience, this relation is repeated here:

$$K_1 = \sigma\sqrt{\pi * a}$$

2. A cracked plate with connection forces, F_i, applied. This problem can be further broken down to two contributions:

   A. An uncracked plate with a connection forces acting on it. If a crack *were* introduced, the crack faces must be free of shear and normal stresses. Therefore, a pressure distribution resulting from the connection forces is determined along fictitious crack faces, as shown. Since this component has no crack in it, the K-factor is zero ($K_2 = 0$)

   B. An equal and opposite set of pressure forces must be exerted on the introduced crack. This distribution opposes the pressure distribution created by the connection forces and fulfills equilibrium, creating the stress-free condition along the crack faces. The stress intensity factor for a pressure distribution along the crack faces is:

$$K_3 = \sum F_i * K_i = \sum \left[-F_i * \sqrt{\pi * a} * \frac{2}{\pi} * \int_0^a \frac{p_i(x)}{\sqrt{a^2 - x^2}} dx \right] \qquad \text{Eqn. 2-12}$$

where F_i is the contribution from the i^{th} set of symmetric rivets, and $p_i(x)$ is the pressure distribution determined using an i^{th} set of unit rivet forces.

The final result is assembled into a total expression for the stress intensity factor:

$$K_{Total} = K_1 + K_2 + K_3 \qquad \text{Eqn. 2-13}$$

The total stress intensity factor is often lumped into a single coefficient to be applied to the solution for the through-thickness crack in a plate subjected to tension. That is, a multiplier is developed as a function of the stringer and its connection:

$$K_{S.P.} = F(\xi, \lambda, \mu) * \sqrt{\pi * a} \qquad \text{Eqn. 2-14}$$

where: ξ represents the rivet spacing ratio, d/2s

λ represents the transverse stiffener spacing ratio, a/2s

μ represents the stiffness ratio of the stiffener to the plate,

$$\mu = \frac{A_{st} * E_{st}}{A_{st} * E_{st} + (2 * s) * E_{pl}} \qquad \text{Eqn. 2-15}$$

Decreasing the rivet spacing to a very small distance simulates the effect of having integral stiffener. The crack may propagate into an integral stiffener and completely sever it. To develop the stress intensity factor, the K-factor was determined for various crack lengths. When the crack is near a stiffener (Around 0.95 * the stiffener spacing), the stiffener is considered completely severed and its load is shed to the remaining net section. Using this procedure, an abrupt jump in the K-factor is noticed due to the immediate loss of the stiffener.

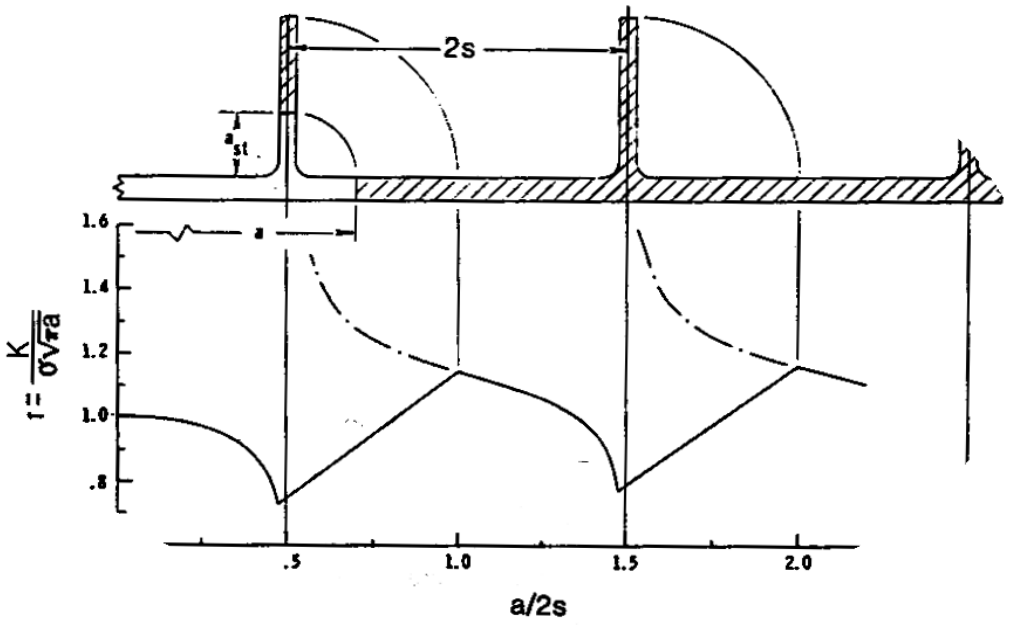

Figure 2-7: K-factor as a function of crack length in plate width in integral stiffeners [123].

Poe noticed that the crack grew at approximately the same rate in the stiffener as it did in the plate, which enabled a linear interpolation of the stress intensity factor between the solution for an intact stiffener and the completely severed stiffener. The figure above shows the results for the stress intensity factor as a function of crack length.

The resulting stress intensity factors could now be utilized in a fatigue crack propagation analysis. Comparing with experimental behavior, the predictions made using the resultant stress intensity factor with the Paris Law showed good agreement. Additionally, the relationship between stiffness ratio and cracking behavior could be directly forecast. Residual stresses, however, were not considered in the study.

Salvetti and Del Puglia conducted a similar study and approach on 6 different riveted stiffener configurations [134]. They studied 60 panels under various constant amplitude loading conditions, and noted discrepancies between Paris Law behavior and experimental at different crack lengths.

Swift later modified Poe's solution for the case of flexible rivets [122] and adhesive panels [70]. Ratwani [71] studied panels with reinforcement attached through adhesion, comparing experimental stress intensity factors with both mathematical and finite element analysis results, including the effects of out-of-plane bending. Arin [8] studied the effects of plate orthotropy in adhesive stiffened panels on the stress intensity factor. He found little variation from that of an isotropic plate with stiffener, validating the initial assumptions made by Sanders in 1959.

Most of the aforementioned studies have been made on aluminum panels, often with riveted or adhesive bond stiffeners. In fact, there has been very little experimentation on welded, stiffened steel panels to determine fatigue crack growth rates. Kinoshita et al. [51] studied the Paris Law applicability to ship structural plate steel in 1973. His findings showed that the Paris Law effectively modeled crack growth in both typical ship structural plate and accurately described crack growth in a ship corner model.

The earliest work most closely fitting the current project's objective was performed by Watanabe et al. in 1979 [166]. The researchers studied crack propagation in a welded, stiffened panel typical of ship structures. Analytical modeling approximated the stress intensity factors for crack growth in the panel with stiffeners, using the Paris Law to evaluate the growth rate. Watanabe found that the predictions compared reasonably well with the actual behavior, although the extent of the investigation was limited to one configuration. The investigation, although limited in scope, demonstrated the possibility of using the Paris law in conjunction with LEFM to compute relatively accurate fatigue crack growth rates.

Petershagen and Fricke [120] conducted several fatigue crack growth experiments on stiffened panels. Experimental testing was emphasized in the study, although the effects of residual stress were neglected. Since much of the fatigue crack growth in ships occurs at low

stresses, where residual stress plays an important role, their inclusion is deemed necessary to correctly predict fatigue crack growth behavior.

Nussbaumer, Dexter, and Fisher [109-11] took residual stresses into account in a study on crack propagation through large-scale experiments on welded box girders. The experiments incorporated several fatigue sensitive details into a three-flanged box beam, an attempt to simulate the structural redundancy found in unidirectional doubled-hulled ship structures.

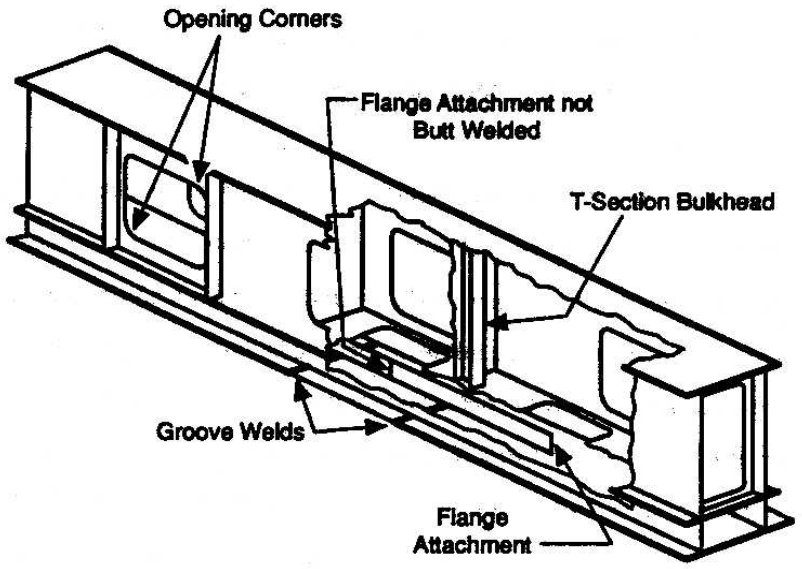

Figure 2-8: Test configuration and details investigated by Nussbaumer [109]

The present research will follow the objectives and methodology of Nussbaumer's work. The present research will extend the research of Nussbaumer et al. to the case of multiple stiffener plate geometry rather than the unstiffened cellular geometry.

Nussbaumer developed both an analytical and finite element models to address fatigue crack propagation based on LEFM. For fatigue crack growth, it was assumed that stresses significantly less than the yield strength of the material comprise the overwhelming majority of fatigue crack growth. Limited amounts of plasticity occur at these service stresses, allowing the principles of superposition and a simplified LEFM stress-intensity factor calculation to be used.

His analytical solution used the basic solution for a center crack in an infinite plate with a series of correction coefficients derived from the work of Isida, Poe, and Grief and Sanders [64, 74-76, 122, 123]. While Poe's work superimposed K-factors from applied loads (uniform axial stress and rivet point forces from stiffener-plate interaction), Nussbaumer's analytical model built upon Poe's model with the addition of a residual stress K-factor. The residual stresses were modeled based on Greene's function, integrating the solution for a pair of splitting forces acting at the crack faces. The K-factor due to residual stress is as follows:

$$K_{RES} = \sqrt{\pi * a} * \frac{2}{\pi} * \int_0^a \frac{\sigma_{RES}(x)}{\sqrt{a^2 - x^2}} dx \qquad \text{Eqn. 2-16}$$

An illustration of the derivation can be seen in Figure 2-9.

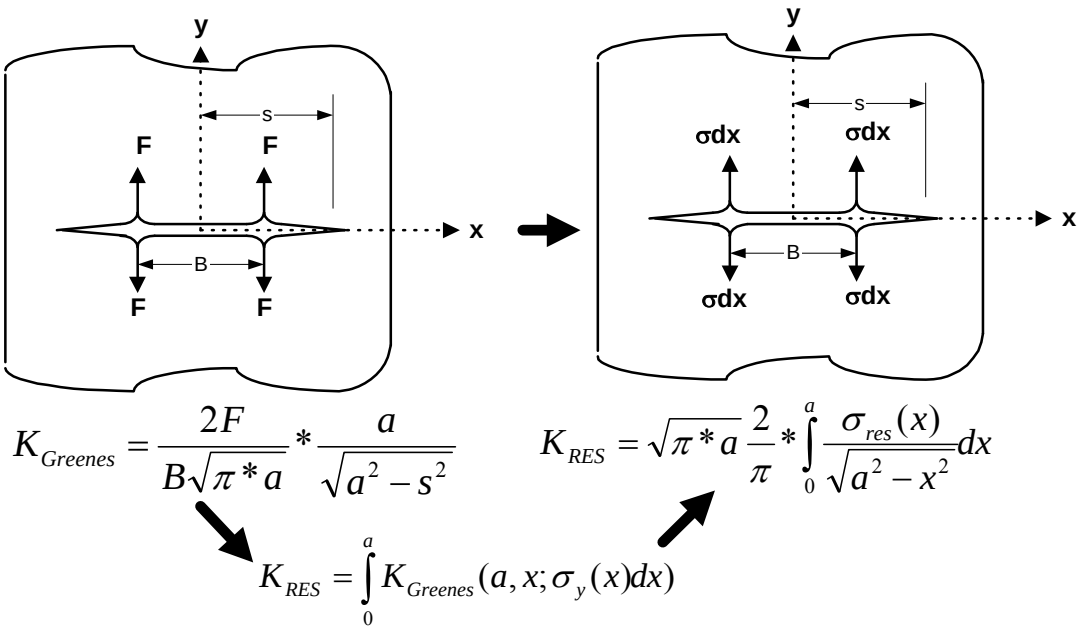

Figure 2-9: Use of Greene's function to develop the stress intensity factor due to the residual stress field [131].

The LEFM K-factor solutions used were all developed for infinite plates subjected to various loads. Several coefficients have been used to correct for the finite width of the plate, but these tend toward infinity as the plate becomes fully cracked.

Nussbaumer proposed a net section coefficient to account for the finite width effect, noting that cracking a stiffened plate in a redundant structure would have the effect of increasing net section stresses. In other words, stiffness of the structure could be expressed as a function of crack length. Such a correction would more adequately simulate the finite width effect than other suggested coefficients. Referencing the initial geometry of the structure, the increase in net section stresses can be determined from the net section modulus:

$$f_\sigma = \frac{\sigma}{\sigma_{nom}} = \frac{I_0 * c(a)}{I(a) * c_0} \qquad \text{Eqn. 2-17}$$

where: I_0 = original moment of inertia

c_0 = original centroid

I(a) = Net section moment of inertia

c(a) = Net section centroid

Nussbaumer's [109-111] finite element model (FEM) consisted of determining J-integral at various crack lengths and translated it to an equivalent K. The J-integral is determined by taking a contour integral around the crack tip. It is a measure of the change in potential energy associated with extending the crack an infinitesimal amount, *da*. Many commercial finite element packages are equipped to perform such a calculation.

Before applying any external loading to the finite element model, residual stresses were input as applied temperatures causing shrinkage. An iterative process was employed on the *uncracked* geometry to develop the stress patterns measured in the specimens. A crack was then introduced, i.e. releasing boundary conditions along the nodes defining the crack faces, and the finite element analysis automatically redistributed the residual stresses by maintaining force equilibrium. Use of contact elements along the crack face prevented overlapping of surfaces. These residual stress patterns redistribute as the crack propagates since they are originally configured on the un-cracked geometry. This procedure will be followed in the current study, and a more detailed procedure will be discussed later.

When the stress intensity factor range is based only on the applied stress range (no residual stresses), both the analytical model and the FEM model predict increasing growth rates. Residual stresses were then considered in these models. A typical distribution of residual stress in a stiffened panel structure is shown in Figure 2-10, along with typical experimental data.

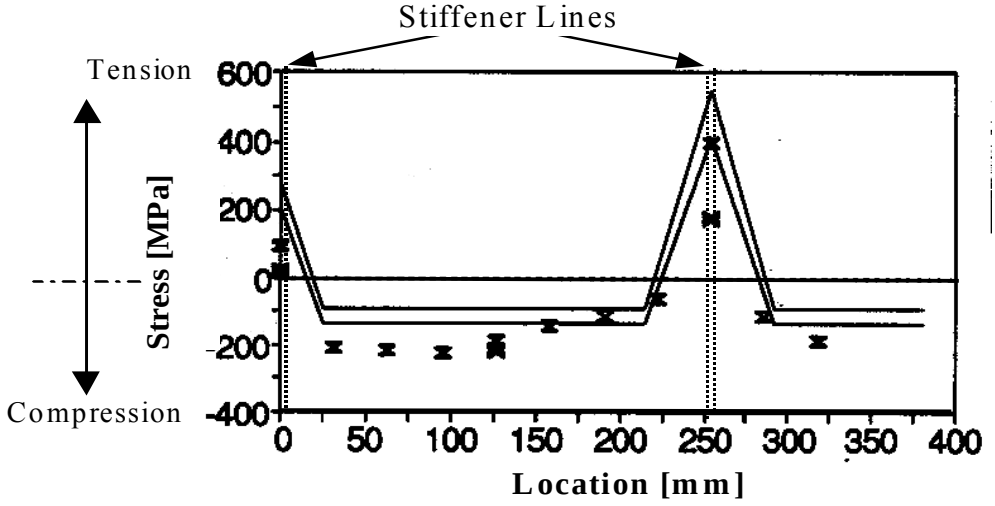

Figure 2-10: Typical residual stress field at fillet welded joints—used in Nussbaumer's analytical model [109-111].

There was significant scatter in the measured residual stress distributions for these experiments. Therefore, three distributions were examined, one based on the lowest observed residual stresses, one based on the largest observed residual stresses, and one that was an average or typical distribution. All of the distributions were in self-equilibrium—that is, compression zone area was equated by the area of tensile zones throughout the entire box section.

All three residual stress distributions were applied to the FEM model. The average distribution gave results that were generally just below the experimental data in terms of the growth rate. The maximum residual stress distribution causes a dramatic decrease in the growth rates to the point of virtual crack arrest. The minimum residual stress distribution

gave results that were good up to 100 mm of crack length but then were too high in growth rate. These results show that the calculations are extremely sensitive to the residual stress within the range of variation that was observed.

In fact many other variables, including the difference between the upper bound growth rate and the lower bound growth rate, made minimal difference in the calculations in comparison to the residual stress. Therefore, if modeling of this type of crack propagation is to be improved, it is not necessary to know the crack growth rate (above threshold) any more accurately, and more effort should be focused on studies of the residual stress and how it is affected by fabrication sequence. Better data on the threshold crack growth rates would improve modeling of the first stage of crack growth, however.

In the analytical model, the average residual stress distribution was used directly in its corresponding K-factor, K_{RES}. The residual stresses were not redistributed as the crack propagated. Such redistribution, although factual, was deemed too complicated to incorporate into the analytical model. Only the tensile part of the stress intensity factor range was considered effective and was used in the Paris law (The effective stress intensity factor is defined in Figure 2-4).

Based on the effective stress-intensity factor range, the analytical model gave reasonable results, as compared to the experimental data in Figure 2-11. The finite element model, where K-factors are determined through converted J-integrals, and residual stresses were redistributed, provided similar results.

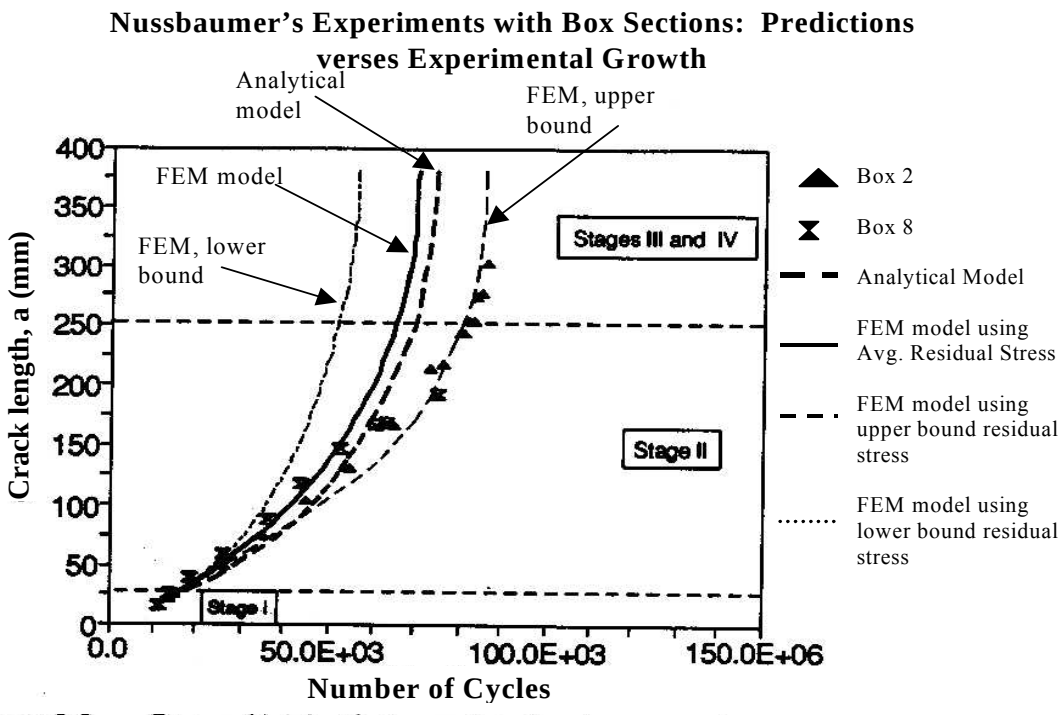

Figure 2-11: Fatigue crack predictions for cellular box beam [109-111].

Nussbaumer found that both the analytical model and the finite-element (FEM) model predicted the behavior reasonably well in the one-celled box beam, and that neglecting the effect of residual stresses increased the error significantly. In addition, the FEM model predicted crack closure at and behind the crack tip, consistent with the observations. In an extension of his research, Nussbaumer analyzed a multi-cellular box structure representative of a ½ scale model of a double-hulled vessel. His FEM predictions indicated that the crack opening stress was significant in accurately modeling the crack growth, due to crack closure effects. With the multi-celled structure, the crack opening stress was predicted through finite element analysis. The analytical model, however, is not capable of accurately predicting crack closure effects. However, no experimental data were available for comparison.

It is noteworthy that in the box girder tests, unless the cracks were repaired, they continued to propagate in a stable manner until it was impossible to load the specimens due to

excessive deflection. The cracks often reached more than 1.5 meters in length, giving a clear demonstration of the inherent structural integrity of a cellular structure fabricated from relatively thin plate (13 mm or less) of reasonably tough steel.

Several other investigators have used techniques similar to Nussbaumer's models. A decade before Nussbaumer, Anil Thayamballi's Ph.D. dissertation [154] outlines an almost identical analytical approach to calculating fatigue crack growth through stiffened panels, including the effects of residual stress. In addition, variable amplitude loading, ship failure assessment and residual strength of ship structure are discussed. The residual stress distribution was determined using the representative block tension and compression regions suggested by Faulkner [48-50], with the same integrated Greene's function as used by Nussbaumer. The dissertation includes an exhaustive reference section of works pertinent to assessing fatigue crack growth, ship structural failure, and wave loading representation. However, no experimental verification was made to verify the approach and its assumptions.

In 1996, Sumi et al. [142] used finite element analysis to study fatigue crack propagation in stiffened panels similar to the deck structure in ship. A single crack in a stiffened panel and an array of three cracks initiated at the stiffener locations was investigated, neglecting the effects of residual stress. Equivalent K-values were computed using ANSYS finite element software. Four specimens were tested: A plate with a center crack, a plate with an array of three cracks, and a stiffened panel with a single crack, and a stiffened panel with an array of three cracks. The applied stress range was 80 MPa, and the initial crack length was 8 mm in all cases.

The research was similar to the present course of study except for the exclusion of residual stress. LEFM ΔK values were used in the Paris Law to predict crack propagation rates in mild steel. For the case of multiple cracks, a simple iterative solution was developed hinging on a reference crack. The predicted results for the plate specimens were reasonably accurate, while the predictions for the stiffened specimens over-estimated the fatigue life by

about 25 percent. The authors attributed the error to lack of residual stress inclusion, noting the behavior in the stiffened specimens with respect to their predictions.

Other researchers using the analytical, LEFM-based approach to fatigue life prediction include Pang in 1991 [116] and Cook et al. in 1992 [29]. Pang explored surface fatigue cracks emanating from both welded cruciform joints and fillet shoulder. His analytical analysis of surface crack propagation used a material threshold stress intensity factor to account for crack closure. This work, however, did not attempt to account for residual stress, and the prediction errors (some being highly conservative) was attributed to the uncertainty in the material threshold.

Cook et al. [29] outline a computer program developed to address cracks propagating from rivet holes in aircraft structures. Although the program addresses fatigue crack growth in aluminum panels with riveted stiffeners, it includes the effects of residual stress at holes with compressive residual stress introduced through cold expansion techniques. Cold expansion, along with interference-fit connections, has become a common technique to increase fatigue resistance at rivet holes in damage tolerant design. A LEFM superposition approach similar to Thayamballi's [154] was used to incorporate a stress intensity factor due to residual stress. The residual stress field, however, was characterized more precisely by Lagrangian interpolation rather than the simple linear interpolation illustrated in Figure 2-9. Stress intensity factors were determined through the use of Green's function, with a resulting expression similar to Equation 2-17. Fitzpatrick and Edwards provide an overview of this technique and its relation to residual stress fields [56]. Essentially this is a means of determining K-values for a specific configuration through weight functions, where 8^{th} order Guassian integration was used to accumulate the total stress intensity factor for a varying stress field.

Cook's approach, although more detailed in determining stress intensity factors, did not resolve the shortcomings of Nussbaumer's analytical model. Namely, the residual stress field was not redistributed with crack growth and crack closure behind the crack tip was not

taken into account. Therefore, the main enhancement of this model was the refined characterization of residual stress field and its subsequent integration. These corrections may be appropriate for application to cold expansion residual stresses, where the stress fields can be characterized with relative accuracy. Welding residual stresses, however, vary so significantly that a refined approximation cannot be justified at this time and a linear, worst-case model is more applicable.

To date, the previously mentioned works were the most significant advances in this subject. Many authors have confirmed the strong influence of residual stress on crack growth, although very little experimentation has been conducted in long fatigue crack growth. The subject of residual stress and its affects on small-scale fatigue and fracture has been studied extensively, however. A review of its role in fracture and plastic collapse is presented by Clayton [27].

2.4 RESIDUAL STRESS

Residual stresses in welded steel structures can contribute to the problems of: 1) hydrogen-assisted cracking during fabrication; 2) brittle fracture during fabrication or in service; or 3) fatigue crack growth in service. Therefore, it is important to be able to predict the magnitude and distribution of residual stress. A good overview of residual stress effects on fatigue and the complexities involved in predicting fatigue crack growth through residual stress fields is provided by Fitzpatrick and Edwards [56]. An excellent work on residual stresses and their effects in ship hulls can be found in an early book by Osgood [114].

Fatigue is more important than fracture in cyclically-loaded structures like ships. The fact that fatigue is not sensitive to microstructure significantly simplifies fatigue design and evaluation, because all ferritic steel can be considered to have the same fatigue strength. Residual stress does not need to be considered for fatigue design or evaluation using S-N curves, because the S-N curves were obtained from a large sample of large-scale tests with the natural residual stress distributions in the specimens. Thus, the appropriate level of residual stress is built into the S-N curves. The high tensile residual stress in welded details means that the mean level of applied stress has little impact on the fatigue life, which also simplifies fatigue design and evaluation procedure. Residual stress is a factor in thickness effects in fatigue, but these are taken care of without explicit consideration of residual stresses.

Residual stresses are very important in fatigue, but normally it is conservatively assumed that there are tensile residual stresses of yield stress magnitude in the vicinity of the crack. This high level of residual stress is built into the S-N curves, so using them implies an assumption of high residual stress. Therefore, there is no need to explicitly consider these residual stresses in a fatigue analysis. There are special situations where residual stress should be explicitly considered in fatigue evaluation using a crack propagation analysis. It is possible that compressive residual stress can protect some buried weld defects from propagation. However, it is probably not prudent to count on this effect for structural

integrity. So the only situation where it is necessary to know the residual stress distribution for fatigue is the analysis of long propagating through-thickness cracks. In fact, it is only necessary to know the compressive part of the residual stress distribution that is far away from the weld. Therefore, the detailed numerical models are really not necessary for this application. Simplified methods, typically idealized representations of residual stress fields based on experimental data, remain the best option for routine engineering assessment.

The uncertainty in this type of long crack propagation analysis is dominated by the uncertainty in the residual stress. Variations in the expected residual stress are due to the initial residual stress in the plates and rolled shapes prior to welding, thermal cutting, and fabrication sequence. Flame straightening may be used to correct plate out-of-flatness or weld distortion, which also alters residual stresses. The resulting uncertainty can change the crack propagation rate by more than two orders of magnitude. Narrowing this uncertainty will have the greatest payoff in terms of increased confidence in structural integrity.

Fracture is very sensitive to microstructure and significant benefits could be obtained by continuing to study how the weld thermal cycle affects fracture toughness. Ductile fracture is not affected by residual stress [57], however brittle fracture is dramatically affected by residual stress. This is only an issue in evaluating existing structures, because new structures should not be designed using brittle materials.

Typically, worst-case assumptions are made regarding the residual stress in brittle fracture evaluations. In fact, this simplifies the evaluations significantly because the peak stresses (applied plus residual) are taken as equal to the actual yield strength. This eliminates the need for determining the applied stresses. In rare cases, it is acceptable to take into account some reduced residual stress other than the worst-case assumption. However, it dangerous to narrow the margin too much on the possibility of brittle fracture. This is the only situation where a detailed description of the residual stress, such as could be obtained with a numerical simulation, would be useful for fatigue and fracture design or evaluation.

A large amount of measured residual stress data from rolled shapes and welded built-up members have been obtained over the years at Lehigh, primarily by Lambert Tall and his colleagues [4, 19, 86, 147, 153]. Experimental data [4, 19, 53, 60, 86, 147, 153] show that the initial residual stress in welded and rolled sections is highly variable and depends on the fabrication process. The ranges in the value of peak tensile residual stress are at least plus or minus 40% about the mean.

Another significant factor that must be taken into account is fabrication sequence. Measured residual stresses in box sections depend strongly on which web is welded to the flange first [53, 115]. When there is excess gap between members to be welded, they are often pulled together using a "come along", which has a profound effect on the built in residual stress in many neighboring members. Flame straightening may be used to correct plate out-of-flatness or weld distortion, which also alters residual stresses.

Many of these issues were faced through compression research of stiffened panels [48-50, 71, 72, 87, 105,124,139, 165]. Vroman took residual stress data in 3 identical steel stiffened sheet panels in 1995 [165]. The configuration was typical of naval vessel structures, and is seen in the Figure 2-13.

The specimens were fabricated at the Naval Surface Warfare Center (NSWC) at Carderock, Maryland, with the welding sequence being typical of naval ship construction. Measurements were taken throughout the fabrication process through use of a Whitmore gage: Once prior to welding, once after tack-welding the stiffeners to the plate, and finally after welding was completed. The data points were spaced at 70 mm in the center bay only, with results for the three panels as indicated in Figure 2-13.

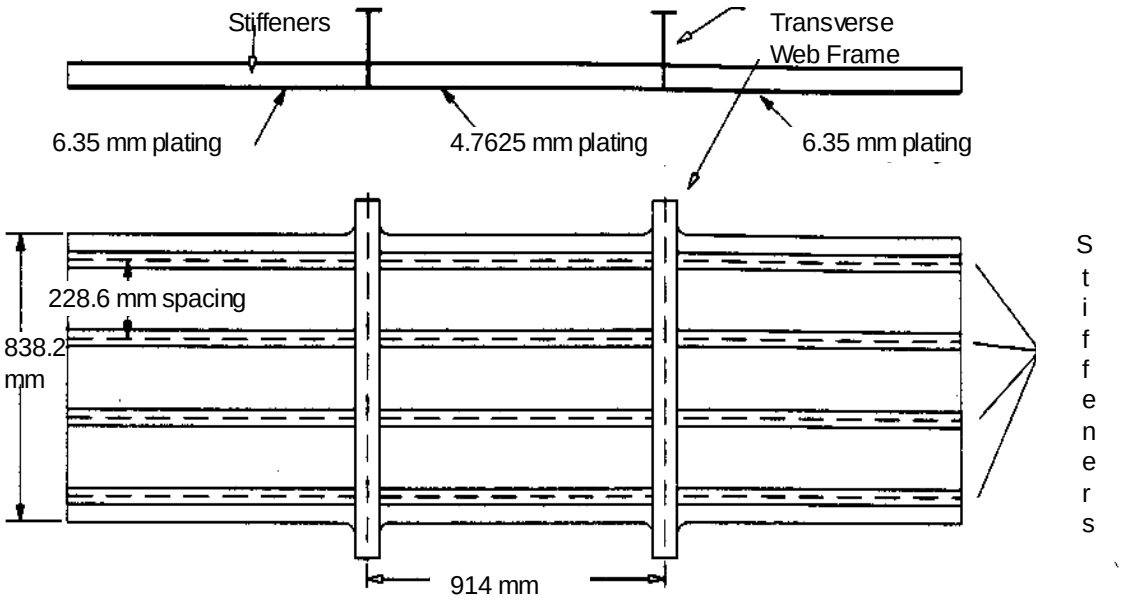

Figure 2-12: Typical grillage tested by Vroman [165].

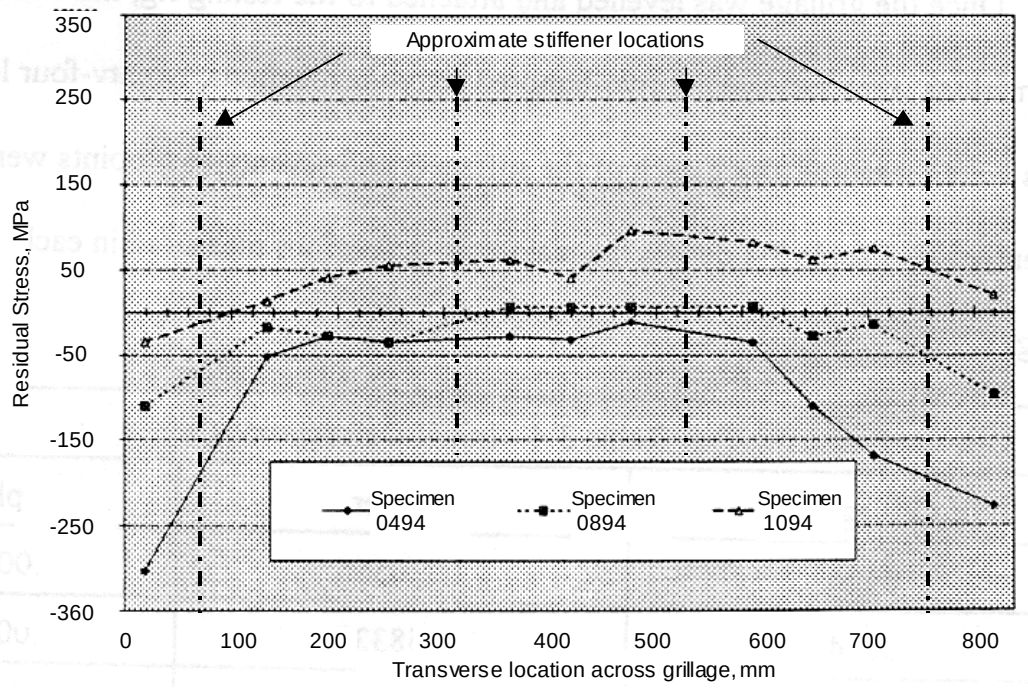

Figure 2-13: Residual stresses in three stiffened panels tested by Vroman [165].

Normally one would expect high tensile regions around the stiffener region, with equilibrating compressive stresses in between stiffeners. The measured forces across the panel do not satisfy equilibrium, and thus the data must be questioned. It is likely that the measurement spacing did not accurately capture the narrow tensile regions surrounding the stiffeners. An important note in Figure 2-13 is the variation in measured residual stresses despite the fact that the steel plating was "carefully selected from a large batch to all exhibit similar strengths, mean stresses, etc." In fact, yield stress measurements in the stiffeners were all matched at 383 MPa, the plating matched at 305 MPa, and the welding pattern unchanged. Even with such rigorous quality control, the difference between the residual stress data in the three identical panels is apparent.

Earlier compression tests by Kondo and Ostapenko provide a more accurate profile of the residual stress field. Their sectioning coupon pattern was more refined (See Figure 2-14).

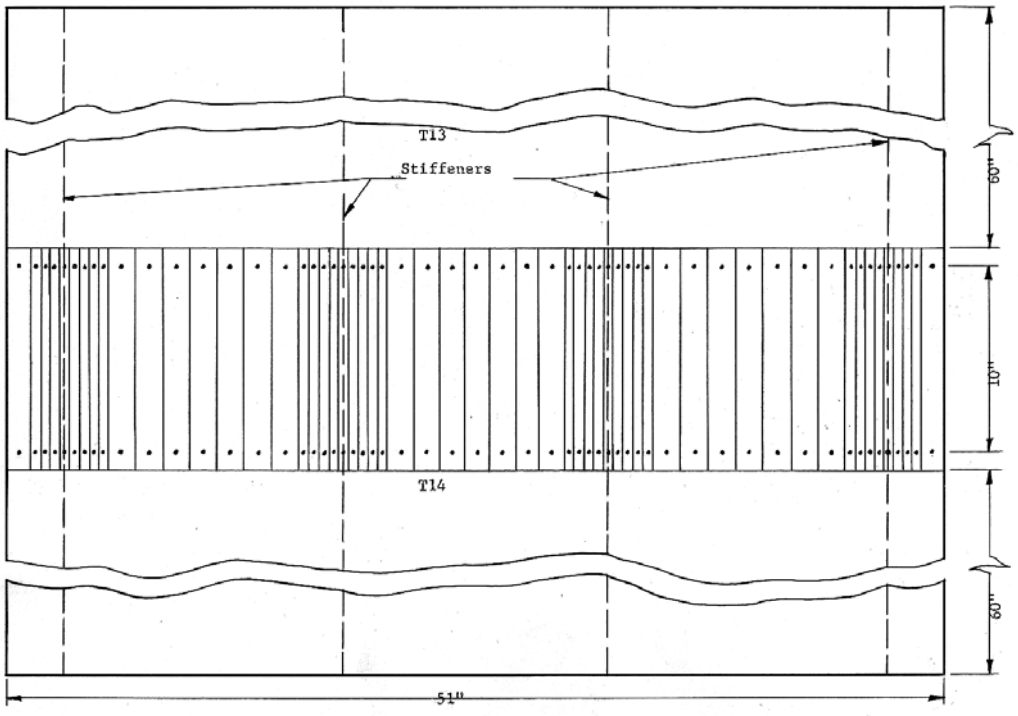

Figure 2-14: Coupon pattern used in sectioning of tested stiffened panels by Kondo and Ostapenko [102].

This fine sectioning pattern was carefully measured and extracted to obtain residual stress measurements. The results may be seen in Figure 2-15.

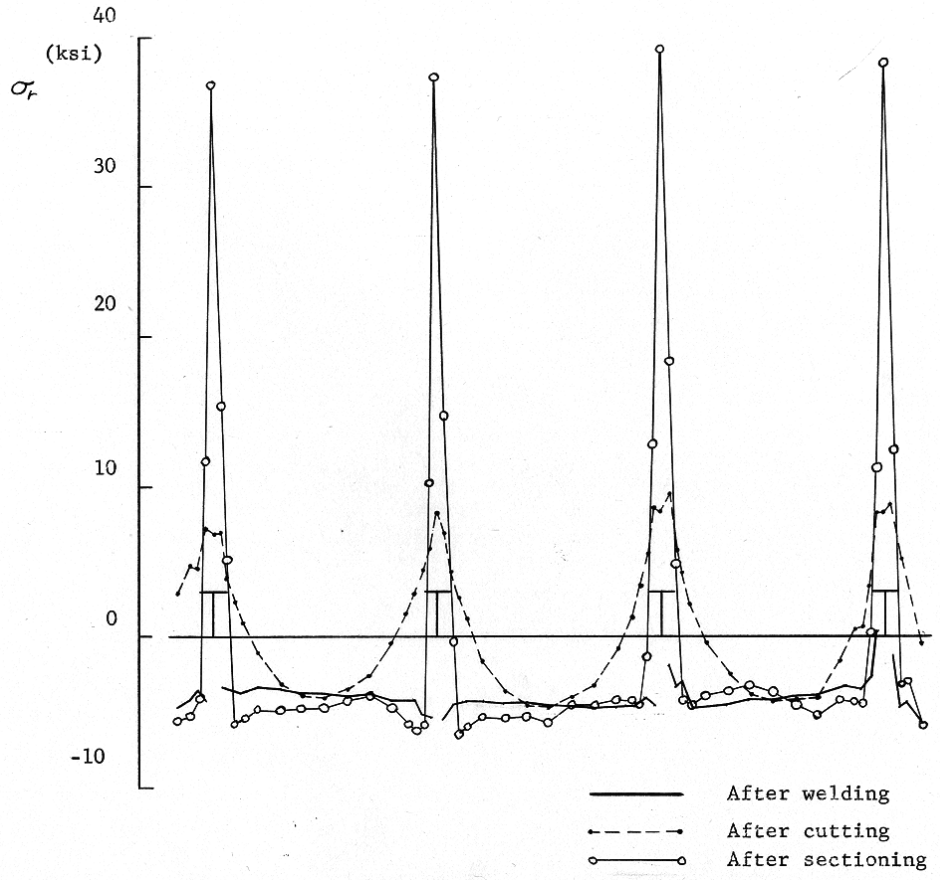

Figure 2-15: Residual stress measurements obtained by Kondo and Ostapenko [102].

Figure 2-15 characterizes the residual stress pattern expected in welded stiffened panels. The measurements capture the tensile zones around the stiffener weld lines and demonstrate the equilibrium conditions found in residual stress patterns.

Compression tests at Simon Engineering Laboratories at the University of Manchester [71, 105], and at Monash University in Australia [105], included measurements of residual stress. Totaling over 40 tests, the results provide residual stress data for a variety of welding configurations on various stiffener geometries. In particular, a large number of hole-drilling measurements were taken across some panels with geometry similar to the current

investigation's configuration, with the exception of a smaller weld size (6-mm). As typical, there was a wide range of residual stress measurements in very similar panels.

Notwithstanding this uncertainty, welding simulation models have been developed and have been used for some practical applications [7, 39-42, 63, 67, 83, 95, 96, 132, 133, 160-162]. Kamtekar [83] provides a review of the development of residual stress prediction attempts. He demonstrated an iterative procedure using the finite difference method to predict residual stress patterns. Significant simplifications are typically used to make the numerical analyses feasible. For example, two-dimensional generalized plane-strain models have been used in most cases. Despite the simplifications, these analyses are far from routine. Yet there is a need to model complex three-dimensional connections. Such three-dimensional calculations require significant labor to set up and significant resources to run. For these reasons, numerical welding simulation has remained primarily a research tool rather than a part of routine engineering assessment of fracture critical structures.

Simplified methods, typically idealized representations of residual stress fields based on experimental data, remain the best option for routine engineering assessment. The simplest method of analysis is to rely on measurements in a similar hot-rolled or welded built-up structural member. Tall and Alpsten [147] state that peak longitudinal residual stresses in hot-rolled and built-up structural members can be estimated within 70 MPa based on experimental data and empirical rules.

The typical residual stress distribution for stiffened panels and box sections was shown in Figure 2-10. This idealized distribution is based on the work of Faulkner [48-50], who stated that the width of the tensile zone, assumed to be at a stress equal to the yield strength, is equal to between 4 and 5 times the thickness of the panel, independent of stiffener spacing. The net tensile force is balanced with a region of constant compression between the stiffeners. In addition, the following formula was given by Faulkner et al. [50] for

characterizing the residual stress field between stiffeners:

$$\frac{\sigma_r}{\sigma_o} = \frac{2*\eta}{\left(\frac{b}{t}\right) - 2*\eta} \qquad \text{Eqn. 2-18}$$

where η = coefficient for determining the width of the tension block, $\eta * t$

σ_r = magnitude of the compressive residual stress block

σ_o = yield stress of the plate

b = stiffener spacing

t = plate thickness

Typical values for η in as-welded ships range from 4.5–6, while values of 3–4.5 were given to account for the shakedown of residual stress in ship service. This equation pertains to idealizing both the compressive and tension zones as rectangular blocks. Modeling the tensile block as a triangular region (Figure 2-10) gave the empirical residual stress distribution used by Nussbaumer, Dexter and Fisher [109-111], a distribution confirmed to be relatively accurate in recent experiments on box sections [115]. This type of residual stress distribution should be used for cracks in the shell of ship structure propagating between stiffeners.

For more complicated geometries, a simple estimation of peak values of residual stress can often be obtained by considering a uniaxial elasto-plastic model. The strain can be estimated with the average coefficient of thermal expansion and the difference between the phase transformation temperature and room temperature. This strain is applied to the uniaxial model to estimate the peak stress [95]. This approach does not give the distribution of residual stresses through the thickness of the plate.

In order to estimate the distribution of the residual stresses, the actual multiaxial behavior of the component must be considered. If simple analytical models exist for the component (e.g. a simple beam or plate), the tendon-force or shrinkage-force approaches [17, 20, 93, 94 146, 167] may be used. In these approaches a force is calculated and applied to the

component along the weld axis. The reaction of the component to this force gives the residual stress. In the simpler applications, this force is taken as 20% of the heat input [94, 167] or proportional to the weld area [17, 20]. The more sophisticated approaches consider the temperature distribution in the weld and are usually attributed to Russian papers by Okerbloom [57].

There are simple numerical models, for example Tall [146], which generally break the plate or other geometry into fibers or strips. The transient temperature distribution is applied and strain compatibility is enforced among the strips. These models are generally applicable to only a specific type of component. The finite-element method offers greater flexibility and accuracy. The justification for the strip models is the savings in computer time relative to advanced nonlinear transient finite-element analyses. Since modern computers are increasingly able to handle these finite-element analyses, there is no longer any reason to consider the strip models.

An example of finite element analysis to determine residual stress distributions is shown by Finch and Burdekin [51]. They illustrated the residual stress field in a butt-welded plate and a butt-welded pipe-on-plate geometry, and calculated J-integrals for various crack lengths and loads. Interestingly, they found [for the butt-welded plate] that the J-integral obtained in a plate with residual stresses was always larger than that of a plate without residual stress, even when the crack was well into the compressive region. Furthermore, they found that at certain loads, the plate with a small crack in the tensile region of residual stress had a higher J-integral than the case where the crack had penetrated the compressive region. The plate with the small crack, therefore, would have the non-intuitive aspect of being more susceptible to cracking than the plate with the larger crack in the compressive residual stress zone.

This behavior of crack propagation was also noted by Almer et al [3]. A series of experiments was performed on compact specimens with and without residual stress introduced. A similar study was conducted by Bucci [24]. X-ray diffraction was used to

quantitatively measure the residual stress field and compared to finite element analysis. The finite element analyses compared relatively well with the x-ray diffraction measurements with the exception of overestimating the residual stress near the source of tensile residual stress. The researchers noted that crack propagation rates became highly sensitive to residual stress as the applied loading decreased. Such behavior reinforces the importance of characterizing worst-case residual stress patterns, especially in ship loading conditions where many of the applied loads are very small.

The beneficial effects of compression zones on crack propagation have been noted for quite some time. Many investigators have sought means of exploiting the compressive regions as crack arresters through a process called "stress coining". An analysis and discussion has been conducted by Ogeman et al. [112] on the applicability of this process to longitudinal connections at web-frame intersections.

Averbach and Lou [11] noted the crack propagation rates in carburized compact specimens. Using superposition, they defined an internal stress intensity factor to account for the residual stress according to a distance, d_i, correlating with the extent of residual stress, and δ_i, the residual stress at a given point. Their simple relation was as follows:

$$K_i = \delta_i d_i^{\frac{1}{2}} \qquad \text{Eqn. 2-19}$$

This relation was added to the applied stress intensity factor to determine the effective stress-intensity factor, K_e.

Beghini et al. [16] studied the effects of residual stress in a series of compact specimen tests in 1994. They modified an expression from Tanaka [148] to account for the plasticity-induced crack closure, an attempt to approximate the effective stress intensity factor actually occurring at the crack tip. Weight functions were used to modify the stress intensity factor, and experiments indicated that the superposition of the residual stress K-factor was only applicable for cracks with no closure. The authors, however, remarked that crack closure would not have significant effects in the case of long cracks [16]. When comparing the

predictions including residual stress with those that neglected residual stress, the results showed conclusively the important influence that residual stresses have.

Torii et al. [155,156] studied surface crack propagation through residual stress fields in 1989, indicating that the crack propagation rate could be based on a combination of the applied stress intensity factor and the maximum stress intensity factor. Their results modified the Paris Law into the form:

$$\frac{da}{dN} = C\{(\Delta K)^p (K_{max})^q \quad \text{Eqn. 2-20}$$

where p and q were empirical coefficients that satisfied the relation: p + q = 1

Although the results were based on an elliptical surface flaw in a compact specimen, the approach provided a new formulation for the Paris Law that could hold significance. Another modification of the Paris Law was presented by Toyosada et al. based on an effective ΔK called the ΔK_{RP} [157, 158]. The ΔK_{RP} parameter is defined as the stress intensity factor of the re-tensile plastic zone. Similar to the crack opening load concept, the re-tensile plastic zone notion attempts to define the amount of tensile load necessary to initiate further fatigue damage at the crack tip. When the crack is opened with significant applied loads, a plastic zone is generated around the crack tip which tends to keep the crack tip closed. With the crack held closed by the plastic zone, part of the applied stress is not effective since a portion of the applied tension is devoted to overcoming the plasticity-induced closure. This means additional tension must be supplied to impart the same amount of crack extension as occurred without the plastic zone.

The ΔK_{RP} is generally larger than the typical crack-opening load, in regions of no residual stress, because it takes into account the plastic deformation ahead of the crack tip that has occurred from previous load cycles. In regions of tensile residual stress, the ΔK_{RP} decreases, translating to more a more effective ΔK range and faster growth rate. In regions of compressive residual stress, the ΔK_{RP} increases, taking into account the beneficial effect of compressive residual stress maintaining the closed crack front.

The study was based on a modification of Newman's crack closure model [139], where plastic shrinkage along the crack faces and redistribution of the plastic zone ahead of the crack was taken into account. Compact experiments showed good agreement with the model, but the improvement of the predictions in tensile-only cycling was negligible. Its merit could be significant in variable amplitude loading where both compressive and tensile cycles exist, although the complexities involved in variable amplitude loading undermine the utility with which the method could be used with ease.

Itoh et al. [77] and Ohji et al. [113] have demonstrated that the use of a simpler LEFM ΔK_{eff} based on the crack opening load was sufficient to produce reasonable crack growth rate correlation. Neglecting the redistribution of residual stress was found to conservative with positive R-ratios, and propagation rates were equivalent with respect to the crack opening ratio, *U* (Elber's ratio) [45]. For convenience, Elber's ratio is restated here:

$$U = \frac{\Delta o_{eff}}{\Delta \sigma} = \frac{o_{\max} - \sigma_{opening}}{\sigma_{\max} - \sigma_{\min}} = \frac{\Delta K_{eff}}{\Delta K_{total}}$$

Itoh et al. programmed this approach into a computer, providing crack growth estimations relatively quickly. A flow chart for such an algorithm is presented in the paper as well. This simplified approach seems prudent in light of the uncertainties involved. It is anticipated that such a procedure will be effective in providing worst-case estimates of crack growth, although the accuracy in any one test may be compromised. Leggatt has confirmed this approach as satisfactory [92]. He comments on the application of the approach in PD6493 procedures and outlines the extension toward CTOD design curves and J-integral schemes, which are comparable to Xiao and Dexter's methodology [169] and the procedure followed by Stenseng [141].

2.5 VARIABLE AMPLITUDE LOADING AND STRUCTURAL RELIABILITY

So far, crack propagation has been discussed as if the loading were constant amplitude. However, the actual service load history of ships consists of cycles with a variety of different load ranges, i.e. variable-amplitude loading. Such wave loading data is found in SSC-268 [68]. Some attempts have been made to model crack growth behavior under a specified loading history [9, 14]. These models, often complex, generally address highly random flight loading and relatively simple models presented hereafter have demonstrated similar accuracy [10].

There are several accepted ways to convert variable stress ranges to an equivalent constant-amplitude stress range with the same number of cycles. SSC-315 addresses some of these methods, although comparisons were made with compact specimen testing [43]. These procedures are based on the damage summation rule jointly credited to Palmgren and Miner (referred to as Miner's rule [103]). Most large-scale experimental studies have confirmed the use of Miner's rule [137]. However, there is some experimental evidence that indicates that Miner's rule can be very conservative in some cases, and unconservative in others [162]. For more information on these effects, the interested reader can consult the work of Gurney [65], Solin [140], Engle [47], and Winter and Maccinnes [168].

The most rigorous way to calculate an equivalent constant-amplitude stress range with measured stress history data is to sort through the stress history in the time domain and count the stress ranges; i.e. specific differences between maximum stress peaks and minimum stress peaks. A stress-range occurrence histogram is then constructed from the cycle-count data. This procedure was analyzed by Thayamballi [154]. Other methods of calculating an equivalent constant-amplitude stress range involve simple relations to statistical measures of the variability of the stress history such as the root-mean-square (rms).

For the cycle-counting approach, there are at least two widely accepted ways to count cycles: 1) the mean-crossing method; and, 2) the rainflow method. The mean-crossing method assumes that the stress-time history is essentially stationary about a mean value (for short periods) and a cycle is counted as the value of the stress passes from below to above the mean. The maximum and the minimum value of stress are the highest and lowest values that occurred in the time interval since the last mean crossing. Intermediate oscillations between successive mean crossings are ignored, counting only the one cycle with range equal to the maximum minus the minimum.

The rainflow method counts cycles as closed loops within a cycle counting period. Essentially, the largest maximum is matched with the largest minimum, then the second largest pair is matched, and so on. The rainflow method does count intermediate oscillations as individual cycles. One problem with rainflow counting is that, depending on how long the cycle-counting periods are, a maximum may not be associated with a minimum until numerous mean crossings have occurred. This seems inconsistent with the fact that a propagating fatigue crack could propagate beyond the location where the maximum occurs before the corresponding minimum occurs and the cycle is counted.

Another issue with cycle counting is a cutoff or threshold. Depending on the sampling frequency and the precision of the data, there will be very large numbers of very small oscillations. It is generally agreed that these very small oscillations do not have a significant effect on the fatigue life, so typically some arbitrary cutoff is used below which cycles are ignored. In practice, a cutoff of about 3.5 MPa is typically used.

Once the stress range occurrence histogram is developed, the equivalent constant-amplitude stress range can then be calculated using Miner's rule [103]. If the exponent of the S-N curve is equal to 3, then the relative "fatigue damage" of stress ranges is proportional to the cube of the stress range. Therefore, the effective stress range is equal to the cube root of the mean cube (rmc) of the stress ranges, i.e.:

$$S_{Re} = [\ \Sigma_i\ (n_i/N_{total})\ \ S_i^{\ 3}\ ]^{\ 1/3} \qquad \text{Eqn. 2-21}$$

where S_{Re} = effective constant-amplitude stress range,

n_i = the number of stress ranges in interval associated with S_I, and

N_{total} = the total number of stress ranges in the stress time history.

The ratio n_i / N_{total} is equal to the fraction of the total stress ranges in the interval of magnitude S_i.

As previously mentioned, there are some simple methods of estimating an equivalent constant-amplitude stress range directly from the statistics of the variability of the stress history. The root-mean-cube (rmc) stress range can be estimated indirectly from the rmc acceleration amplitude from ship motion studies. This approach relies upon a linear relation between the stress range and the acceleration that must be obtained from dynamic structural analysis or from correlation of measured data.

In previous work on fatigue of highway sign structures for the National Cooperative Highway Research Program, another simple approach was used [82]. The effective constant-amplitude stress range is assumed to be equal to 2.8 times the rms of the stress. In this case, the rms can be determined directly from power spectrum data. Note that this rms is the rms of the stress time history itself, not a property of the stress ranges, as is the rmc stress range described above. Therefore, there is no need to count cycles from the actual time histories when using these simple approaches.

An effective constant-amplitude stress range should be estimated for several discrete levels of Sea State. Then, using an estimate of the period from each sea-state such as the significant wave period, the number of cycles in each sea state can be estimated from the number of hours in each sea state.

The fraction of the life that is consumed by a certain duration of a specific sea state can be obtained from the ratio of the number of cycles in that duration to the number of cycles to

failure (N_{total} from Miner's rule) for the effective constant-amplitude stress range associated with that sea state. If a mission profile can be defined that consists of a series of sea-states, the total fraction of life consumed by that mission is the sum of the fractions consumed at each sea state. The total number of missions that can be carried out before failure is the reciprocal of this fraction of life per mission. A good example of this type of analysis can be found in a paper by Sikora et al. [137].

A number of authors have developed methods of fatigue failure assessment through probabilistic methods [10, 28, 59, 79, 82, 90, 139, 168]. A recent report [100] summarizes the state of the art in reliability analyses for ships. Since these methods are statistical analyses and the objectives of the current study focus on the determination of crack growth rate, only a brief summary will be presented.

Freudenthal and Shinozuka [59] considered upper and lower bounds of ship survival. They observed the scatter in fatigue life prediction of aluminum details and concluded that these lives were a random variable with respect to constant and variable loading. They formulated a statistical life-estimation model based on the multiple load path nature of a redundant structure comprised of many of these details.

Jiao [79] discussed a fatigue reliability model based on the Paris law in which the crack growth rate was considered a random variable except its dependence on crack size. This was assumed because of the variability in loading and its corresponding effect on crack size. Sequence effects are incorporated in a model developed by Columbi and Dolinski [28]. Lambrigger [90] provides a commentary on the use of Weibull probability distribution functions for assessing material failure, a commonly used approach for determining critical crack sizes. This approach is outlined by Alaa Mansour for computing peak wave loadings [101], and detailed in SSC-322. For an in-depth review, the reader is directed to the original works.

Soares and Garbatov [139] present a method based on the section modulus of the ship hull at any given point in time. They related a ship's reliability to the incidence of repair and inspection, and compared their methods with case studies of two tankers. The results showed intuitive conclusions—that increased inspection and repair highly contribute to the structural reliability of the hull at any given point.

3 DESCRIPTION OF EXPERIMENTS

3.1 THEORY

Limited testing of stiffened panels has been performed in the past because of the large loading demands involved. These demands present physical and economical issues that often limit the scope that testing may encompass. To perform full scale or half scale tests on specimens with multiple stiffeners, it was conceived to make the stiffened panel the tension flange of a box girder. This configuration maximized the stress that could be imparted on the stiffened panel with minimal loading. In four-point bending, the box girder test setup could achieve a constant moment region where fatigue activity could be monitored. The conceptual setup can be seen in Figure 3-1.

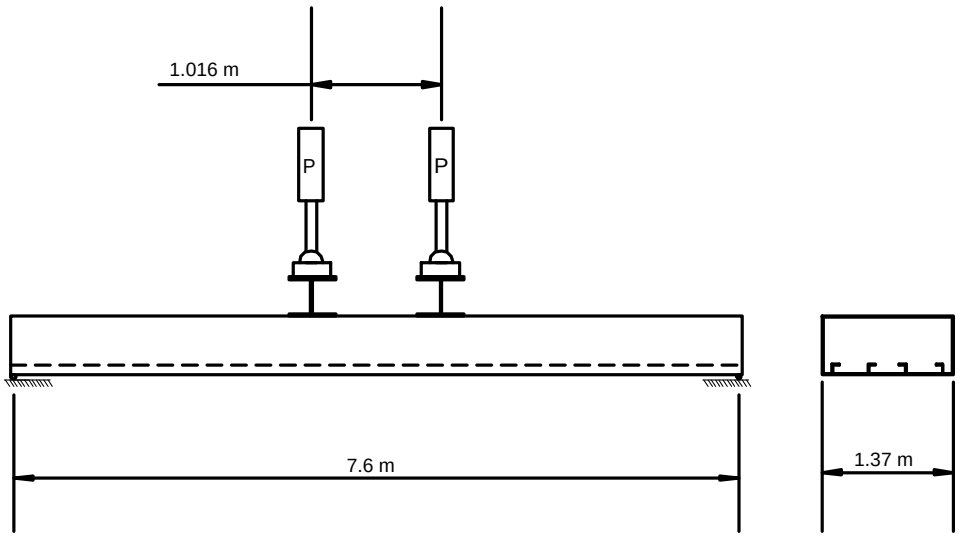

Figure 3-1: Initial conception of testing setup for fatigue experiments.

Financial constraints forced abandonment of monolithic test sections in favor of a bolt-up type specimen with standard W-shapes forming the superstructure. Bolted, slip-critical

connections transform the section from a pair of W12x72 beams at the supports to a large box girder at midspan. These modifications are shown in Figure 3-2.

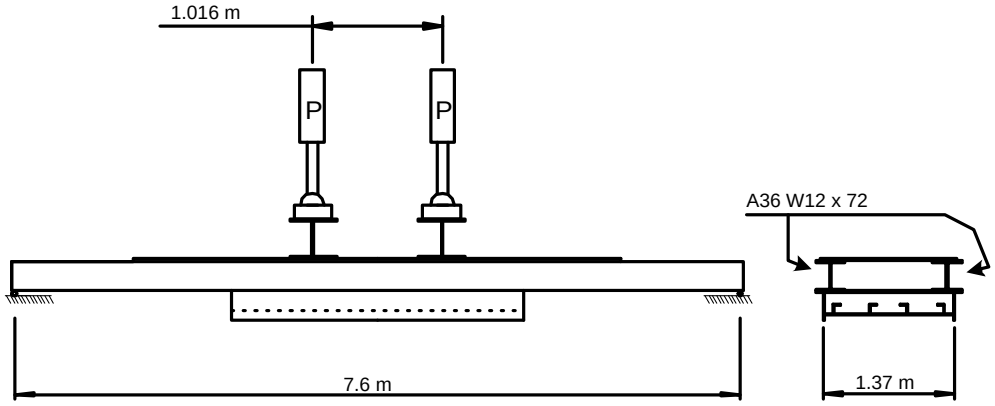

Figure 3-2: Revised experimentation setup after value engineering.

The overall length of the W12 x 72 support beams is 7.62 meters (25 ft) while the distance between supports is 7.112 meters (280 inches). Two 489 kN actuators provide the cyclic load at a distance of 1.016 meters (40 in) apart. A 19-mm thick cover plate spanned the width between the W12x72 beams, tying the beam compression flanges up to a distance 1.27 meters from the ends of the beams. The W12 x 72 beams were drilled with 120 holes matched to a template used for the specimens (Figure 3-3).

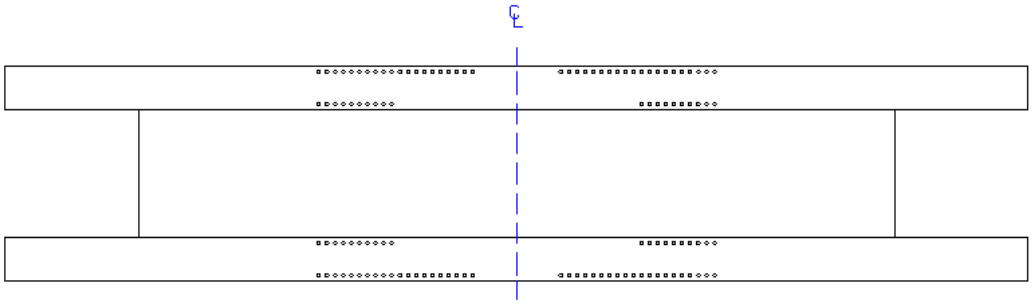

View of support structure from ground level

Figure 3-3: Hole pattern used for experiment assembly with 22-mm A490 bolts.

A490 bolts torqued to 949 N-meters (700 ft-lbs.) connect the top flange of the specimens to the bottom flanges of the W sections. The specimens were fabricated in 3.048-meter lengths, with typical panel widths of 1.37 meters and a plate thickness of 12.7-mm. Four stiffeners were mounted symmetrically in the stiffened panels at a spacing of 190.5-mm. Complete details of the composite cross section is shown in Figure 3-4 while Figure 3-5 illustrates a typical stiffened panel specimen.

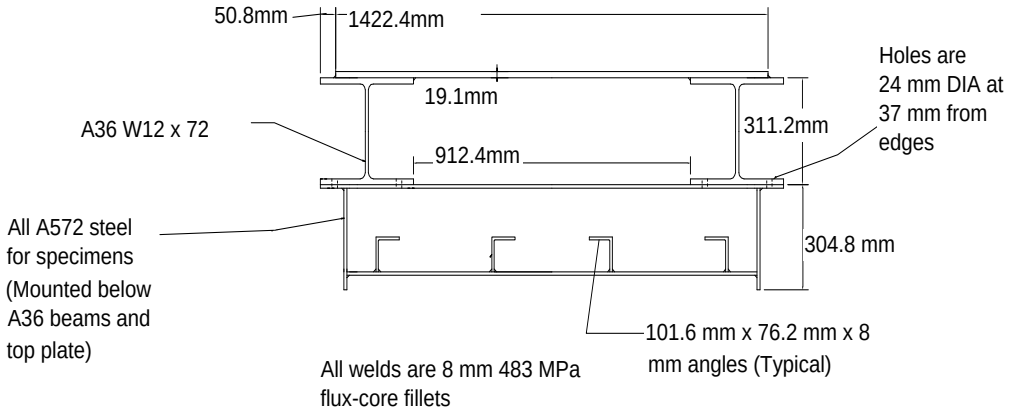

Figure 3-4: Cross section of support structure with specimen mounted below.

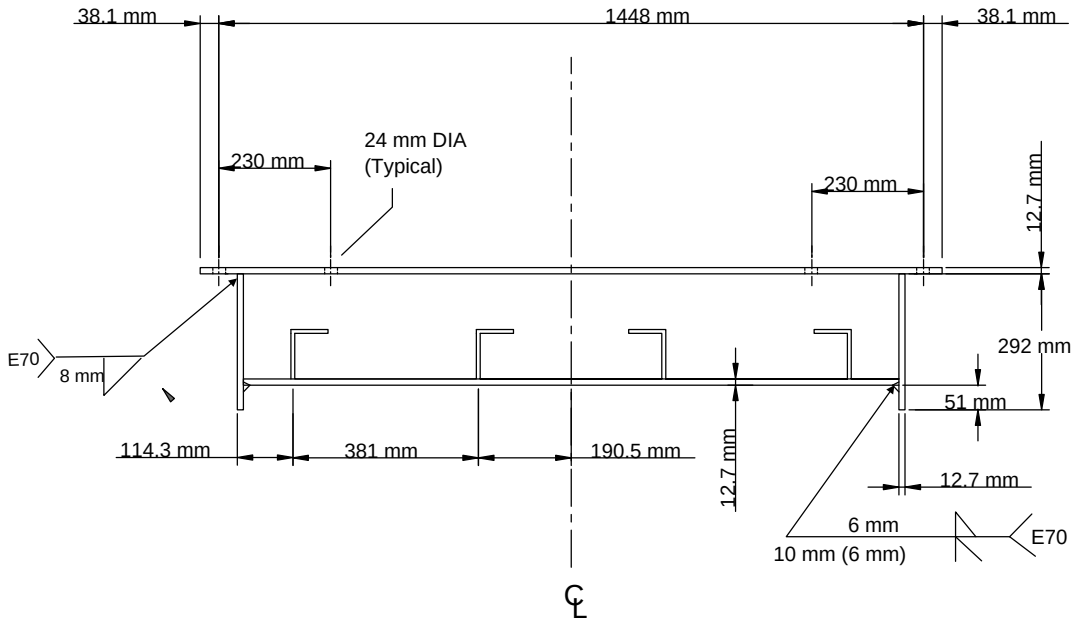

Figure 3-5: Typical stiffened panel specimen employed in experiments.

The total depth of the section is 63.5 cm, with the specimen depth equal to 30.5 cm. A scale of 2:1 was used in correlating specimen component dimensions with typical tanker structure. All of the stiffeners had unequal legs measuring 102 mm and 76 mm with an 8 mm thickness.

Initiation of testing with the baseline test section revealed applied stress ranges of 14 MPa in the stiffened panel, much less than the desired level. In order to raise the stress distribution in the panel and reduce the shear lag effects, vertical webs were fillet welded below the W12 x 72 beams in alignment with the webs of the specimens. Connecting these web additions to the specimens were 12.7 mm x 320-mm plates in a lap splice configuration. Eight A490 bolts were torqued to 949 Newton-meters to provide the slip critical connection. This connection improved the fatigue resistance of the added web at the fillet weld terminations by providing continuity between section changes. The web and splice plate additions can be seen in extending from the specimen.

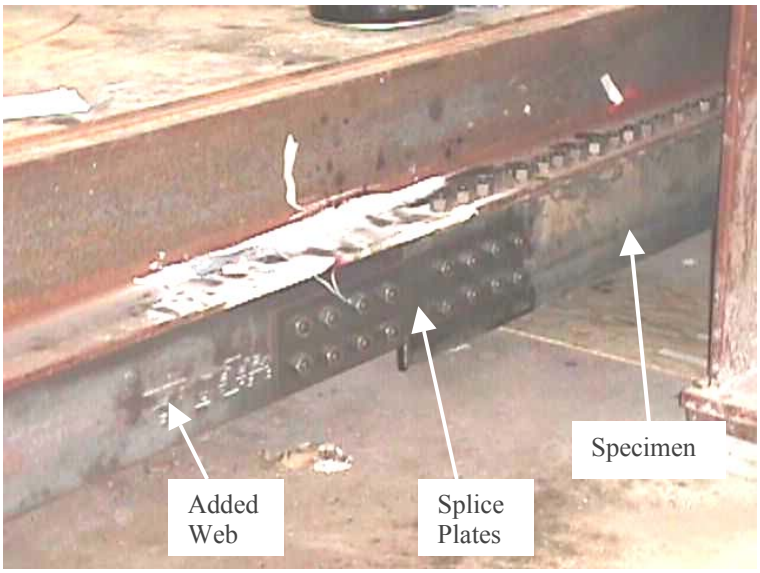

Figure 3-6: Splice plates bridging the gap between specimen and web mounted below W section.

With the splice plate addition, cyclic stress levels in the stiffened panel were increased to an average of 48 MPa. This applied stress range, although low, is very representative of the

overwhelming majority of stress ranges seen in ocean vessels. The extreme wave loading for which ship structure is designed is a rare incidence if it ever is seen during a tanker's life. Consequently, most of the life of the ship undergoes cyclic stresses near the fatigue threshold of the material. The stress ranges in the experiments, therefore, will be a close resemblance of the actual sea state stresses.

However, a stress gradient was still experienced across the specimen width and in the stiffened plate. To monitor the experiments, strain gages were used at varying distances from the crack line. On the bottom plate, six strain gages were mounted 20 cm. from the crack line and an another three were mounted 76 cm. from the crack line. These strain gage locations can be seen in Figure 3-7.

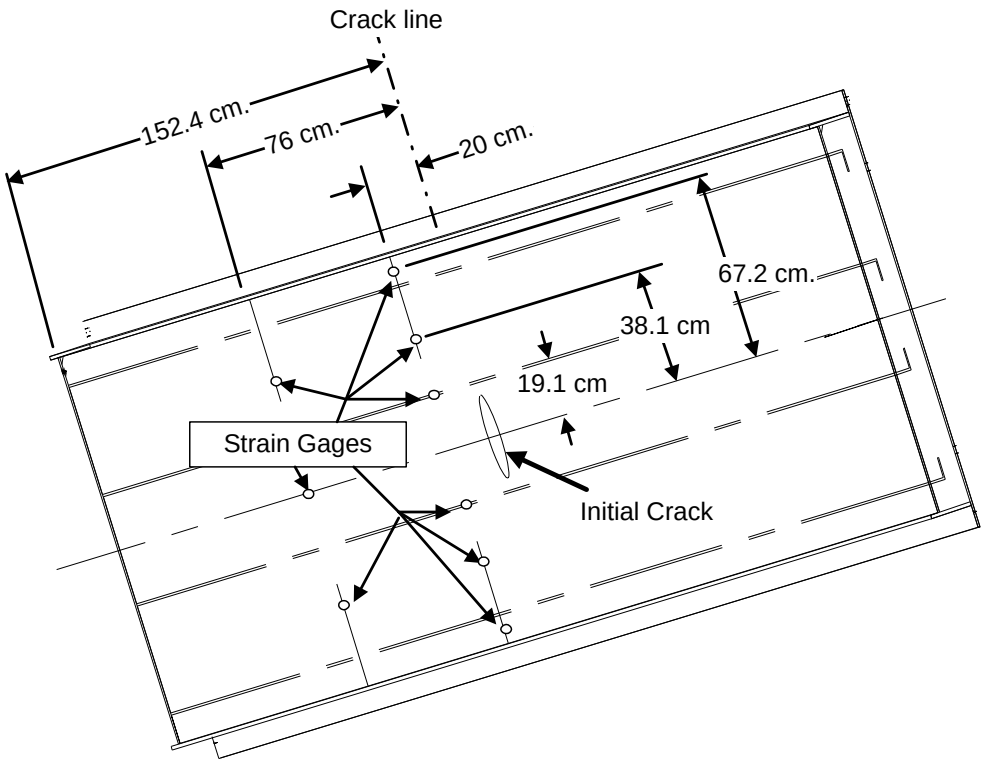

Figure 3-7: Strain gage locations on bottom plate used for stress range monitoring.

In addition, one strain gage was mounted atop the webs of an interior and an exterior stiffener for each specimen. The stiffener gages allowed observation of stress increases as

the plate became cracked and shed load to the stiffeners. They also allowed an estimation of the number of cycles at which a crack would initiate in the stiffener details, i.e., a crack initiating at the top of a weld access hole.

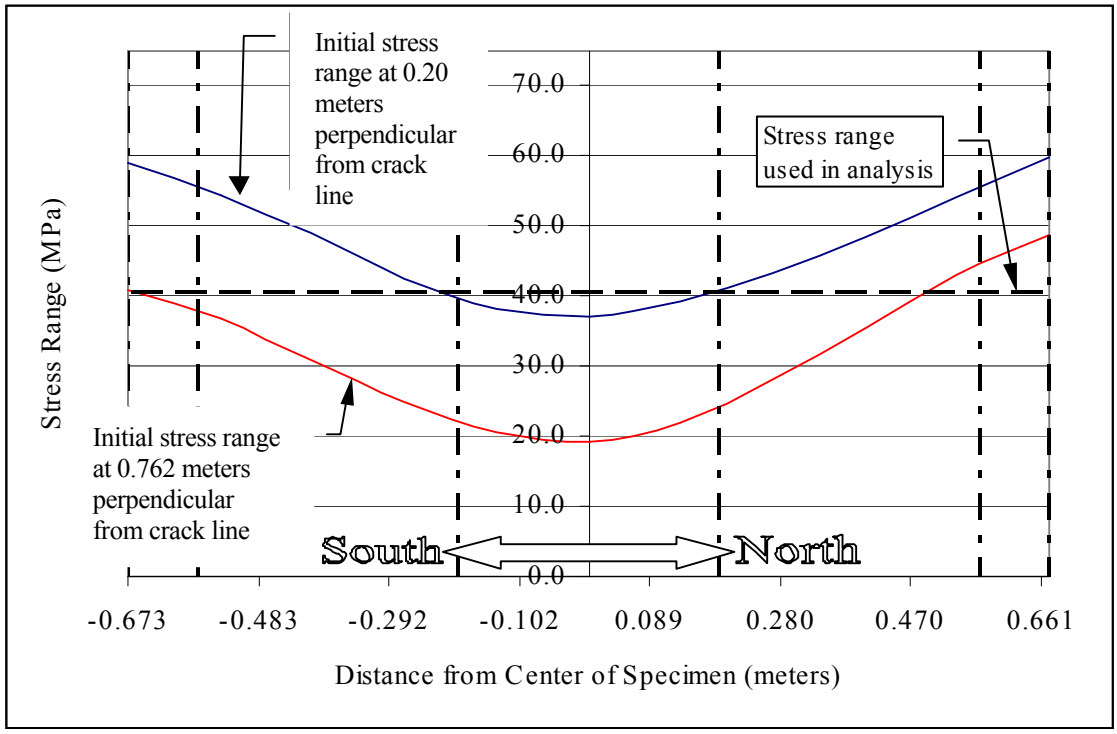

Figure 3-8: Stiffened plate stress gradient experienced in Case 2a (Typical of all cases).

Figure 3-15 illustrates the magnitude of the stress gradient and the gradual increase in stress as one nears the constant moment region. The four vertical centerlines denote the stiffener locations. The stress gradient curves were determined by fitting cubic splines through the strain data points. The instrumentation data and complete record of each experiment can be seen in Appendix C. Individual data sets are not included in this report, however.

The complete test setup allowed easy swapping of specimens, generous access for monitoring crack growth, and full recording of testing stress levels. Figure 3-9 shows a photo of the resulting test setup without a specimen mounted while Figure 3-10 shows a photo with the assembly complete.

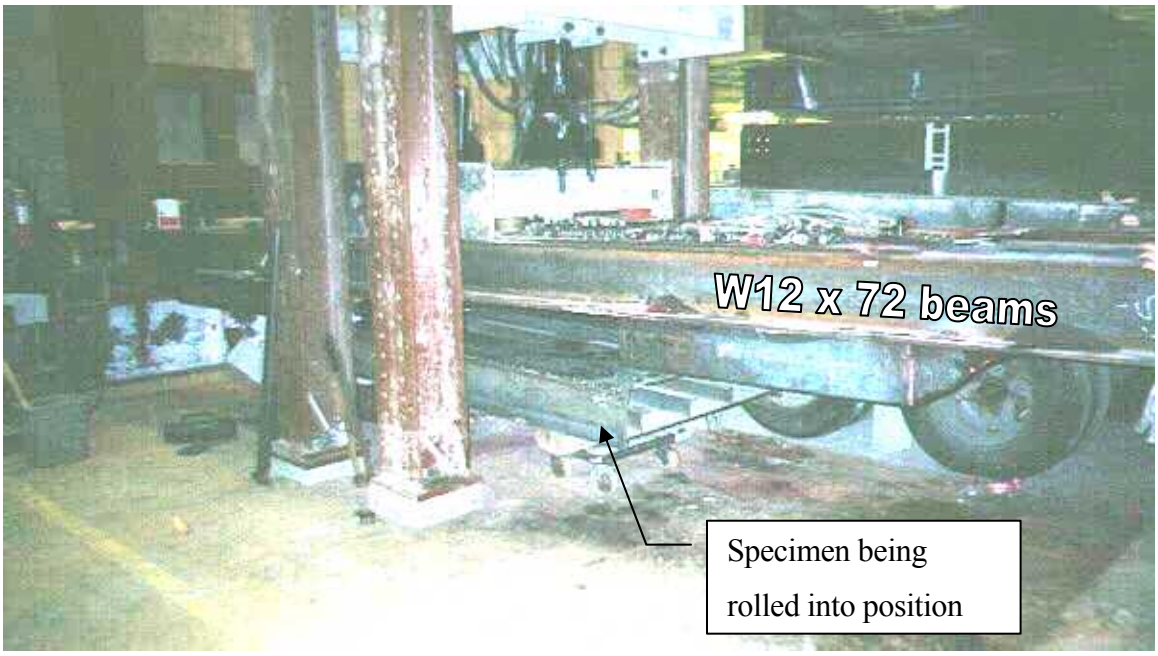

Figure 3-9: Test setup prior to assembly.

Figure 3-10: Test setup with assembly completed.

3.2 FABRICATION

The support structure and the specimens were fabricated at a local AISC certified fabricator, LeJeune Steel Company of Richfield, MN. The support structure material was A36 or better, at the option of the fabricator, while the specimen steel had a minimum yield stress of 345 MPa. Specifically, the 13-mm plate was A572 steel while the angles were A588 steel. Strength tests were performed using full tensile coupons, and results can be found in Table 3-2. The chemical composition of the specimen steel is listed in Table 3-1.

All fillet welds were made using the FCAW process with an 8-mm weld size and 483 MPa wire (E70). Continuous double-sided fillet welds connected the stiffeners to the 12.7-mm thick bottom plate. These overmatched welds were used to maximize any effects of residual stress. A template was used for drilling the 120 holes in the specimen top flange in order to facilitate fit-up problems and minimize mechanical stresses.

Table 3-1: Material composition of steel used in specimens.

Element	Maximum percent by weight	
	A572 12.7 mm plate	A588 101.6mm x 76.2 mm x 8-mm angles (ASTM A709-50W)
Carbon	.05	.13
Manganese	.96	1.04
Phosphorous	.005	.018
Sulfur	.004	.04
Silicon	.03	.26
Copper	.08	.38
Nickel	.05	.17
Chromium	.04	.51
Molybdenum	.01	.048
Vanadium	.059	.044
Aluminum	.032	0
Niobium	.002	0

Table 3-2: Material strength properties.

	Yield Strength, MPa	Tensile Strength, MPa
Plate steel		
Test 1	501.4	628.1
Test 2	500.3	645.3
Angle steel	351.6	524.7

3.3 SPECIMEN DETAILS

Cracking in ship structure often initiates at sources of stress discontinuity and abrupt changes in cross section, such as near hatch openings in the top deck. These discontinuities have been studied for years in order to achieve fatigue improvements and better performance. Nonetheless, fatigue cracks have become a frequent occurrence and the focus is shifted in this report to predicting fatigue crack propagation considering an initially cracked structure.

An existing, identified crack is easier to predict than a nonexistent one. The existing crack occupies a structural setting and has a generally known path--perpendicular to the principle stress path. These facts allow one the benefit of knowing the environment, material, geometry, and loads in advance. The problem remains to simply identify the correct behavioral aspects of the crack under the corresponding conditions. This line of thought led to the development of several details identified as recurring environments for propagating fatigue cracks. The experimental setup does not consider the source of a crack; rather, it provides an ideal environment where specific geometries can be tested for their interaction effects on a running fatigue crack.

With this testing philosophy, six specimens were conceived to characterize common settings in ship structure. The first specimen, the baseline case, contained no stiffeners while five stiffened panels constituted the remainder of the testing schedule. Each of the five stiffened panels focuses on a specific type of detail and cracking scenario. Initially it was idealized to

start all fatigue testing of specimens, except for case 2, with an initial 200-mm notch sawcut in the specimen between the two interior stiffeners. This ideal, however, was soon deemed impractical as it was observed that peak loading conditions failed to propagate the crack with any marked progress. Therefore, initial sawcuts were incrementally lengthened in each specimen until a propagating crack was achieved in less than 300,000 cycles.

Case 1 consists of solid stiffeners with a 40 cm centrally cut notch. This case will attempt to define crack-stiffener interaction in situations where an existing crack intersects a solid stiffener.

Cases 2 and 2a are identically built with 51-mm diameter weld access holes at the centerline of each stiffener. These weld access holes are required at discontinuities in hull plating. Case differences arise in the initially introduced cracks in cases 2 and 2a. The initial notch in case 2a is a 28-cm sawcut centrally located between the interior stiffeners, while case 2 contains short initial notches located at the fillet weld terminations in the weld access holes.

Case 3 incorporates a slotted hole (37-mm x 19-mm) commonly used for drainage at the centerline. The slotted hole was flame cut and the specimen contained a 30-cm initial notch located between the interior stiffeners.

Case 4 contains a transverse butt weld with weld access holes in the stiffeners. This specimen attempts to simulate the master butt weld in ship construction, where two cross sections of ship hull are butted together and welded with a complete penetration butt weld. An initial crack 20-cm in length was saw cut into the specimen 4 between the interior stiffeners.

These different details are shown in Figure 3-11. An illustration of these details in ship structure can be seen in Figure 3-12.

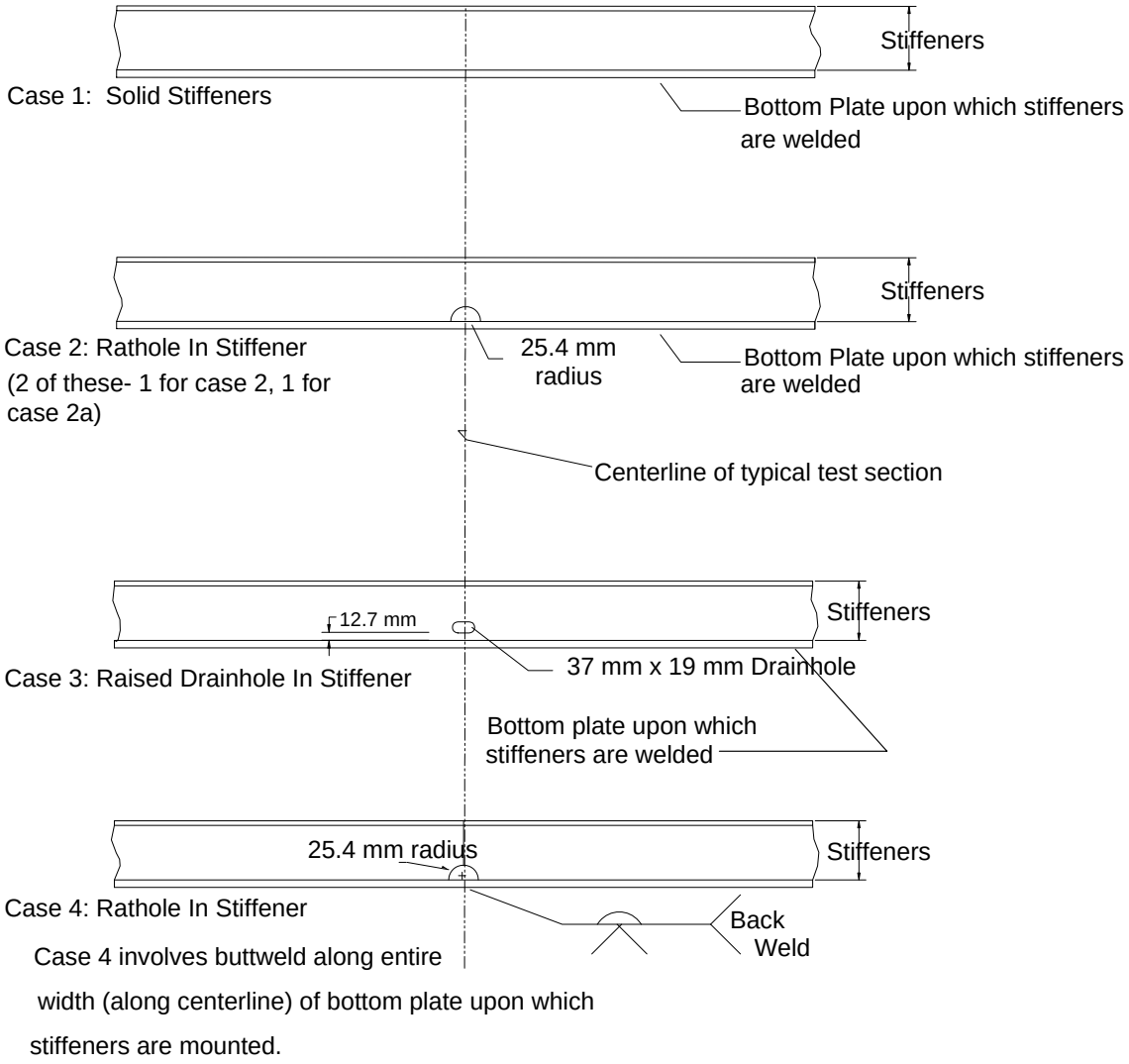

Figure 3-11: Various details tested in experiments.

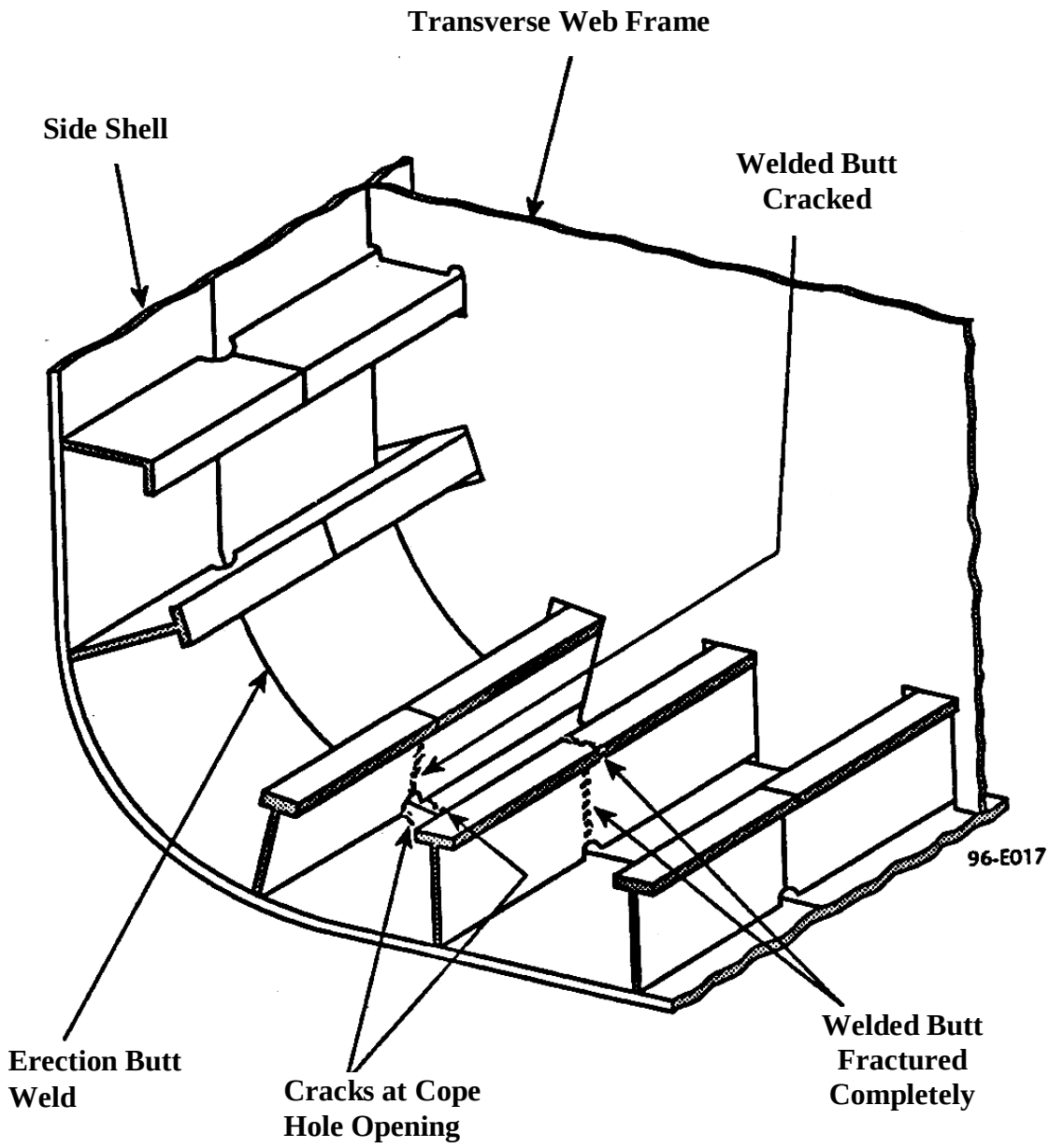

Figure 3-12: Typical fatigue sensitive details in ship structure [35].

Case 4 can be seen in Figure 3-13 prior to installation under the support structure. A large opening was cut into the top flanges of the specimens after testing of the baseline case and case 2a because limited load shedding and negligible displacements were observed with crack growth. The opening also allowed greater access to the interior for crack growth monitoring in the stiffeners.

Figure 3-13: Case 4 with viewport cut into middle flange prior to testing.

Prior to installation under the support structure, the initial crack was cut into the specimens. This initial cut was made by first drilling an access hole for the sawzall blade and then using the sawzall to cut up to the desired length. At the end of the introduced crack, the saw-cut was beveled through the thickness at a 60-degree angle in order to facilitate the formation of a crack. This initial cut can be seen in Figure 3-14.

Figure 3-14: Typical initial crack introduced in specimen with reciprocating saw.

3.4 TESTING PARAMETERS

Ship structure and many other structurally redundant systems exhibit a mixture of load control and displacement control. Load control occurs when the applied loads do not diminish in response to increased compliance in a system. For example, a ship exposed to wave loading has a constant, repeated load applied to it. A reduction in net section will make the structure increase its displacement response, but the applied loading does not diminish. This is the case when a crack forms and releases any forces previously carried by the cracked area, effectively transferring its load to adjacent structural components. This effect is appropriately termed load shedding.

Load shedding contributes to another identifiable structural behavior on a local scale, called displacement control. Displacement control is seen when a crack is limited in the degree it may open by adjacent structural members. The adjacent members simply become more

stressed while restraining the local separation. Structurally redundant ships exhibit a great deal of displacement controlled behavior due to numerous load paths inherent in the cellular structure. These definitions illustrate the complimentary relationship between displacement control and load control that is linked through load shedding. This relationship is very difficult to quantify in a general sense, and thus

Ideally, a variety of testing conditions would be addressed in each specimen configuration. In this testing program, however, the effect of local stiffener geometry was addressed. All of the specimens were tested under the same conditions to single out the effects of the different stiffener details. In fact, many variables were not changed, or altered only slightly, during the experimentation. These include:

- Temperature
- Load ratio
- Material
- Stiffener size
- Weld metal and size
- Weld process
- Testing frequency
- Environmental effects

In the experimental study, the variable of temperature is held constant at the temperature of the laboratory. Temperature may play a significant role in the global stresses that a region in ship structure may experience. Temperature variance between the interior of a ship hull and exterior hull has induced large stresses responsible for crack initiation at susceptible details [6].

Once a crack has developed, temperature effects in ship structure become negligible. This is for several reasons. First of all, the main parameters for fatigue crack propagation are the applied stress range and number of cycles. Since a temperature loading is far less frequent than a wave loading, its contribution to the fatigue crack propagation may be ignored. Secondly, the temperature of the salt water does not drop below its freezing point in a sea environment. The temperature of the steel hull matches that of the water it is in contact with. In other regions of the ship, such as the deck plating, the temperature may be significantly lower in a frigid environment. In these regions the crack propagation rate would increase slightly. Once again, however, the temperature effects are

negligible compared to the effects of applied stress and number of cycles, and can be conservatively accounted for by increasing the coefficient *C* in the Paris Law.

The load ratio has been discussed in the introduction to fracture mechanics, Chapter 2. A load ratio of 0.15 or less is used throughout the experiments. At no point during the testing schedule is a portion of the loading cycle compressive. This has been done to isolate the effects of residual stress on crack growth rate.

All specimens were constructed of the same materials as described earlier in this chapter. Crack propagation rates are virtually identical in most types of steel. This fact is directly seen in the exponent, *m*, of the Paris Law, which has a value of three for steel. Furthermore, the material toughness was not considered or even accounted for in the testing. Toughness was neglected because minimum material toughness levels have existed for several decades in ship construction. These minimum levels assure ductile fracture, and hence stable crack growth, under uniaxial applied stresses. In other words, as long as minimum toughness levels exist in the material the behavior of fatigue crack propagation will not be marked by sudden fracture. As the net section is reduced by fatigue crack propagation, however, a net section fracture based on the ultimate tensile strength of the material can be expected.

Stiffener size was not varied in this project. The stiffeners are approximately ½ scale of full size longitudinals in TAPS trade tankers. Unequal angles having a 101-mm web, a 76-mm flange and a uniform thickness of 9-mm were employed. The stiffener details and their effects on crack propagation were the primary concern in the testing. For this reason, the stiffener size was held constant while the cutouts and local discontinuities were varied. Also, the number of stiffeners in the panel was limited to the physical width of the testing structure and the scaled stiffener spacing. In this regard, four stiffeners were used in each specimen in a symmetric configuration.

Various welding practices and processes are employed in ship construction. To thoroughly test each process in combination with different sequencing methods would be excessive. Instead, the approach taken in this project is to determine worst case crack growth rates and magnify the effects

of residual stress due to welding. With this philosophy, oversized welds were used in assembling the specimens to magnify any residual stress patterns. The welds were all made with E70 wire in a flux-core arc welding (FCAW) process.

Construction sequencing is responsible for mechanical residual stress, or internal stresses that result from improper fit and assembly distortion. There is an intimate relationship between welding-induced residual stress and mechanical residual stress, the latter often being affected by welding distortion. For example, the fabrication of the specimens involved welding the stiffeners to the bottom plate before the top plate and side webs were added. Once the stiffeners were mounted, the side webs were attached. This sequence made the webs "bow out" initially, a reaction to the thermal cooling of the web–bottom plate welds. The web bow was forced into the desired position on the top plate prior to its assembly. This induced mechanical stresses in the specimens.

Special attention was given to specimen four. This specimen incorporated a butt weld typical of the junction of two ship sections, usually termed an erection butt weld. An example of such a joint is shown in Figure 3-5. In order to capture the residual stresses in such a junction, the stiffeners were welded to two separate bottom plates first. Next, the two bottom plates were attached with a full-penetration groove weld, followed by the joining of the side webs and top plate. This sequence attempts to simulate the mechanical and thermal residual stresses resulting from the connection of two ship sections or, alternatively, a weld repair made in a previously cracked section. Constraint from attached stiffeners to the two bottom plates creates large tensile residual stresses in the butt weld region, which can magnify the fatigue crack propagation rate.

Another variable involved in fatigue crack propagation is the cycling frequency. The experiments were conducted with a frequency of 1.2 Hertz. Usually a higher cycling frequency translates to an increased fatigue crack growth rate because the strain rate is increased. An increased strain rate affects crack growth only marginally unless the increase is of several magnitudes. Wave loading in ship structures is stochastic in nature and may be assessed with frequencies less than 2 Hz. However, slamming loading, i.e. the effect of waves impacting a portion of the hull from the side,

can dramatically increase fatigue crack propagation. This type of loading was not investigated in this report.

The frequency effects in ship structure may be tied to environmental effects. A salt-water environment induces corrosion in exposed metal, which is often a source of fatigue loading in itself. When combined with frequency, however, the effects of corrosion may be beneficial. This is because corrosion has the effect of blunting the crack tip, especially at stress ranges near the material threshold. A crack tip must be present for the crack to advance; hence, corrosion-induced blunting forces a new crack tip to be formed on a regular basis and lowers the fatigue crack propagation rate. It is important to note that this behavior occurs when the crack tip is opened only slightly with each cycle, as occurs when the loading is near the material threshold. Larger crack tip opening displacements, associated with high load ratios, advance the crack tip steadily and overcome the blunting benefits provided by corrosion.

High frequency loading in a salt-water environment has the effect of washing the corrosion out and removing any corrosion-induced blunting. Experiments are often made with compact specimens performed at high frequencies, resulting in observations that fail to capture the blunting effect. The observations from these experiments have led many researchers to believe fatigue cracks grow more rapidly in a salt-water environment. For the stochastic loading seen by naval vessels, neglecting the corrosive environment may be more appropriate. For this reason and because of the testing complexities, the environmental effects were ignored in the experiments.

Testing of the specimens was originally designed to be in load control. This type of testing incorporates the net section reduction and the associated increase in the applied stresses caused by cracking. The bolt-up design of the experiment, however, was found to have inadequate connection rigidity to exhibit continuous section behavior. In other words, the stress at a point in the composite cross section could not be predicted using simple flexure theory. To determine the stress distribution through the cross section a number of strain gages were placed along the depth of the section. The results, shown in Figure 3-15, illustrate the lack of bond between the specimen and the support structure.

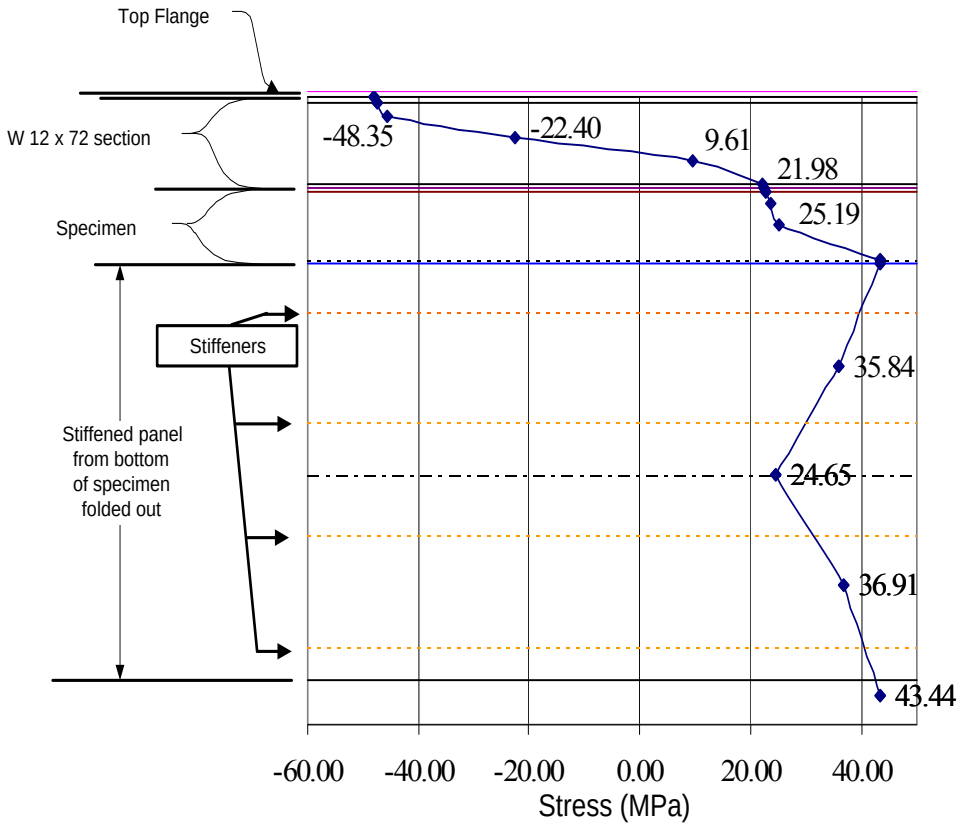

Figure 3-15: Stress gradient experienced in Case 2a (Typical of all cases).

From this investigation it was apparent that the experimentation would be performed at a compromise between displacement-controlled testing and load-controlled testing. The drawback of this situation is that most prediction methods are based on either an applied load analysis or an applied displacement analysis. Since the testing could be classified as neither loading condition completely, it was decided that intermittent stress readings be taken throughout the testing. Such data would assure accurate information would be available for developing prediction models. These stress readings were taken at the points shown in Figure 3-7.

3.5 EXPERIMENTAL PROCEDURE

Six specimens were tested in this investigation. In each case, the preparation required the following steps:

1. Cutting the initial notch in the bottom plate.
2. Bolting the specimen to the support structure.
3. Installing the splice plates to provide for a more continuous structure.
4. Mounting strain gages in the bottom plate of the specimen.

The testing of each specimen ranged from 3-6 weeks at a cycling frequency of 1.2 Hz. Each specimen endured between 1.5 million and 3.5 million cycles before failure was concluded. At no point was unstable crack propagation observed. Rather, incremental crack growth was similar in many of the cases.

To record the crack growth during testing, a red penetrating dye was used. The dye is sprayed around the region of the crack tip and allowed to permeate any imperfections in the material. After several minutes, the dye is removed from the surface with a degreasing agent and a dry cloth. Soon after the surface is cleaned, the dye may re-emerge from the cracked areas either through dispersion or with the aid of a developer. The developer is an agent that is sprayed on the cleaned surface that turns white when dried. It is stained by any red dye that emerges from the crack. Figure 3-16 shows the use of the procedure to identify the crack tip in the baseline specimen.

The use of the red dye to locate the crack tips is particularly effective during testing. Once the surface has been wiped clean, the permeated dye is forced out during cycling. This phenomenon, commonly referred to as pumping, provides an easy means for finding the crack tip.

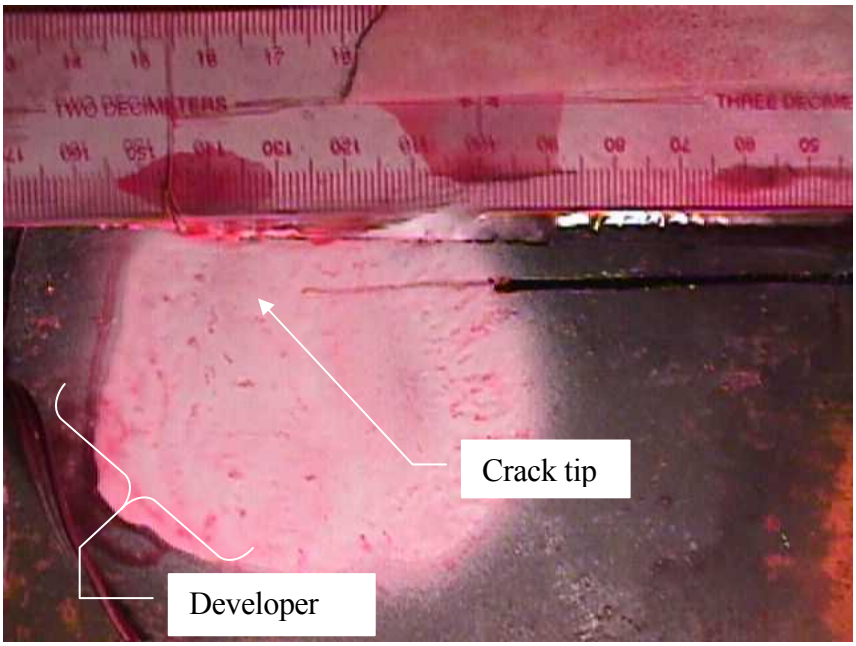

Figure 3-16: Use of red dye penetrant and developer to locate crack tip.

In the stiffened panel cases, excluding case2a, an oval viewport was flame cut in the top flange of the specimens (See Figure 3-13). This viewport increased the applied stresses in the specimen slightly while allowing one to record the crack growth in the stiffeners from the interior of the box section. The crack growth in the stiffeners was mapped to an equivalent distance in the plate. In every case, the growth in the stiffeners virtually matched that of the plate until the stiffener cracks reached approximately ¾ of the height of the stiffener webs.

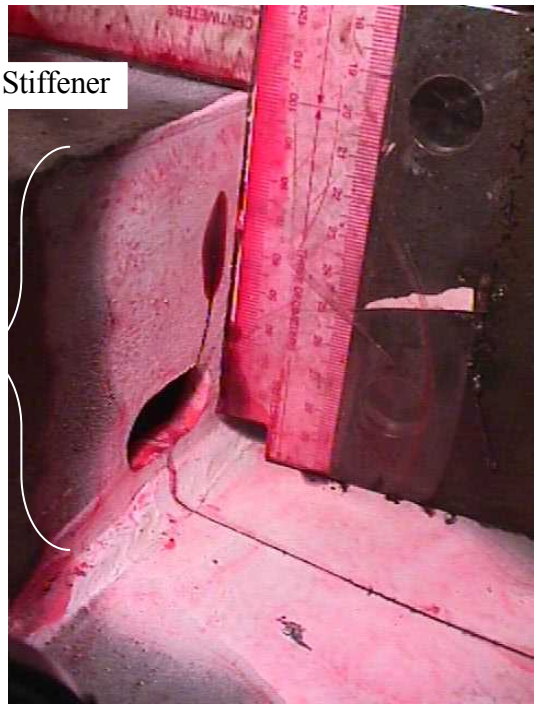

Figure 3-17: Crack growing in stiffener of case 3.

The stiffeners were never completely severed in the test cases. This shortcoming was due to both shear lag effects across the bottom plate and the restraint of the edge webs. To quantify the magnitude of the shear lag effect, stress readings were taken at the top of the stiffener webs before significant cracking occurred. These initial stress readings indicated that the interior stiffeners experienced stress ranges significantly lower than that of the plate. In fact, while the plate was cycled at a stress range of 45 MPa the interior stiffeners only experienced 4 MPa. The exterior stiffeners exhibited greater uniformity with the plate with initial stress ranges of 35 MPa.

The restraint of the edge webs also contributed largely to the lack of stiffener separation. The crack could not be opened wide enough for crack growth to continue in the stiffeners because the edge webs limited the crack opening displacements. This drawback could have been avoided only with a wider and deeper specimen. The loading limitations of the equipment, however, would make such a configuration impossible without scaling down the relative thickness of the shapes used in both the support structure and the specimens.

The lack of stiffener separation does not constitute a failure of the experiments. Actually, the behavior allowed the prediction of a realistic case in which shear lag effects in a structurally redundant system are to be considered. The portion of the stiffener that was severed contributed to crack propagation. The uncracked portion of the flanges, on the other hand, provided little restraint and the cyclic opening of the crack merely pivoted about the horizontal flange like a hinge. An end result to the lower stresses in the stiffeners was to lower the effective stiffener area as it affects crack growth. This point will be discussed in Section 8.3 (Page 146).

Throughout the testing the effects of load shedding were studied by monitoring local stress levels and overall deflection. The prominence of load shedding is characteristic of a structurally redundant system. Load shedding was observed to a great extent in the experiments as the crack progressed through the bottom plate. Normally one would observe increased deflections proportional to the reduction in the net section as the crack propagates. The multiple load paths present in the composite section limited the displacements observed. A maximum mid-span deflection prior to bottom plate cracking was approximately 20-mm. Only a 6-mm. increase in deflection was noted after the crack had propagated into a through-thickness crack in the edge web. This small increase could be attributed to the bolt up design of the experiments; however, no slip was detected between the specimen/support beam interface.

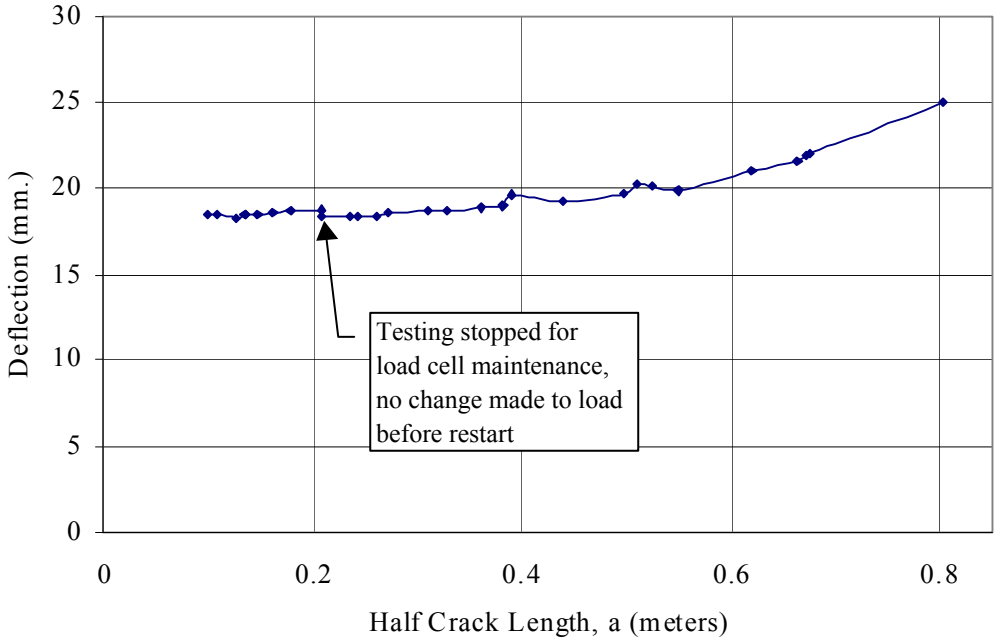

Figure 3-18: Maximum deflections incurred during testing.

3.6 RESIDUAL STRESS MEASUREMENTS

Residual stresses were theorized to affect fatigue crack propagation rates significantly. To quantify the residual stress present in the experiments, residual stress measurements were made on two of the specimens using the sectioning method. Each specimen was sectioned using 41 coupons with a nominal gage length of 254-mm. Four coupons from either side of each stiffener were taken with a width of 12-mm. In addition, three coupons with a width of 37-mm. were taken from the region between stiffeners. The residual stress measurements were made using previously tested panels two and three.

The well-established procedure of sectioning was chosen to be the most economical and convenient method for measuring residual stress. Prior to extraction, gage points were marked at mid-distance between a free edge of the stiffened panel and the crack line. The gage points were then drilled approximately 7-mm.deep with a #2 center drill bit (~3-mm. diameter). Using a digital Whitmore

gage with accuracy to 0.1-mm., the distance between the gage points was obtained and an average of three readings was used. After the initial readings were taken, the full section containing the gage points was removed from the specimen. Each coupon was extracted from the larger section with a bandsaw that was cooled with a steady flow of cutting fluid. After the coupons were removed, final readings were obtained by once again averaging three readings. Figure 3-19 shows the extracted coupons taken from one of the specimens.

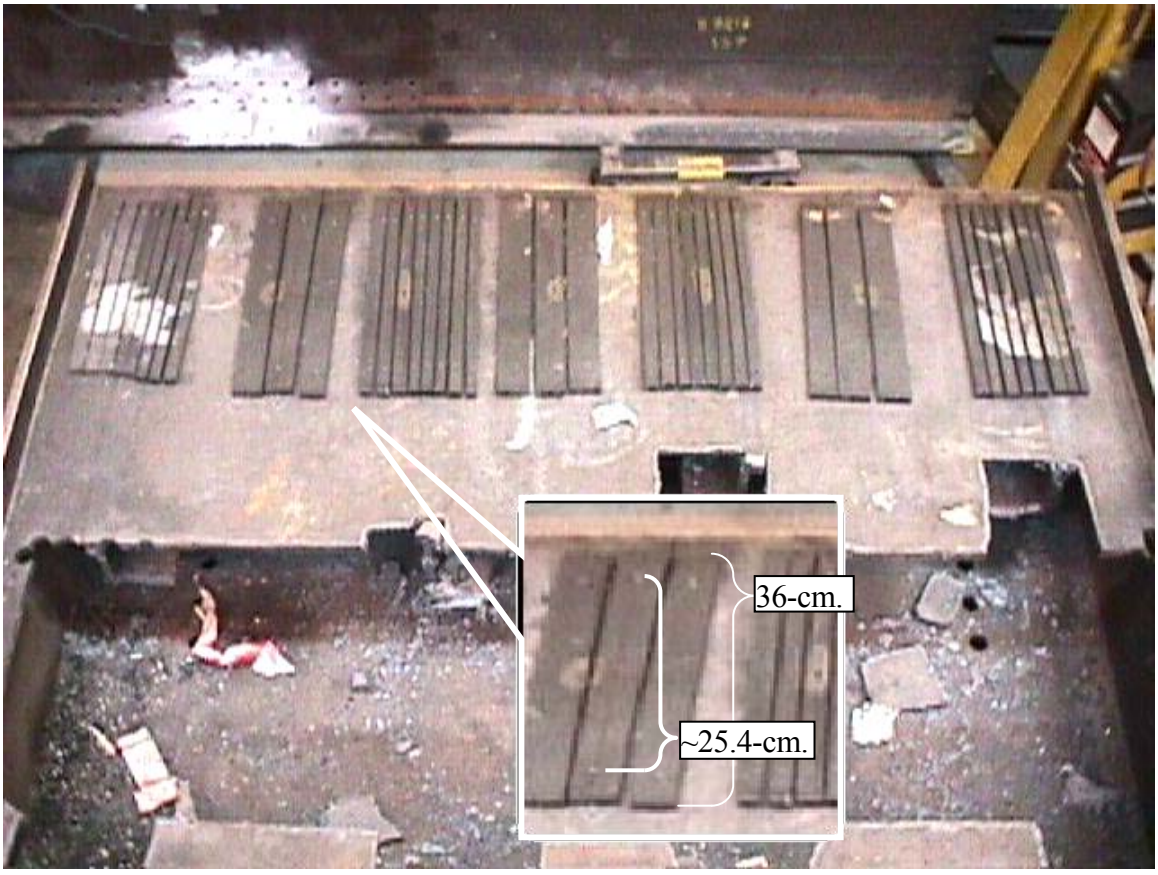

Figure 3-19: Sectioning coupons used for measuring residual stress distributions.

The measured residual stress fields are shown in Figure 3-20. Equilibrium requires offsetting areas of tensile and compressive stress to balance in the specimen. As one may notice, the measured residual stress distribution does not satisfy equilibrium. This discrepancy is likely due to the accuracy of the measurements as well as a minute amount of residual stress-induced curvature in the coupons. A more probable plot of residual stress could be obtained by lowering the x-axis by 60 MPa.

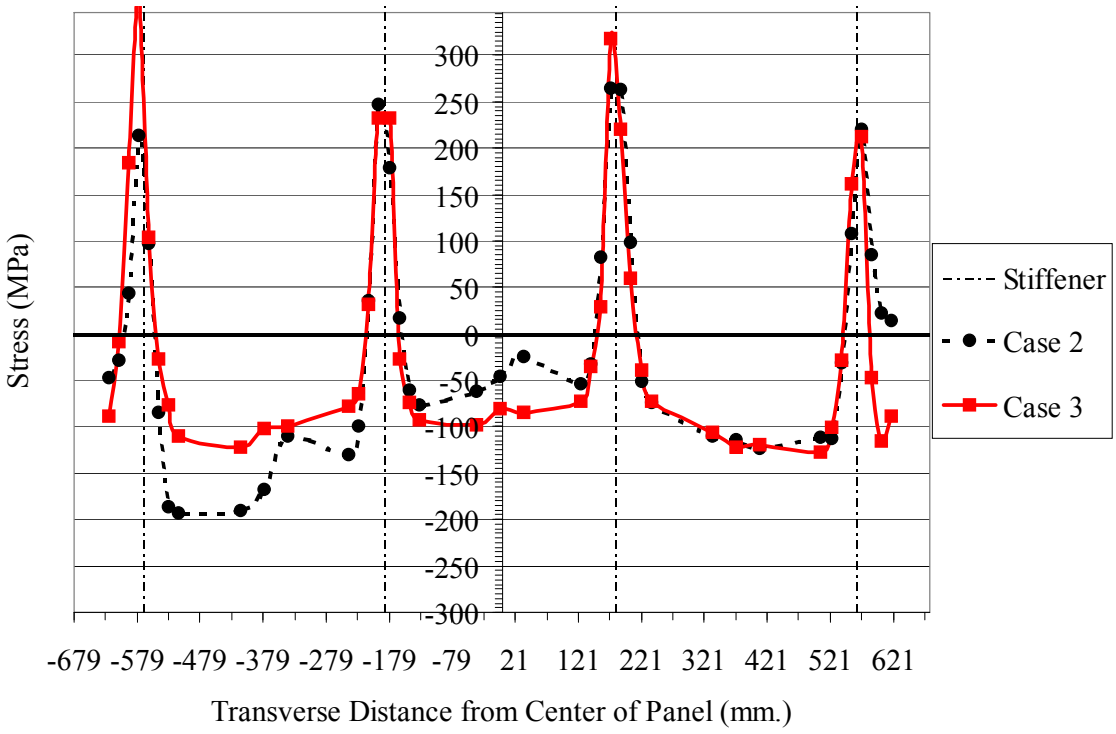

Figure 3-20: Residual stress distributions measured in two specimens.

Faulkner's model for residual stress distribution will be utilized as a simple representation of the actual residual stress in the specimens. This model, as discussed in chapter 3, models the tensile regions around the stiffeners as triangular shapes with a base width proportional to the plate thickness (η). The triangular width typical of as-built ship structures ranges from 3.5 to 4 times the plate width, while values between 3 and 3.5 are more typical of ships after shakedown. The analytical program developed includes a routine for developing the Faulkner representation based on the yield strength of the material, the plate thickness and η.

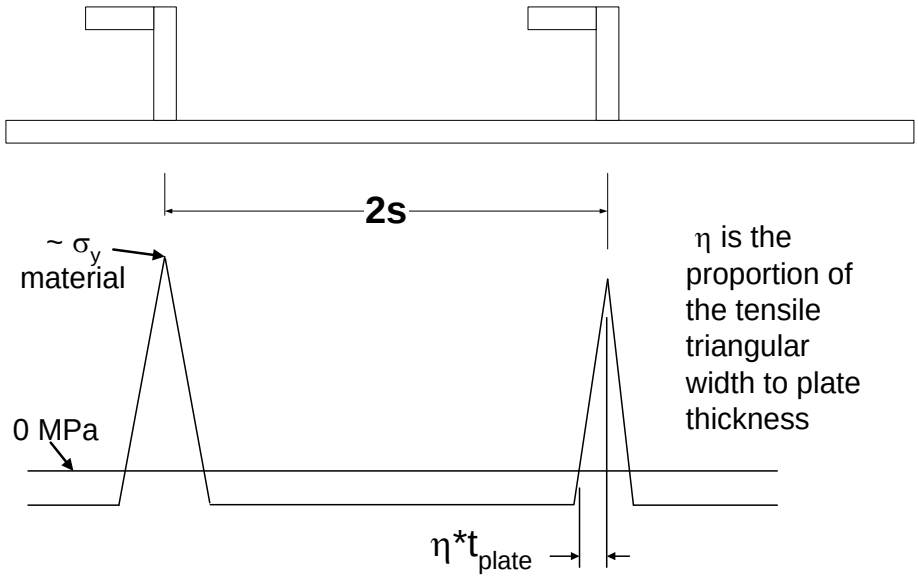

Figure 3-21: Faulkner model for residual stresses.

4 Experimental Results

4.1 Baseline Case

The first specimen tested was the baseline specimen, which consisted of a hollow specimen without stiffeners on the bottom plate. Initially a 204-mm notch was cut in the center of the specimen. After 300,000 cycles measurable crack growth could not be detected. In order to facilitate a crack formation the notch was beveled through the thickness at a thirty-degree angle. The beveling technique successfully initiated crack tips at the notch ends and the crack then grew 2-mm. in 20,000 cycles.

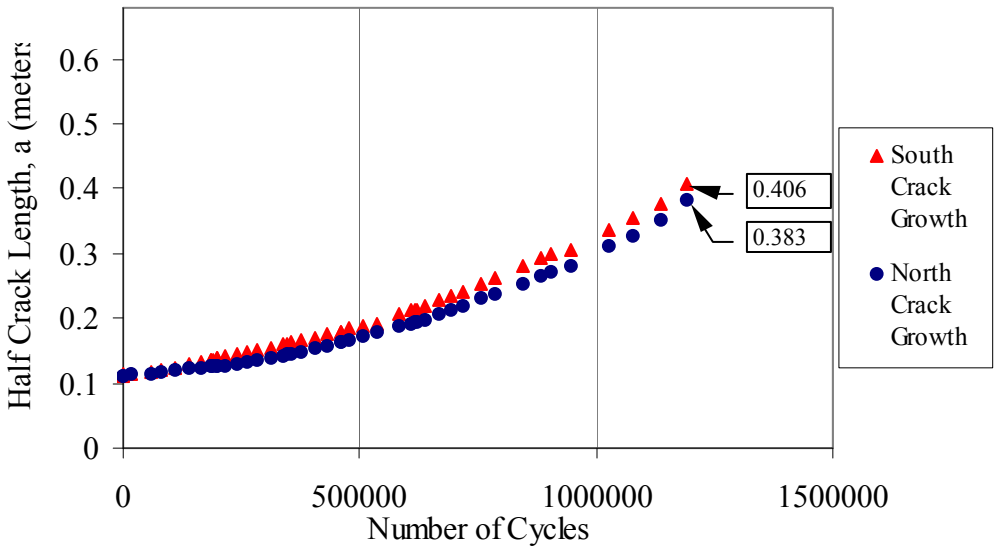

Figure 4-1: Baseline test case data.

The strain gage readings indicated an average applied stress range of 29 MPa. Slow crack growth was noted at this applied stress range and crack size, and at 540,000 cycles the loading range was increased to achieve an average applied stress range of 33 MPa. These stress range values were obtained by taking the average of the center and outer strain gage measurements, whose location was 76-cm from the crack line (See Figure 3-7).

The baseline test was stopped short of the full panel width in order to adhere to a rigorous testing schedule. Its termination was tolerated because the behavior observed was close to what was expected for a CCT specimen.

4.2 OVERVIEW OF STIFFENED PANELS TEST RESULTS

Each stiffened panel was tested under the same loading conditions and frequency. The starting crack length for each specimen was varied because of difficulties initiating a crack within a reasonable number of cycles (≤ ~500,000 cycles). The performance of all the cases, except case2a, can be seen in Figure 4-2. The plot has been constructed to align the crack growth stages, and thus the number of cycles for each test case is shifted horizontally to align its initial crack length with that of case four.

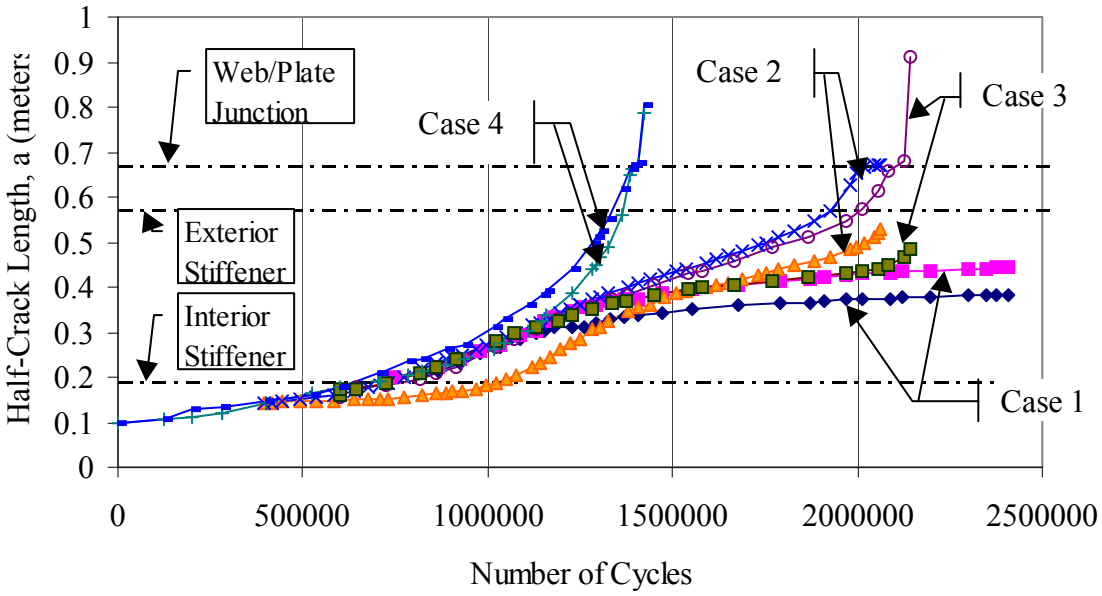

Figure 4-2: Stiffened panel test data (Excluding case 2a).

One will notice a distinct similarity between cases two and three. These tests involved stiffeners with weld access holes (Case 2) and drainholes (Case 3) along the crack path. Case four exhibited

no retardation effects due to the stiffeners or internal residual stress. Case one (Solid stiffeners) did show significant retardation effects, although the last five data points represent a gradual loss in applied stress due to cracking elsewhere in the specimen. The details of each test will be further discussed in the following sections.

4.3 CASE 1: SOLID STIFFENERS

A stiffened panel with solid stiffeners was investigated in test case one. This case represents a situation where an existing crack propagates into a solid stiffener. An initial notch of 28-cm, with a through-thickness bevel, was cut into the specimen and 418,000 cycles accrued with no noticeable crack initiation. At this point, the initial notch was lengthened to 30-cm and testing resumed. Cracking had still not initiated at 1,032,500 cycles. Once again the beveled notch ends were manually advanced, this time to a total notch length of 33-cm, but no crack tip formations were noticed even after an additional 400,000 cycles. Finally, the crack was manually extending to a total sawcut length of 40-cm, a distance which took the initial notch partially into the solid stiffener. With this crack length, crack tips readily formed within 100,000 cycles and the testing was considered officially under way.

The difficulty initiating the crack in this case is a testament to high compressive residual stress and the beneficial restraint of the stiffeners. Modeling observations indicate it is likely that the compressive residual stress played a larger role in crack retardation than the restraint of the stiffener. These observations will be discussed in Section 5.2 (Page 145).

The testing results can be seen in Figure 4-3. Initial crack lengths were identical in both the north and south directions, and variations in growth are the result of variations in residual stress and minute unsymmetric loading.

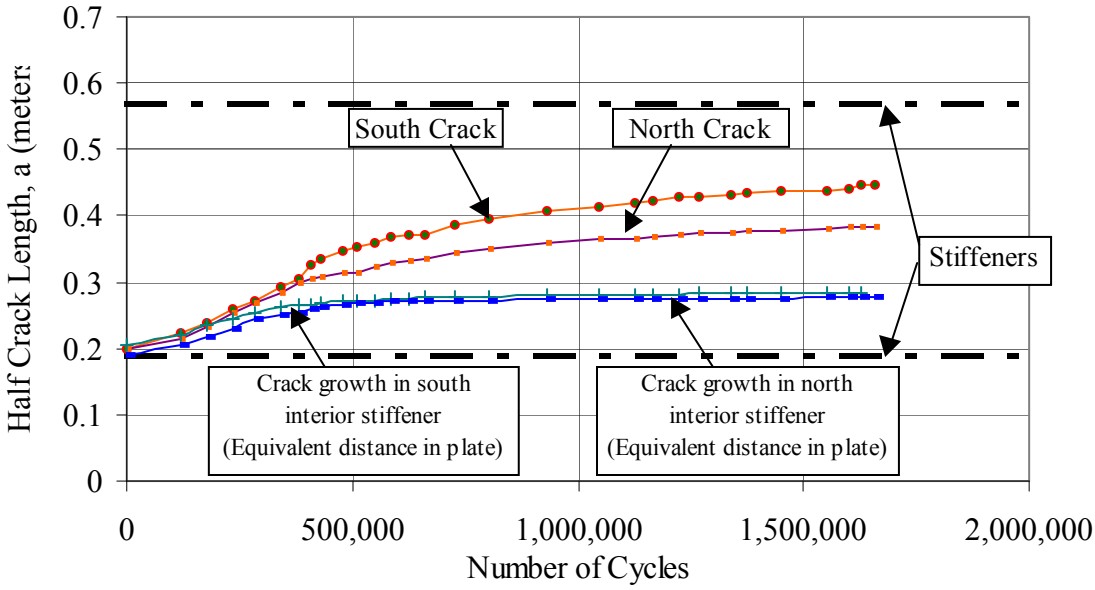

Figure 4-3: Case 1 experiment data.

During the latter part of the test, rubbing along the west end splice plates caused cracking in the edge webs away from the centerline of the specimen (See Figures 4-4,5). The cause of the rubbing was the use of 6-mm thick spacer plates used between the specimen and the splice plates at these locations. The spacer plates became necessary because of small variances in the alignment of the specimen webs. Cracking at these locations reduced the effectiveness of the force transfer into the specimen, and the last four data points reflect diminished stress levels as the remote cracking ensued.

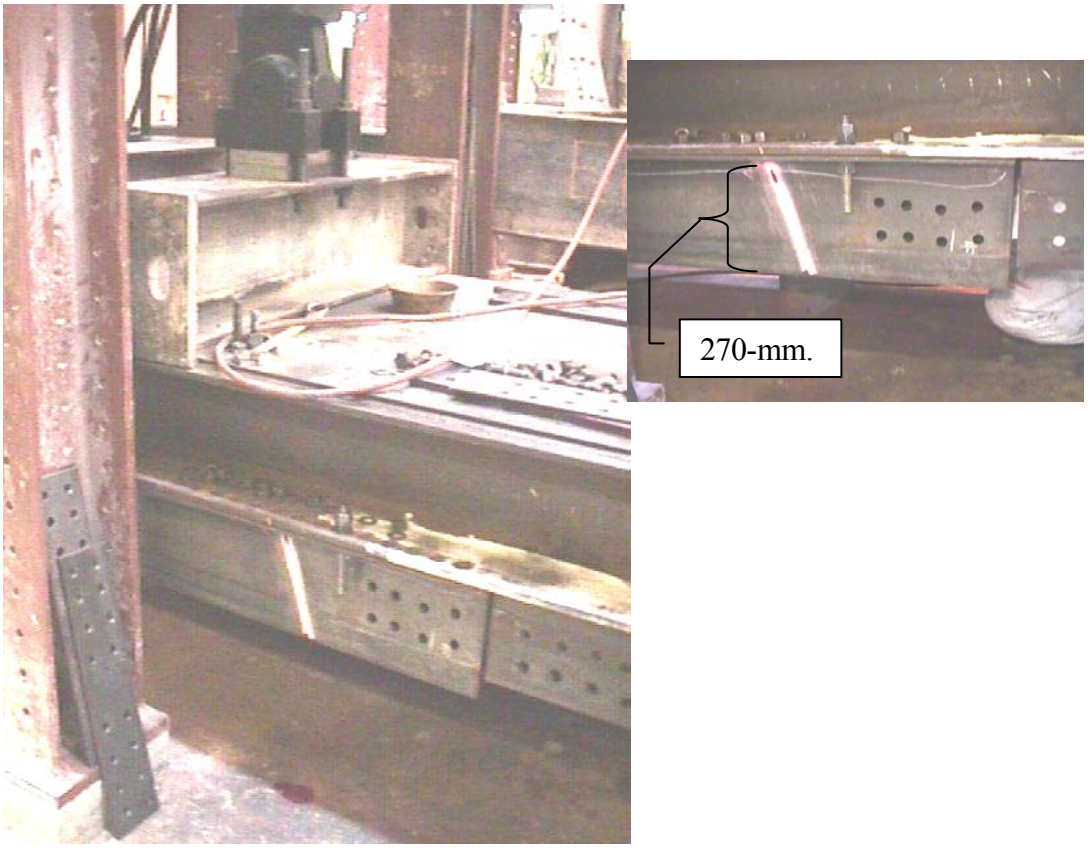

Figures 4-4, 5: Edge web cracking due to rubbing in case one.

As reported earlier, the crack growth in the stiffeners matched that of the plate up to approximately three-fourths of the stiffener height. Cracking in the plate stalled prior to reaching the exterior stiffeners. Stress levels in the plate were monitored and found to be constant up until the last four data points. For this reason, the decrease in growth rate is attributed to the effects of high compressive residual stress; similar to the initial difficulties encountered trying to initiate a crack. Regrettably, no residual stress measurements were obtained from this specimen to quantify the internal compressive stress.

4.4 CASE 2 AND CASE 3: STIFFENERS WITH CUTOUTS AND CENTRAL NOTCHES

Cases two and three represent a variety of cutouts found commonly in ship structure. Case 2 emulates regions where drainholes or miscellaneous cutouts are incorporated. Case 3 contains slotted hole cutouts used for drainage paths. These two tests performed very similarly, with mild crack retardation effects from the stiffeners.

Case two test results may be seen in Figure 4-6. This test started with a manually cut crack length of 20 cm. Only eight millimeters of growth was observed in 980,000 cycles. The rate of growth was documented and then the crack was manually advanced to 28-cm. total length to promote a tolerable test duration. Figure 4-6 shows the crack behavior from this point forward. Crack growth sped up considerably with this new notch length.

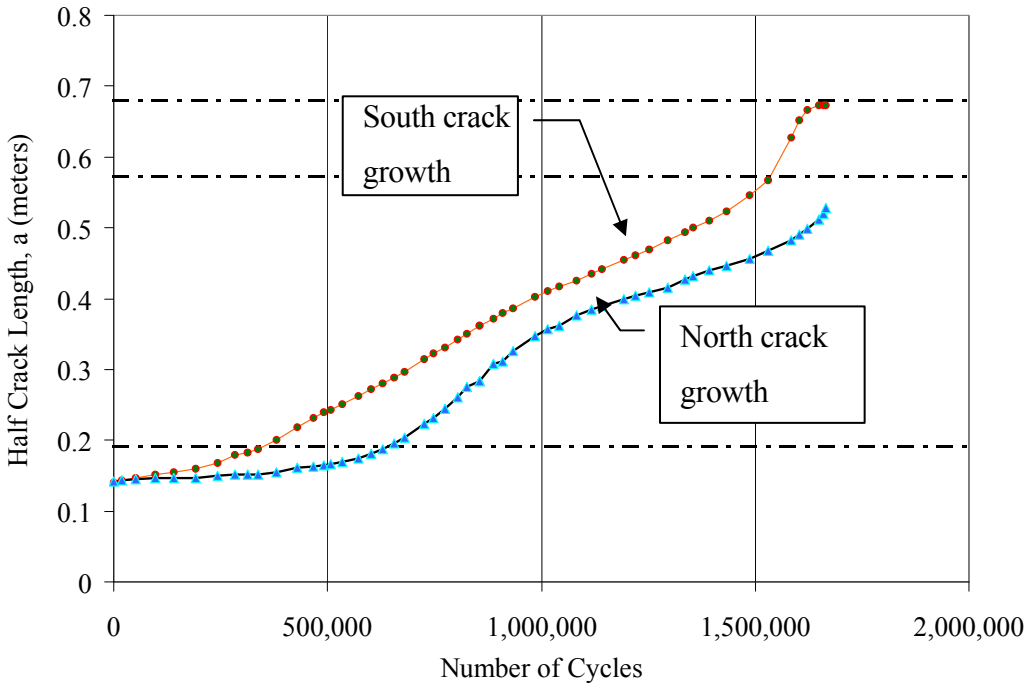

Figure 4-6: Case 2 experiment data.

No measurements were taken of the crack growth in the stiffeners for this test case. The test was completed when the crack had propagated to within 50-mm of the specimen's top plate. Final crack lengths may be seen in Figure 4-7.

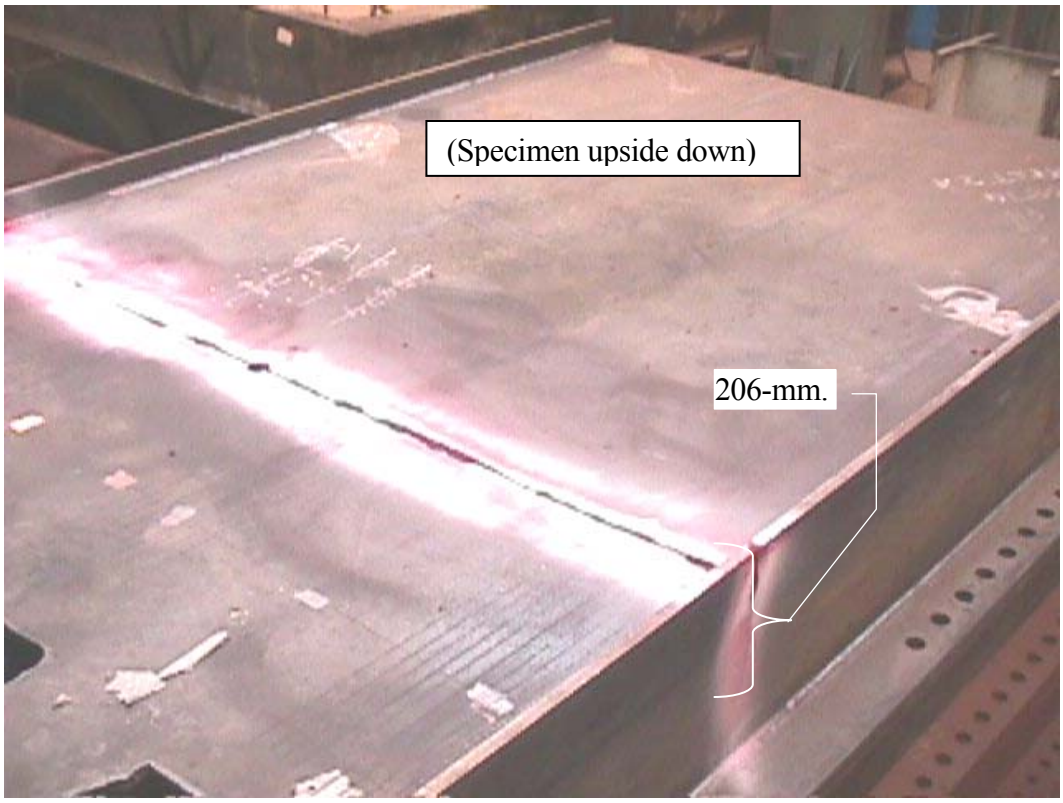

Figure 4-7: Case 2 at failure.

Case 3 exhibited remarkably similar test results. The initial notch length was 155-mm in either direction of the centerline. Once again, this initial crack length proved insufficient to propagate a solidly propagating crack. At 100,000 cycles, the crack was lengthened with a reciprocating saw to a total length of 35-cm. This notch length facilitated more rapid growth and 8-mm of growth was seen in either direction within 100,000 cycles. A full profile of the test results may be seen in Figure 4-8.

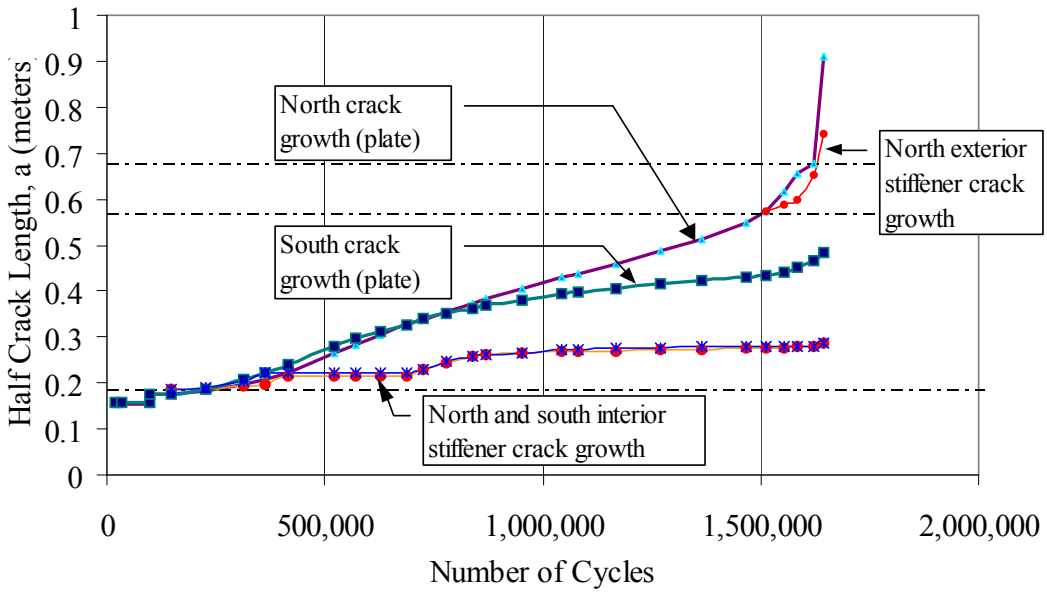

Figure 4-8: Case 3 experiment data.

One may notice the south crack data decreases its growth rate around 750,000 cycles. This deviation from the northern crack growth is a direct result of splice plate cracking in the southeast corner of the experimental setup. The interior splice plate at this location suffered a fatigue crack of its own and led to slightly decreased stress values on the south side of the specimen. The change in stress due the splice plate cracking averaged 6 MPa lower than that of the intact splice plate. For this reason, the south crack growth was significantly retarded compared to that of the north crack.

Earlier the similarities between case 2 and case 3 were noted. Figure 4-9 shows both tests on the same plot.

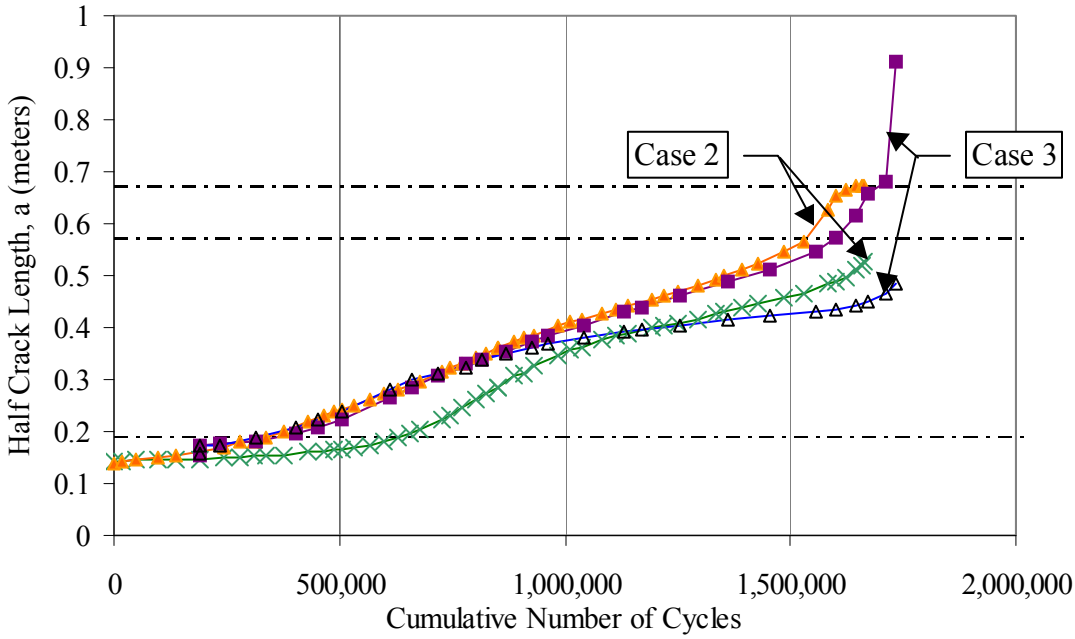

Figure 4-9: Performance similarities of cases two and three.

Only small differences exist between the cases. Previously it was observed that the crack propagation rate for the south tip in case three diminished due to remote cracking in the splice plates and a corresponding stress drop. In case two, however, the opposite behavior is noted with the southern crack tip outpacing the northern tip with no stress fluctuations observed. This behavior signifies that an appropriate growth scenario may be extrapolated from the worst case scenarios.

4.5 CASE 4: PLATE WITH BUTTWELD AND STIFFENERS WITH CUTOUTS

Case four represents a master butt joint in ship structure where two sections of prefabricated hull are joined. It was originally anticipated that the difficulty starting a crack would again be repeated with this specimen. Surprisingly, the 20-cm initial notch was immediately successful in starting crack growth. Within 100,000 cycles an 8-mm. crack had formed and was propagating well.

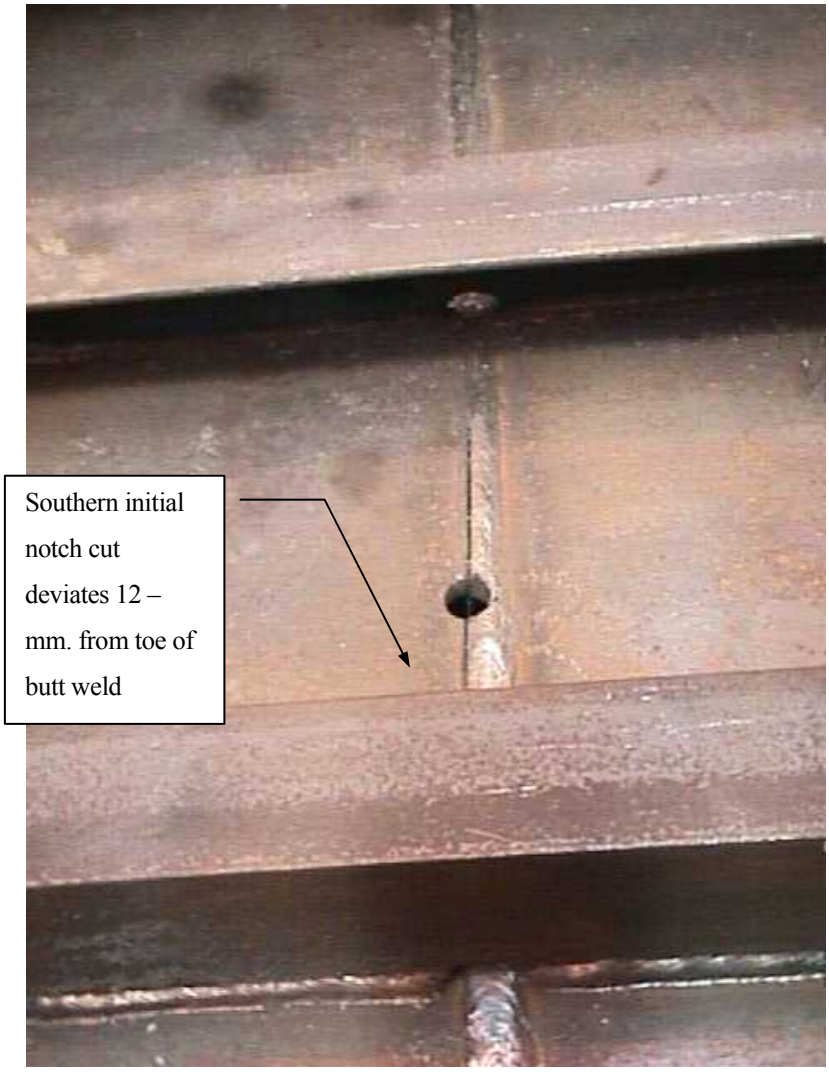

Figure 4-10: South notch end deviates from butt weld.

Rapid initiation was observed even on the southern side of the specimen where the saw-cut notch had inadvertently deviated from the butt weld by almost 12-mm. The crack that initiated away from the toe of the butt weld continued to run parallel to the butt weld for the majority of the experiment.

Crack growth was significantly higher than that of the other specimens including the baseline case. Such ease of crack initiation demonstrates the fatigue sensitivity of this type of detail in ship structure. While unstable crack growth was never observed, the beneficial effects of any internal compressive stress due to the stiffener fillet welds were negated by the butt weld. Furthermore, the stiffeners themselves provided no retardation effects on the crack growth. In this test, the internal

stiffeners still exhibited lower stresses from shear lag in the specimen, as previously discussed in Section 3.5. If the stiffeners had experienced stress levels similar to that of the plate, crack growth would be amplified by the gradual loss of stiffener load-carrying capacity. The complete test results may be seen in Figure 4-11.

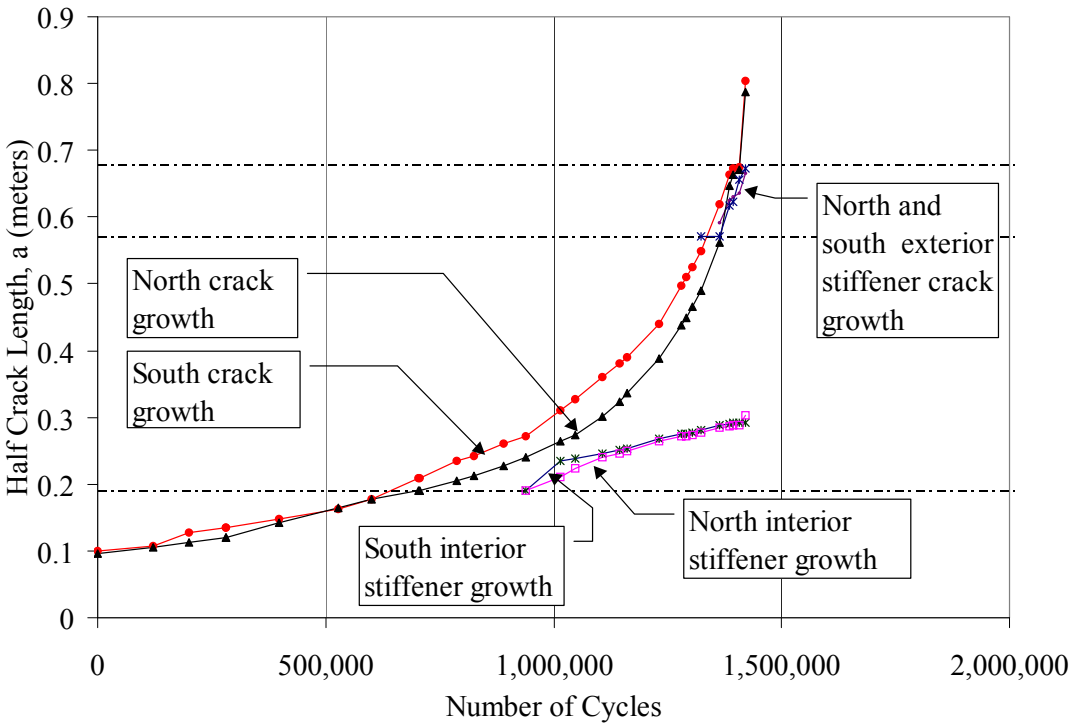

Figure 4-11: Experimental results for case four.

4.6 CASE 2A: MULTIPLE SITE DAMAGE IN STIFFENED PANELS WITH CUTOUTS

In many instances in ship structure, cracks initiate at fillet weld terminations near weld access holes. Furthermore, cracks at these locations are often prevalent in adjacent stiffeners experiencing the same loading conditions. Case 2a attempts to duplicate the propagation behavior that might occur in this situation. This initial cracking scenario is the most realistic among the specimen configurations.

There were many concerns about the proper treatment of this situation given the experimentation setup. First of all, the stress gradient across the bottom of the panel required unequal crack lengths

in order to duplicate four simultaneous running cracks. Because the stress levels near the edges of the panel were 50 percent higher than those in the middle of the panel, it was decided to make the initial interior crack lengths significantly longer than those under the exterior stiffeners. The reasoning for this was the concern that the exterior cracks would propagate through the edge web before the interior cracks showed any significant growth. Another concern was the feasibility of all four cracks behaving realistically in an environment where unequal notches were artificially introduced. The testing configuration could not reasonably be changed, and thus the test was carried out with unequal notches whose lengths were set to minimize the effects of shear lag. The initial notch lengths can be seen in Figure 4-12.

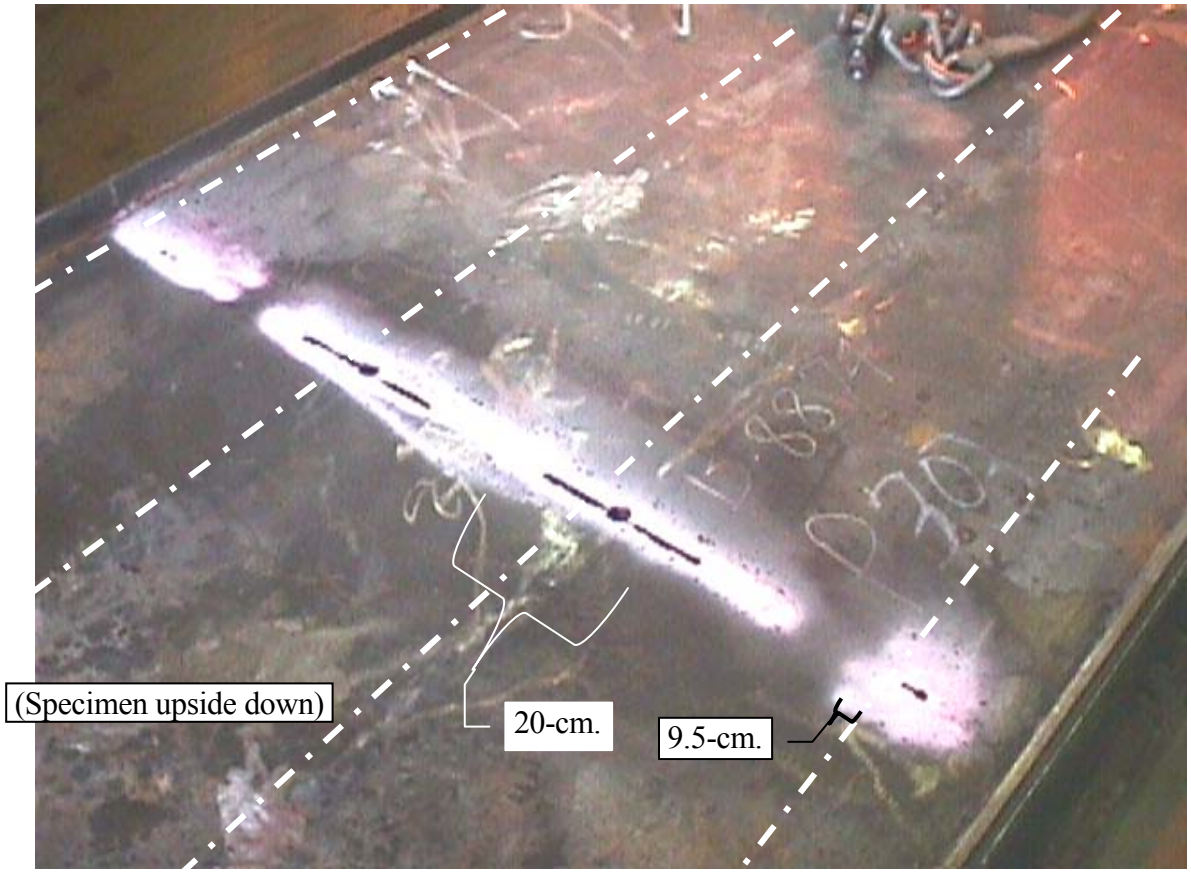

Figure 4-12: Initial crack lengths used in specimen 2a.

The test data for the plate crack growth may be seen in Figure 4-13. The figure displays the whole panel width and the crack length progression. As one can see, the exterior crack lengths proved to

be too small to grow a crack with ease, while the interior crack tips grew at a relatively slow rate. In fact, the interior cracks grew consistently while the exterior cracks had to be manually extended in increments before self-propagation occurred. The length at which the exterior cracks became self-propagating was 10-cm. At this point, the interior cracks had grown to a total length of 27.4-cm. The remainder of the test displayed very symmetric results that yielded identical growth rates in the exterior and interior cracks.

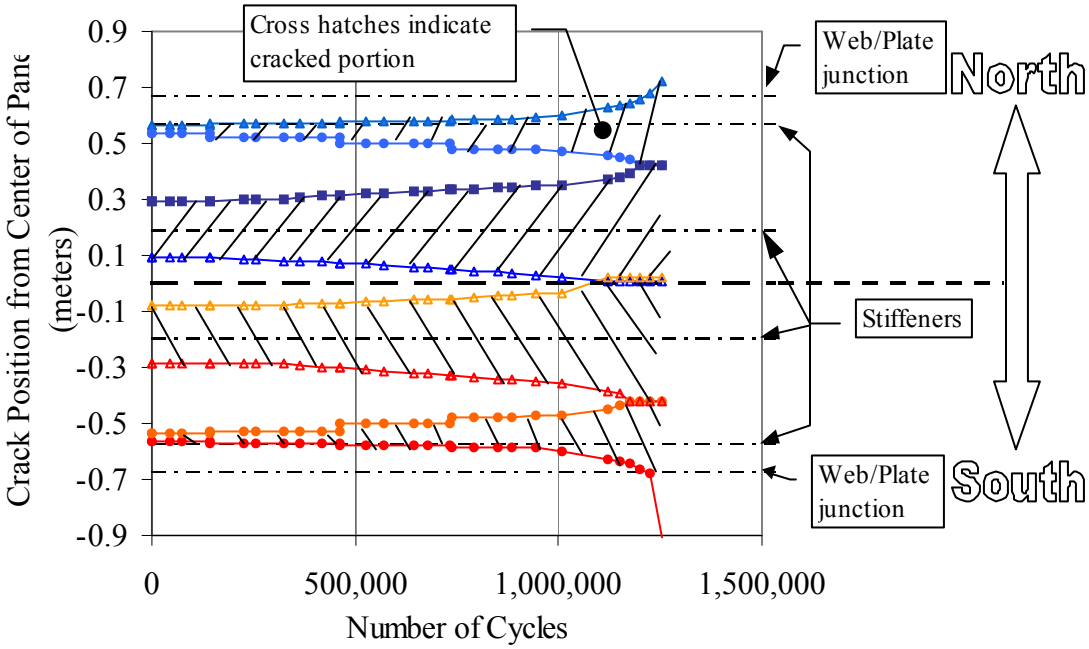

Figure 4-13: Initial crack lengths used in specimen 2a.

The exterior crack growth rates remained fairly slow until all the interior crack tips joined. This behavior could be expected as the intact plate sections minimize crack opening displacements until the cracks merge.

5 Analytical Model

5.1 OVERVIEW

The field of fracture mechanics originated in the early 1950's in the form of analytical solutions. Many of the concepts have been discussed in Chapter 2, and these concepts generally can be applied with little modification to predict crack behavior in virtually any scenario involving elastic materials. The stress intensity factor, or K, serves as the principle parameter for determining the crack driving force. For fatigue crack growth, the stress intensity factor range is used to evaluate the propagation rate through the Paris Law, repeated here for convenience:

$$\frac{da}{dN} = C * (\Delta K)^m$$

A center-cracked panel has long served as a basis for demonstrating the principles of fracture mechanics. In fact, the stress intensity factor for many different cracking situations has been related to the CCT K solution through magnifying coefficients. Cracks in stiffened panels take on this form directly, where the resulting K for a stiffened panel is expressed as a ratio to the unstiffened panel K. This normalization provides an easy means for characterizing the relative severity of a crack scenario.

The analytical model used in this research superimposes K solutions that have been previously developed and are readily available in handbooks. The model was first developed on this basic principle of superposition and then compared with the finite element model, discussed in the following chapter. The results and corresponding modifications will also be discussed in Chapter 7. Chapter two introduced the work of Poe that had been recently used by Nussbaumer in box girder crack prediction. This model serves as the basis for the current model development. Superimposing the effects of stiffener restraint, stiffener separation, and residual stress is the basic procedure that will be defined in this chapter. An overview of the superposition is presented in Figure 5-1.

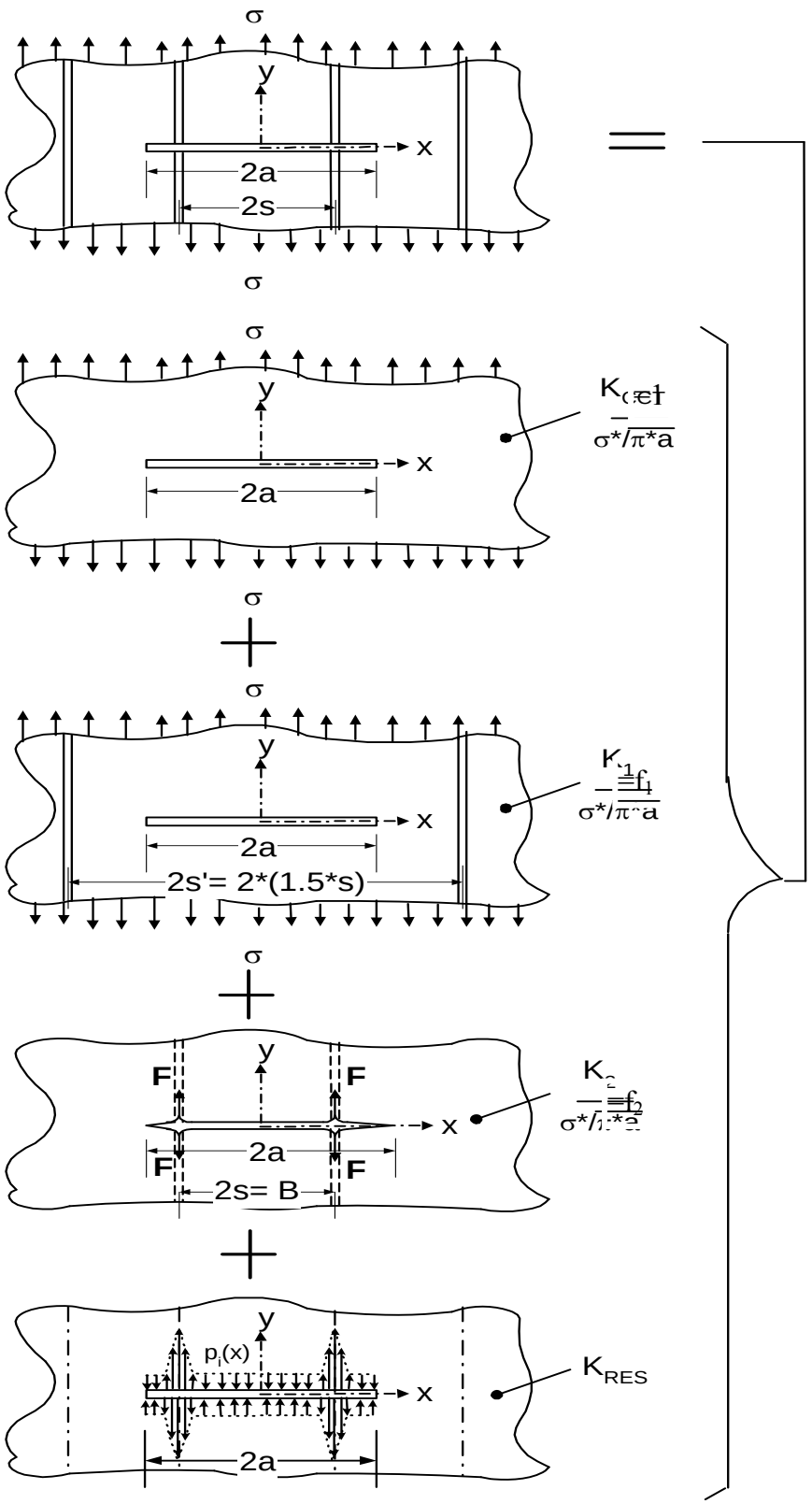

Figure 5-1: Overview of superposition components.

The experimental investigation focused on a case study that would be relatively easy to analyze in order to verify the models. That is, the condition of a crack centrally located between two stiffeners, although unrealistic, provides a valuable basis for model development. The following analytical solutions are developed specifically for a centrally located crack in a stiffened panel. Cracks that are centered about a stiffener would have slightly different K-formulations. Nonetheless, the following analytical model will soundly define the procedure for analysis.

5.2 EFFECT OF STIFFENER RESTRAINT

The first effect that modifies the CCT K is that of stiffener restraint. In Figure 5-1, this effect is represented by f_1. Isida [130] originally developed the stress intensity factor for a sheet with stiffened edges. Nussbaumer manipulated his solution into a form that would be suitable for panels with multiple, continuously attached stiffeners. He modified Isida's work by assuming negligible bending stiffness in the stiffeners and removing the built-in correction for finite width. A brief summary of Nussbaumer's derivation will be provided here.

Isida's stress intensity factor for the finite width sheet with stiffened edges utilized two parameters: β and χ. The first parameter, β, represents the axial stiffness of the stiffeners relative to its tributary plate area. Written expressly:

$$\beta = \frac{A_{st}}{t_{pl} * s} \qquad \text{Eqn. 5-1}$$

where s is half the stiffener spacing and t_{pl} is the plate thickness. The formulation for χ is just the normalized crack distance:

$$\chi = \frac{a}{s} \qquad \text{Eqn. 5-2}$$

where a is half the crack's total length. Isida's solution is accurate for all values of χ less than 0.95. Nussbaumer examined Isida's Fourier series solution for three values of β: 0, 1 and infinity. β-values between one and infinity could be represented adequately by using an abbreviation of Isida's formulation:

$$f_{Isida} = (f_k - 1)\left(\frac{1}{1+\beta}\right)^{\alpha_1} + 1 + 0.3\chi^2\left(\frac{4}{\beta^2 - 2\beta + 4} - 1\right) - \alpha_2\left(\chi^{10} + \chi^{30} + \chi^{50}\right)\left(\frac{4}{\beta^2 - 2\beta + 4} + 1\right) \quad \text{Eqn. 5-3}$$

where α_1 and α_2 characterize the magnitude of the edge stiffener's restraint. Also in the equation is the dimensionless variable f_k known as Koiter's finite width correction. The finite width correction accounts for increased net section stresses, and corresponding higher K values, as a crack grows in a plate of finite size. Koiter's correction is defined as follows:

$$f_k = \frac{1 - 0.5\chi + 0.326\chi^2}{\sqrt{1 - \chi}} \quad \text{Eqn. 5-4}$$

Koiter's solution is a finite width correction factor that is accurate to 1 percent over a wide range of χ. When β is zero, f_{Isida} defaults to Koiter's solution, appropriately so since a β of zero corresponds to an unstiffened plate.

With non-zero β, f_{Isida} provides a reduction factor to account for stiffeners at $\chi = 1$. To obtain the solution for an *infinite plate* with a pair of stiffeners, one merely divides Isida's coefficient by the finite width correction factor. The infinite plate result is as follows:

$$f_1 = \left(1 - \frac{1}{f_k}\right)\left(\frac{1}{1+\beta}\right)^{\alpha_1} + \frac{1}{f_k} + \frac{0.3\chi^2}{f_k}\left(\frac{4}{\beta^2 - 2\beta + 4} - 1\right) - \alpha_2\left(\frac{\chi^{10} + \chi^{30} + \chi^{50}}{f_k}\right)\left(\frac{4}{\beta^2 - 2\beta + 4} + 1\right) \quad \text{for } \chi \le 0.95 \quad \text{Eqn. 5-5}$$

There are a few components that one may take notice of in this equation. First of all, the term $1/f_k$ corresponds to an infinite unstiffened plate. To isolate the reduction in stress intensity factor due to the edge stiffeners, merely subtract one from the above formulation. Secondly, the effect of multiple stiffeners may be addressed by determining $f_{1,i}$ for each i^{th} pair of stiffeners at a distance χ_i from the center of the panel. This approach overestimates the restraining effects of the stiffeners. Therefore, Nussbaumer calibrated the formulation to fit Poe's results by setting $\alpha_1 = 1$ and $\alpha_2 = 0.1$. The restraint contribution of a pair of stiffeners at a distance χ_i may be determined by the following equation:

$$f_1 = \left(1 - \frac{1}{f_{k,i}}\right)\left(\frac{1}{1+\beta_i}\right)^{\alpha_1} + \frac{1}{f_{k,i}} + \frac{0.3\chi_i^{\,2}}{f_{k,i}}\left(\frac{4}{\beta_i^{\,2} - 2\beta_i + 4} - 1\right) - 1$$

$$- \alpha_2\left(\frac{\chi_i^{\,10} + \chi_i^{\,30} + \chi_i^{\,50}}{f_{k,i}}\right)\left(\frac{4}{\beta_i^{\,2} - 2\beta_i + 4} + 1\right) \qquad \text{for } \chi \le 0.95 \qquad \text{Eqn. 5-6}$$

where $\chi_i = \frac{a}{x_i}$ and $\beta_i = \frac{A_{st,i}}{t_{pl} x_i}$. Here x_i is the distance to the i^{th} stiffener and $A_{st,i}$ is its respective area.

The final coefficient may be found by summing the restraint effects for each set of intact stiffeners:

$$f_1 = \sum f_{1,i} \qquad \text{Eqn. 5-7}$$

It is important to note that the effect of stiffener restraint, from this point forward referred to as the "first effect", is only accurate for χ_i less than 0.95. For panels with multiple stiffeners, this limitation becomes evident as a crack is grown across many stiffener spans. Furthermore, this limitation does not allow the crack to grow near or into a stiffener. Therefore, interpolation must be used between a crack of length $\chi_i = 0.95$, using the f_1 coefficient, and a crack that has grown past the stiffener, using the f_2 coefficient. The f_2 coefficient is discussed in the next section.

5.3 EFFECT OF SEVERED STIFFENERS

The second effect to be accounted for is the effect of severed stiffeners. This effect is addressed by a second correction factor termed f_2. Severed stiffeners are treated as point forces applied to the crack face, as shown in Figure 5-2.

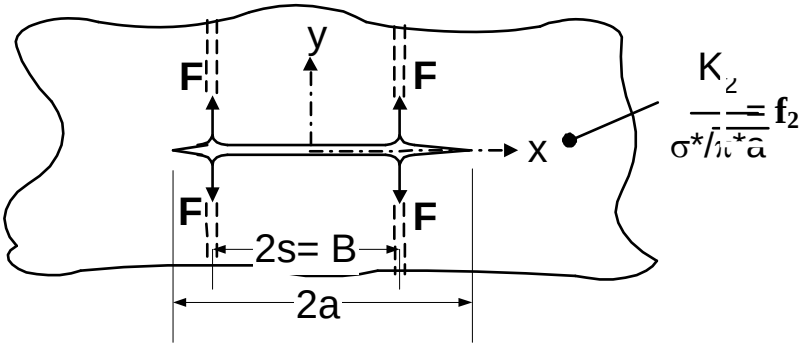

Figure 5-2: Severed stiffeners treated as point forces.

The magnitude of the point force is simply the force that was formerly carried by the intact stiffener,

$$F = \sigma * A_{st,i} = \sigma\left(\frac{\mu}{\mu - 1}\right)\left(A_{pl}\right) \qquad \text{Eqn. 5-8}$$

where $\mu = \dfrac{A_{st}}{A_{st} + A_{pl}}$, and A_{pl} = 2*s* t_{pl} for the crack configuration under investigation. The stress intensity factor is represented as a pair of splitting forces acting on the crack face. Its formulation is readily found in stress intensity factor handbooks as:

$$K = \frac{2F}{t_{pl}\sqrt{\pi a}} \frac{a}{\sqrt{a^2 - s^2}} \qquad \text{Eqn. 5-9}$$

As in the formulation of the first effect, the second effect may be transformed to a magnification of the unstiffened plate K with the same crack length. This transformation turns the above stress intensity factor into the correction factor f_2. Further algebraic manipulation of the equation allows the use of common parameters χ_i and μ:

$$f_{2,i} = \frac{2\mu}{\pi(1-\mu)} \frac{2s / x_i}{\sqrt{\chi_i^{\,2} - 1}} \quad \text{for } \chi_i > 1 \qquad \text{Eqn. 5-10}$$

where x_i is the actual distance to the i^{th} severed stiffener and χ_i is the normalized distance to the i^{th} severed stiffener. The above equation is used for each pair of severed stiffeners and summed to give the total f_2 coefficient.

5.4 ASSEMBLY OF STIFFENED PANEL COEFFICIENT

Now that the first and second effects have been formulated, one may assemble the coefficients to obtain the complete coefficient for an individual crack length. The assembly may be expressed as:

$$f_{st} = 1 + \sum f_{1,i} + \sum f_{2,i} \qquad \text{Eqn. 5-11}$$

where one represents the unstiffened plate. The following chart shows the assembled coefficient and the relative contributions of the first and second effects.

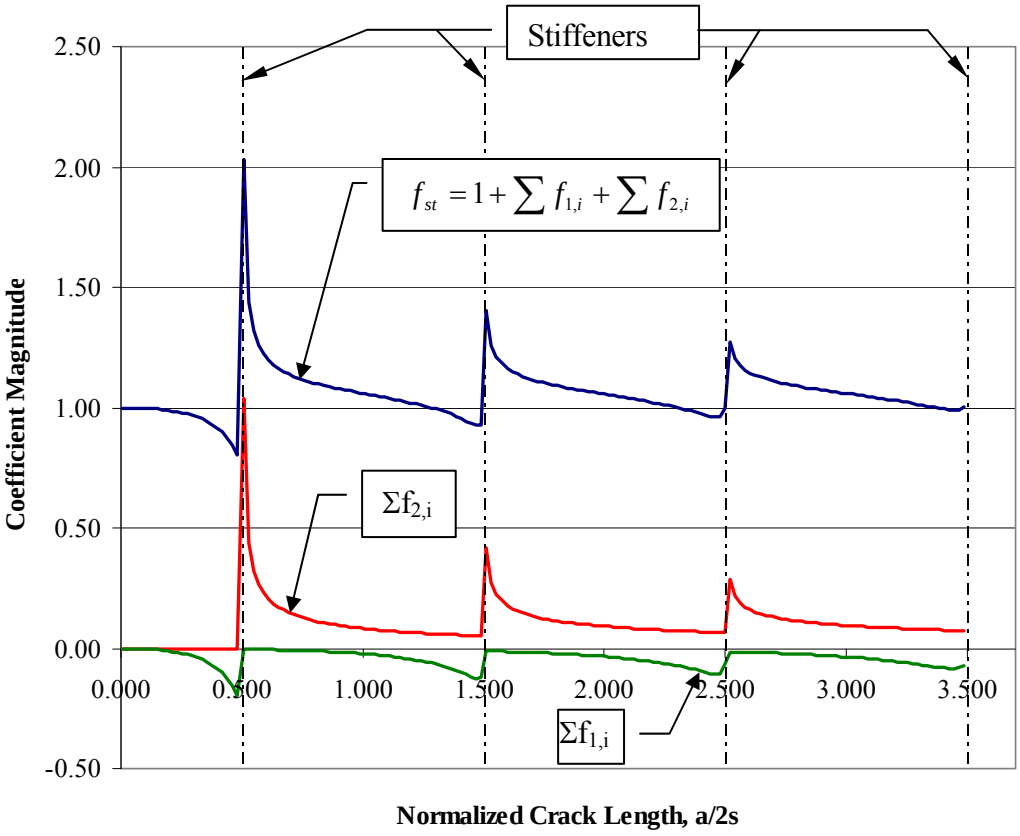

Figure 5-3: Assembly of stiffened panel correction coefficient.

One may observe the sharp discontinuity that forms as a crack approaches the stiffener. The discontinuity results from the assumption that the stiffener is severed immediately once the crack reaches it. In reality, the stiffener crack growth has been observed to match the growth in the plate.

Using this observation, one may use linear interpolation between the coefficient for an unsevered stiffener and a severed stiffener.

The first point of interpolation is defined as the last accurate correction coefficient prior to a crack surpassing a stiffener, namely $\chi_i = 0.95$. One may find the second interpolation point by assuming a radius equal to the distance of the plate crack from the stiffener centerline. Poe originally developed this procedure, which may be seen graphically in Figure 5-4.

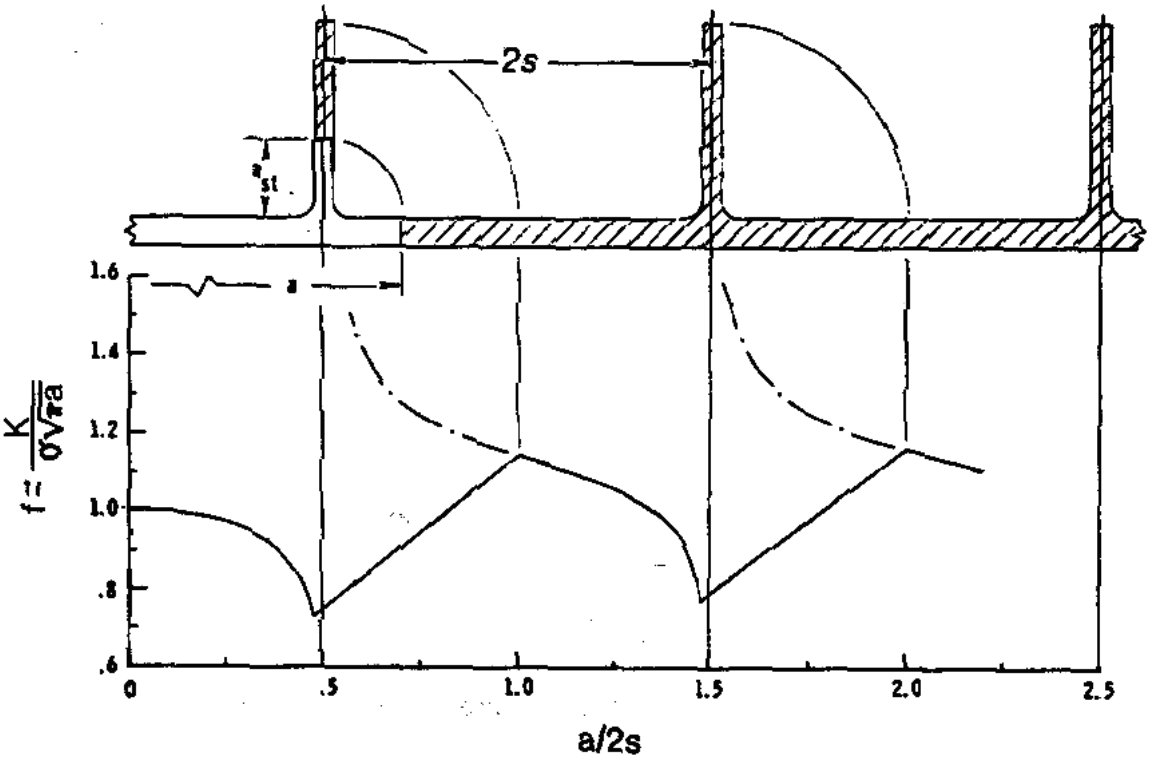

Figure 5-4: Interpolation between unbroken and broken stiffeners [Poe, 66].

Using this procedure, a comparison may be made between various stiffness ratios. Figure 5-5 shows the effect of changing the stiffness ratio.

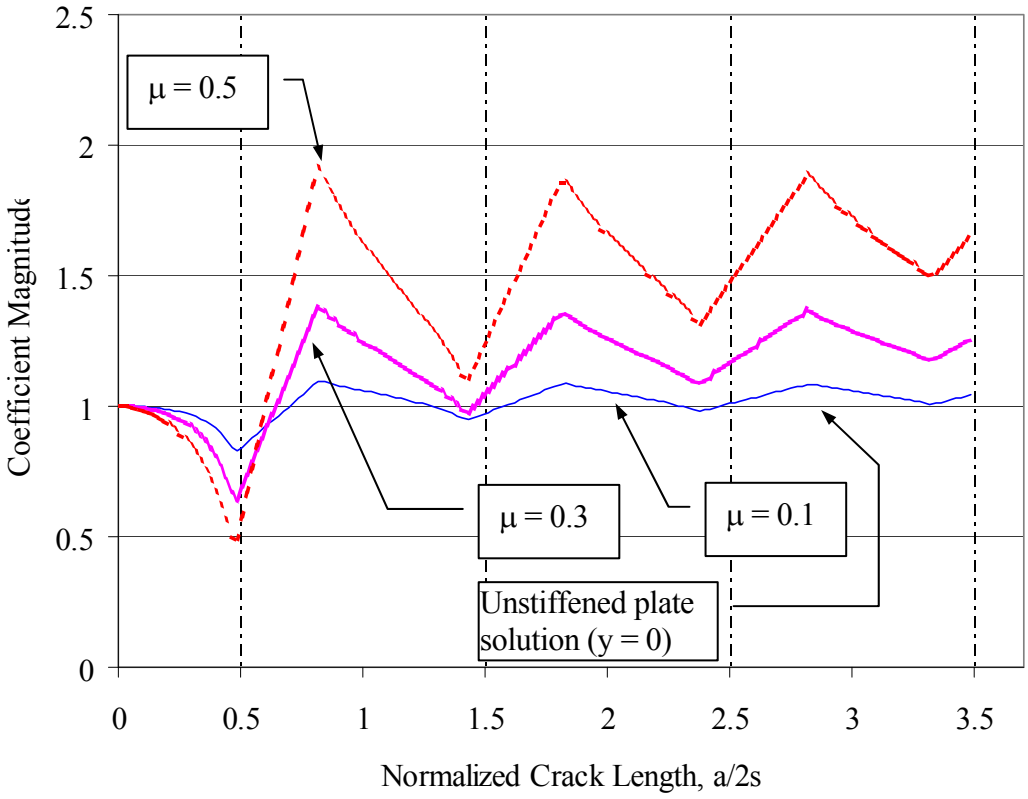

Figure 5-5: Effect of changing stiffness ratio on correction factor.

As the stiffness ratio increases, the curves for f_1 and f_2 diverge. Nussbaumer found that stiffness ratios less than 0.7 result in behavior resembling that of Poe's work. He noted that, in typical cellular structure, stiffness ratios are less than 0.5 and thus the model is applicable. In the experimental scope of this research the stiffness ratios were held constant at μ=0.22.

The stiffened panel stress intensity factor has so far been illustrated without correcting for the effects of finite width. Many functions exist to make this correction, including the net section change coefficient presented by Nussbaumer. This compliance coefficient, which is Equation 2-17, is repeated here for convenience:

$$f_\sigma = \frac{\sigma}{\sigma_{nom}} = \frac{I_0 * c(a)}{I(a) * c_0} \qquad \text{Eqn. 5-12}$$

This correction factor is used as a multiplier to the total stress intensity factor. It provides an easy means of relating the increase in applied stresses to crack growth. The final result for the stiffened panel stress intensity factor is expressed as follows:

$$K_{st}(a, f_1, f_2) = f_\sigma\left(1 + \sum f_{1,i} + \sum f_{2,i}\right)\left(\sigma\sqrt{\pi a}\right) = f_\sigma f_{st}\sigma\sqrt{\pi a} \qquad \text{Eqn. 5-13}$$

5.5 RESIDUAL STRESS INTENSITY FACTOR

Residual stress effects on crack growth are taken into consideration separately from the previous components. This is because the applied stresses are assumed to not affect the magnitude of the residual stress distribution. A stress intensity factor is developed to account for its presence assuming no redistribution during cracking. After the residual stress intensity factor is determined, it is added to the applied stress intensity factor as explained in Figure 2-5.

The analytical model presented uses the same residual stress intensity factor as utilized by Nussbaumer [109] and Thayamballi [154]. Its formulation has been previously shown in Figure 2-10 but will be repeated here for convenience:

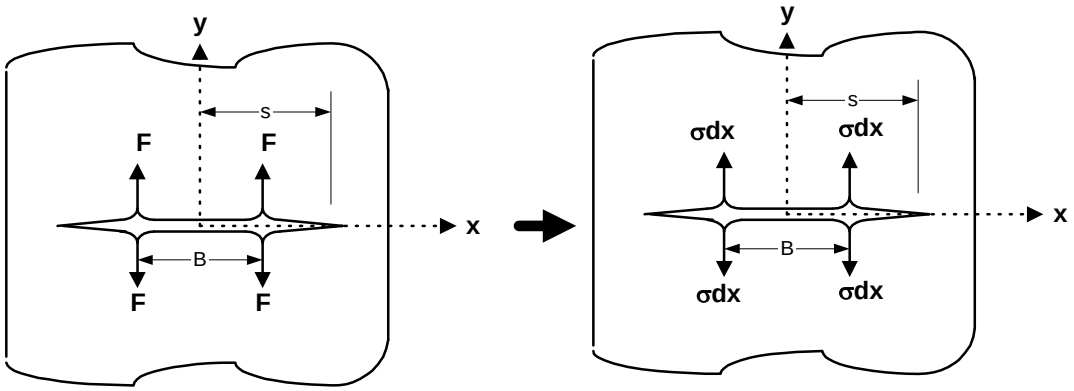

Figure 5-6: Development of residual stress intensity factor.

The residual stress intensity factor requires that the residual stress distribution be defined. In this analytical model, Faulkner's recommendations will be utilized. Faulkner's characterization of residual stress has been previously discussed in Section 3.6. The relatively simple model is practical in light of the scatter in residual stress data both in the laboratory and in actual ship measurements [114].

The residual stress distribution used in most of the analytical analyses is shown in Figure 5-7. For comparison, the measured data is presented also. The triangular tensile region has a base width of 3.5 times the plate thickness on either side of a stiffener. The peak of the tensile stress is the material yield stress. In determining the residual stress field, residual stress contributions from the stiffeners were neglected. This methodology provides an extremely simple means to develop the residual stress field for use in the residual stress intensity factor.

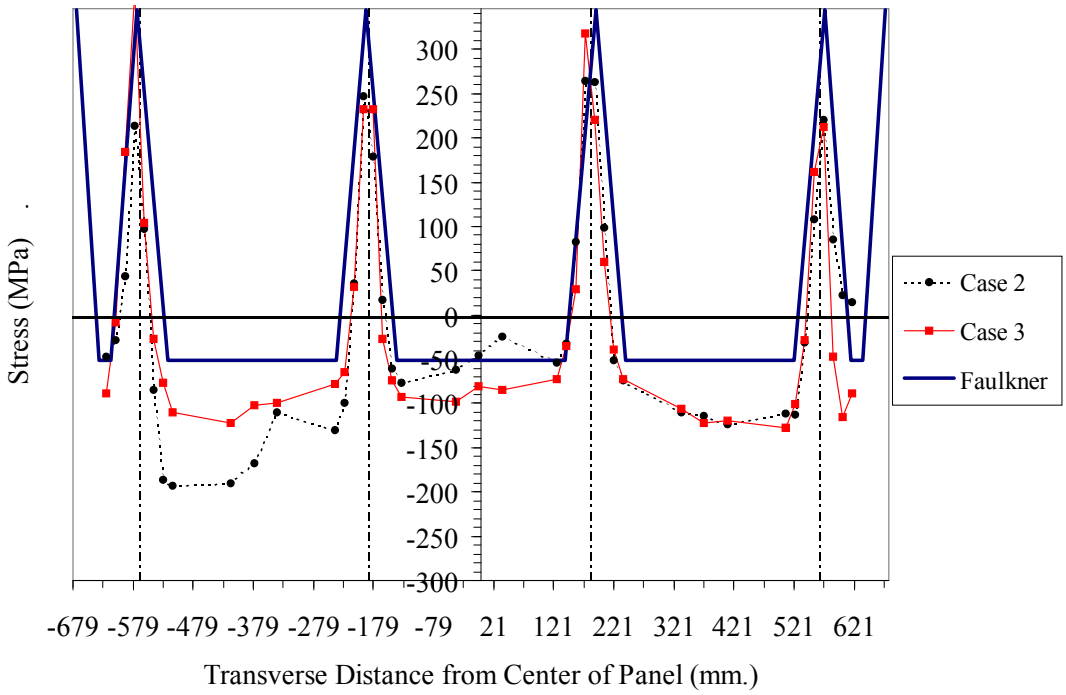

Figure 5-7: Faulkner residual stress model compared to measured values.

It is important to realize that the only effect residual stress has on the proposed models is to reduce the growth rate in regions of high compressive stress. In regions of tensile stress, the residual stress poses no impact on the analysis prediction since crack growth is a function of the effective stress

range. That is, for positive residual stress intensity factors, crack growth is affected only by the applied stress range regardless of the magnitude of the residual stress intensity factor.

An evaluation of the residual stress intensity factor may be seen in Figure 5-8.

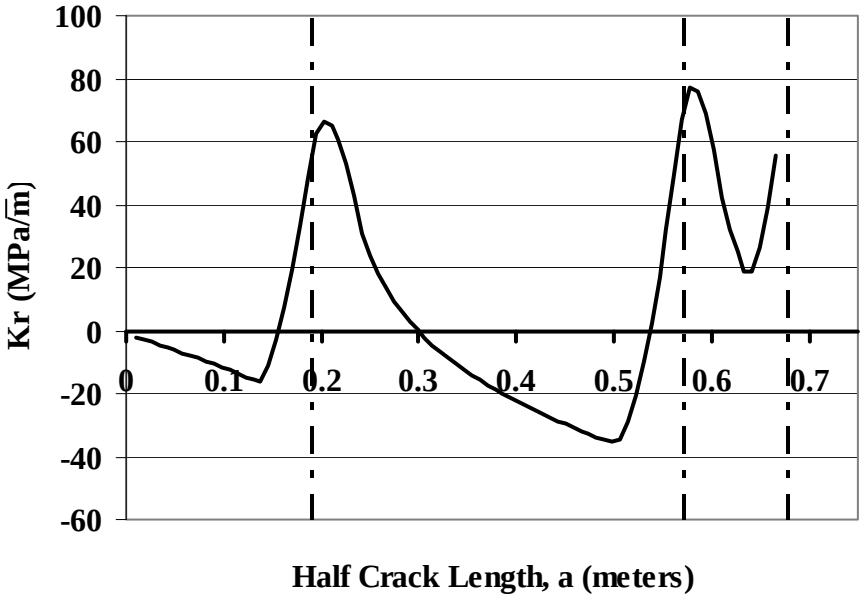

Figure 5-8: Resulting residual stress intensity factor for typical specimen.

5.6 PLASTICITY EFFECTS

Plasticity effects become important as applied stresses increase. In the course of this research, however, the effects of plasticity have been ignored. Justification lies in the low stress ranges used in the experiments, where plasticity effects are deemed negligible and are set to zero. This justification extends to the use of the models for evaluation of fatigue cracking in ship structure because most of the life of the ship undergoes stress ranges well below the yield strength of the material.

Nussbaumer [109] discredited the inclusion of plasticity effects in his models as well. He cited similar reasoning while also noticing that the effects of local plastic strain reversal tend to propagate

cracks "in a manner proportional to $(\Delta K)^m$." For these reasons, $K_{pl} = 0$ in the models proposed and analyses made.

5.7 SUPERPOSITION OF ANALYTICAL MODEL COMPONENTS

In this section a procedure will be reviewed to obtain the effective stress intensity factor range, the key parameter used in fatigue life prediction. The effective stress intensity factor is directly used in the Paris Law to predict the number of cycles for an incremental growth, *da*. Solving Equation 2-4 for the number of cycles yields:

$$dN = \frac{da}{C\left(\Delta K_{eff}\right)^m}$$

where $C = 9.5 \times 10^{-12}$ and m =3 for steel. There is some debate over the values to be used for C (Discussed in more detail in Chapter 2), but the author has chosen these values for upper bounds in connection with BSI PD6493 [23].

Figure 2-5, repeated here for convenience, provides the most straightforward instruction for determining the effective stress intensity factor. Recall that $K_{pl} = 0$ in the models proposed.

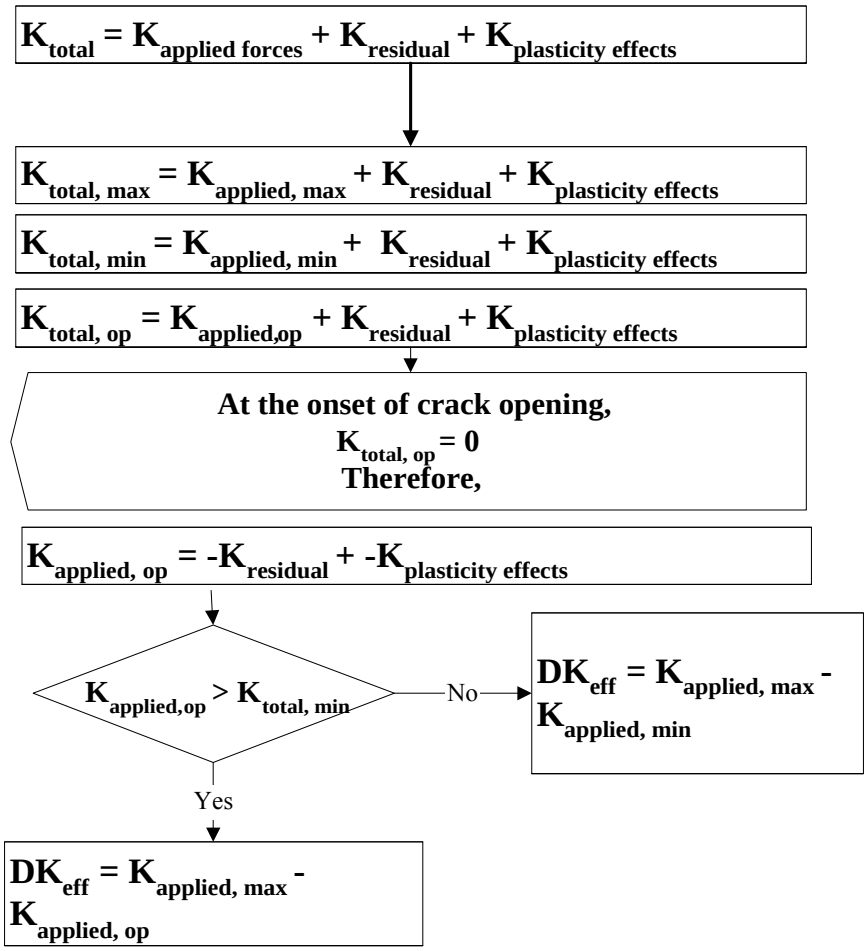

Figure 5-9: Procedure for determining stress intensity actor range.

In essence, one determines the stress intensity factor for both the minimum and maximum applied stresses. These quantities are appropriately termed the applied stress intensity factors. For example, the maximum applied stress intensity factor would be:

$$K_{app,\max} = f_\sigma f_{st} \sigma_{\max} \sqrt{\pi a} \qquad \text{Eqn. 5-14}$$

Next, one adds the residual stress intensity factor, a constant, to both of the applied stress intensity factors. The quantities are now called the total stress intensity factors. If neither of the total stress intensity factors is positive, it indicates that the crack is not opening even under the maximum applied stress. The effective stress intensity factor would be zero, then, and crack growth could not occur.

If the only the maximum total stress intensity factor is positive, it indicates that only part of the applied stress range is effective. Finally, the whole stress range is effective if both maximum and minimum total stress intensity factors are positive. A plot of an analytical model analysis can be seen in Figure 5-10.

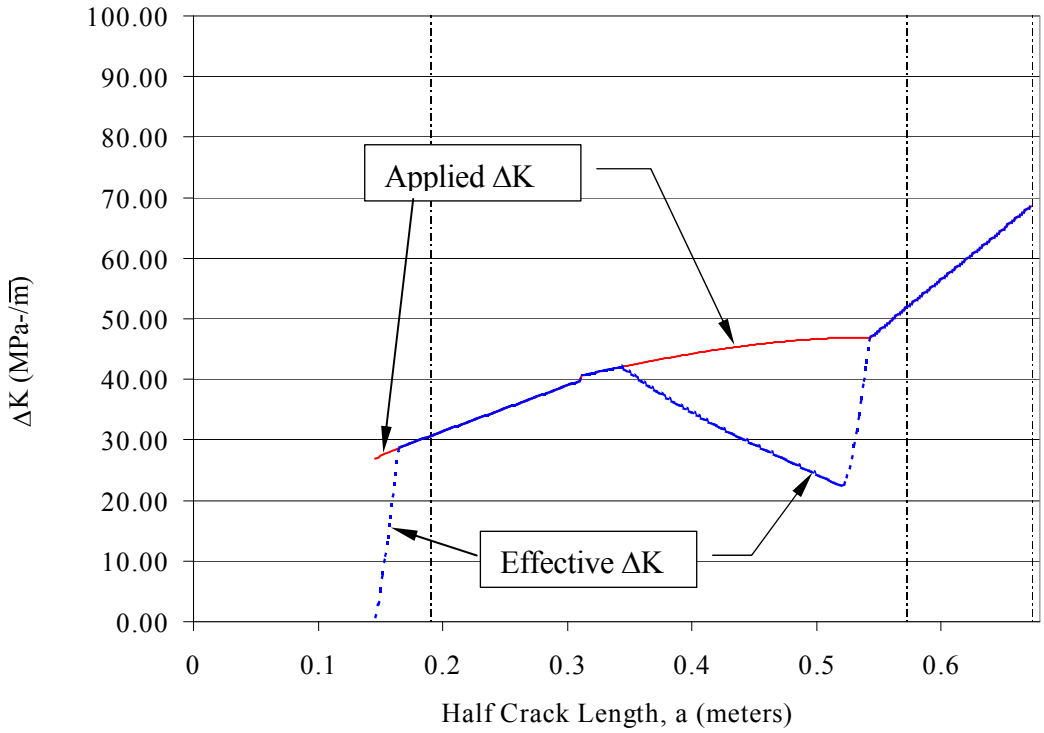

Figure 5-10: Difference between ΔK_{app} and ΔK_{eff} for stiffened panel with σ_{max}=46 MPa and σ_{min}=6 MPa.

The effective stress range is defined as Elber's ratio, U, defined in Equation 2-8. Plotting Elber's ratio allows one to observe the residual stress influence on the effective stress intensity factor. Since the residual stresses are treated as constants, they do not promote increased fatigue crack growth in these models for any given crack length.

The region before the crack meets the first stiffener is highly sensitive to the compressive residual stress. In fact, for half crack lengths less than 146-mm no propagation would occur, as illustrated by Figure 5-11. Notice the rise in Elber's ratio between a = 0.145 meters and a = 0.175 meters. For

cracks starting in a compressive residual stress region, this steep rise is an indicator that several analyses with different starting lengths should be performed.

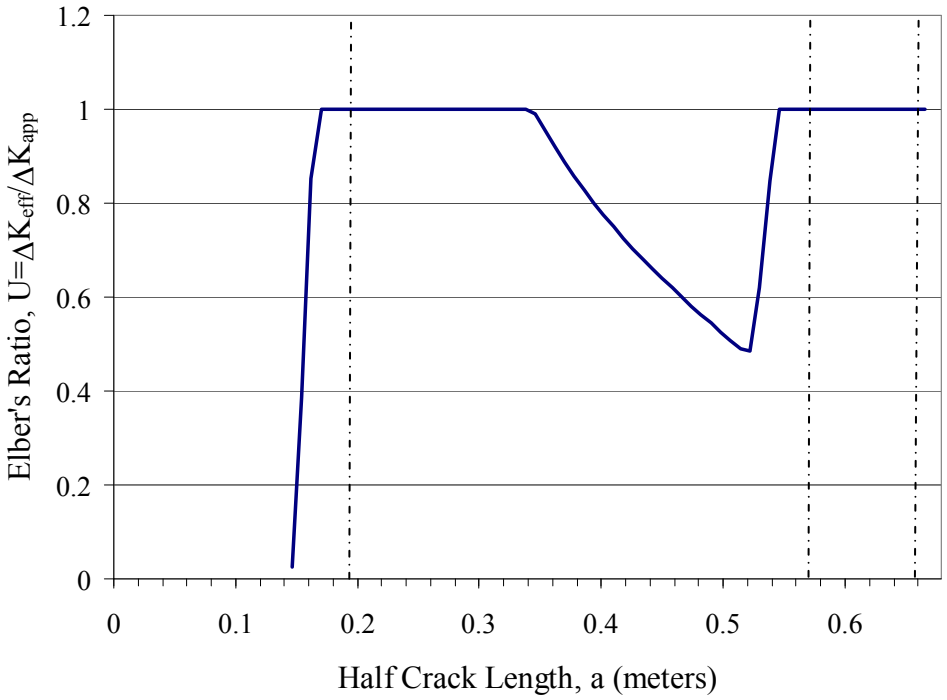

Figure 5-11: Elber's ratio for a stiffened panel with σ_{max}=46 MPa and σ_{min}=6 MPa.

To illustrate this reasoning, suppose one performed an analyses with an initial crack size of a = 0.150 meters and desired a prediction estimate for the crack to reach a = 0.671 meters. The effective stress intensity factors would be very low in the initial crack lengths. As a result, the number of cycles predicted would be very high. On the other hand, if one performed the analysis with an initial crack length with a = 0.165 meters, the initial effective stress intensity factor would be significantly greater. The number of cycles predicted would also be significantly lower, sometimes as small as 10 percent of the previous analysis' estimate. Therefore, it is important to perform the analysis with several starting lengths if the crack originates in a region of compressive stress.

This caution is not as significant in other situations (i.e. running cracks encountering compressive stress) because the applied K continually increases with crack length while the K_r is limited by its self-equilibrium.

5.8 ANALYTICAL PROGRAM

The analytical model may easily be developed in a spreadsheet application. Furthermore, each component may be coded in a separate routine to provide reasonable estimates in a very short amount of time. The analytical model used in this project was developed using Microsoft Excel and accompanying Visual Basic code. The Visual Basic code, which is simply BASIC coding language within the Excel program environment, is integrated into the spreadsheet and may be easily accessed for revisions. A complete program was developed that includes extensive comments for easy interpretation. The routines and flowchart can be found in the Appendix.

The program was developed for the case of a central crack in either an unstiffened plate or stiffened plate. The program does not address a crack emanating from underneath a stiffener or an unsymmetric crack, but it does provide a solid basis for developing further crack prediction codes. Other assumptions made include:

1. Equal crack growth rates in the stiffener and the plate. The stiffener is considered severed when the plate crack has propagated a distance equal to the radius of the tangential stiffener distance.

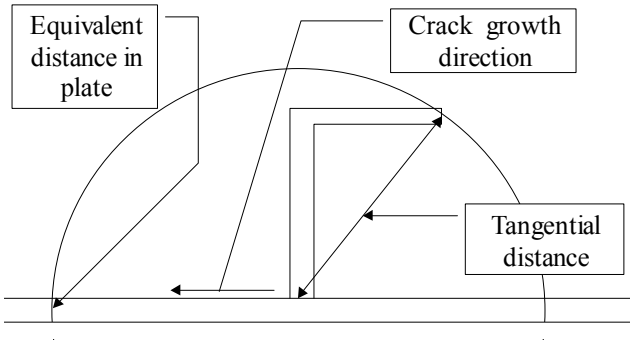

Figure 5-12: Tangential distance for stiffener.

2. Low stress ranges are used and only tensile portion of stress range is considered.

3. Residual stress distribution is unaffected by crack growth.
4. Plasticity affects are negligible or plastic strain reversals provide offsetting results.

Several features have been included in the spreadsheet including a routine that produces Faulkner's residual stress distribution. In addition, instruction is available for each parameter that is required by the program. The end result provides a user-friendly program that was effectively applied in predicting the experimental behavior.

6 Finite Element Model

6.1 INTRODUCTION

The finite element model is more appropriately a modeling technique than a model. Basically, a finite element analysis is performed on the specified geometry with a given crack length. An output request is made for the J-integral to be calculated, specifying the node at a crack tip and the crack's propagation direction. The J-Integral can then be converted it into an equivalent stress intensity factor. Henceforth the procedure is equivalent to that of the analytical model—determining K_{eff} and utilizing it in Equation 2-4 for many discrete crack lengths.

6.2 J-INTEGRAL BACKGROUND

The J-Integral was previously introduced in Chapter 2. It is a measure of the energy released by moving the crack tip forward an incremental length, da. The formal definition is as follows:

$$J = \int_{\Gamma} \left(W dy - T \frac{\partial u}{\partial x} \right) ds = -\frac{\partial V}{\partial a} \qquad \text{Eqn. 6-1}$$

where W is the strain energy density, T is a traction vector on a point in the contour being evaluated, u is the displacement and s corresponds to the arc length along the contour Γ. The right side of the equation defines the J-integral as the change in potential energy associated with the virtual crack extension, *da*. A graphical aid is shown below in Figure 6-1.

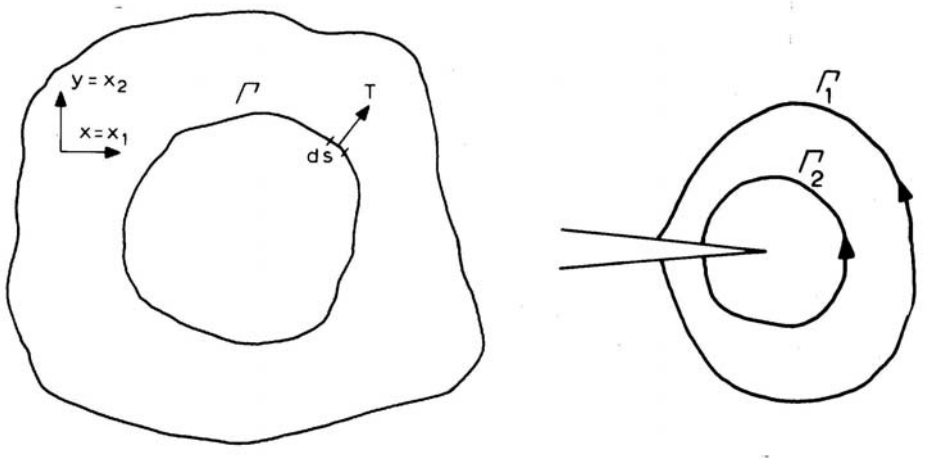

Figure 6-1: Visualization of J-integral evaluation.

The J-integral is calculated using any closed path that encircles the crack tip. A number of separate evaluations may be made along different paths. Each of these evaluations should yield the same value for J since the quantity is path independent in linear elastic materials. In finite element analyses, the first evaluation is usually made using the row of elements immediately surrounding the crack tip. For the modeling put forth in this report, it is suggested that the average of the second and third J-integrals be evaluated. This is because the row of elements immediately adjacent to the crack tip can be subject to stress inaccuracies and therefore yield higher error than subsequent contour paths. J-integral values for paths higher than the third row of elements may also exhibit slight errors in J in regions of high stress gradients.

The path-independent property of the J-integral serves as a check on the accuracy of the J results. It does not, however, assert that the mesh is sufficiently refined to yield the correct stress and displacement values. Therefore, one should perform preliminary mesh studies to find a proper element size. Another useful quality of the path independence is that no special elements are required around the crack tip in most cases. It has been argued in the past that the proper way to model the elastic crack is to include the stress singularity at the crack tip (See Figure 2-4). Barsoum [15] advocated moving the mid-side nodes of six or eight-noded elements to the ¼ points to correctly recreate the stress singularity. In reality, accurate values for J may be obtained without

recreating the stress singularity. Nussbaumer found deviations were 5% on the first contour and less than 1% on the second contour.

The J-integral is only applicable to planar mode I cracks in linear elastic materials [136]. It has been argued that the J-integral may be used for nonlinear material evaluation as well, and the interested reader is referred to the work of [22, 136, 169]. For the proposed fatigue crack growth models, however, one implicitly assumes linear elastic behavior and relatively low stresses. Therefore, the J-integral is well suited for the current research.

Once the J-integral is determined it can be converted into an equivalent K through use of Equation 2-3:

$$K = \sqrt{JE} \quad \text{for plane stress}$$

where E is the material's elastic modulus (MPa), J is in Joules, and K has units of $MPa\sqrt{m}$. The uniqueness of the finite element model ends with the formulation of K, at which point it is used as shown previously in Figure 5-9.

The finite element model was developed using ABAQUS, a powerful finite element software package that was available through the University of Minnesota's Supercomputing Institute. This widely used software is certainly not unique in its capabilities of evaluating the J-Integral, and many F.E. packages exist today with similar features. One such program, ADINA, was used by Nussbaumer to determine stress intensity factors by a method other than the one is this report.

A small plate model will be used in the first section to thoroughly detail the methodology. This case study would be an excellent learning aid for anyone interested in using this method. In Section 6.4, an approach to allow a single set of analyses to be used for various stress ranges is demonstrated. Finally, Section 6.5 details the results of several stiffened panel analyses.

6.3 SMALL MODEL CASE STUDY

The small case study involves modeling a CCT plate with residual stresses. Modeling the CCT specimen requires only a quarter of the plate to be modeled (See Figure 6-2).

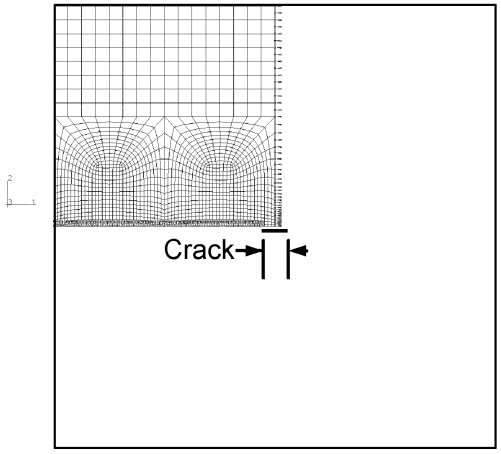

Figure 6-2: Small case study of CCT specimen.

Symmetry conditions are placed along the centerline of the specimen in both the x and y directions. Figure 6-3 shows the mesh and model used, with tensile stress to be applied in the positive y-direction. To simulate a crack, boundary conditions are released along the crack face up to the tip.

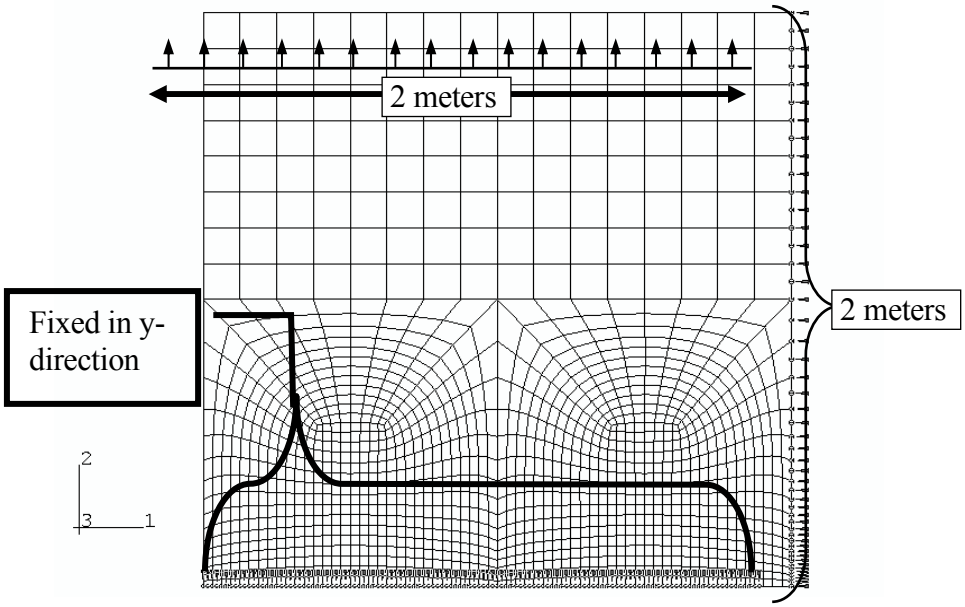

Figure 6-3: Mesh used in small case study.

All elements used in the analyses were 8-noded shell elements with reduced integration. These elements were also used in the three-dimensional stiffened panels, however ABAQUS automatically [and appropriately] uses shell elements with full integration at plate intersections. The

element size near the crack tip should be roughly the thickness of the plate for reasonable accuracy. This element size may be increased away from the crack tip as long as the geometry of each element is not warped beyond software recommendations.

Fatigue crack growth requires that many crack lengths be evaluated along the crack line. For this reason it was found convenient to make a zone of refined mesh along the entire crack path. When a new crack length was to be analyzed, no remeshing was required and it was only necessary to release the boundary conditions along the advanced crack face.

Nussbaumer utilized special elements along the crack face to prevent the faces from overlapping in regions of compressive stress. These elements, called "gap elements," yield values for contact forces that occur when two crack faces come together. The resultant contact forces, however, are not included in the J formulation. Therefore, it was decided to examine the effects of using the gap elements in the small CCT study. Case A of the study examines a crack in a tensile residual stress field while Case B examines the same length crack in a region of compressive residual stress. Both cases were subjected to analyses with and without the use of gap elements.

The rest of the finite element procedure is very basic. Forces may be applied as displacements, body forces, temperatures, or nodal forces. A linear static analysis is performed with an output request for the J-integral to be calculated. This request requires the direction cosine of crack propagation to be specified as well as the node number at the crack tip. Applying the forces incrementally allows the computation of the J-Integral at various levels of stress. Typically a load was applied in 10-12 increments over an analyses step. In addition, each type of load (e.g. body forces or temperature) was applied during the analysis as distinct analyses step. Figure 6-4 shows the results of a typical analysis.

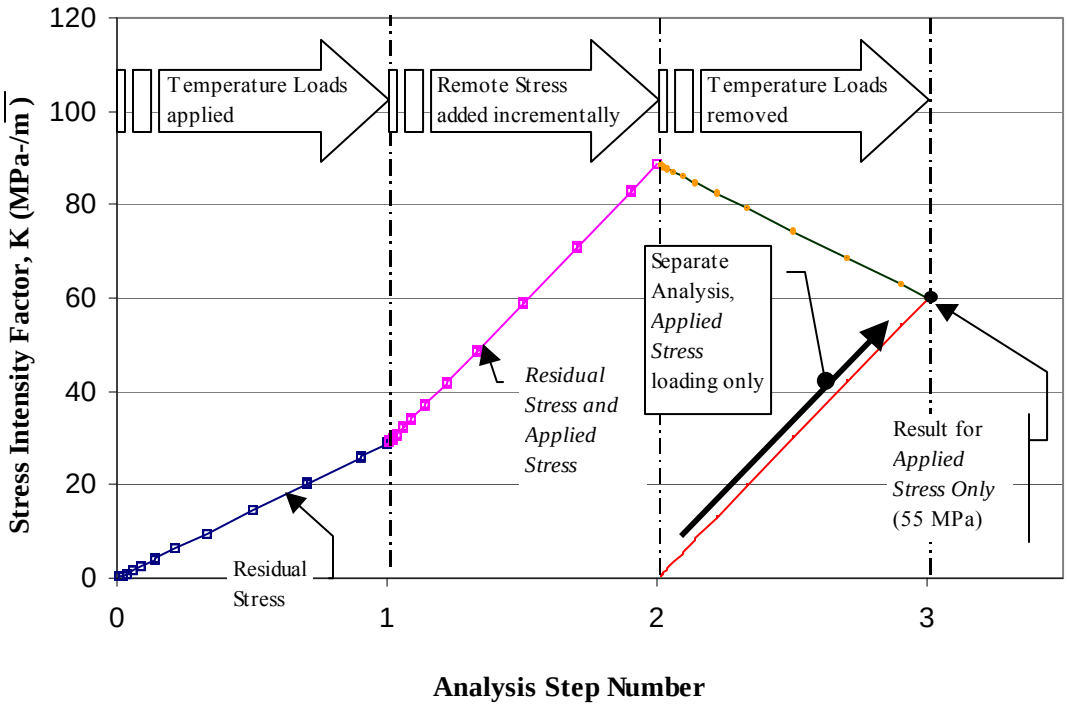

Figure 6-4: Typical plot of analysis procedure.

Residual stresses were modeled by changing the temperature in a region of the specimen. The results of one such analysis, case one, is shown in Figure 6-5. In this figure the temperature of the nodes on the right have been set to –200 Celsius while temperatures on the left have been set to +200 Celsius. The net effect is to create a self-equilibrated bending gradient throughout the specimen, with tensile stresses in the cooled region and compressive stresses in the heated region.

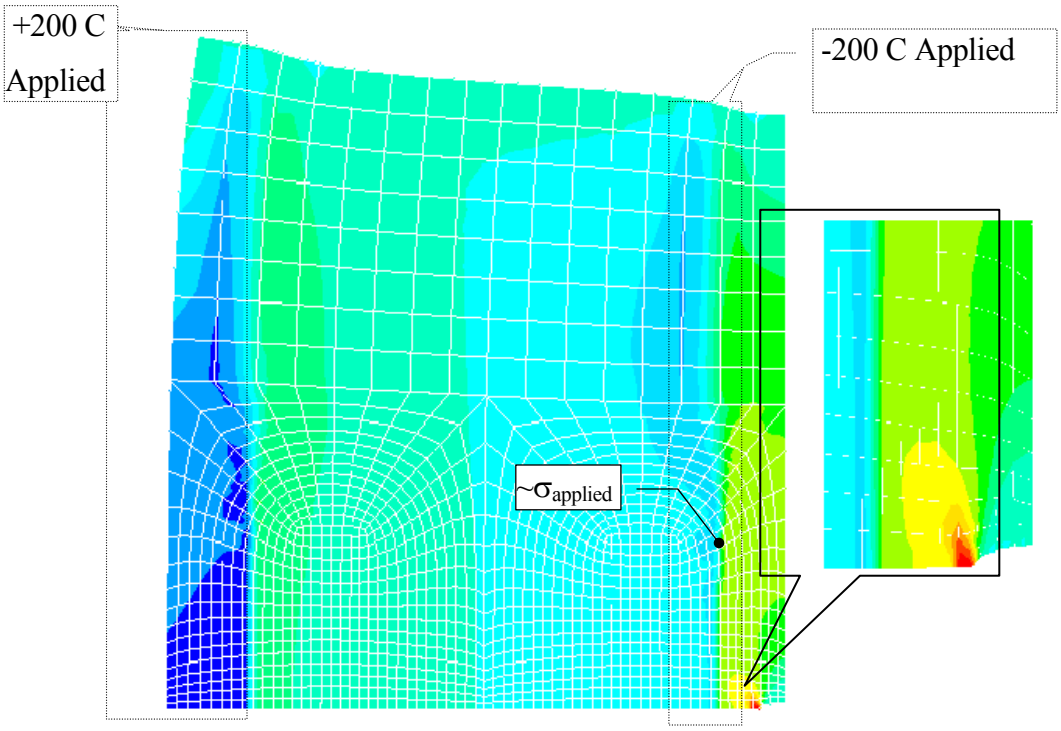

Figure 6-5: Case residual stresses applied by temperature loading.
(100x displacement magnification)

At nodes where the temperature has not been set, the F.E. software applies the default temperature of zero. To roughly verify the computed J-integral, one may take an approximation of the stress above the crack tip and use it in the CCT formula. The computed result should yield a K-value within 35% of the F.E.A. equivalent K value. This crude verification will let the user realize immediately if the approach has been implemented correctly.

An examination of the interaction between residual stress and applied stresses will now be made. Referring to Figure 6-4, one can observe three steps to the analysis. First, the temperature loads are applied and residual stress fields are formed. By performing this step separately, one may directly observe the magnitude of the residual stress J integral. The second step consists of applying forces incrementally without changing the temperature loading. In this CCT study, only body forces were used because they are easily translated into an applied uniform stress by the analysis. The final step maintains the applied body forces [or other external loading] and incrementally removes the temperature loading. This final step should provide a J estimate equal to that of an applied stress

analysis only. To prove this, a separate analysis was performed using the applied body forces only. It is shown plotted with a shift in step number for illustration purposes only.

The use of gap elements makes the analysis more time consuming and difficult. Without their use, however, greater care must be exercised to use the correct J value. To explain, first consider Case A of the study. Its residual stress field has been shown in Figure 6-5. The majority of the crack is subjected to the tensile residual stress field and consequently there are no effects of crack closure. Accordingly, there is no difference between an analysis made using gap elements and that without gap elements. The J integral results for this case are presented in Figure 6-5. A fourth step has been added removing the applied loads to verify the load application cycle.

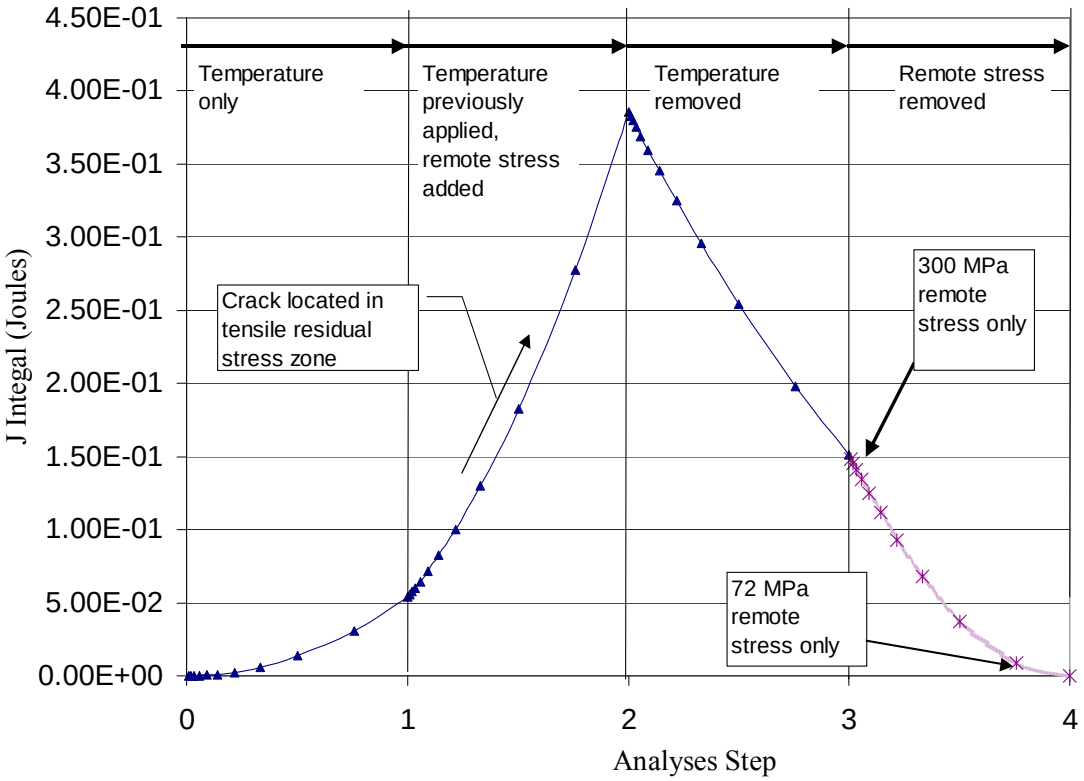

Figure 6-6: Case A of CCT study results.

Notice that the above plot is nonlinear because it plots J instead of K. This point must be kept in mind when using superposition and the Paris Law: A J value must first be converted to an

equivalent K before any ΔK is calculated. In other words, do not make the mistake of equating ΔJ with ΔK.

Case B of the CCT study uses the same crack length with reversed temperature loading. Figure 6-7 shows the residual stress distribution from an analysis which did not use gap elements. The overlap caused by compressive residual stress can clearly be seen. With gap elements, no such overlap would occur, effectively maintaining the compressive residual stress at a level equivalent to that of a plate without a crack present.

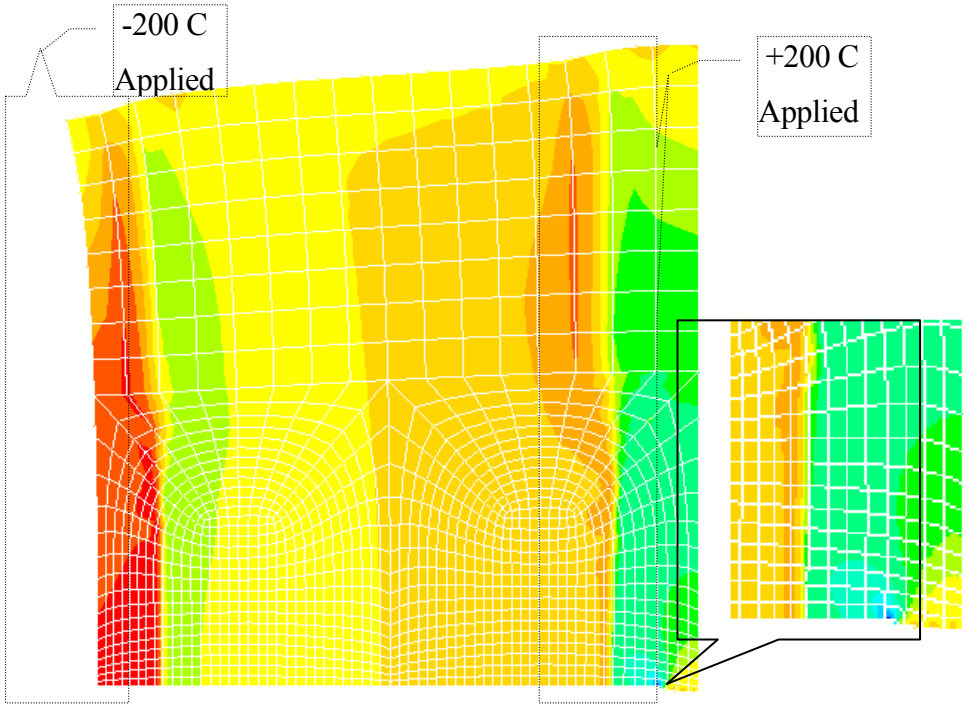

Figure 6-7: Case B residual stresses applied by temperature loading.
(100x displacement magnification)

What's interesting about this study is the behavior of J when gap elements are introduced. The results of Case B are shown in Figure 6-8.

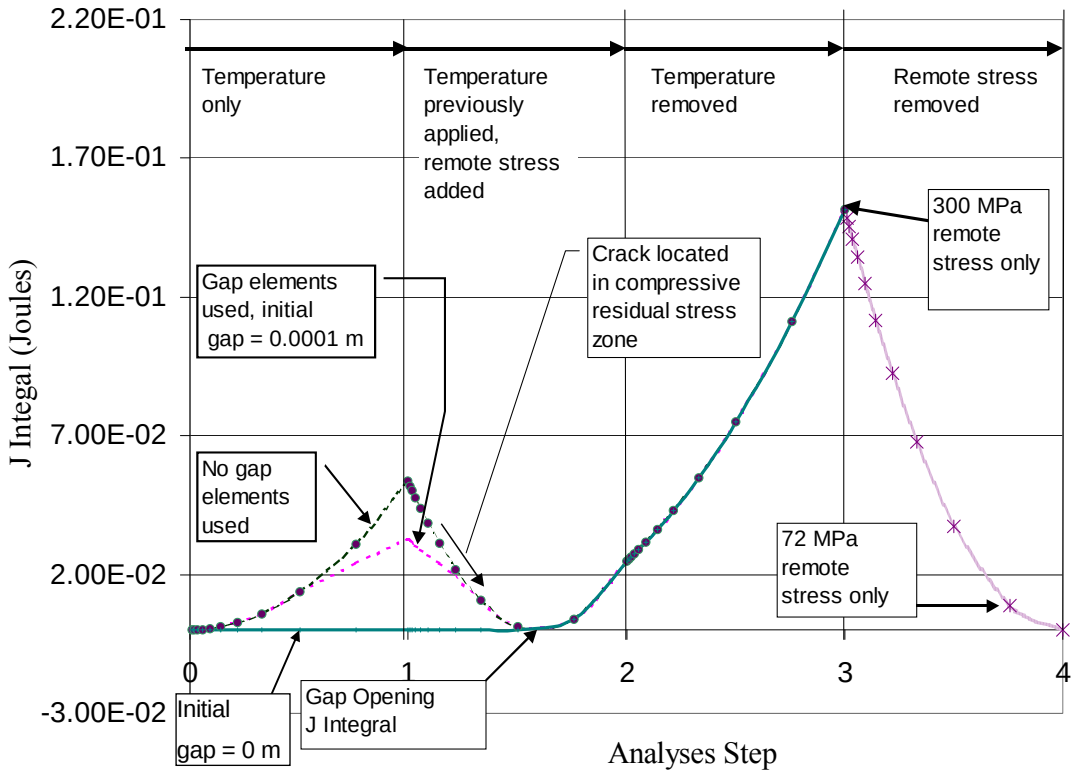

Figure 6-8: Case B of CCT study results.

Some observations can be immediately made from this analysis. First, the J integral is always an absolute value. By omitting gap elements, one is able to observe this characteristic. By including gap elements and specifying an initial gap of zero meters, the J integral remains zero until applied external loads overcome the residual stress-induced closure. By using gap elements with an initial gap of 0.0001 meters, one obtains similar results as would be found without the use of gap elements. This seems to indicate that the J integral may not yield values for the case when there *appears* to be no crack, as in specifying an initial gap of 0 meters.

Without gap elements the J integral is output as an absolute value. A decreasing J with applied tensile load indicates that compressive residual stresses are inducing crack closure. Usually this decrease in J reaches a minimum at the same point as the gap element analysis indicates a non-zero J. The point at which J reaches a minimum under applied loading is the *opening* applied load, indicating the applied loads are becoming effective. As the crack tip is moved away from of a region of compressive stress the opening load is decreased. Figure 6-9 demonstrates this for various

crack lengths in Case B. At a crack length of 109-mm, the crack is entirely within a region of compressive residual stress. Consequently, the opening load is significantly greater than for a longer crack, especially one that is not completely contained within a compressive residual stress zone.

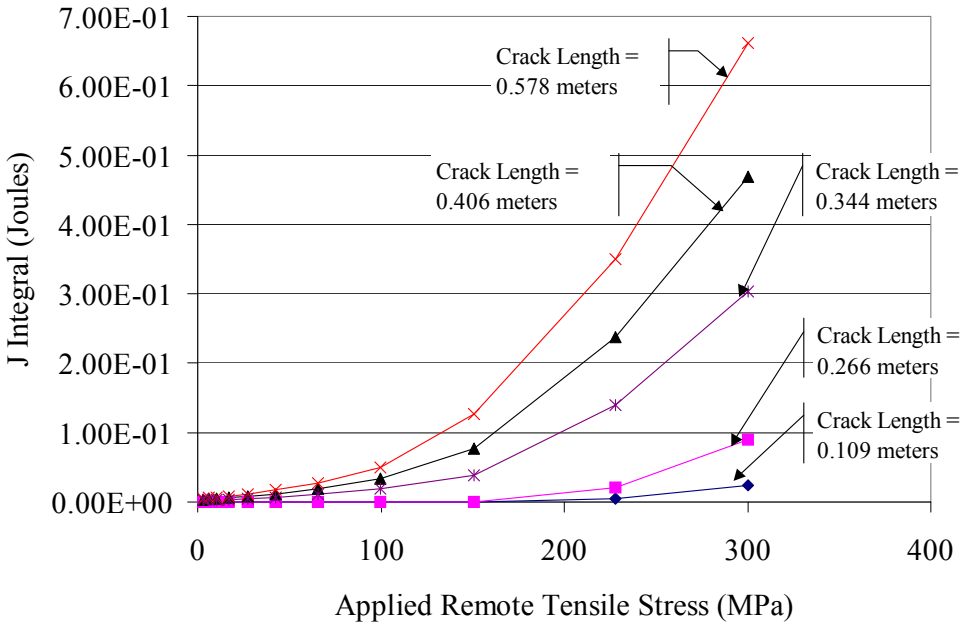

Figure 6-9: Closure effects on effective applied load for Case B.

The three variations of analyzing Case B all converge to a common opening load. This seems to imply the same results could be obtained with or without the use of gap elements. However, the convergence to a common opening load is not always observed. Gap elements take into account closure along the entire crack front, and in some situations the crack may be open near the crack tip while closure occurs behind the crack tip. To illustrate, several variations of closure are illustrated in Figure 6-10 (Adapted from Nussbaumer).

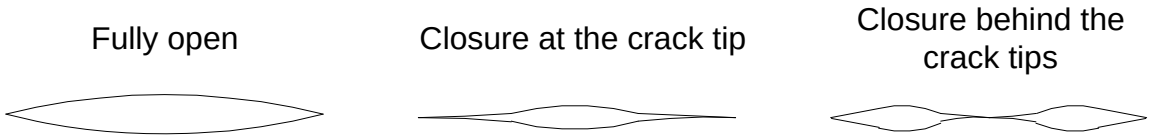

Figure 6-10: Variations of crack shape.

Closure effects behind the crack tip cannot be modeled without the use of gap elements.

Proof of this statement was observed in one of the stiffened panel F.E. analyses. In the analysis, a crack was introduced that extended beyond the first severed stiffener. A view of the crack in the panel is seen in Figure 6-11. In this picture, both residual stress and an applied uniform tensile stress of 200 MPa are present.

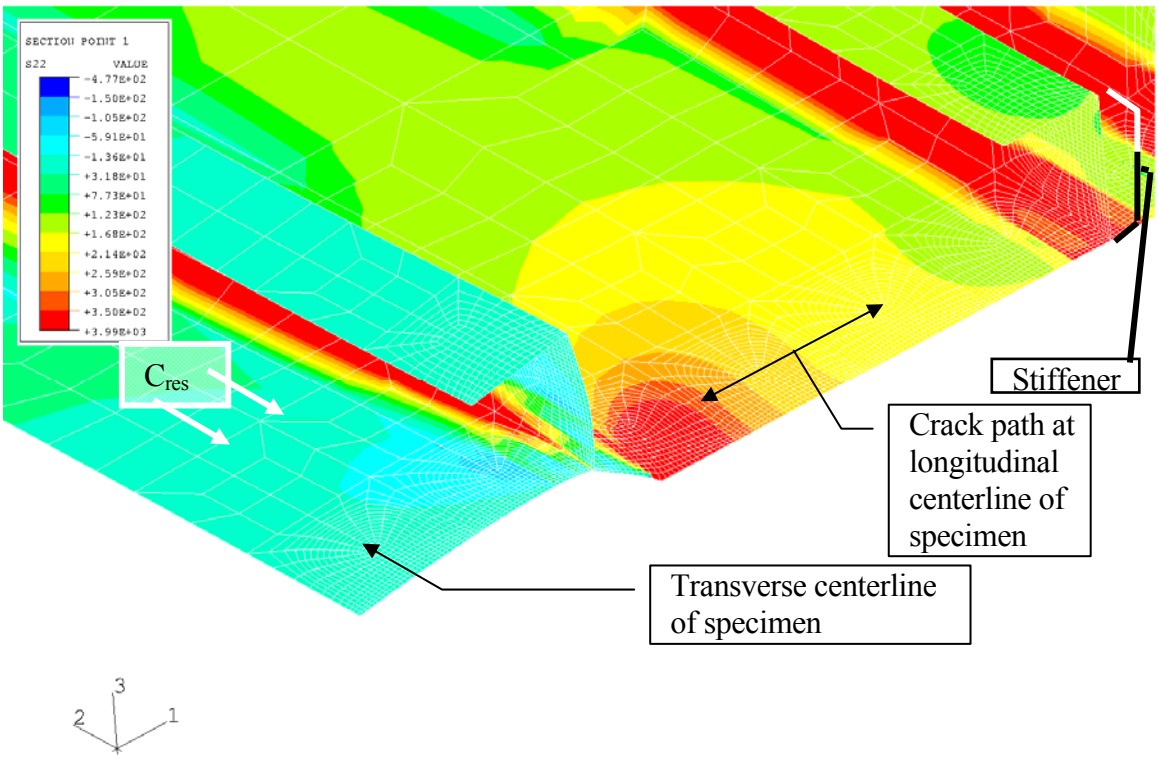

Figure 6-11: Closure effects on effective applied load for Case B.
(100x displacement magnification)

The crack tip was on the outer edge of a tensile residual stress zone, insuring that it would be open even without any applied external load. A region of compressive residual stress exists behind the crack tip. This compressive stress [behind the crack tip] affects the manner in which the crack opens and different results were obtained depending on whether or not gap elements were used. These differences are quantified in Figure 6-12, where K_{total} is plotted for various phases of load application.

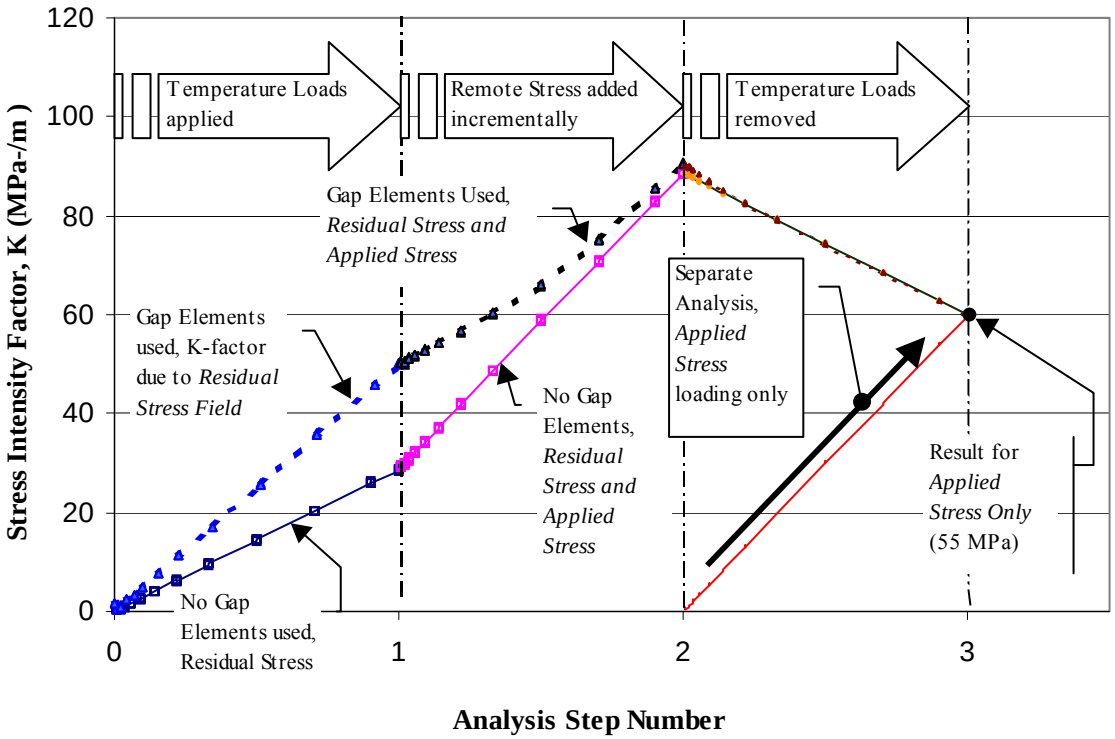

Figure 6-12: Stiffened panel analysis with closure behind crack tips.

Figure 6-12 represents an analysis made with the peak external loading producing 55 MPa of tension in the specimen. Comparing the analysis using gap elements to the one without gap elements provides insight into the merits of each. In the gap element analysis, no overlapping behind the crack tip has occurred and redistribution of residual stress has occurred due to the contact forces. For this reason, the K_{res} derived from a gap element analysis is higher than the analysis where overlapping is permitted. Overlapping, therefore, magnifies closure effects in the analysis without gap elements.

Now consider step two of the analyses. As external load is applied and tensile stresses are induced, the crack starts to open and both analyses converge at a point where closure disappears. The nonlinear behavior of the gap element analysis indicates that residual stress redistribution is more prominent in the model. In step three, the temperature loading is removed and hence the residual stress field as well. Removing the residual stress field results in no closure effects as pure tension exists in the panel. The fact that removing the residual stress field reduces K_{total} reveals that local

tensile residual stress (around the crack tip) was making a significant contribution to K_{total}. A separate analysis has been made without residual stress to show that the same $K_{applied}$ is obtained independently of the three-step analysis method.

One additional observation can be made in reference to Figure 6-12—that of superposition validity. Superposition is only valid in a F.E. analysis made without gap elements. The consequences of nonlinearity will be shown later in comparisons with the analytical model.

Deciding whether or not to use gap elements can now be addressed. The impact of choosing either type of analysis is best illustrated in Figure 6-13. Closure effects that increase the residual stress intensity factor have the effect of decreasing the possible ΔK_{eff}. The Paris Law is a function of the stress intensity factor range, and a smaller available ΔK_{eff} translates into a greater life prediction. While this investigation has isolated the case of closure behind the crack tips, its impact is dramatic on the overall prediction.

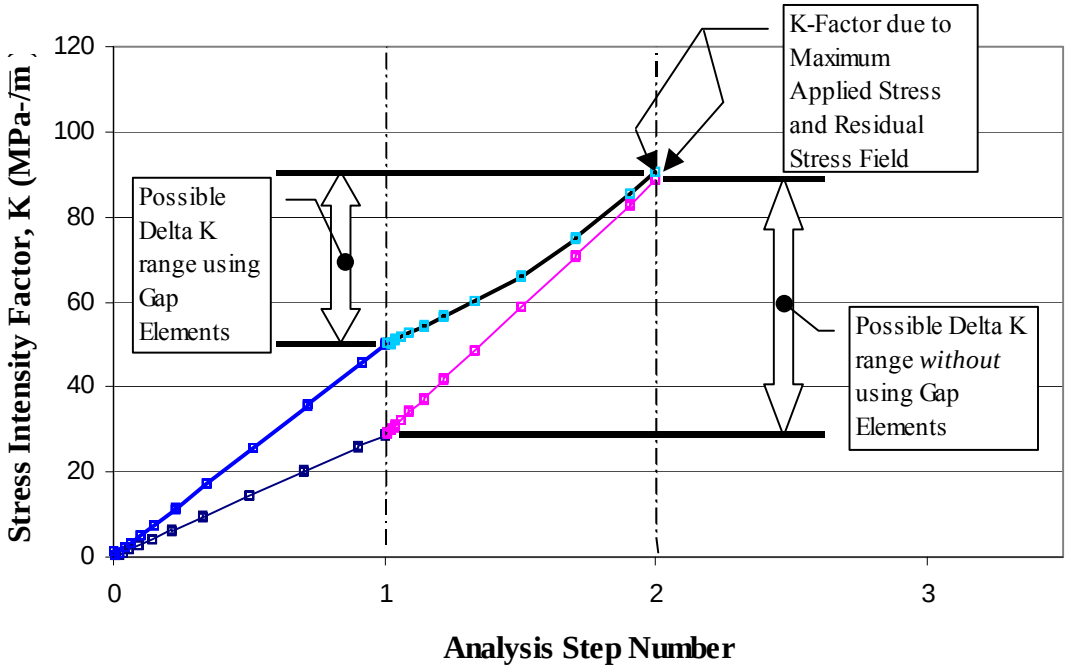

Figure 6-13: Effect of using gap elements in analyses.

Many argue that preventing overlap is the proper way to model cracking in residual stress zones. Specifying an initial gap of zero meters may be called into question. Justification lies in the observation that crack faces are usually jagged and slightly deformed. A perfect meshing of crack faces at the unloaded state is never the case. Instead, contact between crack faces occurs even at initial tensile loading of the structure. Crack tip plasticity after an overload will, of course, prevent contact of crack faces at the unloaded state. Considering the loading history is unrealistic, however, since the analysis already averages all natural variables (e.g. applied stress, material properties, etc.). In addition, it has been emphasized that fatigue crack growth in ship structure often occurs at low stress levels. Such low stress levels advocate low plasticity at the crack tip. For this reason, the initial gap of zero meters is suggested if one intends to model fatigue considering the contact of crack faces.

Is there a correct choice on the use of gap elements? The experimental predictions, presented in Chapter 8, will show better correlation without the use of gap elements. The lack of superposition validity is also a strong argument to not use gap elements in an analysis that is used for LEFM prediction. In addition, F.E. results obtained from an analysis without gap elements correlate well with the analytical model (See following chapter). Furthermore, the increased complexities of the modeling and increased analysis time make eliminating gap elements favorable. All of these reasons support not using finite element analysis. However, by eliminating gap elements caution must be exercised in making sure the correct opening load (See Figure 6-8) is obtained for all crack lengths. From the current research, it was inconclusive on whether or not gap elements should be utilized. Realistically, contact behind the crack tips should be negligible for cracks greater than one stiffener span. For this reason and because excluding gap elements is conservative, the recommendation is that they are not necessary if proper care is taken in assessing the sign of J (i.e., negative or positive).

There is a convenient way to extrapolate non-gap element results from an analysis that includes gap elements. This method is explained in Figure 6-14. First, an analysis with gap elements is performed with the loads applied in separate steps. This analysis will yield three values for K:

- $K_{res,\ gap}$ (Point 1)
- $K_{total,\ gap} = K_{res,\ gap} + K_{app,\ gap}$ (Point 2)
- K_{app} (Point 3)

The applied stress K, K_{app}, is the same whether or not gap elements are used (Point 3). This fact allows one to merely subtract K_{app} at point three from K_{total} of point 2 to yield the residual stress K that would be obtained from an analysis without gap elements.

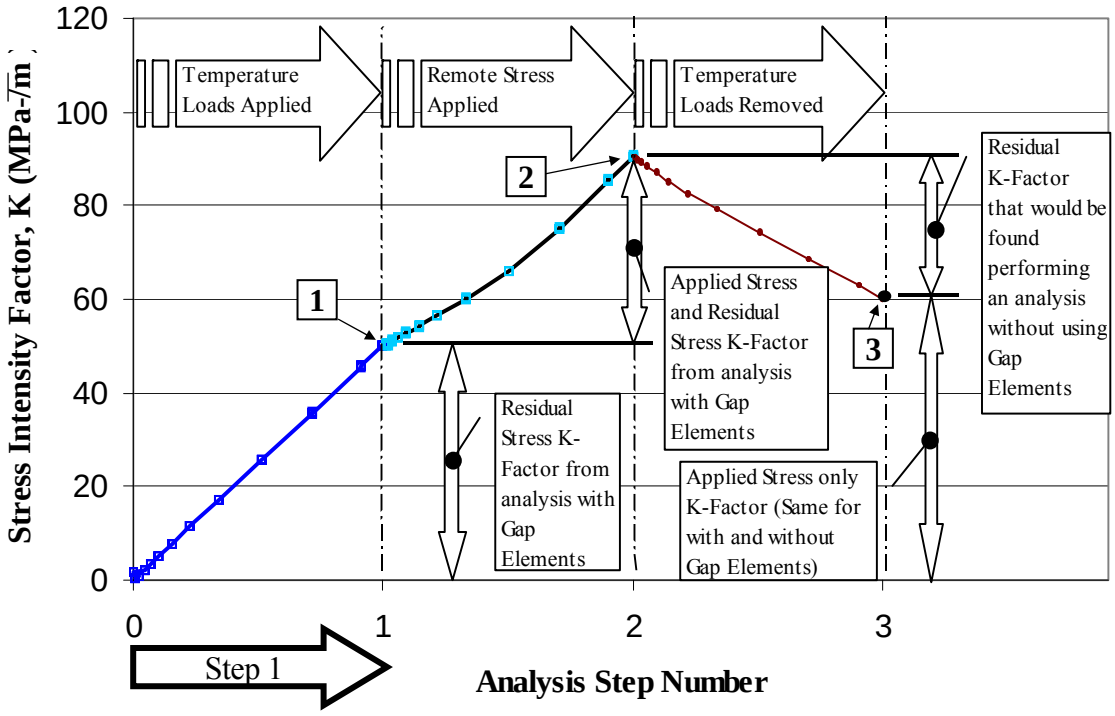

Figure 6-14: Extrapolation of superposition results from a single analysis.

A formal set of expressions clarifies the different obtainable values:

$K_{app,\ gap} = K_{app,\ no\ gap}$	where both values are at point 3
$K_{res,\ no\ gap} = K_{total,\ gap} - K_{app}$	where $K_{total,\ gap}$ is the value at point 2
$K_{res,\ no\ gap} \neq K_{res,\ gap}$	where $K_{res,\ gap}$ is the value at point 1
$K_{res,\ gap} \neq K_{total,\ gap} - K_{app}$	

An important requirement for this procedure to work is that all closure effects disappear at peak applied loading. Therefore, one should make the applied stresses large enough to remove any closure effects by the end of step 2.

Applying the loads incrementally has several advantages that will now become evident. Incremental loading allows the history of the J integral to be recorded at discrete values of applied load for a given crack length. The J value for any specific load may be obtained by first fitting the J history with a natural cubic spline. With little effort, accurate splines were formulated for over 450 step histories of J integrals. One such spline is seen in Figure 6-15. Use of the natural cubic spline has been very successful in comparisons with J integrals determined for the specified load in a separate analysis.

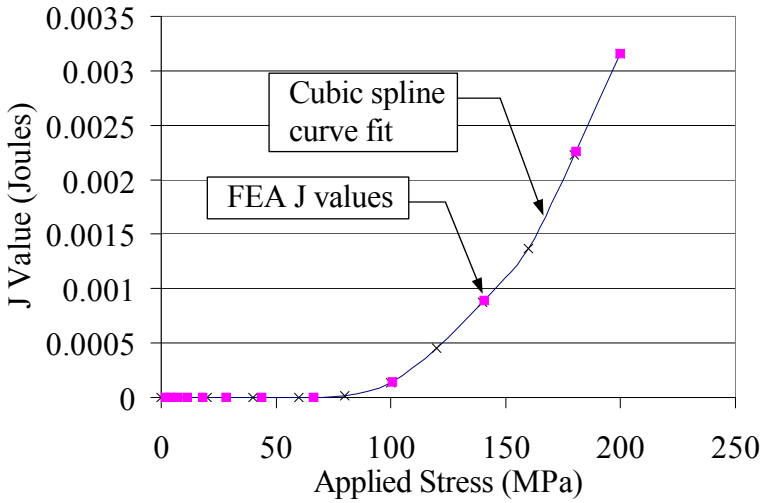

Figure 6-15: Cubic spline fit to incremental J values.

One could also take a simplified yet conservative approach by fitting a linear slope through the equivalent K values as performed by Nussbaumer. This works well for analyses that do not use gap elements because the slopes of K are linear. Either method of extrapolating an equivalent K provides the maximum and minimum values needed to calculate ΔK_{eff}. At this point the Paris Law may be used for prediction.

6.4 STIFFENED PANEL ANALYSES

The finite element model was developed as a tool to model fatigue crack growth in complex geometries. The modeling technique was verified through comparisons with the analytical modeling technique and textbook solutions, such as the CCT specimen in the previous section. This section will detail the implementation of the model as it was used for formulating equivalent K values in the stiffened panels.

A view of the typical mesh used in these analyses is seen in Figure 6-16. As in the CCT example, symmetry conditions were utilized to model only a quarter of the specimen. Element sizes were typically 12-mm square around the region of the crack line. Smaller element sizes (~5.5-mm) were required to compute converged J estimates in regions of high residual stress gradients. Such high residual stress gradients exist near the transition from compressive to tensile residual stress at stiffener weld lines. In addition, J convergence cannot be obtained close to stiffener/plate intersections. This is because the J integral is a two dimensional quantity.

The crack advancement between analyses should therefore be reduced when the crack is near a stiffener. The trend in J will then reveal any inaccuracies around plate/stiffener junctions.

Crack growth in the stiffeners is a difficult behavior to predict because a crack length must be known as part of the analysis. Therefore, the approach taken was exactly as was done in the analytic model where linear interpolation was used assuming equal crack growth rates in both the stiffener and the plate. Analyses were performed for crack lengths up to the complete plate width for three scenarios: No severed stiffeners, the first stiffener severed, and both stiffeners severed. The broken stiffener analyses were considered only in situations where the crack length was past the stiffener in question. The behavior was usually similar to the plot in Figure 6-17.

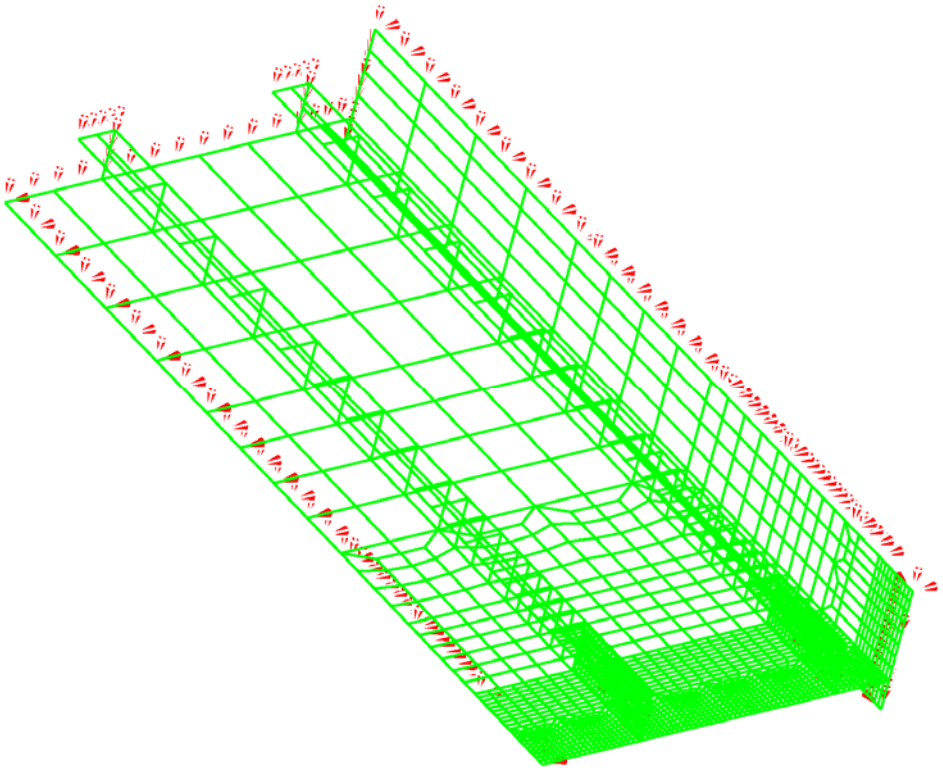

Figure 6-16: Typical mesh of stiffened panel.

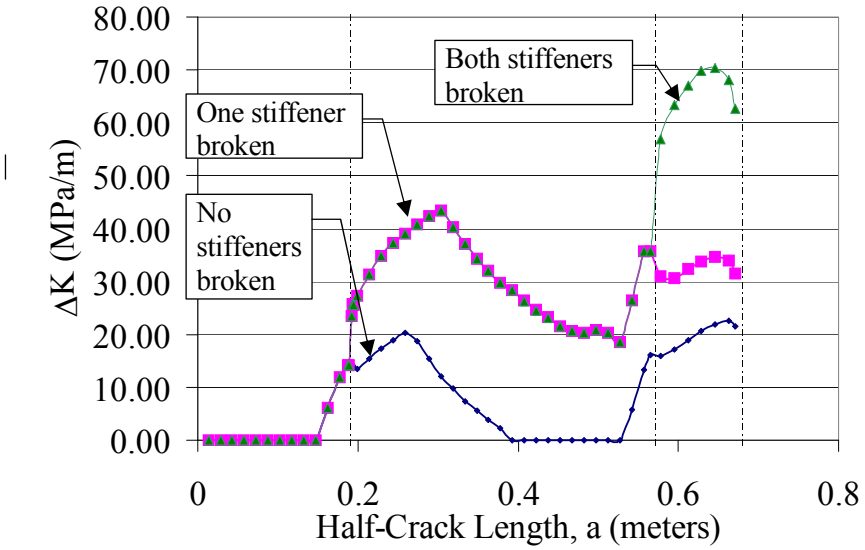

Figure 6-17: K_{total} for typical analysis of stiffened plate.

To create accurate residual stress fields, temperature gradients were applied to nodes near the weld line. A thermal expansion coefficient of 1.2 x 10^{-5}/ degree Celsius and an initial temperature of 25 degrees Celsius were used in defining the material properties. Iteration was required to find the appropriate temperature values, but it was found that cooling the material to a temperature (in Celsius) roughly equal to two-thirds the stress desired (MPa) produced an appropriate distribution. An upper bound residual stress field was obtained by applying the following temperature profile to the nodes within 3.5 times the plate thickness from a weld line.

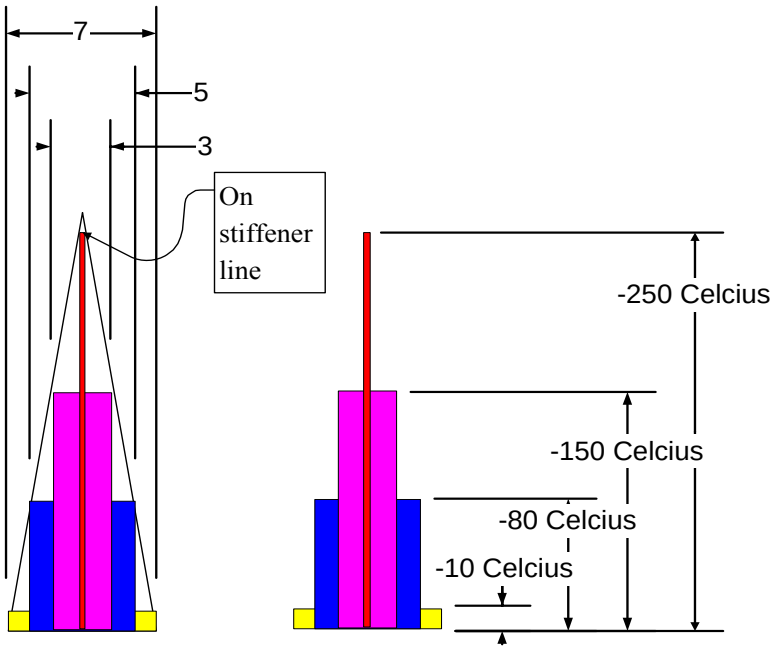

Figure 6-18: Temperature distribution applied to weld lines.

All nodes within a distance specified by the drawing on the left were applied the corresponding temperatures on the right drawing. The distances given are multipliers of the plate thickness. By using this methodology a good approximation to welding residual stresses can be created.

Compressive residual stresses were essentially constant at a value of –70 MPa between tensile regions. Tensile stresses along weld lines sometimes exceeded the yield strength of the material by

40 MPa, but this discrepancy was deemed acceptable. A view of the residual stresses imparted on a typical specimen may be seen in Figure 6-19.

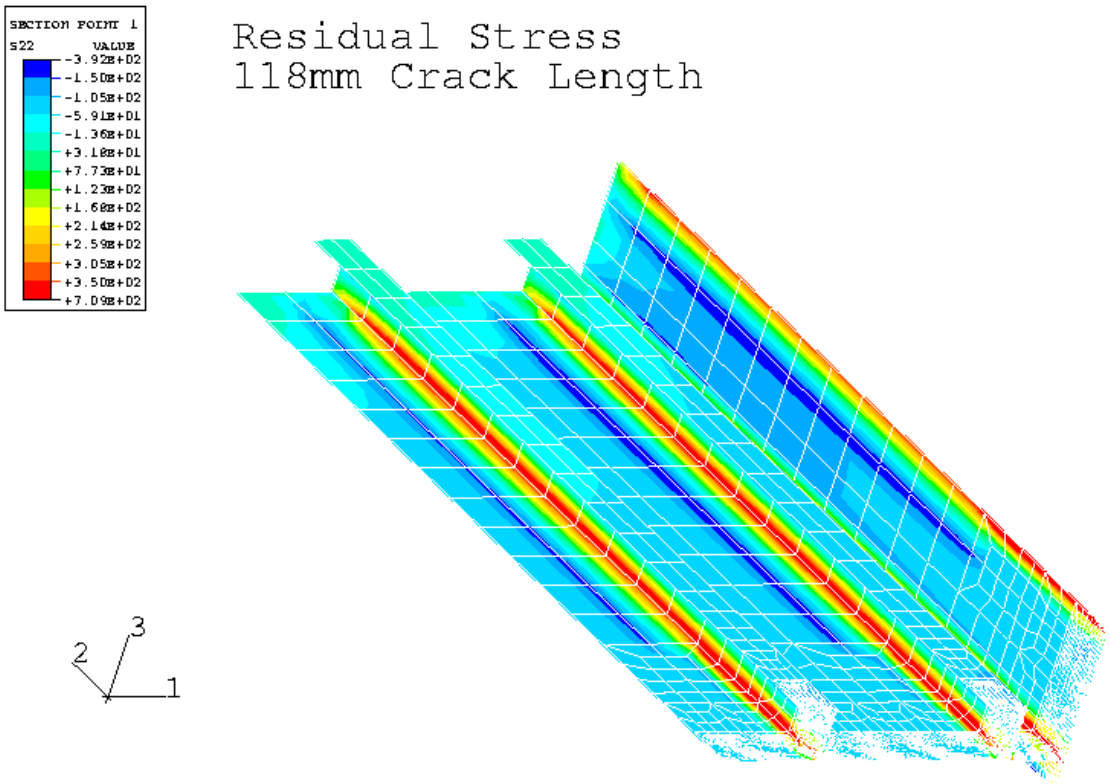

Figure 6-19: Typical residual stress distribution created in specimens.

Comparisons were made between applied displacements and applied stresses. As expected, equivalent K values were progressively less than those of the applied stress analyses. The stagger is especially noticeable when stiffeners are severed as may be seen in Figure 6-20. Here the equivalent K values have been normalized by the CCT K equivalent for the crack length. Also, the crack distance has been normalized by the stiffener spacing.

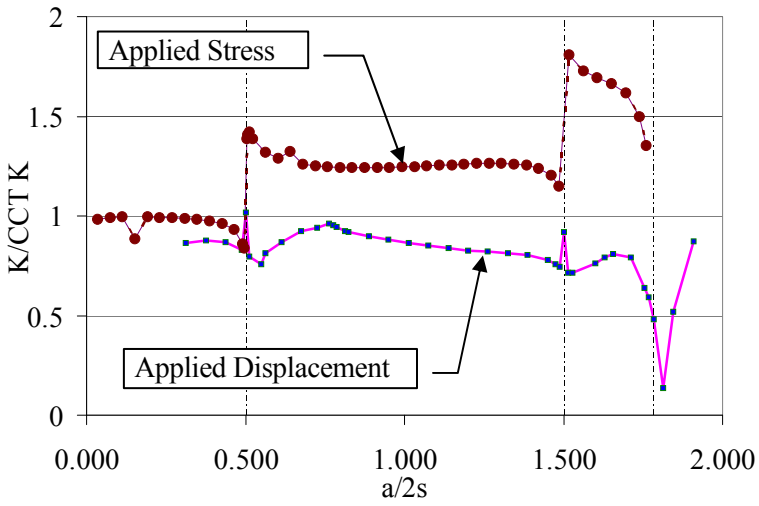

Figure 6-20: Applied stress verses displacement results in Case 1.

One may notice a few data points that deflect from the any smooth path. It should be expected that inconsistent J's will be found at times even with mesh refinement. It is therefore important to combine a number of crack length analyses with plotting, such as the above figure, to realize any discontinuities.

7 Differences Between Analytical and Finite Element Models

7.1 INTRODUCTION

The finite element model was developed as an alternative to the simpler analytical model. Comparisons were made to verify both models would produce similar results under similar testing variables. This chapter explains the comparisons made and details the pros and cons of each model.

7.2 APPLIED STRESS INTENSITY FACTOR COMPARISONS

The basis for both the analytical and F.E. model is the ability to predict the applied stress intensity factor. The applied stress intensity factor is the same whether gap elements are used or not in a F.E. analysis. Figure 7-1 demonstrates the applied stress intensity factor for both maximum and minimum stress in the specimen with solid stiffeners, case 1.

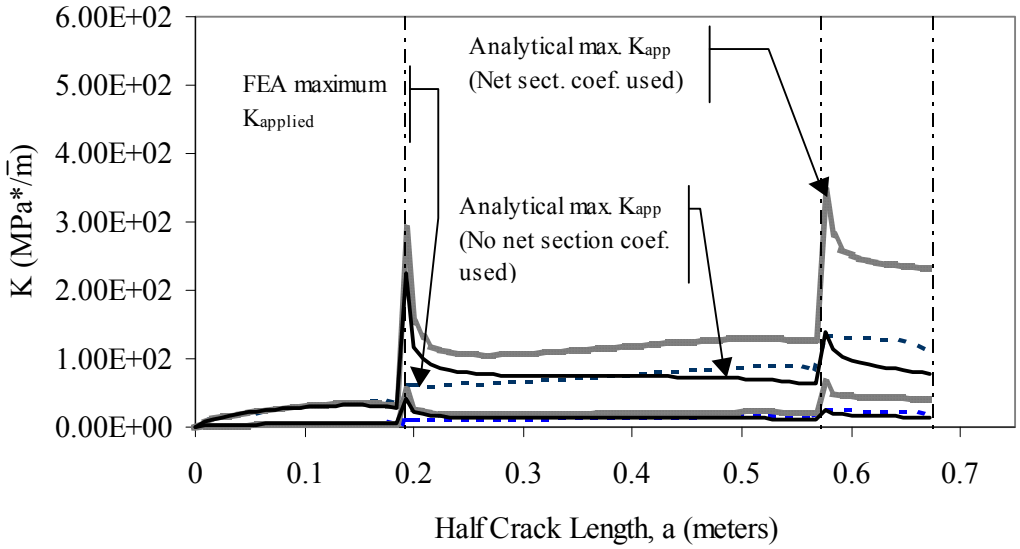

Figure 7-1: $K_{app,max}$ and $K_{app,min}$ for both finite element and analytical models, immediately severed stiffeners.

This plot depicts the assumption that the stiffeners are severed immediately once the crack has reached them. Only the maximum K_{app} curves have been pointed out to prevent clutter in the figure, but the type of line is held constant in the minimum K_{app} curves. Better agreement between the analytical and finite element models is obtained if the net section coefficient is not used in the analytical model. This characteristic will be noted in many of the comparisons.

Interpolation between intact and severed stiffeners is seen in Figure 7-2. Here the results shown in Figure 7-1 have merely included the assumption of equal growth rates in the stiffener and the plate.

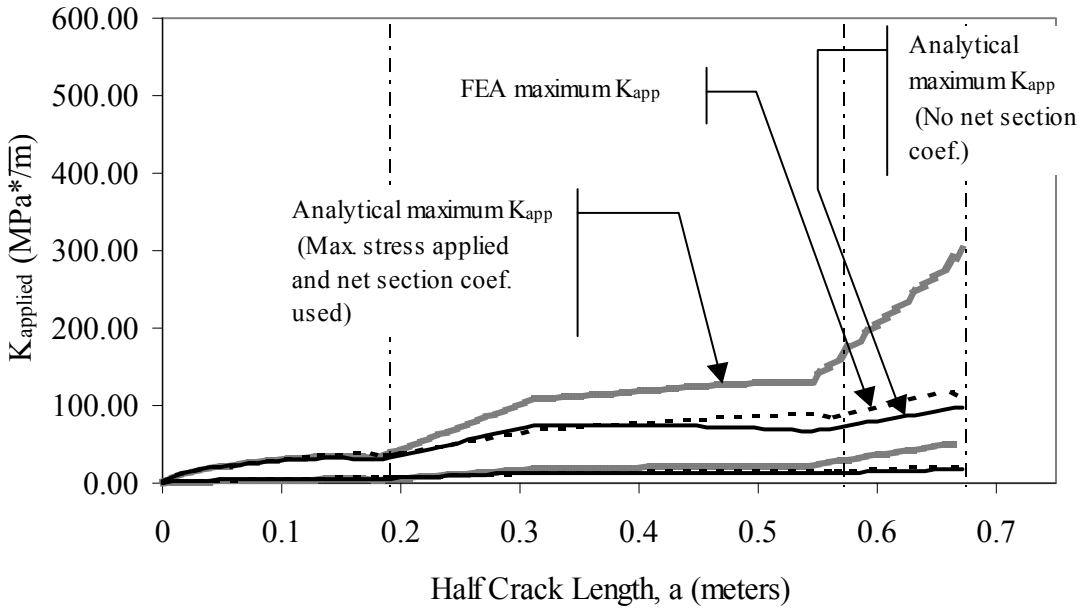

Figure 7-2: $K_{app,max}$ and $K_{app,min}$ for both finite element and analytical models, stiffener interpolation used.

These comparisons show that good duplication between the analytical and finite element models exist without residual stresses included.

7.3 RESIDUAL STRESS INTENSITY FACTOR COMPARISON

The next comparison made was that of the residual stress intensity factor. The residual stress intensity factor showed the most scatter between models. Varied results were attained between the models, and therefore a more in-depth study was made concerning the overall effects on K_{total}. Figure 7-3 shows the different curves that comprised the study.

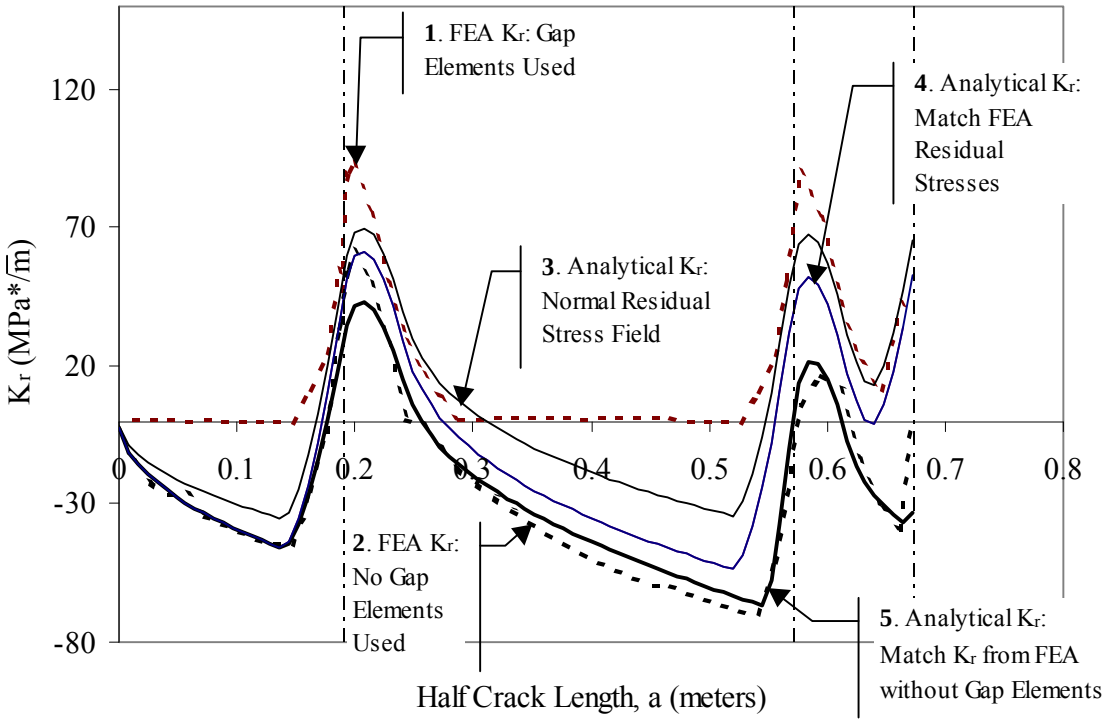

Figure 7-3: K_r for both finite element and analytical models.

The study included the following components:

1. The finite element K_r obtained using gap elements and upper bound residual stress.
2. The finite element K_r obtained without gap elements (Extrapolated from the gap element analysis with upper bound residual stress).
3. K_r from an analytical model using a typical Faulkner residual stress determination.
4. K_r from analytical model using the same residual stress distribution input into the finite element models (F.E. upper bound residual stress)
5. K_r from an analytical model that matches K_r from number 2. Iteration was used to determine the residual stress distribution necessary in the analytical model to reproduce the K_r derived in study point two.

Figure 7-3 has several characteristics that may be immediately observed. First, Kr from 1 never becomes negative. This is because the gap elements were specified with an initial gap of zero meters. Consequently, J remains zero in compressive residual stress regions until sufficient external load is applied to separate the crack faces.

In the F.E. analysis without gap elements, curve 2, J values and subsequent K_r values were determined by subtracting K_{app} from K_{total}. Recall the criteria that, in order to perform this extrapolation, the external load must at least match the opening load before K_r can be obtained. It is not clear why this K_r differs significantly from K_r in 1), and so both K_r values were studied in their correlation with the analytical model.

Analytical modeling provided residual stress intensity factors that corresponded well within the range suggested by both F.E. analyses. When the residual stress distribution that was created in the finite element analysis was used in the analytical model, a Kr resulted (Curve 4) that averaged both finite element analyses. Increasing the residual compressive stresses in the analytical model allowed curve 5 to be formulated. Finally, curve 3 shows that K_r obtained by using Faulkner's residual stress distribution provides an average K_r curve that emulates the gap element K_r quite well. The Faulkner residual stress distribution is what would normally be used in a standalone analytical model, where residual stress values are not obtained in connection with F.E. modeling. The excellent correlation with the finite element K_r curves promotes its use as a simplification to the more complex F.E. modeling.

7.4 TOTAL STRESS INTENSITY FACTOR COMPARISONS

Minute differences in K_r and K_{app} between the models have been very acceptable in the results presented so far. The additive effects of these differences are seen in comparing K_{total} for the various analyses. Figure 7-4 plots each K_{total} curve for direct comparison.

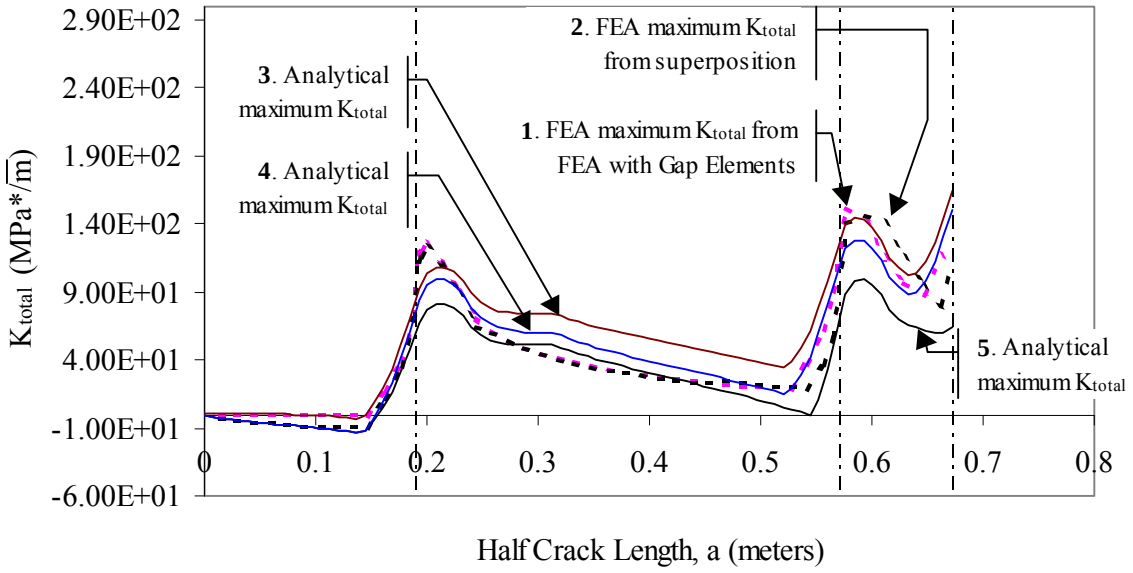

Figure 7-4: K_{total} for both finite element and analytical models.
(Analytical results do not include a finite width correction.)

No finite width correction was used in the analytical curves. Good agreement seems consistent throughout the models plotted in Figure 7-4. However, small variations in K_{total} are cubed in the Paris Law, so it is important to correctly identify which curve is most appropriate. For example, curve 5 would predict cracking stop altogether at 545-mm while the other models do not indicate this drastic a reduction in K_{total}.

Degraded correlation is seen when the net section coefficient or other finite width correction is used in the analytical model. Figure 7-5 shows the increased K_{total} values in the analytical model.

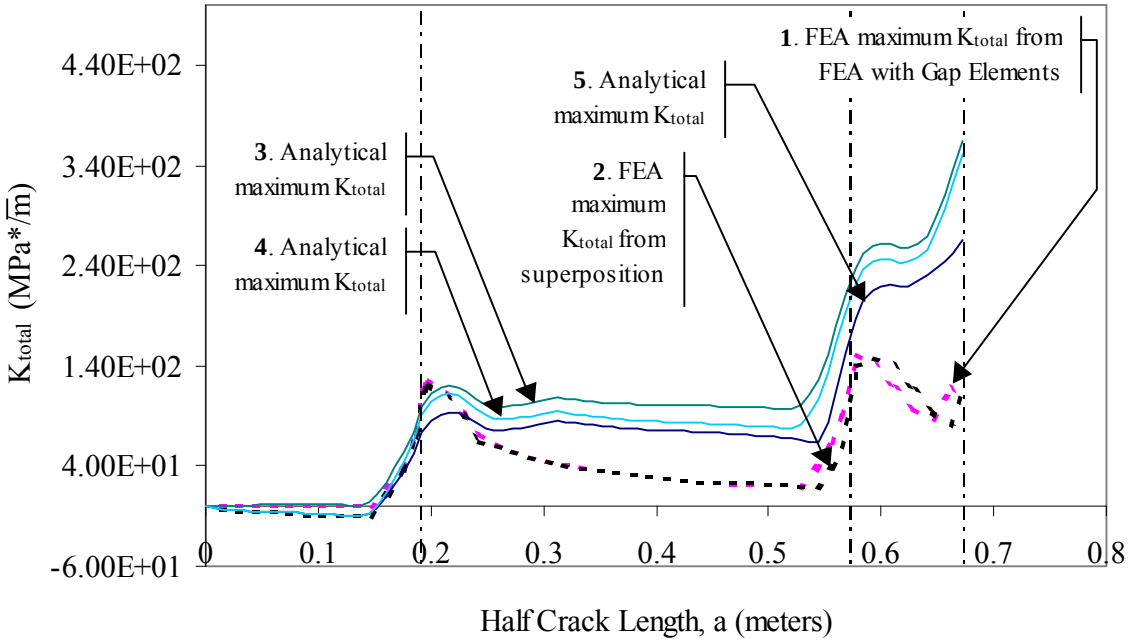

Figure 7-5: K_{total} for both finite element and analytical models.
(Finite width correction included in analytical models.)

7.5 STRESS INTENSITY FACTOR RANGE COMPARISONS

Comparing ΔK provides the most direct view of discrepancies between F.E. and analytical modeling. The comparison is also the most significant because these values are cubed in the Paris Law for crack growth prediction. Two figures are put forth to demonstrate the results: Figure 7-6 plots ΔK_{app} and Figure 3-12 plots ΔK_{eff}. Once again it may be seen that the net section coefficient decreases the compliance between the models.

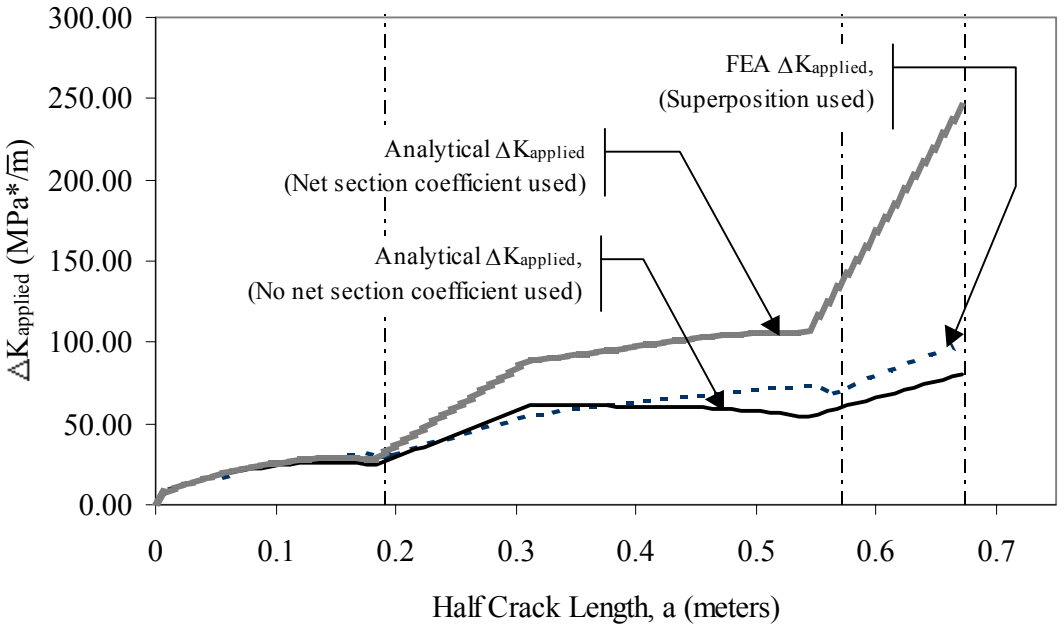

Figure 7-6: ΔK_{app} for both finite element and analytical models.
(Analytical results do not include a finite width correction.)

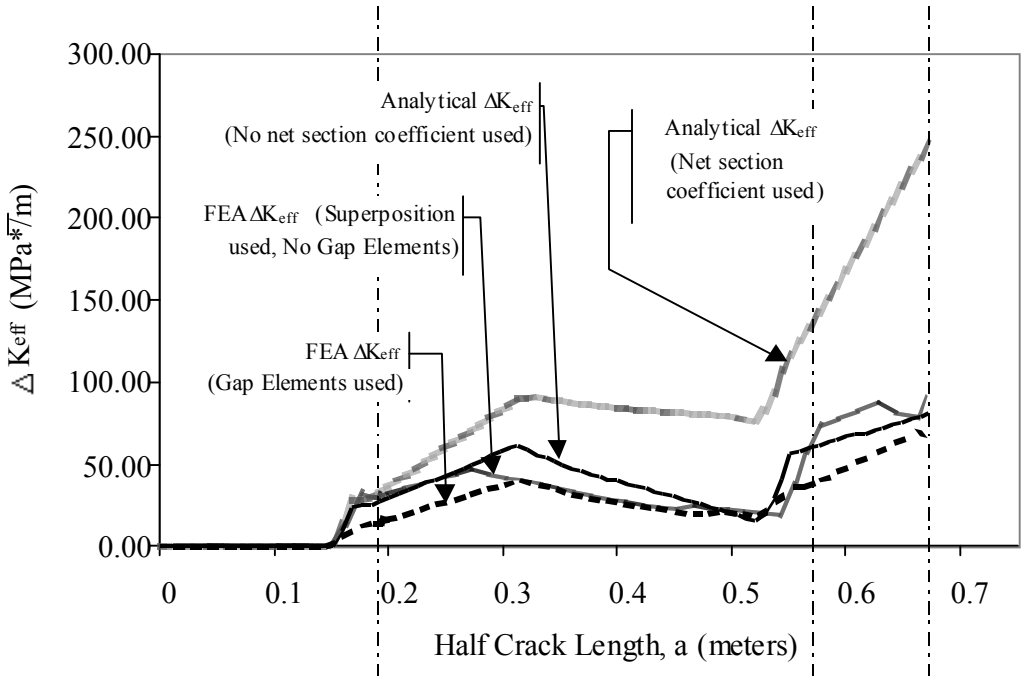

Figure 7-7: ΔK_{eff} for both finite element and analytical models.
(Finite width correction included in analytical models.)

The increase in error caused by including the net section coefficient is difficult to explain. One reason may be that the increase in net section stress is not realized until the full panel width is cracked and a crack has entered the edge web. The edge web might be providing sufficient restraint to reduce the effects of increased net section stresses. This uncertainty should be investigated further, but the true test of the models is their ability to predict the experiments.

As will be seen in the next chapter, experimental comparisons support neglecting the finite width correction. However, the net section correction for cracks in ship hulls will likely be very close to unity for even long cracks. For this reason, it could be used to add an increased factor of safety to one's predictions.

8 Prediction Success with Experimental Cases

8.1 INTRODUCTION

Previously it has been shown that the analytical model can readily be used to obtain the same results as the finite element model. This fact was taken advantage of in refining the analysis to produce better results. For example, instead of re-running a complete set of F.E. analyses with a different residual stress field the analytical model was used with the new residual stress field input. The result was then obtained in three minutes as opposed to several days of running F.E. analyses and J value interpolation.

Many variables affected the predictions made in the stiffened panels. Correlation between the analytical and finite element model alone required a number of investigations to be made. These investigations led to observations that were necessary to develop a cohesive set of results under the same conditions. The same procedure will be taken in the following sections.

It is not enough to show the final results and expect an individual to reproduce them under the same conditions without certain error. Therefore, the focus of the predictions will be the revisions made to achieve good results. With this approach, one will learn the correct procedure while avoiding the pitfalls that had occurred in developing the current final results.

8.2 BASELINE SPECIMEN

Determining the applied stress ranges and values is the most significant source of error in prediction accuracy. Such difficulty was realized early on in baseline case predictions. The initial predictions were made using the average of the three strain gages mounted at 76-cm. from the crack line (See Figure 3-7). These predictions, shown in Figure 8-1, indicated that the correct uniform stress should be higher and within the constant moment region of the experiment configuration. Good correlation with the experiments was obtained using a uniform stress as indicated in Figure 3-8.

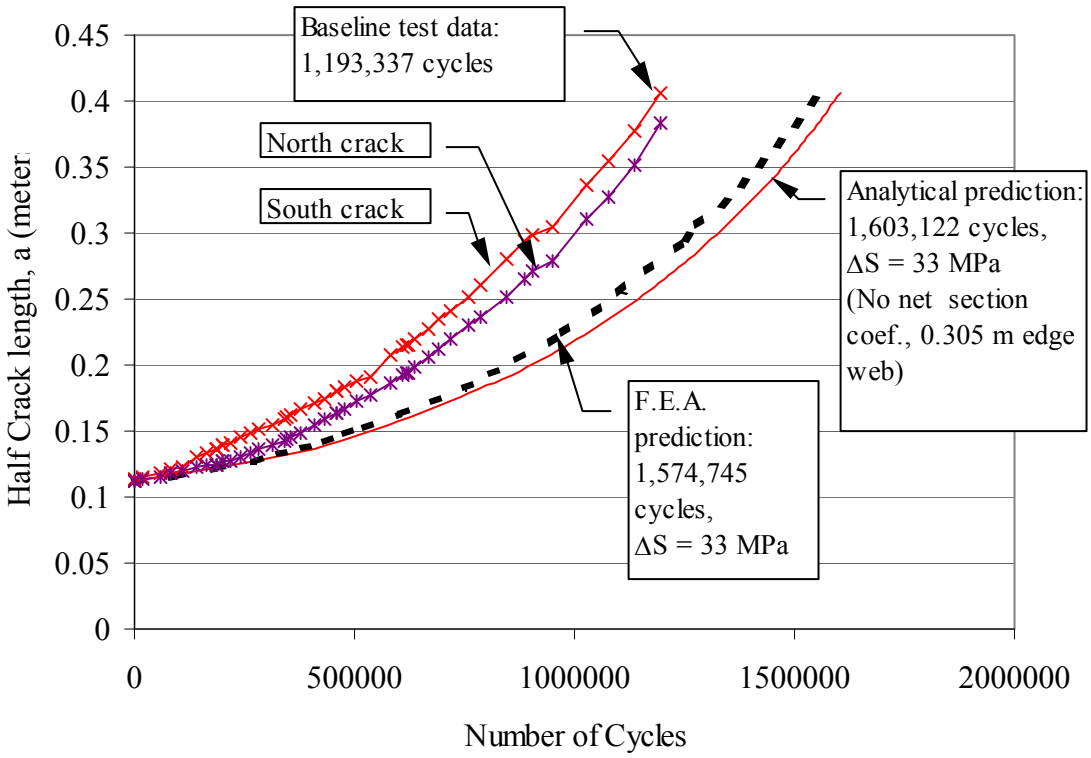

Figure 8-1: Initial predictions made for baseline test specimen.

This location of stress monitoring was used for the remainder of the experiment predictions to prevent bias in one prediction over another. The prediction based on the final stress measurement point is shown in Figure 8-2.

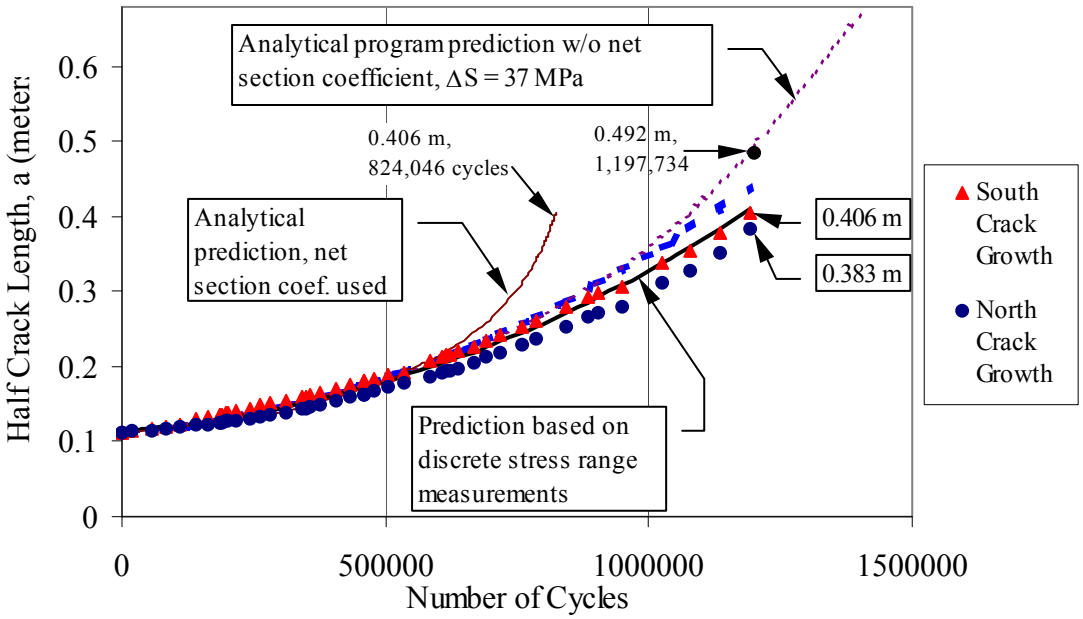

Figure 8-2: Final predictions made for baseline test specimen.

Note that use of a finite width correction dramatically skews the accuracy of the prediction. The finite width correction is seen as the only contributor to the error, because the error becomes exponentially larger as the crack becomes larger. If the error were due to improper stress definition, the deviation from the experimental results would be consistent from the initial crack lengths.

The excellent correlation in the baseline case demonstrated that a uniform stress could be used to predict crack growth in a plate with large stress gradients. Additional modeling was done to try to directly use the measured stress gradient for predictions, but no improvement in accuracy was attainable. In fact, using the low stress values at the interior of the plate predicted low initial growth rates while the stress values at the exterior of the plate predicted the higher than observed final crack growth rates. Therefore it is recommended that a uniform stress be used to represent a stress gradient across a plate or stiffened plate. The location to measure this uniform stress should be near enough to the crack line that little increase in stress would be expected to be seen at the crack line. In other words, the stress should be taken as the stress acting on *that* cross section and not a true "remote stress" as the analytical formulations theoretically apply to.

8.3 CASE 1: SOLID STIFFENERS

Many analyses are presented in Figure 8-3 that attempt to duplicate the test behavior. Prediction A was made using a F.E. analysis without gap elements and compressive residual stress of –70 MPa between weld lines. A similar result was obtained with the analytical model by matching the F.E.A. K_r (Curve 5 of Figure 7-3) and using the net section coefficient. This curve is shown as Curve B. Curve D was obtained by repeating the analysis used in Curve B with the exclusion of the finite width correction. There is significantly better accuracy obtained by removing the net section coefficient. The unconservative growth rate exhibited in curve D is attributed to the high compressive residual stresses and subsequent K_r used in the analysis.

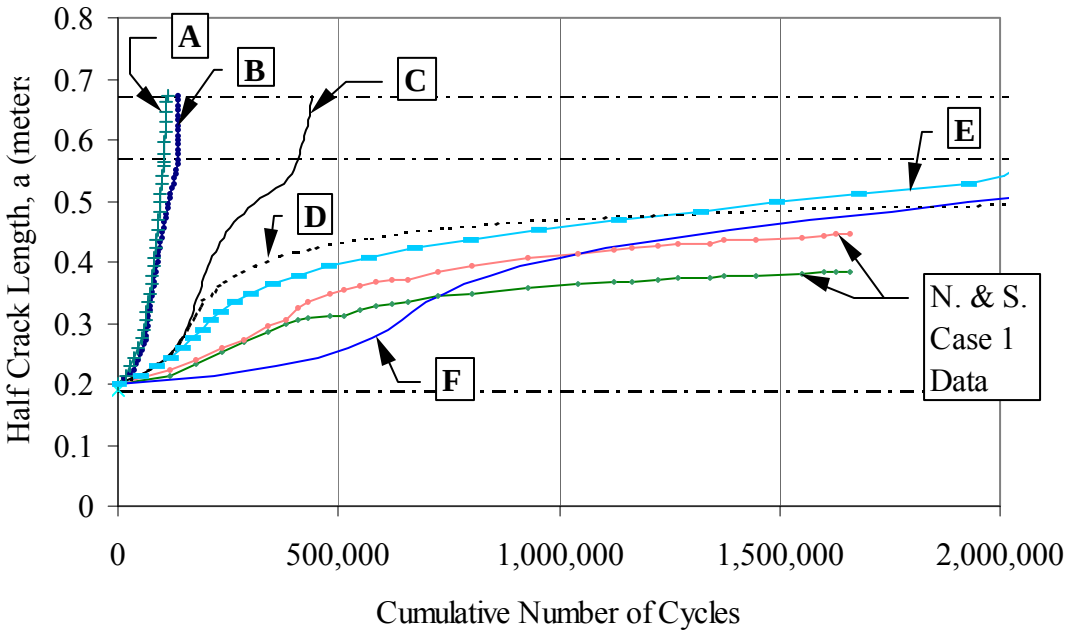

Figure 8-3: Predictions made for Case 1: Solid Stiffeners.

Prediction C is the normal analytic model prediction. It uses Faulkner's method of specifying the residual stress distribution with a triangular tensile region equal to 3.5 times the plate thickness. It is felt that this result would be very accurate had the plate been uniformly stressed without the steep gradient as seen in Figure 3-8. Low stresses in the stiffeners were also reported, and these likely promoted slower crack growth than would be present in a uniformly stressed panel.

Curve E is the result of finite element analyses made with gap elements and the assumption that stiffeners were immediately severed. In contrast, curve F represents the same analyses with the exception that linear interpolation was used between an unbroken and broken stiffener scenario.

Of these analyses, prediction C is the most recommended. It is the analytical model that incorporates a simple estimation of the residual stress and does not include the net section correction. Had the finite element analysis been performed with lesser residual stress magnitudes this curve would have been reproduced well. The testing of this specimen ended with cracking in remote regions of the specimen. The remote cracking, in combination with the large stress gradient, support using this conservative approach to estimate crack growth in situations where a larger structure provides a more continuous force transfer into the full stiffened plate section.

Cases two and three produced more uniform testing results and were not affected by any remote cracks and subsequent loss in applied stresses. For these reasons, more accurate modeling was justified and the stress gradient was directly accounted for.

8.4 CASES 2 AND 3: STIFFENED PANELS WITH CUTOUTS

Cases two and three of the experimental study gave very similar results. Consequently, refinement in the modeling could be achieved with greater certainty that the behavior could be expected in real structures. A progression of different analyses will be shown to arrive at the recommended modeling technique.

The first predictions demonstrate the inadequacy of simple rule-of-thumb coefficients applied to the CCT K. The CCT DK was used without a finite width correction to produce the results shown in Figure 8-4. Rolfe's reduction factor for multiple stiffeners was applied to the same CCT ΔK and produced highly unconservative predictions.

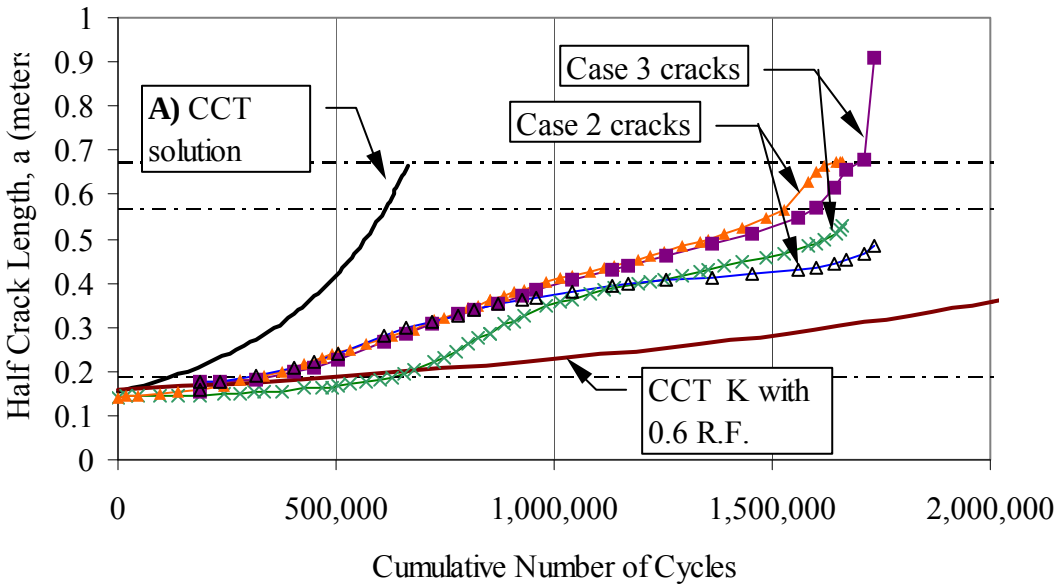

Figure 8-4: Predictions based on simple CCT ΔK without finite width correction.

The next plot, Figure 8-5, demonstrates the differences obtained in finite element modeling. By using gap elements in the finite element analysis, prediction H was made. Excluding gap elements and using simple addition of F.E. K_r and K_{app} values resulted in curve I. Both of these prediction methods showed that the compressive residual stress was retarding crack growth too much. Therefore, the residual stress distribution was reduced by five percent. This reduction brought compressive stress to a constant value of -66 MPa between weld lines. The effect of the residual stress reduction is seen in curve F.

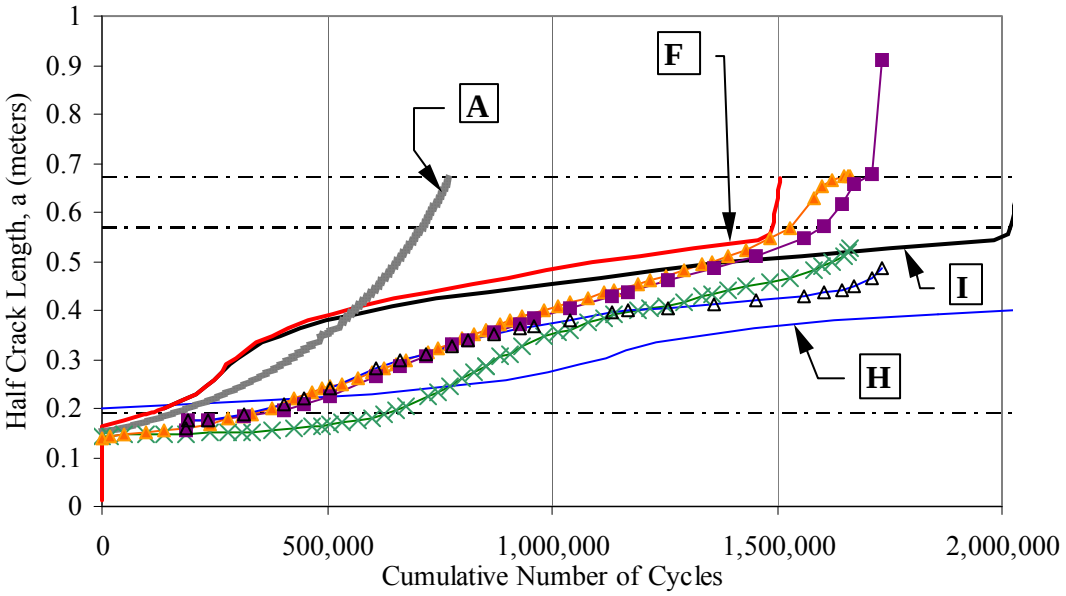

Figure 8-5: Predictions based on F.E. analyses with and without the use of gap elements.

The finite element predictions generally exhibited poor reproduction of the experimental data shape. Finite element modeling is only effective if valid input is specified, such as accurate applied stressed. It was hypothesized that the poor curve appearance was attributable to both low stresses seen in the interior stiffeners and lack of restraint effects in the all the stiffeners. An investigation was conducted on this speculation to improve the prediction curve appearance. Since the analytical model duplicated the finite element model results well, it was used as a quick means of representing results that would be obtained had either model been used.

The lack of stiffener restraint on crack growth was the first modification addressed. It directly addresses observations of Petershagen and Fricke, where they reported that the stiffeners with cutouts were ineffective in slowing down an approaching crack tip. This behavior was confirmed when observing the experiments involving stiffeners with cutouts. The F.E. analyses verified that there was virtually no decrease in K as a crack approached a weld access hole. The finite element method did, however, predict decreasing K-values in the case of solid stiffeners.

A better understanding of crack retardation due to geometry may be obtained by taking a closer look at the plate/stiffener interface. It is intuitive that a rathole would hinge more easily than a continuous stiffener. This is seen in Figure 8-6. However, since the crack propagates into the solid stiffener readily, the benefits of slowing down a running crack are limited.

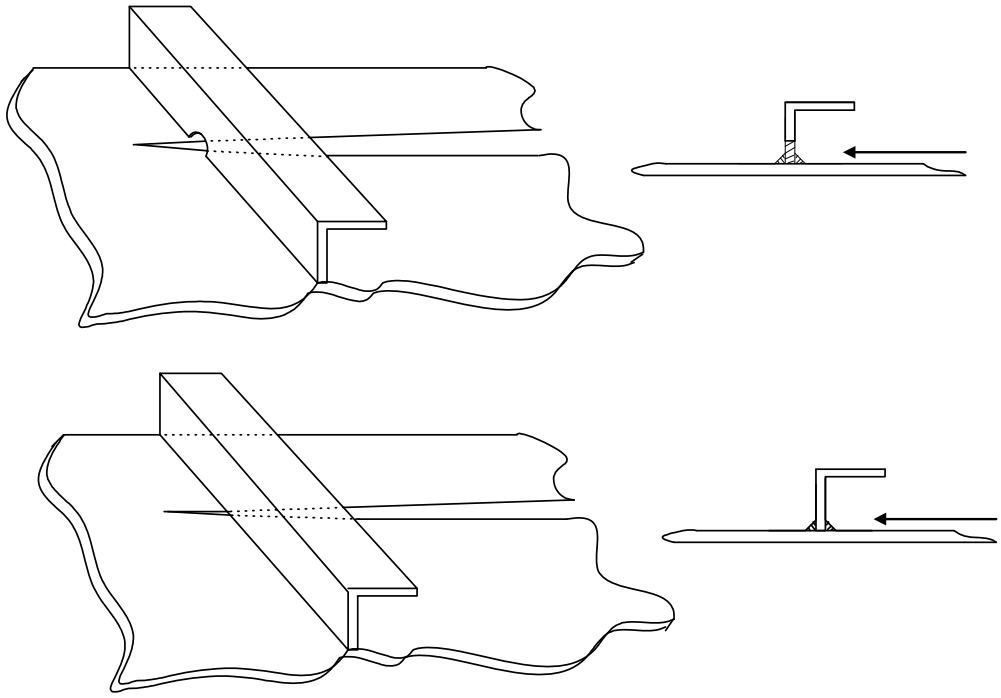

Figure 8-6: Effects of geometry on crack opening.

To accommodate the lack of stiffener restraint in panels with cutouts is relatively easy. All that is necessary is to set the f_1 coefficient to zero. This will eliminate any contribution of the first effect discussed in Section 5.2 found on page 96.

Modeling the low stress in the stiffeners was considered next. An appropriate modification that could be made to the model was reducing the force imparted by a severed stiffener. Recall that the effect of a severed stiffener in the model is treated as a pair of splitting forces on the crack line. To reduce the magnitude of the splitting forces, the thickness of the stiffener was decreased. A smaller stiffener area translates to a smaller amount of force that the stiffener is responsible for, and the modification effectively represents a stiffener with lower stress than the plate. One can accurately

model different stress levels in many stiffeners by specifying a ratio of the stiffener stress to the plate stress.

These changes were made to the analytical model and the results may be seen in Figure 8-7. Curve E was made using an exterior stiffener stress ratio of 0.68 and an interior stress ratio of 0.16. These ratios were determined from strain gage readings from atop the stiffener webs in the uncracked specimen. By lowering the interior stiffener stress ratio to 0.13 even better correlation was obtained, as seen in curve J. Both curves E and J were generated with the analytical model neglecting the f_1 coefficient and the net section correction. They illustrate that the analytical model can be very precise if the true stress distribution is known. Furthermore, shear lag effects in the stiffened panel may be accounted for by specifying only the individual stiffener stress ratios and an approximation to the uniform plate stress.

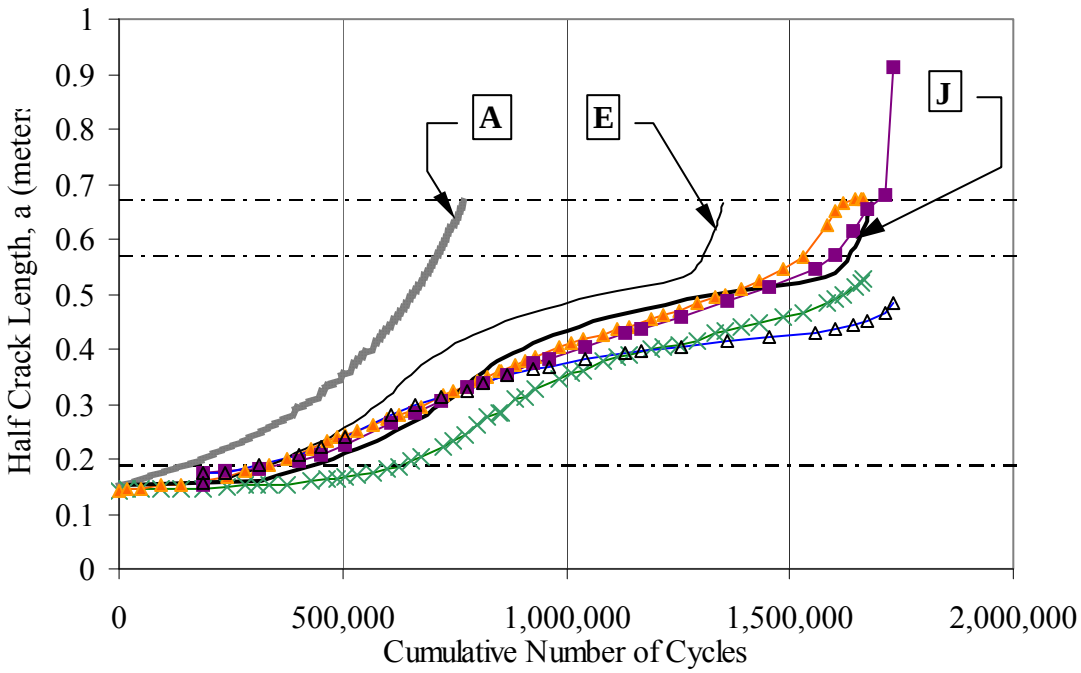

Figure 8-7: Refined analytical modeling.

The results of Figure 8-7 show much promise for the successful modeling of fatigue crack growth in stiffened panels. Curve E doubled the prediction life estimate made by curve A, the CCT ΔK prediction. The modifications to the analytical approach could easily be duplicated in finite element

modeling by changing the uniform stress applied to the stiffeners into a more realistic applied stress. The uniform stress should still be applied to the plate, however, because analyses that directly used the stress gradient underestimate crack growth rates while the crack length was less than one stiffener spacing.

For comparison, the ΔK_{eff} values for many of the predictions made for case two and three are shown in Figure 8-8. Data points in the figure represent extrapolated ΔK_{eff} values from the experimental data.

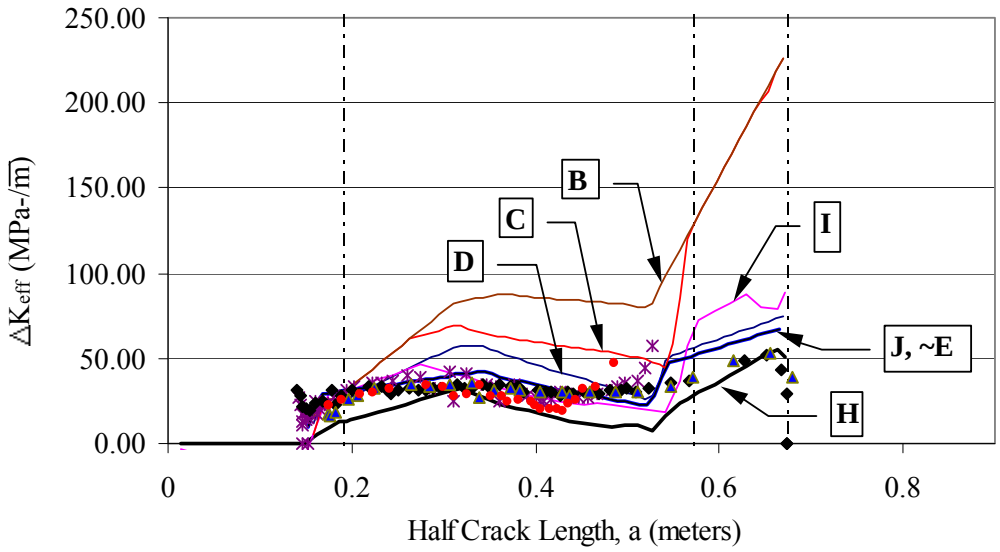

Figure 8-8: ΔK_{eff} for various prediction methods in cases 2 and 3.

Now that an appropriate modeling technique has been defined, it is important to look at some precautions that should be made in such an analysis. The first and most important precaution is to use either a good estimate of the actual stress range or a slightly conservative estimate. The stress range affects the final cycle count tremendously and if one wishes to obtain an accurate or conservative measurement, due care should be exercised. Secondly, analyzing several starting crack lengths is essential—especially for situations where the initial crack length may be affected by compressive residual stresses. To illustrate, consider Figure 8-9. Curve G was made using the actual starting crack length of 316-mm., where the crack was theoretically located in a compressive residual stress zone. This theoretical value of residual stress exceeded the actual residual stress

distribution and caused extremely low ΔK_{eff} values to be obtained. Consequently, the prediction made gave an extremely high number of cycles necessary to propagate the crack a short distance. On the other hand, using an initial crack length of 322-mm, in the exact same analysis, resulted in the prediction seen as curve C.

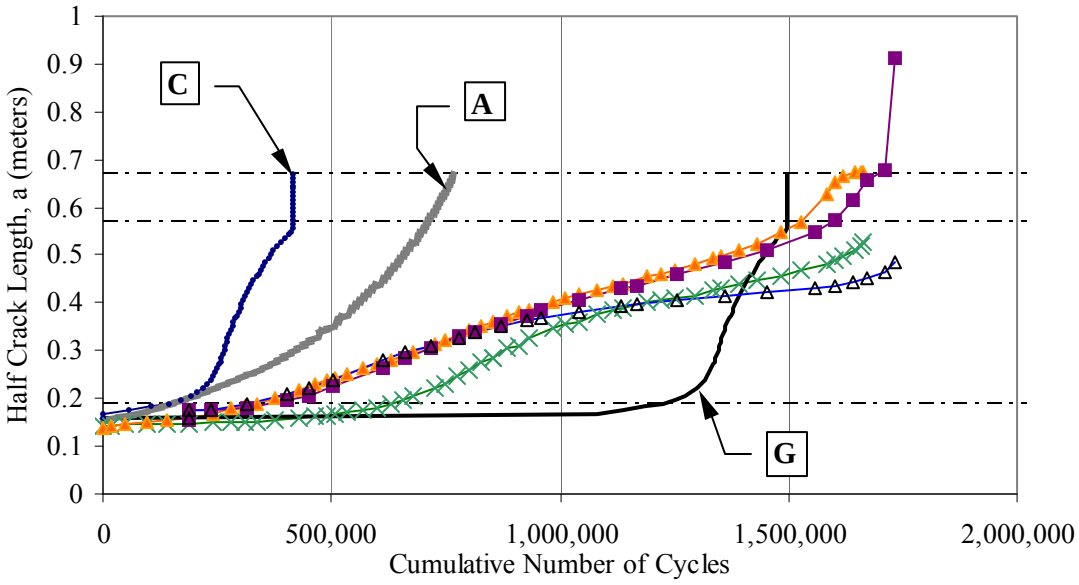

Figure 8-9: Possible prediction variation for cracks growing out of initial residual stress zone.

The wide range is not an error in modeling procedure. Rather, it illustrates that the variability in residual stress may cause limited success in small crack growth estimates. A small crack growth estimate in the course of this study means a crack less than one stiffener spacing in length. To alleviate any unconservative estimates for small cracks, one could set the compressive residual stress in the first stiffener span to zero.

8.5 CASE 4: STIFFENERS WITH CUTOUT AND MASTER BUTT WELD

Case four showed accelerated crack growth more typical of a plate specimen than a stiffened panel. Therefore, predictions were appropriately made by using variations on the simple CCT stress intensity factor without accounting for any residual stress interaction. Curve A was made using a finite width correction factor and a stress range as determined in the same fashion as developed in

section 8.1. Instead of using the net section correction to account for specimen finite width, a simple secant formula was used:

$$f_w = \sqrt{\sec\left(\frac{\pi a}{2b}\right)}$$

where 2a is the half-crack width and 2b is the total plate width taken as the plate width plus the 30.5-cm edge webs.

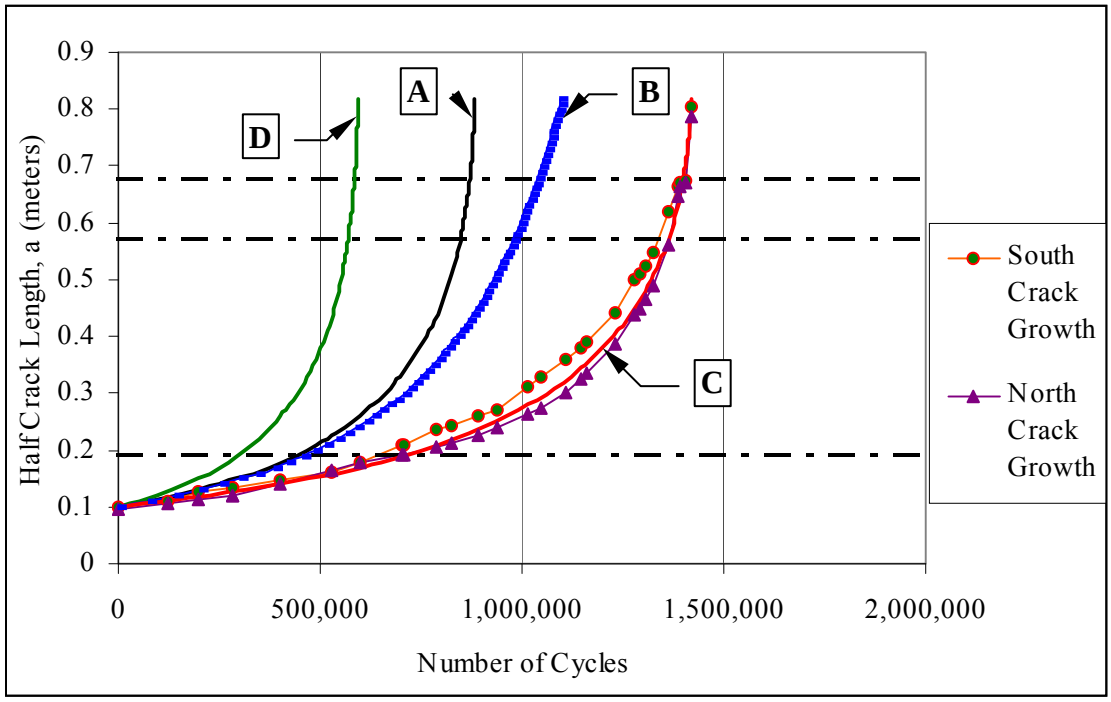

Figure 8-10: Case four predictions.

This finite width correction was used for both its simplicity and because the net section coefficient did not perform well under the current testing configuration. The net section coefficient yielded higher amplification than was probable for shorter crack lengths in the plate. The secant formula, however, exhibits a delayed amplification until the majority of the plate is cracked. This behavior better suited the observations in the experiment. It should be noted that the secant formula does not usually include the width of the edge webs, but it certainly is not appropriate for a plate with stiffened edges. Therefore, the inclusion of the edge web plates in the total plate distance was a compromise between a theoretical application and real world observations.

Curve B represents the same analysis without the finite width correction. Finally, curve D was made using the suggested weight function of Petershagen and Fricke to account for stiffener seperation:

$$f_s = \frac{2b_s t + A_s}{2b_s t} \qquad \text{Eqn. 8-1}$$

where b_s is the distance between stiffeners, t is the plate thickness, and A_s is the cross sectional area of the stiffener. This coefficient was applied to the CCT K solution in the following manner:

$$K_I = f_s f_w \left(\sigma_n \sqrt{\pi a}\right) \qquad \text{Eqn. 8-2}$$

In making these predictions, it was quite noticeable that the actual fatigue data could be better mapped by deterring from the stress range definition determined in section 8.1. Iterating on the stress range resulted in an excellent data fit for $\Delta\sigma$ = 35 MPa. This prediction, curve C, includes the finite width correction used in prediction A. The luxury of iteration is not an option for practice, however, and therefore a reasonable expectation should fall in the range of curves A, B and D. For case four it is recommended that the CCT K be used in conjunction with the secant finite width correction.

8.6 CASE 2A: MULTIPLE SITE DAMAGE IN STIFFENERS WITH CUTOUTS

Case 2a represented a stiffened panel with cracks initiating at weld access holes. A complete description of the experiment was made in Section 4.7 on page 91. The testing of specimen 2a was marked by frequent compromises between an engineered test and one that behaved naturally. Creating four running cracks that would be represent the same four cracks in a much wider structure was hampered by the stiffener proximity to the edge webs and the large stress gradient across the panel. The results of the test, therefore, gave limited confidence in developing a refined model that would work well in realistic applications.

A simplified and conservative analysis was promoted based on the information from the test. The prediction approach was similar to that of case four, where the CCT K was applied and modifying

coefficients investigated. The resulting model is developed in two stages: Stage one is shown in Figure 8-11 and stage 2 in Figure 8-12.

Stage one involved making six predictions based on the CCT K equation. First, a prediction curve is made for each crack tip except those propagating away from the exterior stiffeners. A new crack length definition is used in the CCT K formula:

$$K_{mc} = \sigma\sqrt{\pi * c} \qquad \text{Eqn. 8-3}$$

where c is the distance of the crack tip from the stiffener centerline.

This crack length was defined because sometimes the crack length would not be symmetric about a stiffener, and best results were found if this definition was used. For the crack tips propagating away from the exterior stiffeners, no K was determined directly. Rather, the incremental crack growth was defined as twice that of the crack tip on the interior side of the same stiffener. The stress values were taken from the values along each respective stiffener line. For example, for the interior stiffeners the stress was determined by estimating the stress at the stiffener line and approximately 20-cm from the crack line in the uncracked body. The results of this first phase may be seen in Figure 8-11.

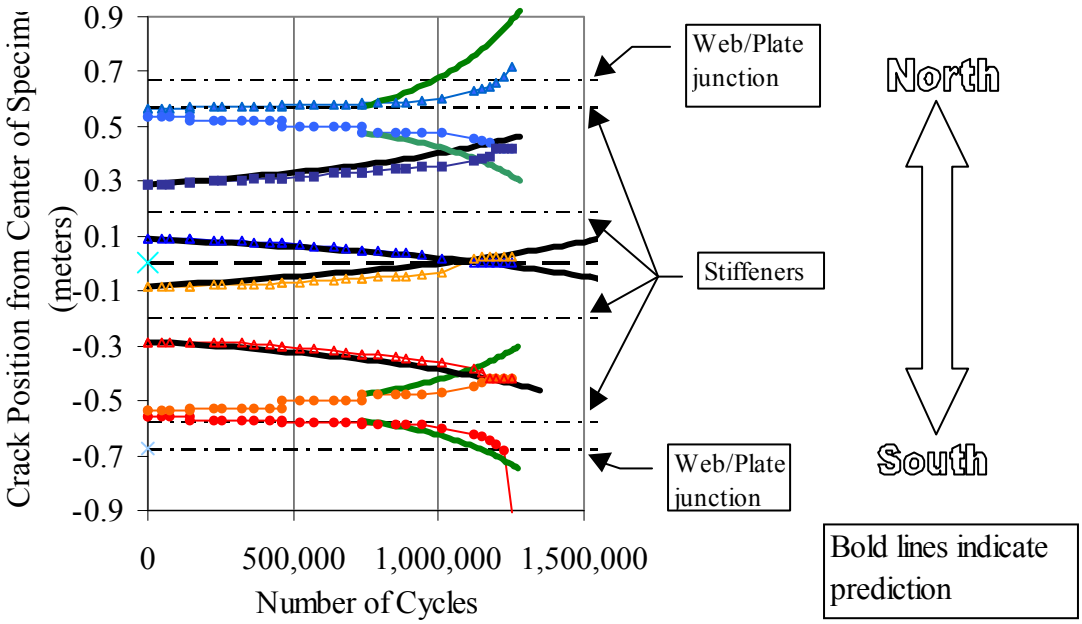

Figure 8-11: Stage one of prediction for case 2a.

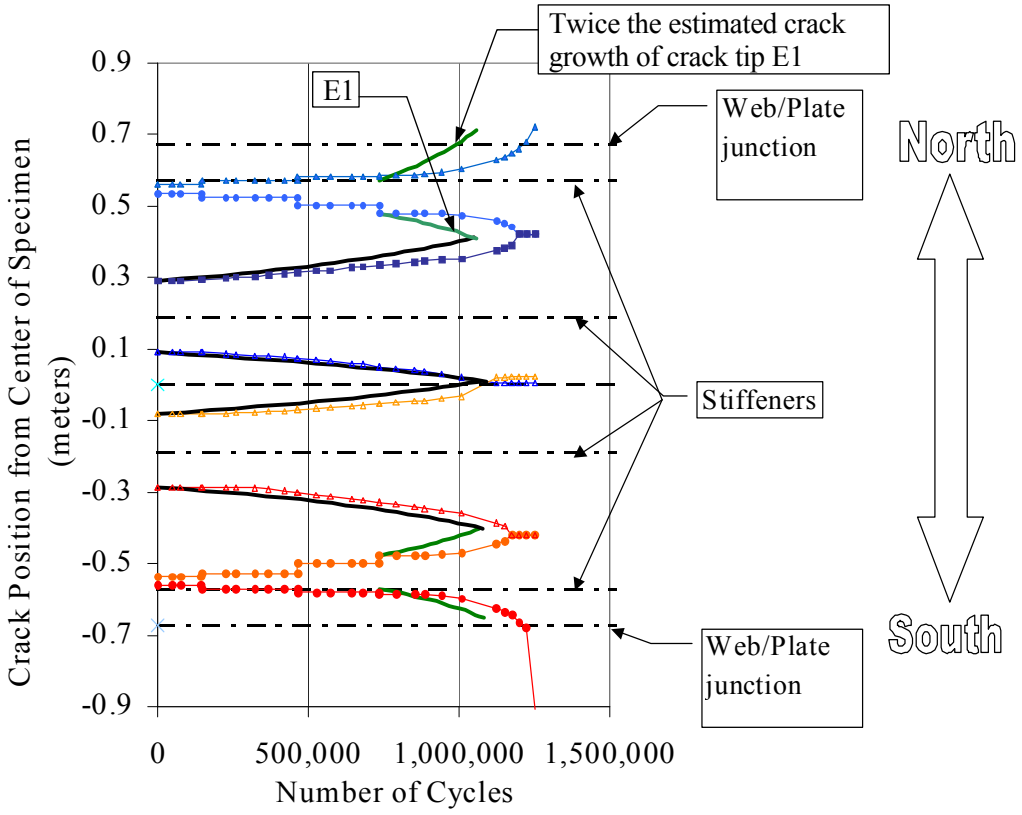

Figure 8-12: Beginning of stage two of prediction for case 2a.

The prediction of stage one generates crack lengths that overlap rather than grow together. By plotting the predictions, we may visualize number of cycles necessary for the cracks to merge. This cycle count is recorded as the product of a stage one prediction. Next, the crack is treated as a continuous crack similar to those modeled in the previous specimens. The continuous crack may be seen in Figure 8-12, where the stage one predictions have been cut off to represent merged crack tips. Any prediction made assuming the crack is continuous comprises a stage two prediction. Since the specimen width prevented continued growth of the crack, no stage two prediction was made.

The approach may be considered crude but offers a conservative model for assessment in light of the uncertainty in the test results. Estimating the extreme stiffener crack tips as twice the interior half provides a safe yet feasible behavior in the configuration. Undoubtedly better models could be created if multiple, wider specimens were involved in the experiment. However, loading and financial limitations make such a study impractical.

9 Conclusions

9.1 SUMMARY

A series of six experiments were conducted to define crack behavior in stiffened panels. These tests provided valuable information regarding the effects of both stiffener geometry and residual stress on crack growth rates. Variability of crack tip growth rates was seen within each test. This variability was attributed primarily to differences in the residual stress distribution. To assess the residual stresses, measurements were made in two of the specimens. Also, complete records of stress levels were recorded as the crack grew in the panel. These stress readings were used to develop guidelines on choosing a representative uniform stress for use in crack growth prediction.

Analytical modeling was performed to predict the experiments. A simple model for the residual stress distribution was included. The analytical model demonstrated that simple fracture mechanics principles could be used to effectively determine crack growth rates. Superposition was used in the analytical model to combine the effects of residual stresses, stiffener separation, and stiffener restraint on crack growth rates. The effect of the finite width correction was also reviewed throughout the modeling. Parametric investigations with the model resulted in guidelines for proper life prediction.

A finite element modeling technique was developed as well, including an evaluation into the use of gap elements. The gap elements prevented overlapping of crack faces but also introduced nonlinearity in the formulation. A finite element model that excluded the gap elements was developed in which superposition was valid. This finite element model gave virtually identical results as the analytical model. By including gap elements, however, small differences were seen between analytical model and the F.E. model. A method was developed to obtain the results obtained with gap elements from a FE model without gap elements. The differences between models with and without gap elements diminish when the applied load overcomes the effects of crack closure.

Both the finite-element and the analytical models can simulate measured crack growth rates reasonably well. Finite element modeling is more time consuming but may be necessary for cracks in complicated geometries. All of the prediction methods were sensitive to the specified residual stress distribution for low applied stresses. The inherent variability of residual stress does not allow for accurate predictions, however. Therefore, the approach taken is to develop conservative models based on worst-case residual stress distributions.

Finally, it was noted that the effects of residual stress could only decrease crack growth rates. This is because the applied stress range is used in the Paris Law, and compressive residual stress may make the applied stress range less effective by contributing to crack closure.

9.2 FINDINGS

The findings of this research may be divided into sections:

I. Experimental observations
    A. Solid stiffeners will slightly slow down an approaching crack. Stiffeners with cutouts, however, provide no restraint on crack opening and consequently no retardation can be expected. If there as a buttweld in the plate nearby and parallel to the crack, accelerated growth similar to an unstiffened, cracked plate may be expected.
    B. Residual stress distributions have substantial variability. At low stresses typical for fatigue crack growth, this variability will significantly influence the accuracy of predictions. In the stiffened panel tests, compressive residual stress between stiffener spacings significantly retarded crack growth rates. In fact, there was significant difficulty starting a crack centered between stiffeners. The effect of residual stresses far outweighs the effect of other variables.
    C. Shear lag effects led to non-uniform applied stress distributions in the specimens. These shear lag effects also occur in ship structure, however. Continuous stress monitoring was used to record the history of stress changes.

D. After the cracks encountered the solid stiffeners, the rate of propagation up the web of the stiffener was similar to the rate of propagation in the plate beyond the stiffener. Even in the stiffeners with weld access holes or drainage holes in the propagation path, cracks started at the apex of the holes as soon as the plate crack had reached a distance from the stiffener equivalent to that of the cutout height above the plate. This equivalent growth rate persisted until the stiffener crack encountered the flange of the stiffener.

II. Analytical Model Observations

A. The analytical model correlated well with finite element modeling.

B. An attempt to correct for the increase in stress due to a reduction in the net section overestimated crack growth rates. The correction becomes more applicable with decreasing redundancy in a structure. In other situations, such as the test setup, load was redistributed in a manner not proportional to the flexure formula.

C. Stress gradients across the width of the panel are easily incorporated into the analytical model by adjusting the stiffener areas.

D. For butt-welded plates and multiple propagating cracks, an analytical prediction based on the stress-intensity factor for a flat plate is sufficient.

III. Finite Element Modeling Observations

A. Using gap elements reduces the available effective range in stress-intensity factor (ΔK_{eff}) in some situations. This occurs because crack closure effects behind the crack tip promote residual stress redistribution. Excluding gap elements allows superposition to be used in determining K_{total}. The results without gap elements compare well with the analytical model. Finite element modeling generally predicts less conservative results by including gap elements with an initial gap of zero meters.

B. Any effects of gap elements are negligible when external load completely opens the crack.

C. Applying temperature loads to nodes within the weld regions can reproduce residual stress distributions.

D. Finite element modeling can be quite time consuming compared to the analytical model. Furthermore, no greater accuracy is seen in the typical studies conducted in this report. It is recommended to use finite element modeling to determining a local uniform stress

in the structure (without a crack) and then use this stress in the analytical model to include the effect of the crack.

IV. Miscellaneous Observations

A. The support structure was subjected to repeated instance of fatigue cracking. These cracks were repaired by a variety of methods. As testing continued, some repairs performed better than others. A complete report of the cracking, repair method, and repair performance at a number of locations is included in the appendix.

B. Redundant structures exhibit a great amount of symmetry. For instance, cracking in an area of one support beam promoted cracking in its parallel counterpart. This was due to load shedding.

C. Fatigue cracks may often be repaired by simply drilling out the crack tip and welding the crack faces together. The repair is discussed in detail in Appendix A. This repair significantly increases fatigue life with little effort since the majority of fatigue life is seen when the crack is relatively short. The downside to this quick repair is that any future crack growth will occur at a slightly increased rate.

D. Other performance-based repairs make treating these fatigue crack problems in older ship structure more economical. These types of repairs are suggested for review in the next section.

9.3 MAIN CONCLUSIONS

1. The behavior of cracks in welded stiffened panels is substantially different than predicted using conventional faracture mechanics solutions for a crack in a plate.
2. Compressive residual stresses between stiffeners significantly retards the rate of crack growth. However, if there as a buttweld in the plate nearby and parallel to the crack, accelerated growth similar to an unstiffened, cracked plate occurs.
3. An analytical model was developed that can simulate these effects of welded stiffeners and provide reasonable worst-case predictions of the propagation of very long cracks in welded stiffened panels.
4. Residual stress distributions have substantial variability. At low stresses typical for fatigue crack growth, this variability will significantly influence the accuracy of predictions. The effect of residual stresses far outweighs the effect of other variables.
5. Finite-element modelling of the cracked stiffened panels verified the analytical model but offered no greater accuracy for the cases studied. It is recommended to use finite element modeling to determining the stress distribution in the structure (without a crack) and then use this stress in the analytical model to include the effect of the crack.

9.4 RECOMMENDATIONS FOR FUTURE WORK

The analytical model described in this report should yield a reasonably adequate prediction, especially considering the high variability seen under even constant amplitude loading.

The experiments suggest further review of several parameters, however. First, the stiffener sizes remained constant throughout the testing. The crack propagation in panels with different stiffener areas is likely to be similar and therefore reasonably well predicted by the model. However,

confirmation of the behavior with different stiffener areas would facilitate wider acceptance of the model.

The added effects of pressure loading should also be investigated. Watanabe and Kawano performed a limited study of this situation and predicted crack growth through finite element analysis. The effect of pressure on the shell can be significant.

Residual stress is inherently highly variable. Further investigation into quantifying residual stress will not improve the situation unless assembly order is known a priori and carefully controlled during fabrication.

Predicting fatigue cracks allowed for speculation on the best and easiest repairs to make in cracking situations. Stiffeners that are not welded to the plate will significantly decrease crack growth rates. For this reason, it would be worth examining the feasibility of using adhesive-bonded plates to arrest crack propagation.

An immediately applicable repair involves a more conventional welding approach. Holes are drilled at the crack tips and the crack faces are welded up to the weld holes. Additional reinforcement can be added by welding plate strips across the crack. This repair detail will not perform as well as the original continuous base metal, but the repair can be quickly implemented resulting in considerable additional life. For example, a section in the support structure repeatedly cracked and was repaired with a complete penetration plug weld. Each repair afforded continued use of the section for one million cycles at a measured stress range of 80 MPa. This type of performance-based repair could serve the aging tankships in the TAPS trade until they are slated for retirement.

Fatigue involves a great amount of variability. When combined with an equally variable loading environment, the possibility of developing a model that correctly addresses all parameters is impossible. Reasonable models, such as the ones presented in this report, should be coupled with a reasonable models to predict the loading.

10 REFERENCES

1) Aihara, S., et al. (1995, December) Fracture Mechanical Modeling of Brittle Crack Propagation and Arrest in Steel. J. Soc. of Naval Arch. of Japan, Vol. 178, pp. 545-555.

2) Alman, P., W.A. Cleary, Jr., M.G. Dyer, and J.R. Pauling. (1992) The International Load-Line Convention: Crossroads to the Future. Marine Technology, Vol 29, N 4, pp. 233-249.

3) Almer, J.D., K.R. McCallum, and R.A. Winholtz. X-Ray Diffraction and Finite Element Study of Residual Stress Effects on Fatigue Crack Growth. Technical Report #34. Office of Naval Research, May 1997.

4) Alpsten, GA, and L. Tall. (1970) Residual Stresses in Heavy Welded Shapes. Welding Journal, Vol. 49, Research Supplement. pp. 93-s to 105-s.

5) American Bureau of Shipbuilding, Guide for Fatigue Assessment of Tankers. New York, NY: ABS, 1992.

6) Anderson, T.L. Fracture Mechanics - Fundamentals and Applications. (2nd ed.) Boca Raton, Florida: CRC Press, 1995.

7) Argyris, J.H., J. Szimmat, and K.J. William. (1982) Computational Aspects of Welding Stress Analysis. Computer Methods in Applied Mechanics and Engineering, Vol. 33, pp. 635-666.

8) Arin, K. (1979) Several Intact or Broken Stringers Attached to an Orthotropic Sheet with a Crack. Engineering Fracture Mechanics, Vol 3, pp. 1-8.

9) ASTM. Methods and Models for Predicting Fatigue Crack Growth Under Random Loading. ASTM Special Technical Publication 748. Ed. J.B. Chang and C.M. Hudson. Philadelphia, PA: American Society for testing and Materials, 1981.

10) ASTM. Probabilistic Fracture Mechanics and Fatigue Methods: Applications for Structural Design and Maintenance. ASTM Special Technical Publication 798. Ed. J.M. Bloom and J.C. Ekvall. Philadelphia, PA: American Society for testing and Materials, 1981.

11) Averbach, B.L. and Bingzhe Lou. (1984) Fatigue Crack Propagation through Residual Stress Fields. Metal Trans. A (USA), pp. 1631-1640.

12) Bacci, A. and S. Ligaro. (1996) Competition Between Brittle fracture and Plastic Collapse in the Failure of Thin Rectangular Panels. Intl. J. of Fracture, Vol 77, pp. 185-198.

13) Barsoum, R.S.. (1976) On the Use of Isoparametric Finite Elements in Linear Fracture Mechanics,' International Journal for Numerical Methods in Engineering, Vol. 10, pp. 25-37.

14) Barsom, J.M. Fatigue Crack Growth Under Spectrum Loads. ASTM Special Technical Publication 595. Philadelphia, PA: American Society for testing and Materials, 1976. pp. 217-235.

15) Barsom, J.M. and S.T. Rolfe. (1987). Fracture and Fatigue Control in Structures. 2nd ed. Englewood Cliffs, New Jersey: Prentice-Hall.

16) Beghini, M., L. Bertini and E. Vitale. (1994) Fatigue Crack Growth in Residual Stress Fields: Experimental Results and Modeling. Fatigue and Fracture of Engineering Materials, Vol. 17, N 12, pp. 1433-1444.

17) Bibby, M.J. and Goldak, J.A. "Weld Induced Camber in Structural Sections." Weldments: Physical Metallurgy and Failure Phenomena. Proceedings of the Fifth Bolton Landing Conference, August 1978, Cristoffel, R.J. et al. (eds.), ISBN 0-931690-07-2, General Electric Company, Schenectady, NY, 12305, pp. 101-115, 1979.

18) Biggs, W.D. (1960). The Brittle Fracture of Steel. London: MacDonald and Evans LTD.

19) Bjorhovde, R., J. Brozetti, G.A. Alpsten, and L. Tall. (1972) Residual Stresses in Thick Welded Plates. Welding Journal, Vol. 51, Research Supplement, pp. 392-s to 405-s.

20) Blodgett, O. (1976, March) Distortion (Part III)." Canadian Welder and Fabricator, p. 15.

21) Bloom, J.M. and J.L. Sanders. (1966). The Effect of a Riveted Stringer on the Stress in a Cracked Sheet. Journal of Applied Mechanics, Vol 33 , pp. 561-570.

22) Broek, D. (1987). Elementary Fracture Mechanics. 4th ed. Dordrecht, Netherlands: Martinis Nijhoff Publishers.

23) BSI. Guidance on the Methods for Assessing the Acceptability of Flaws in Fusion Welded Structures, PD6493: 1991. British Standards Institution (BSI): 1991.

24) Bucci, R.J. "Effect of Residual Stress on Fatigue Crack Growth Rate Measurement." Fracture Mechanics: Thirteenth Conference. ASTM STP 743. Ed. Richard Roberts. American Society for testing and Materials, 1981. pp. 28-47.

25) Burnside, O.H. et al. Long-Term Corrosion Fatigue of Welded Marine Steels. SSC-326. Washington, D.C.: Ship Structure Committee, 1984.

26) Cartwright, D.J. and T.P. Rich. Plastic Strip Yielding for a Crack in a Stiffened Sheet. First Intl. Conf. on Numerical Methods in Fracture Mechanics, 1978. University College, Swansea.

27) Clayton, A.M. (1993). Design of Welded Structures to Avoid Fracture and Plastic Collapse." Welding in the World, Vol 32, pp. 25-32.

28) Columbi, P., and Dolinski, K. "Fatigue Reliability under Stochastic Load." Safety and Reliability, Proc. 1995 OMAE Conference. ASME, 1995. pp. 207-214.

29) Cook, R., S. Dorey and D.P. Rooke. A Computer Program to Calculate Growth Rates for Cracks at Notches in Regions of Residual Stress. Tech. Memorandum Materials and Structures 1207. Farnborough, England: Defence Research Agency, 1992.

30) Cramer, E. et al. Fatigue Assessment of Ship Structures. DNV Report No. 93-0432, N-1322. HOVIK, DNV: Division Ship and Offshore, Norway, 1994.

31) Dalzell, J.F., N.M. Maniar, and M.W. Hsu. Examination of Service and Stress Data of Three Ships for Development of Hull Girder Load Criteria. SSC-287. Washington, D.C.: Ship Structures Committee, 1979.

32) Demsetz, Laura. Optimal Strategies for Inspection of Ships for Fatigue and/or Corrosion Damage. Ship Structure Committee, Project SR-1365. Interim Report of U.C. Berkeley, 1997.

33) Dexter, R.J. and Fisher, J.W. "Fatigue and Fracture." Steel Design Handbook: LRFD Method, Ed. A.R. Tamboli. New York, New York: McGraw Hill, 1997. pp. 8-1 to 8-53.

34) Dexter, R.J., J.W. Fisher, and J.E. Beach. “Fatigue Behavior of Welded HSLA-80 Members.” 12th International Conference on Offshore Mechanics and Arctic Engineering (OMAE), 1993: ASME.

35) Dexter, R.J. and M.L. Gentilcore. Evaluation of Ductile Fracture Models for Ship Structural Details. SSC-393. Washington, D.C.: Ship Structure Committee, 1996.

36) Dexter, R.J., S.J. Hudak, and D.L. Davidson. (1989). Modeling and Measurement of Crack Closure and Crack Growth Following Overloads and Underloads. Engineering Fracture Mechanics, Vol 33, N 6, pp. 855-870.

37) Dexter, R.J, E.B. Norris, W.R. Schick, and P.D. Watson. Performance of Underwater Weldments. SSC 335. Washington, D.C.: Ship Structure Committee, 1990.

38) Dexter, Robert J. and Pilarski, P. J. “Growth and Instability of Large Cracks in Redundant Structures.” Proceedings of the 12th Engineering Mechanics Conference, ASCE, 17-20 May 1998. La Jolla, CA: ASCE, 1998.

39) Dexter, R.J., A. Pellissier-Tanon, D. Pont, C.-P. Leung, and M. Behravesh. "Residual Stress Analysis of Reactor Pressure Vessel Attachments." International Conference on Residual Stresses (ICRS3), Osaka, Japan, July 20-24, 1991.

40) Dexter, R.J., A. Pellissier-Tanon, D. Pont, C.-P. Leung, and M. Behravesh, "The Use of Residual Stress Analysis in Reactor Pressure Vessel Attachments." Presented at the Structural Mechanics in Reactor Technology (SMiRT 11), Post-Conference Seminar (PCS) 2, Taipei, August 26-28, 1991.

41) Dexter, R.J., C.-P. Leung, and D Pont. Residual Stress Analysis in BWR Pressure Vessel Attachments, Electric Power Research Institute Report EPRI TR-1--651, Project C102-3, June 1992.

42) Dexter, R.J., S.C. Grigory, and W.R. Schick. Residual Stress and Deformation Prediction in Welded Structural Components. SwRI Internal Research Project 06-9497, Final Report, July 1989.

43) Dobson, W.G., et al. Fatigue Considerations in View of Measured Load Spectra. SSC-315. Washington, D.C.: Ship Structures Committee, 1982.

44) Dugdale, D.S. (1960). Yielding of Steel Sheets Containing Slits." J. Mech. Phys. Solids, Vol 8 , N 2 , pp. 100-104.

45) Elber, W. (1970). Fatigue Crack Closure under Cyclic Tension. Engineering Fracture Mechanics, Vol 2, pp. 37-40.

46) Ellyin, F. (1997). Fatigue Damage, Crack Growth and Life Prediction. (1st ed.) London: Chapman and Hall.

47) Engle, R.M. Damage Accumulation Techniques in Metallic Structures: Analysis Methods and Applications. STP 842. Philadelphia, PA: ASTM, 1984.

48) Faulkner, D. (1975, March). A Review of Effective Plating for Use in the Analysis of Stiffened Plating in Bending and Compression. Journal of Ship Research, Vol. 19, N 1, pp. 1-17.

49) Faulkner, D. "Compression Tests on Welded Eccentrically Stiffened Plate Panels." Steel Plate Structures. Ed. P.J. Dowling et al., Crosby Lockwood. pp. 581-617.

50) Faulkner, D., et al. (1993). Synthesis of Welded Grillages to Withstand Compression and Normal Loads. Great Britain: Permagon Press. Computers and Structures, Vol 3, pp. 221-246.

51) Finch, D.M. and F.M. Burdekin. (1992). Effects of Welding Residual Stresses on Significance of Defects in Various Types of Welded Joints. Engineering Fracture Mechanics, Vol 41 , N 5 , pp. 721-735.

52) Fisher, J.W., K.H. Frank, M.A. Hirt, and B.M. McNamee. Effect of Weldments on the Fatigue Strength of Steel Beams. Washington, D.C.: National Cooperative Highway Research Program (NCHRP) 102, Highway Research Board, 1970.

53) Fisher, J.W., et al. Phase I: Final Report--Development of Advanced Double Hull Concepts. TDL 91-01 Phase 1.3(a). Philadelphia, PA: ATLSS/FFP and U.S. Navy MANTECH, Fleet of the Future Program, 1993.

54) Fisher, J.W., et al. Fatigue Strength of Steel Beams with Welded Stiffeners and Attachments. Washington, D.C.: National Cooperative Highway Research Program (NCHRP) 147, Transportation Research Board, 1974.

55) Fisher, J.W., et al. Resistance of Welded Details Under Variable Amplitude Long-Life Fatigue Loading. National Cooperative Highway Research Program Report 354. Washington, D.C.: Transportation Research Board, 1993.

56) Fitzpatrick, M.E., and L. Edwards. (1998). Fatigue Crack/Residual Stress Field Interactions and Their Implications for Damage Tolerance Design." JMEPEG, Vol 7, pp. 190-98.

57) Formby, C.L., and J.R. Griffiths. "The Role of Residual Stresses in the Fracture of Steel." Proceedings of the International Conference "Residual Stresses in Welded Construction and

Their Effects," 15-17 November 1977, London, The Welding Institute, Abington Hall, Abington, Cambridge, CB1 6AL, UK, pp. 359, 1977.

58) Francis, P.H., J. Lankford, Jr., and F.F. Lyle, Jr. (1976, April) Subcritical Crack Growth and Ship Structural Design." Marine Technology, Vol 13, N 2, pp.152-160.

59) Freudenthal, A.M. and M. Shinozuka. "On Fatigue Failure of a Multiple-Load-Path Redundant Structure." First Intl. Conf. on Fracture, 1965. Sendai, Japan: Jpn Soc. for Strength and Fracture of Materials, 1965.

60) Galambos, T.V., Guide to Stability Design Criteria for Metal Structures. 4th ed. NY: Wiley-Interscience, 1988.

61) Garwood, S.J., R.H. Leggat, and T. Ingham. (1994). Structural Collapse, The Failure Assessment Diagram and "Off-The-Shelf" Operation. Fatigue and Fracture of Engineering Materials, Vol 17 , N 12 , pp. 1418-1431.

62) Ghassem, Mansoor Mohammad. "Fracture Diagram for Stiffened Panel and Computer Based Approach for Structural Life Prediction." Ph.D. Dissertation: Mechanical Engineering. Texas A&M University: College Station, 1980.

63) Goldak, J., et al. "Progress in Computing Residual Stress and Strain in Welds." Advances in Welding Science and Technology, TWR '86. International Conference on Trends in Welding Research, Gatlinburg, Tennessee, USA. 18-22 May, 1986.

64) Grief, R. and J.L. Sanders, Jr. (1965). The Effect of a Stringer on the Stress in a Cracked Sheet. J. of Applied Mechanics, Series E, Vol 32 , N 1, pp. 647-665.

65) Gurney, T.R. "Comparative Fatigue Tests on Fillet Welded Joints under Various Types of Variable Amplitude Loading in Air." 12th Intl. Conf. on OMAE, 1993: ASME, 1993.

66) Hahn, G.T., and M. Sarrate. "Failure Criteria for Through-Cracked Vessels." Practical Fracture Mechanics for Structural Steel. Proc. of the Symposium on Fracture Toughness Concepts for Structural Steel, April 1969. Ed. M.O. Dobson. Risley, U.K.:U.K. Atomic Energy Authority, 1969.

67) Hibbitt, H.D. and Pedro V. Marcal. (1972). A Numerical Thermo-Mechanical Model for the Welding and Subsequent Loading of a Fabricated Structure. Computers & Structures, Vol. 3, pp. 1145-1174.

68) Hoffman, D., and Walden, D.A. Wojnarowski. Environmental Wave Data for Determining Hull Structural Loadings. SSC 268. Washington, D.C.: Ship Structures Committee, 1979.

69) Hollister, S.C., J. Garcia, and T.R. Cuykendahl. Fatigue Tests of Ship Welds. Washington, D.C.: Ship Structure Committee, SSC-7, 1946.

70) Hollister, S.C., J. Garcia, and T.R. Cuykendall. Final Report on Fatigue Tests in Ship Welds. Washington, D.C.: SSC-14, Ship Structure Committee, 1948.

71) Horne, M.R., and R. Narayanan. (1976). The Strength of Straightened Welded Steel Stiffened Plates. The Structural Engineer, Vol 54, N 11, pp. 437-43.

72) Horne, M.R., P. Montague, and R. Narayanan. "Influence on Strength of Compression Panels of Stiffener Section, Spacing, and Welded Connection." Proc. of the Institute of Civil Engineers, Part 2, 1977a. p. 63.

73) Irwin, G.R. (1957). Analysis of Stresses and Strains near the End of a Crack Traversing a Plate. Journal of Applied Mechanics, Vol 24 , pp. 361-364.

74) Isida, M. (1966). Stress Intensity Factors for the Tension of an Eccentrically Cracked Strip. Trans. ASME, J. Applied Mechanics, Vol 33, p. 674.

75) Isida, M. (1970). On the Determination of Stress Intensity Factors for Some Common Structural Problems. Eng. Fract. Mech., Vol 2 , pp. 61-69.

76) Isida, M. (1973). Analysis of Stress Intensity Factors for the Tension of a Centrally Cracked Strip with Stiffened Edges. Engineering Fracture Mechanics, Vol 5, pp. 647-665.

77) Itoh, Y.Z., S. Suraga, and H. Kashiwaya. (1989). Prediction of Fatigue Crack Growth Rate in Welding Residual Stress Field. Engineering Fracture Mechanics, Vol 33, N 3, pp. 397-407.

78) Jan, H.-Y., K.-T. Chang, and M.E. Wojnarowski. Comparison of Stresses Calculated Using the Daisy System to Those Measured on the SL-7 Containership Program. SSC-282. Washington, D.C.: Ship Structures Committee, 1979.

79) Jiao, Guoyang. "Reliability Analysis of Crack Growth with Inspection Planning." OMAE, Vol 2 , 1992: pp. 227-235.

80) Jordan, C.R. and L.T. Knight. Further Survey of In-Service Performance of Structural Details. SSC –294. Washington, D.C.: Ship Structure Committee, 1980.

81) Jordan, C.R. and R.P. Krumpen, Jr. Design Guide for Ship Structural Details. SSC-331. Washington D.C.: Ship Structure Committee, 1985.

82) Kaczinski, M.R., R.J. Dexter, and JP. Van Dien. Fatigue-Resistant Design of Cantilevered Signal, Sign and Light Supports. NCHRP Report 412. Washington, D.C.: National Cooperative Highway Research Program, 1998.

83) Kamtekar, A.G. (1978). The Calculation of Welding Residual Stresses in Thin Steel Plates. Int. J. Mech. Sci., Vol 20, pp. 207-227.

84) Kim, S.C., Y. Fujimoto, and E. Shintaku. "Study on Fatigue Reliability and Inspection of Ship Structures Based on Questionnaire Information." PACOMS, 1996.

85) Kinoshita, M., K. Kono, and K. Shingai. (1973).Estimation of Fatigue Crack Propagation Life of Steel Plates and of Structural Member Model of Ship Hull. Engineering Fracture Mechanics, Vol 5, pp. 563-584.

86) Kishima, Y., G.A. Alpsten, and L. Tall. Residual Stresses in Welded Shapes of Flame Cut Plates in ASTM A572(50) Steel. Fritz Laboratory Report No. 321.2. Bethleham, PA: Lehigh University, 1969.

87) Kondo, J., and A. Ostapenko. Tests on Longitudinally Stiffened Plate Panels with Fixed Ends—Effect of Lateral Loading. Report No. 248.12. Fritz Engineering Laboratory, 1964.

88) de Koning, A.U. "A Simple Crack Closure Model for the Prediction of Fatigue Crack Growth Rates Under Variable-Amplitude Loading." Fracture Mechanics: Thirteenth Conference. ASTM STP 743. Ed. Richard Roberts. American Society for Testing and Materials, 1981. pp. 63-85.

89) Kujawski, D., and F. Ellyin. (1984). A Fatigue Crack Propagation Model. Engineering Fracture Mechanics, Vol 20, N 5/6, pp. 695-704.

90) Lambrigger, M. (1997, February). Weibull Master Curves, Residual Stress Fields and Stable Crack Growth. J. Materials Science Letters, Vol 16, N 4, pp. 298-300.

91) Larrson, L.H. Subcritical Crack Growth Due to Fatigue, Stress Corrosion and Creep. New York: Elsevier Applied Sciences Publishers, 1984.

92) Leggat, R.H. Fracture Assessment in the Presence of Residual Stresses. England: The Welding Institute: Cambridge, 1984. pp 1239-1246.

93) Leggatt, R.H. "Residual Stresses at Girth Welds in Pipes." Proceedings of the International Conference "Welding in Energy-Related Projects," 20-21 September 1983, Toronto, pp. 429-439.

94) Leggatt, R.H. and J.D. White. "Predicting Shrinkage and Distortion in a Welded Plate," Proceedings of the International Conference "Residual Stresses in Welded Construction and Their Effects," 15-17 November 1977, London, The Welding Institute, Abington Hall, Abington, Cambridge.

95) Leung, C.K. and R.J. Pick. "The Use of Generalized Plane Strain Elements in The Prediction of Residual Stresses in Welded Flat Plates." Symposium on Computer Modelling of Fabrication Processes and Constitutive Behavior of Metals, Ottawa, Canada, May 25-16, 1986, Too, J. (ed.), CANMET, Ottawa. pp. 563-585.

96) Leung, C.K. and R.J. Pick. Finite Element Analysis of Multi-Pass Welds. Bulletin 356. Welding Research Council Bulletin, August 1990. pp. 11-33.

97) Liu, D. and Thayamballi, A. "Local Cracking in Ships--Causes, Consequences, and Control." Workshop and Symposium on the Prevention of Fracture in Ship Structure. 1995.

Washington, D.C.: Marine Board, Committee on Marine Structures, National Research Council.

98) Maddox, S.J. Fatigue Strength of Welded Structures. 2nd ed. Cambridge, U.K.: Abington Publishing, 1991.

99) Mansour, Alaa E. Gross Panel Strength Under Combined Loading. SSC 270. Washington, D.C.: Ship Structures Committee, 1977.

100) Mansour, A., et al. Assessment of Reliability of Existing Ship Structures. SSC-398. Washington, D.C.: Ship Structure Committee, 1997.

101) Mansour, Alaa. (1972, June)Methods of Computing the Probability of Failure Under Extreme Values of Bending Moment. J. Ship Research, pp. 113-123.

102) Marine Digest and Transportation News. March, 1998

103) Miner, M.A. (1945) Cumulative Damage in Fatigue. Journal of Applied Mechanics, Vol. 12, 1945: p. A-159.

104) Murakami, Y., et al. Stress Intensity Factors Handbook. Oxford, U.K.: Permagon Press, 1987.

105) Murray, N.W. (1975). Analysis and Design of Stiffened Plates for Collapse Load. The Structural Engineer, Vol 53, N 3, pp. 153-8.

106) Nagaraja Rao, N.R., and Tall, L. (1961). Residual Stresses in Welded Plates. Welding Journal, Vol. 40, Research Supplement, pp. 468-s to 480-s.

107) National Research Council. Marine Board. Committee on Marine Structures. Prevention of Fracture in Ship Structure. Proc. of the Symposium and Workshop on the Prevention of Fracture in Ship Structure. 30-31 March 1995. Washington, D.C.: National Research Council, 1997.

108) Newman, J.C. Jr. A Crack-Closure Model for Predicting Fatigue Crack Growth Under Aircraft Spectrum Loading, Technical Memo 81941, NASA, 1981.

109) Nussbaumer, Alain. "Propagation of Long Fatigue Cracks in Multi-Cellular Box Beams." Ph.D. dissertation in Civil Engineering, 1993. Bethlehem, Pennsylvania: Lehigh University.

110) Nussbaumer, A.C., R.J. Dexter, J.W. Fisher, and E.J. Kaufmann, Propagation of Very Long Fatigue Cracks in a Cellular Box Beam, Fracture Mechanics, Twenty-Fifth Volume, ASTM STP 1220, F. Erdogan and Ronald J. Hartranft, Eds., American Society for Testing and Materials, Philadelphia, pp.518-532, 1994.

111) A.C. Nussbaumer, J.W. Fisher, and R.J. Dexter. (1998). Behavior of Long Fatigue Cracks in a Cellular Box Beam. Submitted for review to ASCE Journal of Structural Engineering, 1998.

112) Ogeman, Rutger T., B. Josefson, and Anders Ulfarson. (1995). Residual Stresses at a Longitudinal Stiffener--Web Frame Intersection and Their Effects on Crack Growth. Marine Structures, Vol 8 , pp. 603-616.

113) Ohji, K, et al. (1987). Methods of Predicting Fatigue Crack Growth Lives in Residual Stress Fields. Trans. Japanese Soc. Mech. Eng., Vol 53 , N 492, p. 1516.

114) Osgood, William R. Residual Stresses in Metals and Metal Construction. New York:Reinhold Publishing Corp. Prepared for the Ship Structure Committee, 1954.

115) Pang, A.A.-K., R. Tiberi, L.-W. Lu, J.M. Ricles, and R.J. Dexter. (1995, February) Measured Imperfections and Their Effects on Strength of Component Plates of a Prototype Double Hull Structure. Journal of Ship Production, Vol. 11, No. 1, pp. 47-52.

116) Pang, H.L.J. A Linear Elastic Fracture Mechanics Assessment of the Fatigue-Crack-Growth Behaviour for a Semi-Elliptical Surface Crack in Machined and Welded Specimens Subjected to Constant Amplitude Tension Loading. Dept.of Trade and Industry. National Engineering Laboratory, 1991.

117) Paris, P. and F. Erdogan. (1963). A Critical Analysis of Crack Propagation Laws. Trans. ASME, Ser. D. Journal of Basic Engineering, Vol 85 , N 4, pp. 528-534.

118) Petershagen, H. (1986). Fatigue Problems in Ship Structures. Advances in Marine Structures. London: Elsevier Applied Science, pp 281-304.

119) Petershagen, H. (1993). Stress Analysis and Fatigue Life Prediction of Ship Structures. Welding in the World, Vol 32, pp.75-82.

120) Petershagen, H., and Fricke, W. Fatigue Crack Propagation in Plate Panels with Welded Stiffeners. IIW-Doc. XIII-1272-88. Technical University of Hamburg Harburg, 1988.

121) Pisarski, H.G. and S. Slatcher. "Assessment of the Significance of LBZ's in Steels Using a Probabilistic Model." OMAE, Vol 2 , 1993: pp. 89-97.

122) Poe, Clarence C. "The Effect of Riveted and Uniformly Spaced Stringers on the Stress Intensity Factor of a Cracked Sheet." M.S. Thesis: Mechanical Engineering. Virginia Polytechnic Institute, 1969.

123) Poe, C.C., Jr. Fatigue Crack Propagation in Stiffened Panels. ASTM STP 486. 1971: ASTM.

124) Rampetstreiter, R.H., T. Lee, and A. Ostapenko. Tests on Longitudinally Stiffened Plate Panels—Effect of Residual Stresses and Rotational Restraint by Stiffeners. Report No. 248.5. Fritz Engineering Laboratory, 1962.

125) Ratwani, M.M. (1978). A Parametric Study of Fatigue Crack Growth Behavior in Adhesively Bonded Metallic Structures. Trans. ASME, Vol 77, pp. 1-6.

126) Reemsnyder, H.S. "Fatigue and Fracture of Ship Structures." Symposium on the Prevention of Fracture in Ship Structure. 30-31 March 1995. Washington, D.C.: Marine Board, Committee on Marine Structures, National Research Council.

127) Riemelmoser, F.O. and R. Pippan. (1997). Crack Closure: A Concept of Fatigue Crack Growth under Examination. Fatigue and Fracture of Materials and Structure, Vol 20, N 11, pp. 1529-1540.

128) Rolfe, S.T. Fracture Mechanics, Fracture Criteria and Fracture Control for Welded Steel Ship Hulls. Report 244. Washington, D.C.: The Society of Naval Architects and Marine Engineers, 1974.

129) Rolfe, S.T., K.T. Hays, and A.E. Henn. "Fracture Mechanics Methodology for Fracture Control in VLCC's." Ship Structures Symposium, 1993. Arlington, VA: SNAME and SSC.

130) Rolfe, S.T., D.M. Rhea, and B.O. Kuzmanovic. Fracture Control Guidelines for Welded Steel Ship Hulls. SSC-244. Washington, D.C.: Ship Structures Committee, 1974.

131) Rooke, D.P. and D.J. Cartwright. Compendium of Stress Intensity Factors. Uxbridge, Middex, U.K.: HIllington Press, 1976.

132) Rybicki, E.F., et al. (1988). Experimental and Computational Residual Stress Evaluation of a Weld Clad Plate and Machined Test Specimens. Journal of Engineering Materials and Technology, Vol. 110, pp. 297-304.

133) Rybicki, E.F., and R.B. Stonesifer. "An Analysis Procedure for Predicting Weld Repair Residual Stresses in Thick Walled Vessels." Pressure Vessels and Piping Conference, 25-29 June 1979. San Francisco, California: ASME,1979.

134) Salvetti, A. and A. Del Puglia. "Fatigue Crack Propagation in Stiffened Panels." The Eighth Congress of the International Council of the Aeronautical Sciences, 1972. Amsterdam, The Netherlands: AIAA, 1972.

135) Sanders, J. Jr. Effect of a Stringer on the Stress Concentration Due to a Crack in a Thin Sheet, Technical Report R-13, NASA, 1959.

136) Sih, G.C. and Faria, L. (1984). Fracture Mechanics Methodology. Martinus Nijhoff Publishers, The Hague, Netherlands.

137) Sikora, J.P., A. Dinsenbacher, and J.E. Beach. (1983, May). A Method for Estimating Lifetime Loads and Fatigue Lives for SWATH and Conventional Monohull Ships. Naval Engineers Journal, pp. 63-85.

138) Smith, C.S. (1975). Compressive Strength of Welded Steel Ship Grillages. Transactions RINA, Vol 117, pp. 325-359.

139) Soares, G. and Y. Garbatov. "Influence of Inspection and Repair on the Fatigue Reliability of Oil Tankers." OMAE, Vol 2, 1996: pp. 245-254.

140) Solin, J. “Analysis of Spectrum Fatigue Tests in Sea Water.” Ninth Intl. Conf. on OMAE Symposium, 1990. New York, NY, USA: ASME.

141) Stenseng, Arne. (1996). Cracks and Structural Redundancy. Marine Technology, Vol 33, N 4, pp. 290-298.

142) Sumi, Yoichi, Hisashi Iyama, Zeljko Bozic, and Yasumi Kawamura. (1996), Multiple Fatigue Cracks Propagating in a Stiffened Panel. Journal of the Society of Naval Architects of Japan, Vol 179, pp. 407-412.

143) Swift, T. “The Effects of Fastener Flexibility and Stiffener Geometry on the Stress Intensity Factor for a Stiffened Cracked Sheet.” Intl. Conf. on Prospects of Fracture Mechanics, 1974. Noordoff, Leyden, The Netherlands: Delft Univ. of Tech., 1974.

144) Swift, T. “Fracture Analysis of Adhesively Bonded Cracked Panels.” Transactions of the American Society of Mechanical Engineers, 1978. Atlanta, GA: ASME, 1978.

145) Tada, H. (1985). The Stress Analysis of Cracks Handbook. Saint Louis: Paris Productions, Inc.

146) Tall, L. (1964, January). Residual Stresses in Welded Plates--A Theoretical Study. Welding Journal, Research Supplement, 10s-23s.

147) Tall, L., and G.A. Alpsten. “On the Scatter in Yield Strength and Residual Stress in Steel Members.” Symposium on Concepts of Safety of Structures and Methods of Design. September 1969. London: International Association for Bridge and Structural Engineering, pp. 151-163.

148) Tanaka, K. “Mechanics and Micromechanics of Fatigue Crack Propagation.” 20th Symposium on Fracture Mechanics: Perspectives and Directions, 1989. Philadelphia, PA: ASTM.

149) Tanker Structure Co-operative Forum. Int'l Chamber of Shipping and Oil Companies Int'l Marine Forum. Guidance Manual for the Inspection and Condition Assessment of Tanker Structures. London, England: Witherby & Co., Ltd., 1986.

150) Tanker Structure Co-operative Forum. Int'l Chamber of Shipping and Oil Companies Int'l Marine Forum. Guidelines for the Inspection and Maintenance of Double Hull Tanker Structures. London, England: Witherby & Co., Ltd., 1995.

151) Tanker Structure Co-operative Forum. Condition Evaluation and Maintenance of Tanker Structures. London, England: Witherby & Co., Ltd., 1992.

152) Terada, H. Stress Analysis of a Crack in the Residual Stress Field by Welding and Its Application to the Fatigue Crack Propagation. Tokyo, Japan: National Aerospace Laboratory, 1994.

153) Tebedge, N., and L. Tall. Residual Stresses in Structural Steel Shapes: A Summary of Measured Values. Fritz Laboratory Report No. 337.34. Bethleham, PA: Lehigh University, 1973.

154) Thayamballi Mathummal, Anil Kumar. “Reliability of Ship Hull in the Fracture and Fatigue Modes of Failure.” Ph.D. dissertation in Engineering. 1983. University of California, Berkeley.

155) Torii, Tashiyuki; Kazuo Honda, and Masahiko Sugiyam. (1989). Surface Fatigue Crack Propagation Behavior in a Residual Stress Field. JSME International Journal, Vol 32, N 3, pp. 450-457.

156) Torii, T., K. Honda, and T. Hamano. (1988). Fatigue Crack Propagation Behavior in a Tensile Residual Stress Field. Trans. Japan Soc. Mech. Eng., Vol 54, N 500, pp. 679.

157) Toyosada, Masashiro; Toshio Niwa and Junichi Sakai. (1997). Physical Meaning of Delta KRP and Fatigue Crack Propagation in the Residual Stress Distribution Field. International Journal of Fatigue, Vol 19 , Suppl. 1, pp. S161-S166.

158) Toyosada, Masahiro and Toshio Niwa. (1995). Fatigue Crack Propagation Behavior in the Field of Residual Stress Distribution: Study of Fatigue Crack Propagation Based Upon RPG Load (7th Report). Journal of the Society of Naval Architects of Japan, Vol 178 , pp. 505-511.

159) Troitsky, M.S. Stiffened Plates: Bending, Stability and Vibrations. Oxford: Elsevier Scientific Publishing Co., 1976.

160) Ueda, Y., K. Fukuda, and K. Nakacho. "Basic Procedures in Analysis and Measurement of Welding Residual Stresses by the Finite Element Method." Proceedings of the International Conference "Residual Stresses in Welded Construction and Their Effects," 15-17 November, 1977, London, The Welding Institute: Abington Hall, Abington, Cambridge, CB1 6AL, UK.

161) Ueda, Y. and K. Nakacho. (1982). Simplifying Methods for Analysis of Transient and Residual Stresses and Deformations Due to Multipass Welding. Transactions of JWRI, Vol. 11 (1), pp. 95-103.

162) Ueda, Y. and H. Murakawa. (1984). Applications of Computer and Numerical Analysis Techniques in Welding Research. Transactions of JWRI, Vol. 13, No. 2, pp. 337-346.

163) U.S. Coast Guard. Circular 15-91. USCG NVIC 15-91. Washington, D.C.: U.S. Coast Guard, 1991.

164) Vlieger, H. (1973). The Residual Strength Characteristics of Stiffened Panels Containing Fatigue Cracks. Engineering Fracture Mechanics, Vol 5, N 2, pp. 447-477.

165) Vroman, R.H. An Analysis into the Uncertainty of Stiffened Panel Ultimate Strength. Trident Report 234. Annapolis, MD: U.S. Naval Academy, 1995.

166) Watanabe, M., H. Yajima, and H. Kawano. (1979). Analysis of the Crack Strength of a Stiffened Panel in a Ship Hull Structure. J. Soc. Naval Arch. Japan, Vol 146, pp. 314-320, 530.

167) White, J.D. and J.B. Dwight. "Weld Shrinkage in Large Stiffened Tubulars." Proceedings of the International Conference "Residual Stresses in Welded Construction and Their Effects", 15-17 November 1977. London: The Welding Institute, Abington Hall, Abington, Cambridge, CB1 6AL, UK, Paper 21. pp. 337-344.

168) Winter, P.W., and Macinnes, Don A. "Fatigue under Variable Amplitude Loading: A New Approach." Safety and Reliability, Proc. 1993 OMAE Conference. ASME, 1993. pp. 99-106.

169) Xiao, Dayton and R.J. Dexter. (1998). Finite Element Calculation of Applied J-Integral for Cracked Ship Structural Details. Engineering Fracture Mechanics, Vol 60, N 1, pp. 58-82.

11 Appendix A: Support Structure Cracking and Repair Methods

11.1 INTRODUCTION

Cracks occurred in a variety of locations during the testing of the specimens. These cracks provide additional information about welded and bolted details outside the scope of the original project. Many of the cracks started at discontinuities in the support structure, such as the cover plate termination. Other cracks starting due to rubbing, improper bolt tightness, and weld defects. All of these cracking incidences required repair in order to continue testing. These repairs were observed for effectiveness and crack recurrence.

This appendix details a number of cracks, the repairs made and their general effectiveness. When possible, a detailed account of the repair is made through illustrations and photographs. The overall setup may be seen in Figure 11-1. Particularly sensitive details are pointed out for later reference.

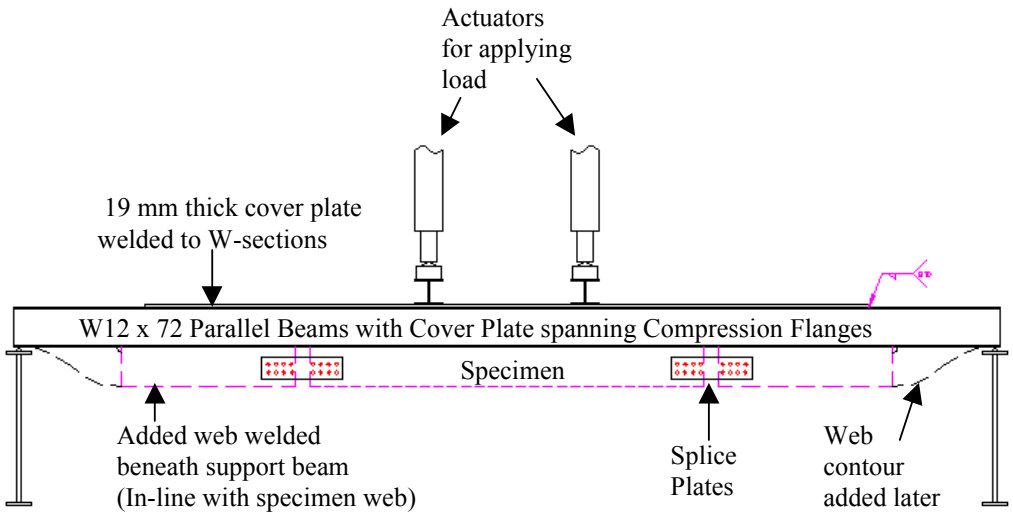

Figure 11-1: Testing setup with problem fatigue areas indicated.

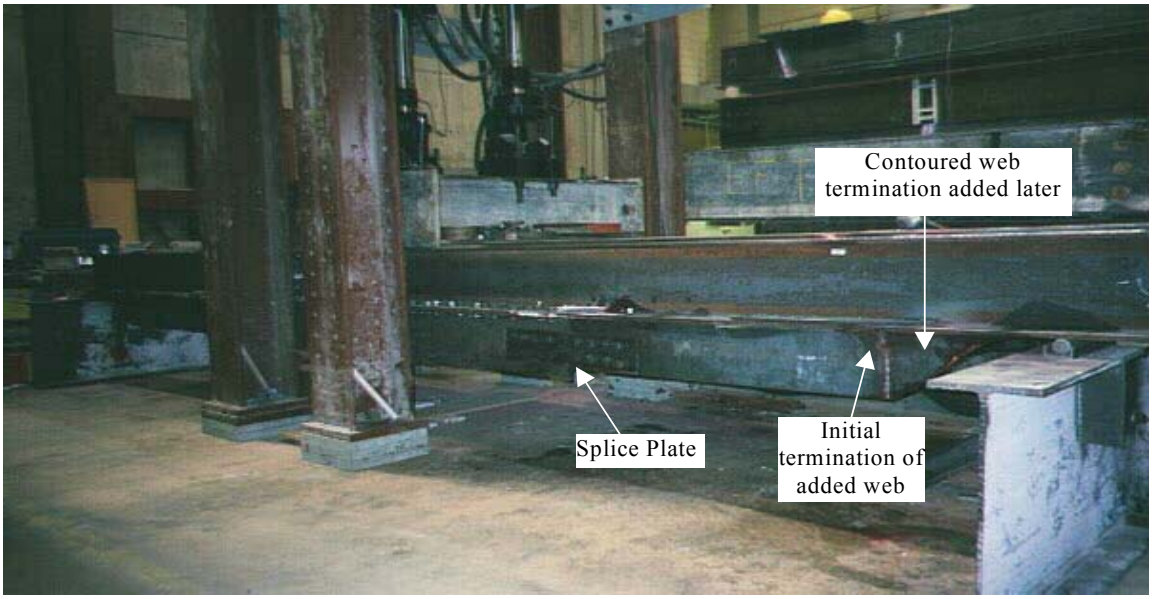

Figure 11-2: Testing setup with structural details clarified.

An actual photo of the experiment is seen above. The splice plates bridge the gap between the added web and the specimen. The thickness of the added web and each splice plate was 13-mm. Each added web was attached to the W12x72 beams by 8-mm double-sided fillet welds. These welds were made with the FCAW process and terminated approximately 3-cm from the end of either side of the added web. The web was tack welded at either side prior to making the full longitudinal fillet welds.

Eight A490 bolts, each 22-mm in diameter, were tightened to 75% of the yield strength of the bolt to provide a slip critical connection in the splice plates. The capacity of this bolt setup was considered highly conservative. However, variations in web placement in the specimens created alignment problems with web permanently mounted below the beam support structure. Spacer plates were used to provide smooth, aligned surfaces that the splice plates could be fastened to. The spacer plates, though, reduced the capacity of the connection and slippage was noticed if the bolts were not torqued to at least 80% of the nominal yield strength. An example of the spacer plates is seen in Figure 11-3.

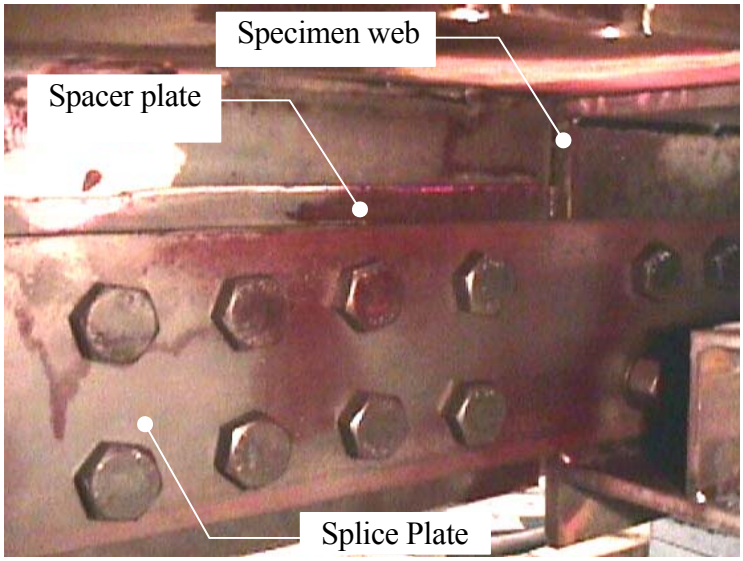

Figure 11-3: Spacer plates used to line up added web and specimen web.

Further detail will be now shown in outlining the cracking incidences.

11.2 FILLET WELD TERMINATION CRACKING

The first incidence of cracking was observed when webs were added below the W12x72 beams in line with the specimen webs. Splice plates connected the webs to each specimen as seen in Figure 11-4. The web and splice plate addition was made to promote force transfer to the composite section of the specimen and the support structure. These modifications, however, initially caused high stresses to be located in fatigue-sensitive areas, such as the added web termination.

Initially there was no smooth contour used to gradually taper the added web. Excluding the taper caused a high stress concentration at the fillet weld terminations. These fillet weld terminations were located 20-cms from the support. It was thought that the net section stress at this point would be below the S-N fatigue limit for fillet weld terminations, a Category E detail. The stress ranges exceeded the constant amplitude fatigue limit (CAFL), however, and cracking ensued at all four corners. The figure below illustrates the point of cracking.

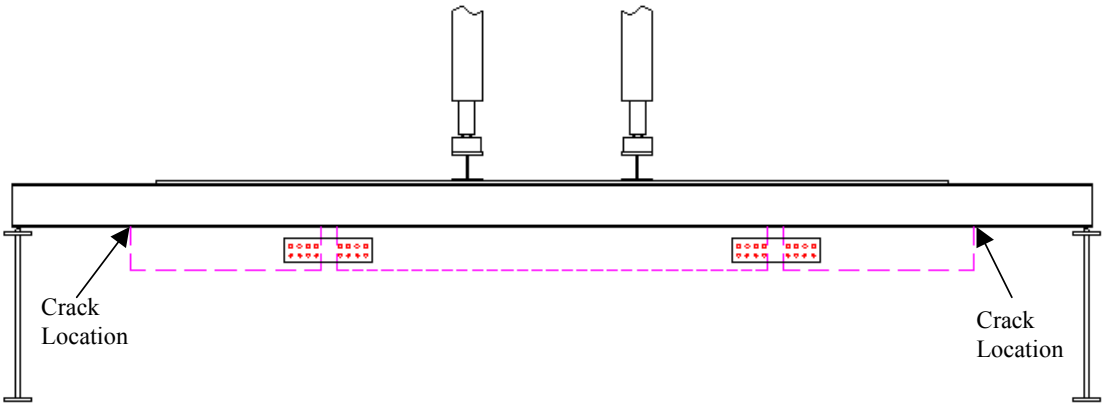

Figure 11-4: Initial testing setup with abrupt web terminations.

A typical crack may be seen in Figure 11-5. These were relatively long, through-thickness cracks that had not yet entered the beam web. Although the crackswere located at all four corners of the structural setup, they were not noticed until a detailed inspection was performed. An appreciation for the difficulties of field inspection may developed from this experience.

Table 11-1: Initial cracking in added web fillet weld terminations.

Crack Description	Corner Location/Through -thickness final length (mm)	Estimated Stress Range	Estimated Number of Cycles	Repair Method (More detail follows)
Fillet weld termination	SE: 100 NE:105 SW: 110 NW: 45	39 MPa	1.2×10^6	Remove part of added web, drill out crack tips, buttweld crack in flange between drill holes, add contoured web

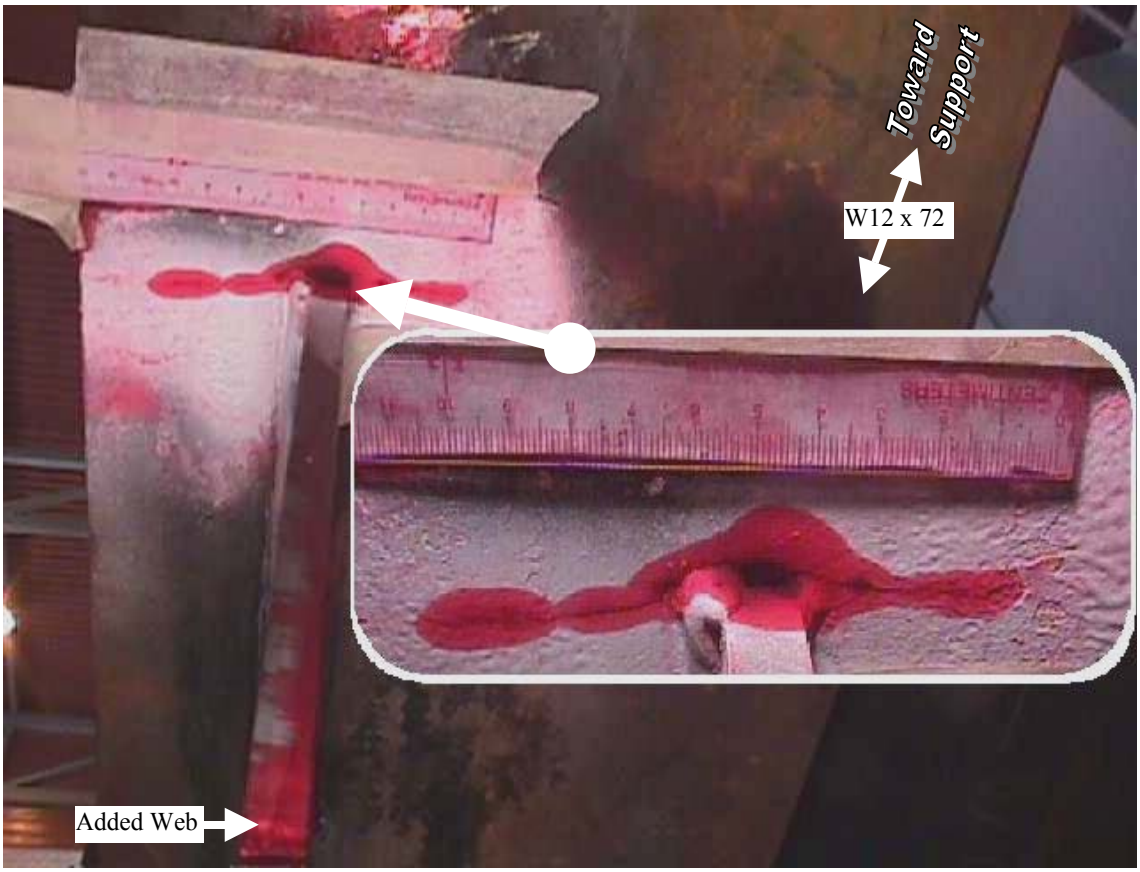

Figure 11-5: Typical crack at fillet weld termination of added web.

Notice the offset of the added web from that of the flange centerline. The eccentricity of the added web was necessary to maintain alignment with the specimen webs.

At this point one might question the design W-sections, but these were painstakingly chosen for their dimensions. A brief aside will be used to justify the design and provide insight into the beam size selection. It is presented here because the consequences of the design are most pronounced in the fatigue problems that are presented in this appendix. The beam size of W12x72 was chosen for several reasons:

- First of all, a greater depth beam would reduce the stresses available in the stiffened panel for testing. Since the composite section (i.e. Support beams and test specimen) has a large section

modulus, the overall depth of the structure had to be minimized to reach the desired stress levels in the stiffened plate of the specimen.

- Secondly, the beam flanges had to be wide enough to accomodate the bolt-up assembly of the specimens. Bolting patterns were detailed to provide the easiest assembly possible considering both bolt strength requirements and the feasibility of tightening the bolts to slip-critical specifications.
- Finally, the capacity of the actuators and laboratory was a factor in developing a specimen the optimized the use of transverse width limitations.

The experimental testing could not procede without repair of the cracks at these loacation. The repair of the cracks will be detailed through the use of photographs and accompanying description.

The first step in rhe repair was to locate the crack tips. This was performed with the red penetrating dye previously discussed in this report. A 19-mm hole was drilled at the crack tips once they were located. A photograph of one crack tip being drilled out may be seen in Figure 11-6.

Figure 11-6: Drilling out the crack tips.

Drilling out the crack tips removes any existance of a sharp notch that might promote further cracking. A typical location with holes drilled at the crack tips may be seen in Figure 11-7. With the crack tips drilled out, a 10-cm portion of the added web was removed to increase accessability to the cracked region. A recipricating saw was used as seen in Figure 11-8.

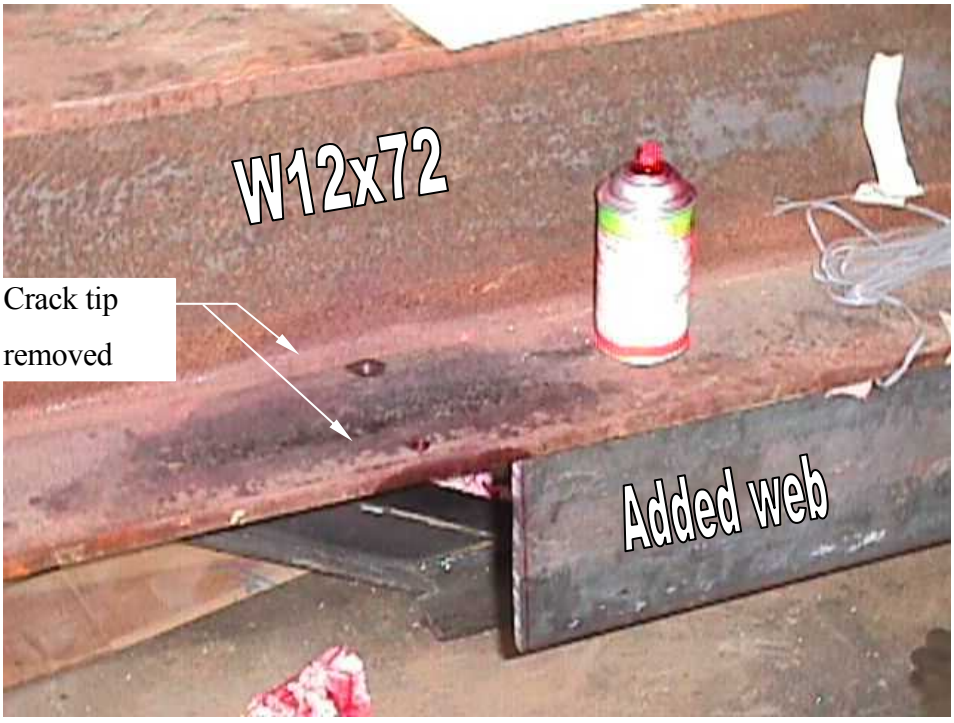

Figure 11-7: Drilled out crack tips in beam flange.

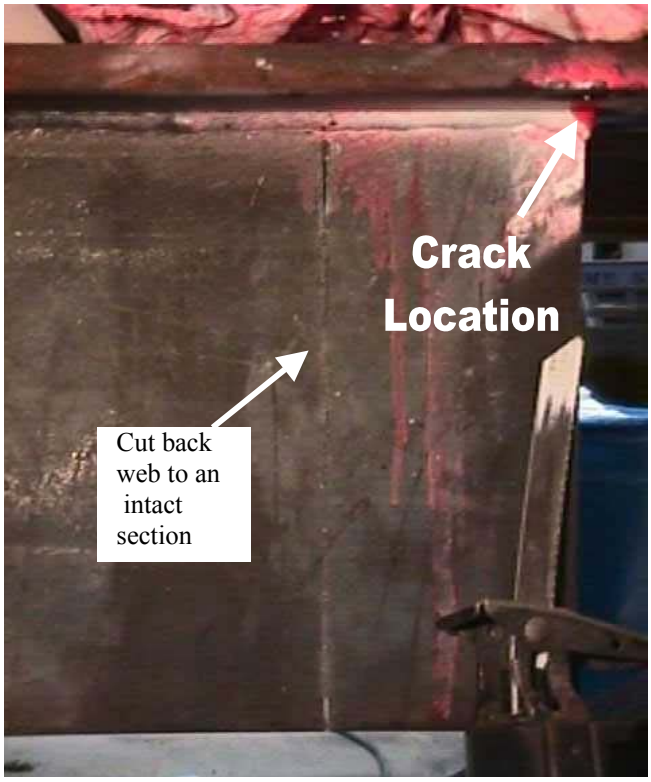

Figure 11-8: Increasing accessibility for weld repair.

Figure 11-9: Resultant weld between drilled-out crack tips.

Increased accessibility to the crack allowed a complete penetration weld to be made between the drilled holes. The end result may be seen in Figure 11-9. Normally one should not weld the drilled holes shut as this creates an area of high constraint once the weld cools. Instead, the weld should be

made between the holes and the the holes should be enlarged to remove any roughness that might exist at the weld termination.

After repairing the cracks in the beam flanges, an overall improvement to the added web termination was necessary. The abrupt termination of the added web was replaced with a contoured web. The addition of the contoured web termination may be seen in Figure 11-10.

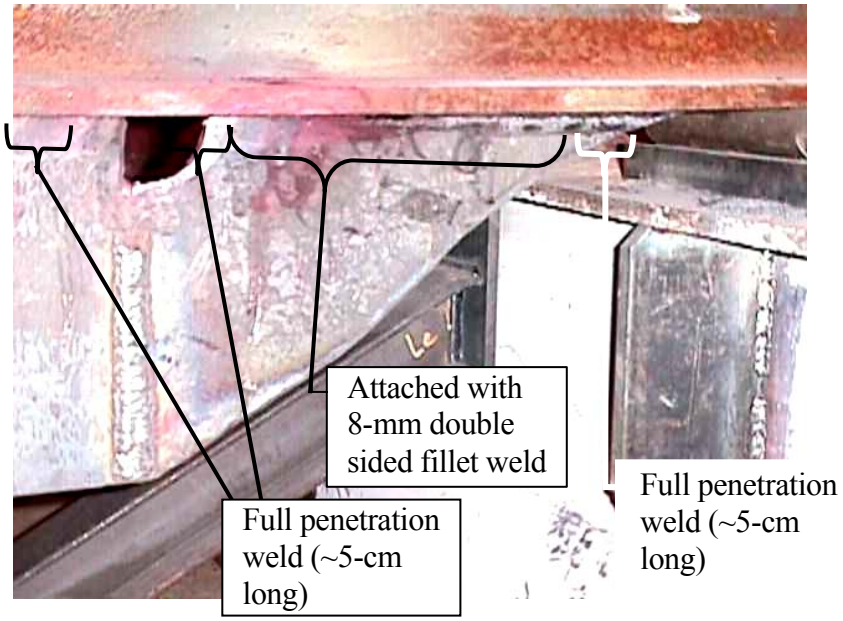

Figure 11-10: Attachment of contoured web to existing web.

It was predicted that adding the contoured web would gradually transfer the force from the web into the support beam. For increased fatigue resistance, the terminations of the added web were made with full penetration welds. The remainder of the contour was attached with 8-mm double sided fillet welds.

The contour web addition was made to all four corners of the supprot structure. A picture of the resultant repair may be seen in Figure 11-11.

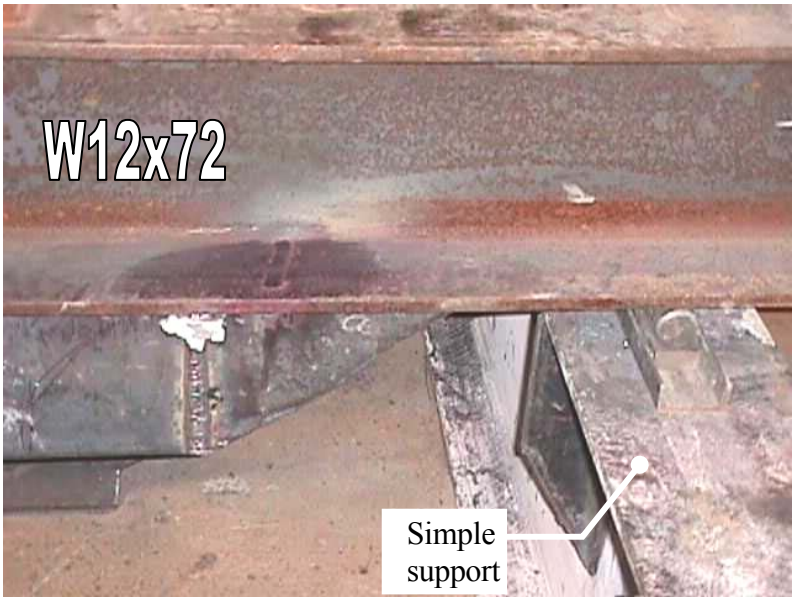

Figure 11-11: Typical repair for web terminations at four corners.

11.3 CRACKING IN FULL PENETRATION WELD AND BASE METAL

Modifying the abrupt termination of the added web was originally predicted to solve the fatigue cracking issue at these locations. It was soon found, however, that the state of stress was high enough even near the support to induce fatigue cracking. Fatigue cracks developed at both the contour web terminations and the weld access holes. All of these locations had been improved with a full-penetrations weld. Several small defects, however, were noticed in the welds. Fatigue cracks initiated at these flaws as wellas in the base metal of the added web. These cracks had grown to an average length of 15-mm within 1.5×10^6 cycles. Parallel cracks were noticed at several corner locations indicating a large amount of stress existed in the region. The crack tips were immediately drilled out once the crack had prograssed into the beam flange. Figure 11-12 and Figure 11-13 show a pair of cracks emanating from the end of the contoured web termination with the crack tips already drilled out.

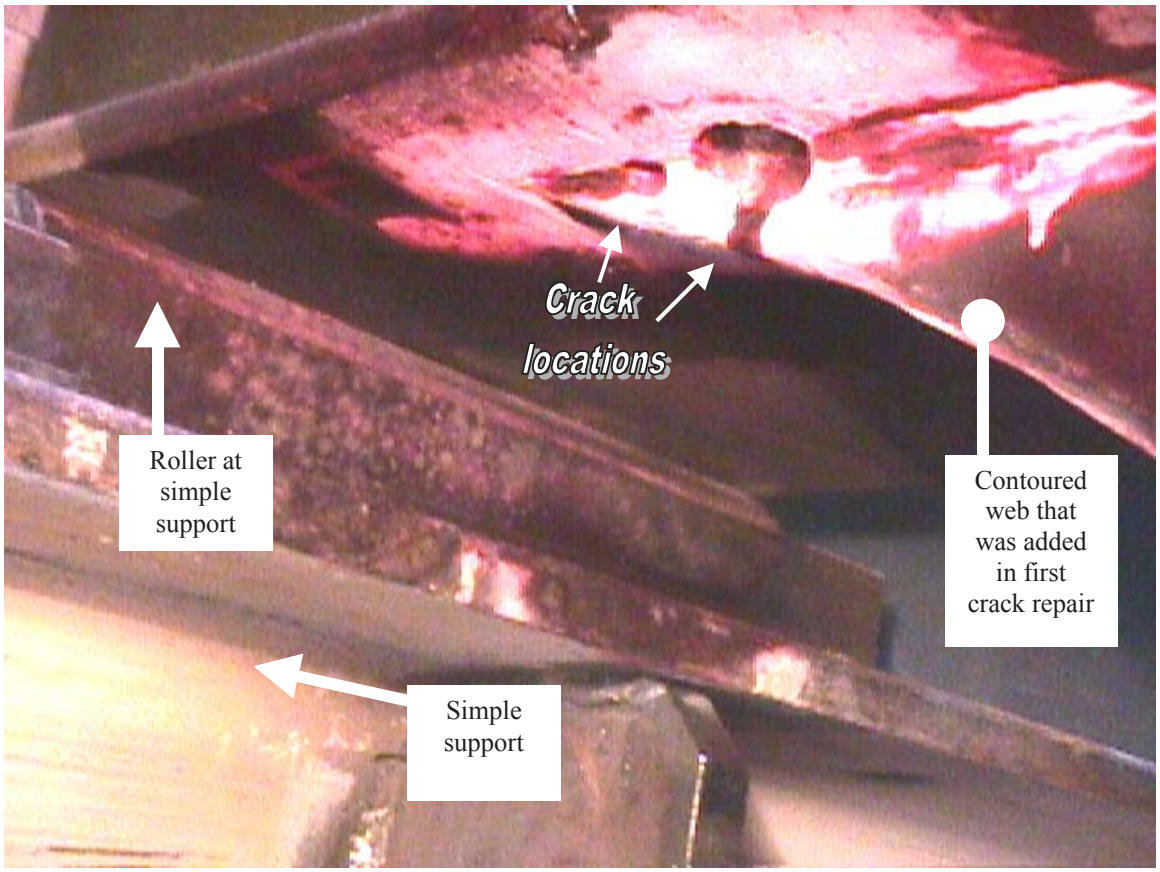

Figure 11-12: Cracking in full penetration weld after contour repair was made.

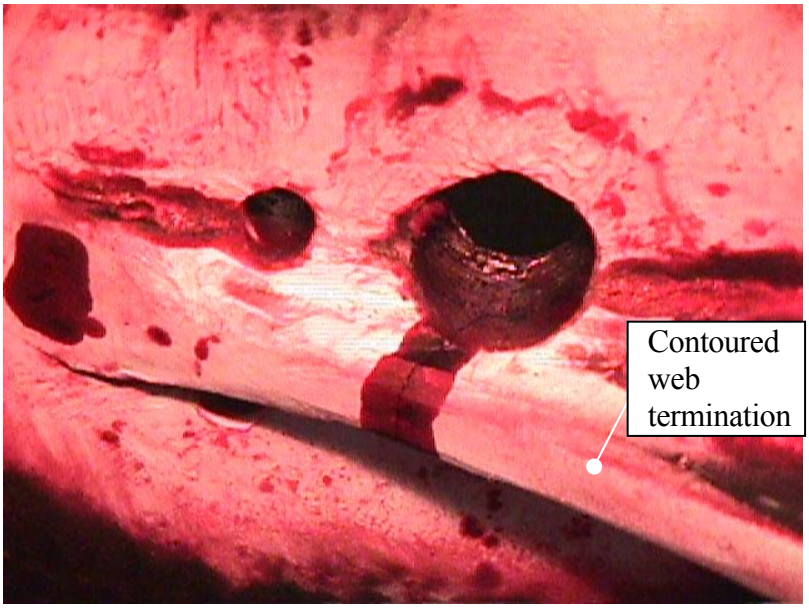

Figure 11-13: Detail of crack occurring in full penetration weld with tips drilled out.

Table 11-2: Cracking in contoured web additions at full penetration weld.

Crack Description	Corner Location/Crack Length (mm)	Estimated Stress Range	Estimated Number of Cycles	Repair Method
Full penetration weld termination	SE: 15 NE:12 SW: 20 NW: 12	55 MPa 55 MPa 55 MPa 55 MPa	$2.5x10^6$ $2.5x10^6$ $2.5x10^6$ $3.0x10^6$	Drill hole at crack tips. Hole diameter ~1/3-1/2 crack length

The only repair that could feasibly address this problem area was drilling out the crack tips. Hole drilling has been used for years as a crack arrestor. By drilling a hole at the crack tip, two goals are accompliched:

1) The region is made more flexible relieving highly constrained areas.
2) The sharp crack is replaced with a smooth circular profile which readily opens.

New cracks can only develop if a new notch is introduced. With a drilled hole, the surrounding material simply hinges about the hole and new notches cannot be developed. This behavior can be expected provided the hole is large enough. The hole size required to arrest a crack may be determined from the equation:

$$\rho > \left[\frac{\Delta K}{10.5\sqrt{\sigma_y}} \right]^2 \qquad \text{Eqn. 11-1}$$

where ρ is the required hole diameter in meters, ΔK is the applied stress intensity factor range, and σ_y is the yield stress of the material in MPa. This relation was originally developed by John Fisher to address fatigue cracking in brigde structures. Roughly speaking, the hole diameter should be approximately 1/3 the total crack length to arrest the crack in a steel structure. Obviously this is not amenable to long cracks, but for instances of distortion-induced cracking such as this one it is exceptionally effective.

The cracks at all for corners were repaired by drilling holes typically 16-mm in diameter. For the larger cracks, the hole size was increased to a 25-mm diameter. With the holes drilled, testing continued and no further cracking was noticed even after an additional 10 million cycles were applied. This number of cycles is approximately four times the number of cycles that previously initiated and propagated the termination cracks. Therefore, this repair method is highly recommended in areas where a hole may be tolerated and cracking is intiated due to high local constraint.

11.4 BASE METAL CRACK IN ADDED WEB

Previously it was mentioned that the webs of the specimens did not always line up with the added web. This presented a problem when attaching the splice plates between the specimen and the added web. An in-line connection was achieved by placing spacer plates between the splice plates and the webs.

At one location, the southeast corner, the alignment of the webs was off as much as 13-mm. When the spacer plates were used at this location, the slip-critical connection was poor and a crack initiated at the last bolt hole within 50,000 cycles. The crack quickly propagated through the entire added web and into the beam flange. Figure 11-14 shows the location being discussed.

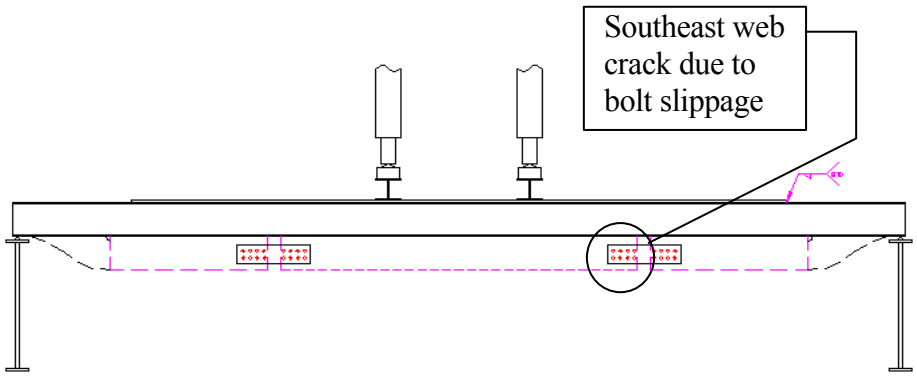

Figure 11-14: Area where clamping force in slip-critical connection was poor.

A simulation of the crack location may be seen in Figure 11-15. A closer view of the initial crack is presented in Figure 11-16.

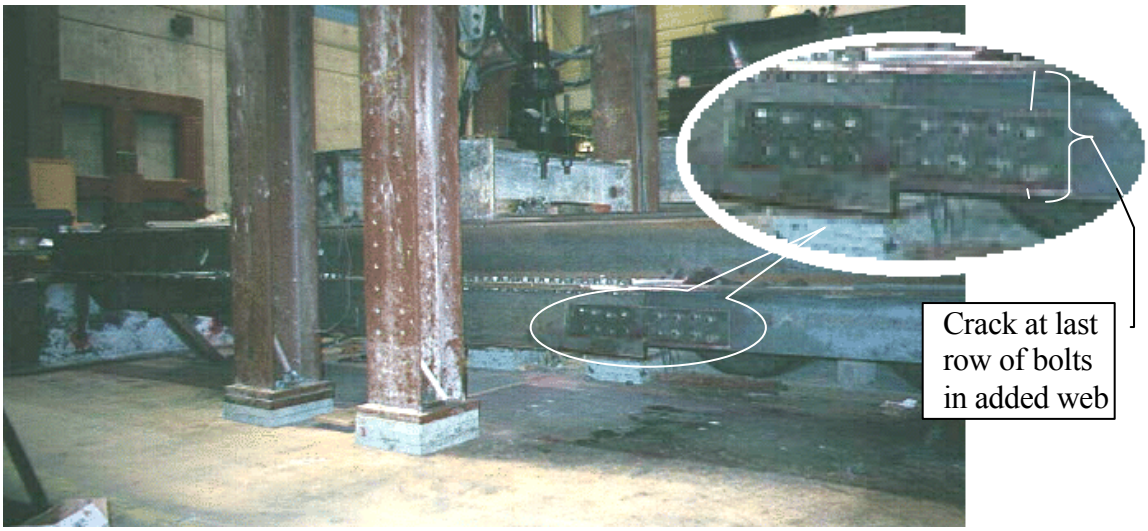

Figure 11-15: Detail of crack occurring in full penetration weld with tips drilled out.

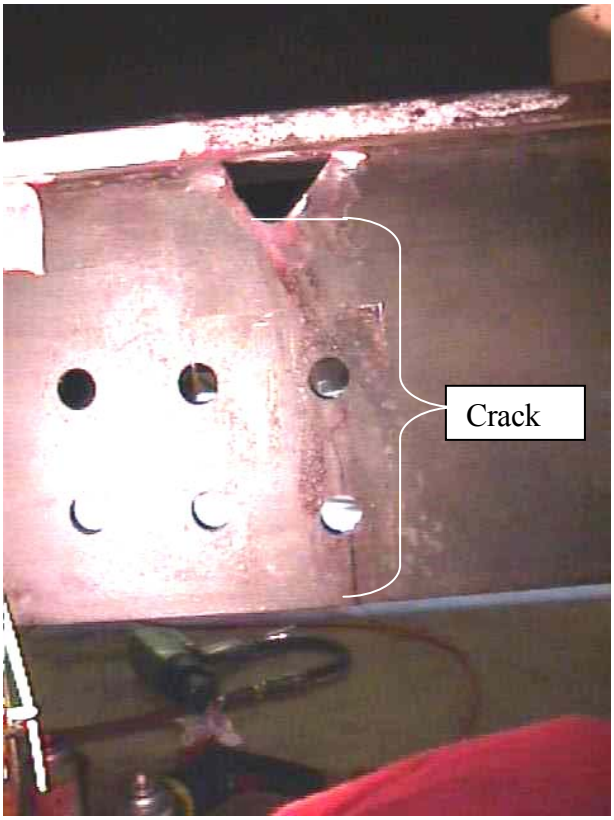

Figure 11-16: Detail of crack in added web with weld access hole already prepared.

The repair was made similarly to the first repair discussed: First drilling out the crack tips, then cutting in a weld access hole, arc-gouging the crack faces, and finally making a complete penetration butt weld between the cracked faces. This repair was accompanied by adding 3 rows of bolts and a longer splice plate.

A series of photographs detail this repair. Figure 11-18 shows the holes drilled in the bottom flange of the support beam to remove the crack tips. The weld access hole has also been roughly cut in with a reciprocating saw. One may also notice the arc-gouged crack in preparation for a complete penetration weld. Arc-gouging the crack faces was found to be a useful technique for both tracing the crack line and preparing the detail for a butt weld. Grinding is the alternative method of preparing for the butt weld, but tracking the crack can be extremely difficult when an abrasive wheel is used to remove material. A closer view of the prepared crack and drilled holes may be seen in Figure 11-17.

Figure 11-18: Crack faces arc-gouged and crack tips drilled.

Figure 11-17: Detail of crack at prepared weld access hole prior to welding.

The entire length of the crack would be gouged to mid-thickness prior to welding two crack faces together. After this first weld was made, the opposite side was back-gouged and

welded to no trace of the previous crack existed within the weld.

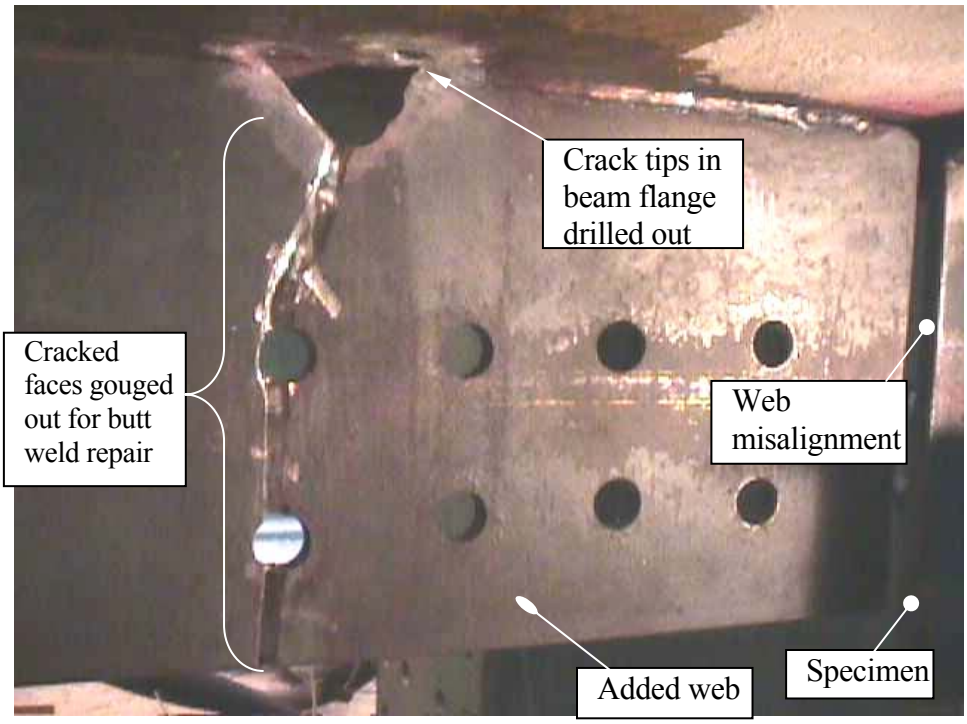

Figure 11-19: Full view of cracked area prior to weld repair.

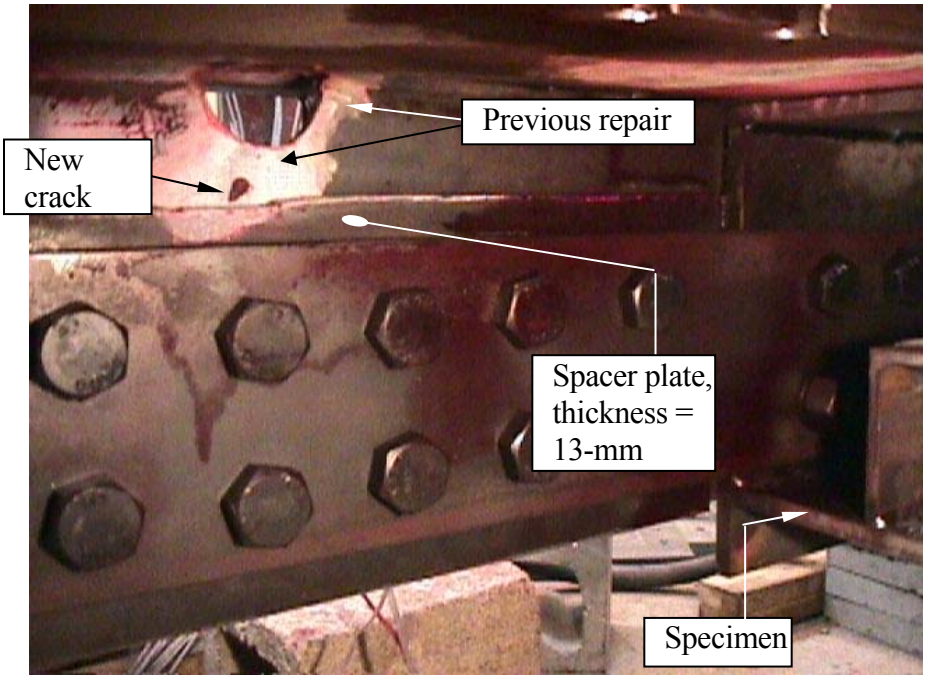

Figure 11-20: Full view of repaired crack.

The repair with the splice plates attached is shown in Figure 11-20. Notice the splice plates were extended to overlap the previously cracked area.

This repair was successful only as a temporary solution. Cracks repeatedly emerged from the weld access hole, the bolt holes, or a defect in the butt weld itself (See Figure 11-21). These cracks were allowed to propagate if they were contained to the added web for the duration of the particular specimen's test.

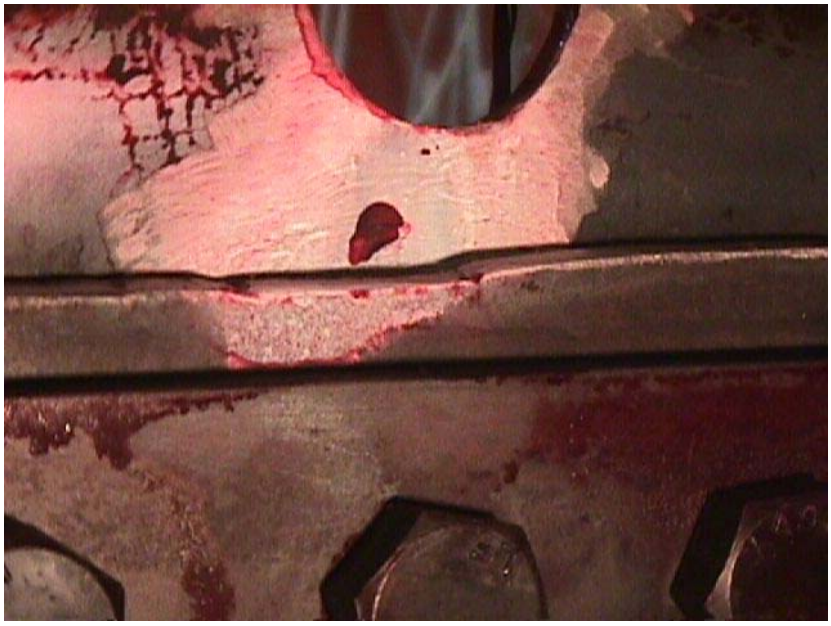

Figure 11-21: Re-initiation of crack from internal weld defect.

A new repair was made at the time specimens were changed. The repair was repeated four times during the span of the testing schedule. After the second repair, a strain gage was mounted 3-cm below the weld access hole. The stress range at this location was measured to be 80 MPa. At this stress range, new cracks emerged reliably at one million cycles after each repair. A record of the crack recurrence at this location may be seen in Table 11-3. The crack lengths and number of cycles shown correspond to the point at which the cracks were first noticed.

Table 11-3: Cracking in butt weld repair at splice location.

Crack Description (Weld access hole = W.A.H.)	Crack Length (mm)	Estimated Stress Range	Estimated Number of Cycles	Repair Method
From bolt hole due to slipping	134	60 MPa	0.4×10^5	Full repair as described above
1st butt weld repair, from bolt hole	25	80 MPa	9.8×10^5	
2nd buttweld repair, from crack at W.A.H.	19	80 MPa	1.0×10^5	
3rd butt weld repair, from butt weld defect	8	80 MPa	1.3×10^5	
4th butt weld repair, from W.A.H.	12	80 MPa	1.1×10^5	

11.5 SPLICE PLATE CRACKING

Cracking occurred in the splice plates for a variety of reasons despite being over-designed for the theoretical conditions. For the majority of the cracking incidents, the misalignment of the specimen web and the added web played a major role in crack initiation. Splice plate failure occurred a number of times and the failures can be categorized in one of three categories:

A) Crack initiation due to ineffective clamping force
B) Crack initiation due to high tensile stress ranges
C) Crack initiation due to rubbing

These three cases may be seen in Figure 11-22. A close view of the fatigue crack surface in case B is shown in the photo on the right.

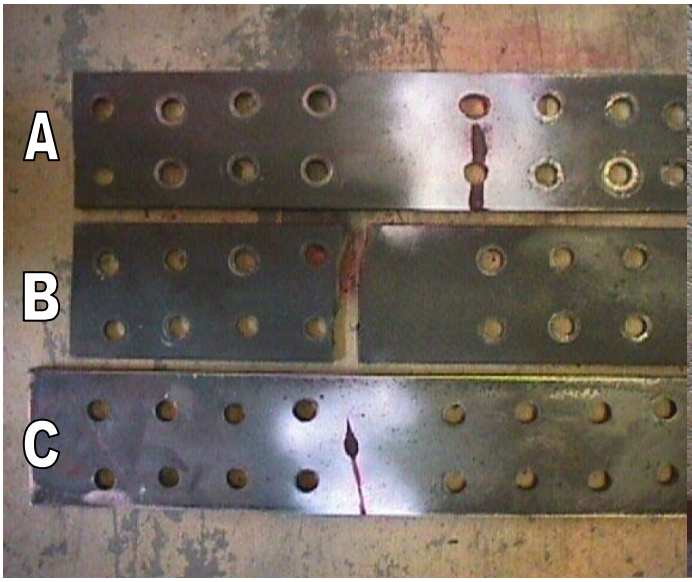

Figure 11-22: Various cracks observed in splice plates

Figure 11-23: Fatigue striations on crack faces of Case B.

Case A can be attributed to both web misalignment and improper clamping force. The slight misalignment of the webs, even with spacer plates, induced a small amount of prying when tensile load was applied. This prying action prevented the first row of bolts from sufficiently providing a slip-critical connection. Without a slip critical connection, the bolted tension member drops from a Category B detail to a Category D detail. Such a shift represents a 56 percent reduction in the constant amplitude fatigue limit.

Case B has occurred for similar reasons to that of Case A. Web misalignment probably induced loading other than pure tension. In this case, however, the crack did not initiate at the bolt hole. For this reason, it is believed that cracking in splice plates at other locations in the frame increased the loading demands placed on splice plate B. The failure is seen as a pure base metal failure, a Category A detail. Category A details have a constant amplitude fatigue limit (CAFL) 50 percent higher than that of a slip-critical connection. The development of this type of crack indicates that a large amount of load shedding to this detail occurred when the other splice plates cracked.

Case C is the direct result of rubbing between the splice plate and one of the webs it connected. The rubbing initiation is recognized because the crack initiated in the gap between the specimen and the added web.

Usually splice plates were discarded and replaced with newly drilled plate steel. After the initial cracking, the splice plate thickness was increased 50 percent at all locations. This was the maximum thickness which could be tolerated in the setup because the exterior stiffeners were closely spaced next to the edge web. The actual clearance was 10-cm and may be seen in Figure 11-24.

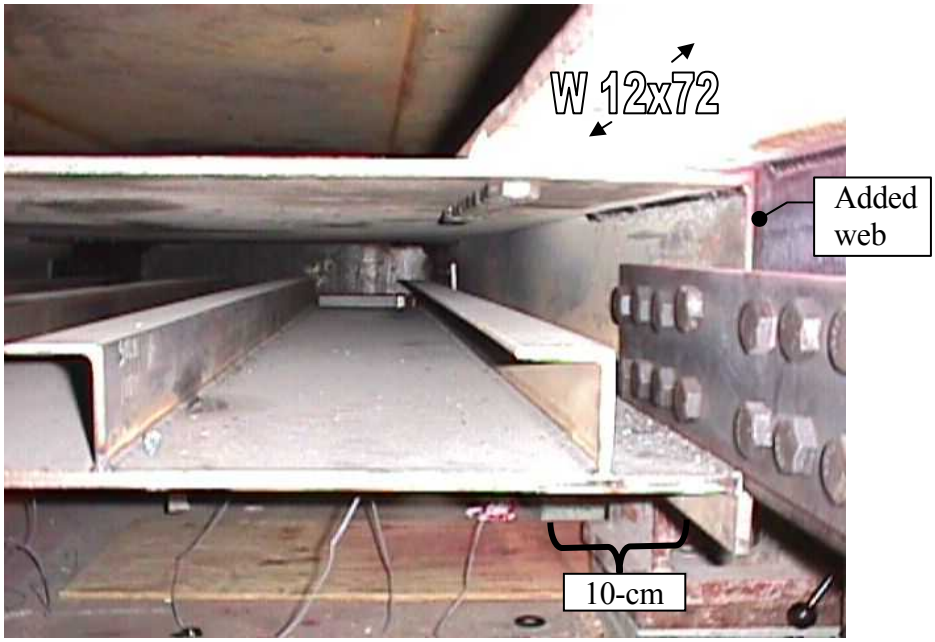

Figure 11-24: Tight clearances for bolting splice plates.

Even with the increased thickness all of these cracks reocurred. In several of the plates it was decided to show the effectiveness of the previously described welding repair technique. The repair was made similarly to the other weld repairs: Finding and drilling out the crack tip, weld repairing the crack, and re-drilling the weld tremination to provide a clean termination. The performance of the repaired plate was very good and the plate was able to be re-used as shown in Figure 11-25. Poorer performance was seen in the repair of plates with cracks emanating from bolt holes. In these repairs, the weld terminated in an active bolt hole which had to be oversized to provide the clean

weld termination. Oversizing, however, reduced the capacity at that particular location and cracking re-initiated at the bolt hole at approximately 800,000 cycles.

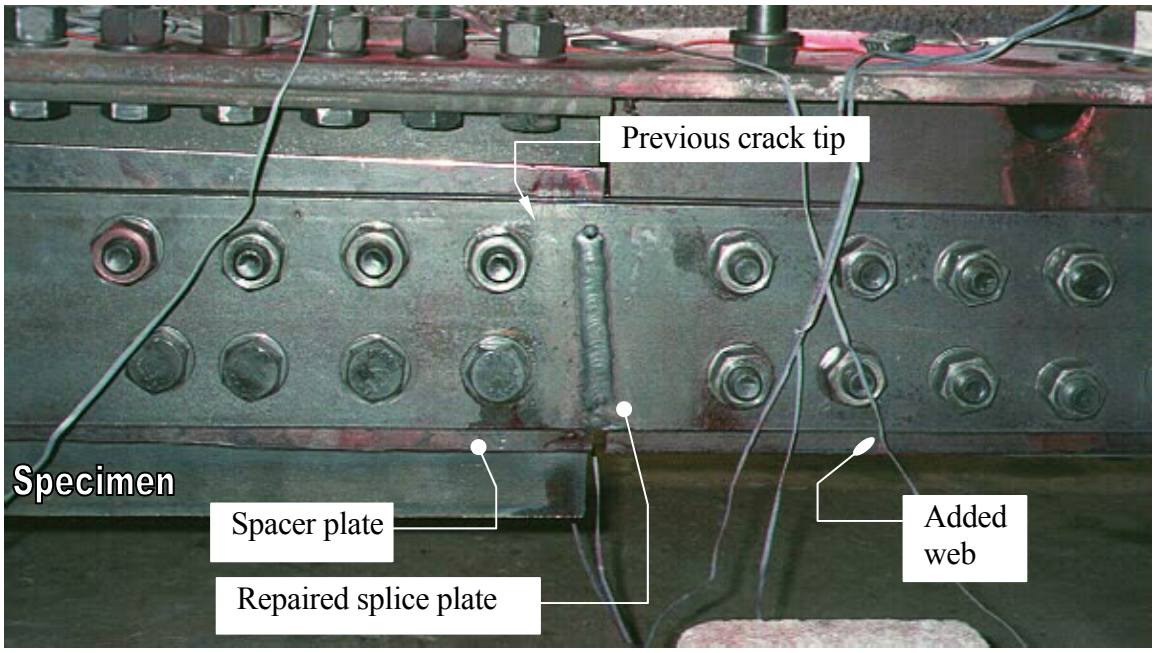

Figure 11-25: Repaired splice plate assembled in test setup.

11.6 COVER PLATE CRACKING

The support structure boasted a 19-mm thick cover plate that was fillet welded to parallel W12x72 beams. The cover plate was attached continuously to the beams by 8-mm fillet welds with E70 weld material. During the testing of the second specimen, a large crack was noticed at the southwest corner of the structure. The crack discovered had propagated to almost the full width of the beam flange and had penetrated the beam web. Cracking was not noticed at the other cover plate termination locations, however. Figure 11-26 illustrates the crack propagation direction and cover plate detail.

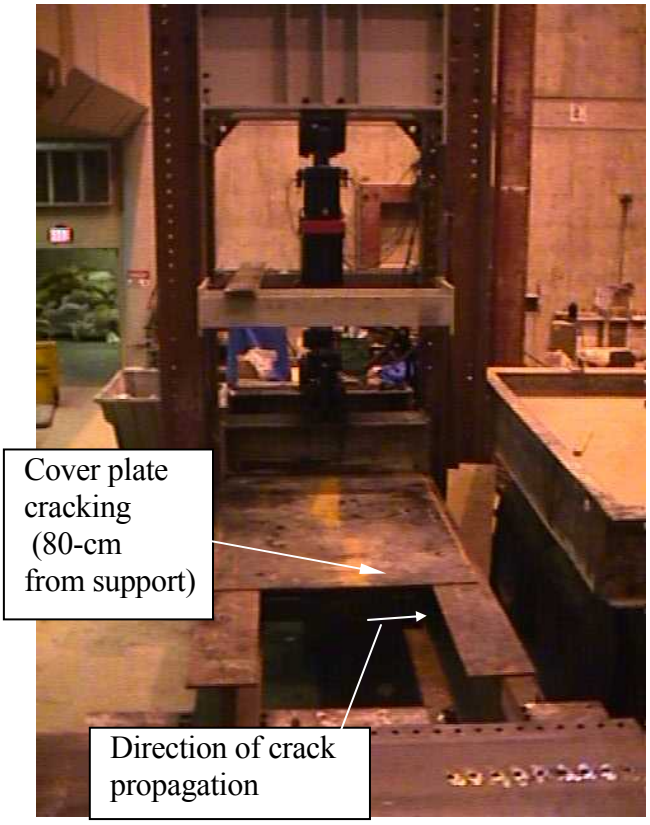

Figure 11-26: Cover plate detail prior to repair with and crack propagation direction indicated.

Table 11-4: Cracking at end of cover plate.

Crack Description	Crack Length (mm)	Estimated Stress Range	Estimated Number of Cycles	Repair Method
Fillet weld termination (Category E detail)	267-mm in beam flange, 37-mm in beam web	20 MPa nominal	3.4×10^6	Gouge crack path and buttweld, drill out crack tip, add section transition

The repair to the cover plate crack involved completely gouging out the cracked area and welding the crack faces with a full-penetration, one-sided weld. In the web, the cracked area was completely removed and a large opening was created to erase any presence of sharp discontinuities. Once the

compression flange of the beam was repaired, the cover plate was extended with both a rectangular and triangular plate addition. The cover plate extension may be seen in Figure 11-28.

Figure 11-27: Plates added to smooth transition of cover plate width.

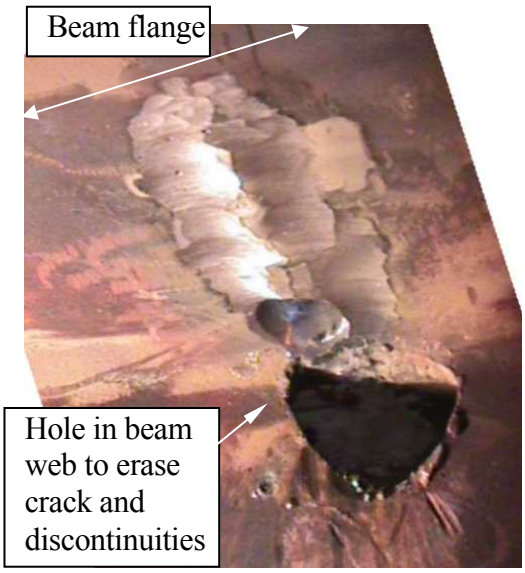

Figure 11-28: Gouged hole in beam web to erase crack tips.

The triangular section was the source of small fatigue cracks after 500,000 cycles at the point where it connected with the rectangular plate. These cracks were successfully ground out and then the triangular piece was ground to a smooth contour as seen in Figure 11-27 and Figure 2-9. After one million cycles, cracks re-emerged from defects in the butt weld and holes were drilled, as seen in Figure 11-29, to contain the crack to a small region.

Figure 11-29: Holes drilled to contain crack propagating from internal weld defect.

The cover plate extensions were provided on the east side of the support structure only. On the west side, surface cracks were found at both north and south transverse fillet welds. These surface cracks were each 76-mm long and had not progressed the full depth of the fillet weld. Instead of a more costly repair performed on the east end, peening was used with an air-powered impact chisel. The toe of the transverse fillet weld was thoroughly hammered with the impact chisel, making a 3-mm depression in the base metal and weld material. The surface crack at the toe of the weld never re-appeared. However, a small surface crack appeared mid-way in the testing in the fillet weld exterior surface. To repair this crack, the impact chisel was used over the entire transverse fillet weld and part of the longitudinal weld. This operation successfully erased all incidence of cracking for the remainder of the testing (~7 million additional cycles) at the west end cover plate terminations. Such success re-iterates the well-known benefits of peening in fatigue-sensitive areas.

11.7 BEAM TENSION FLANGE CRACKING

The initial fabrication of the support structure included angles that connected the bottom flanges of the parallel W-sections. These transverse attachments were fillet welded to the bottom flanges with a 10-cm long fillet weld for stability during transport. The angles were removed in the laboratory once the support structure was set in place. The area of connection was roughly ground smooth at three locations, while the fourth location was left with a flame-cut section of angle remaining.

Late in the testing, a faulty wire gave erratic signals to one of the actuators. When this happened, control devices in the system would abruptly stop the testing, resulting in a slight impact loading to the testing setup. The problem could not be immediately identified, and the impact loading continued sporadically over the course of one million cycles. This impact loading caused fatigue cracks at the locations where the fillet welded attachments previously existed. In fact, at one location over 60 percent of the tension flange of the W12x72 beam had cracked. The crack had penetrated 18-mm up the beam web as well. This crack may be seen in Figure 11-30 and in Figure 11-31.

The procedure for repair was performed exactly as illustrated before. Figure 11-32 shows where the tip of the crack in the beam flange was replaced with a drilled hole. Similarly, Figure 11-33 shows the tip in the beam web drilled out.

Figure 11-30: Crack in beam tension flange due to abrupt stops in loading.

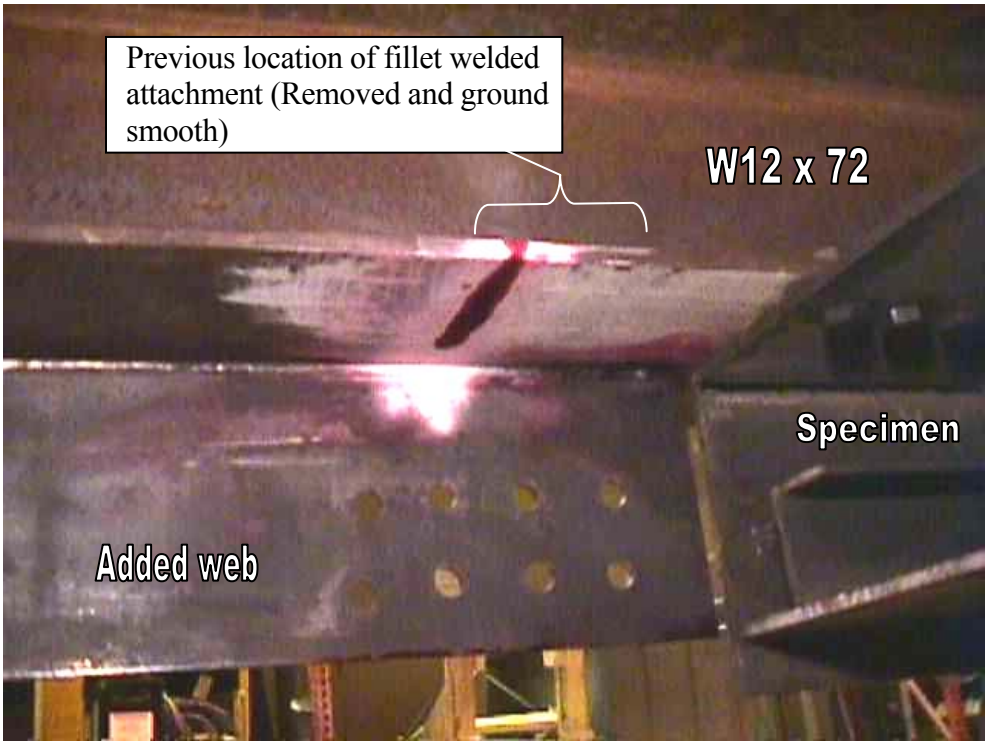

Figure 11-31: Bottom view of cracked beam flange.

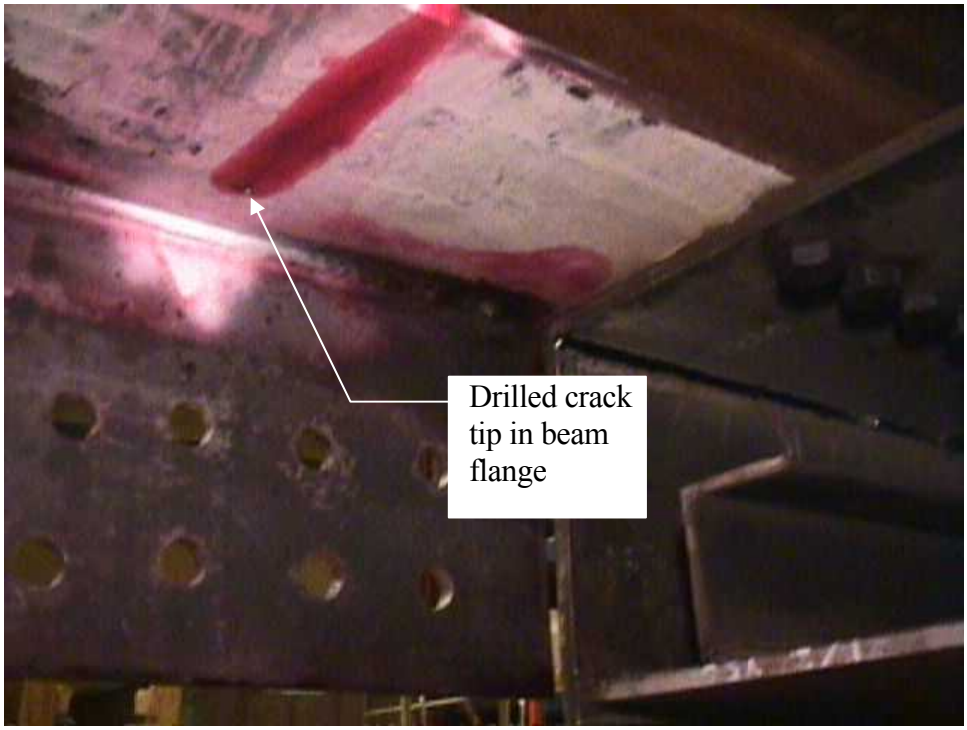

Figure 11-32: Crack tip in tension flange drilled out.

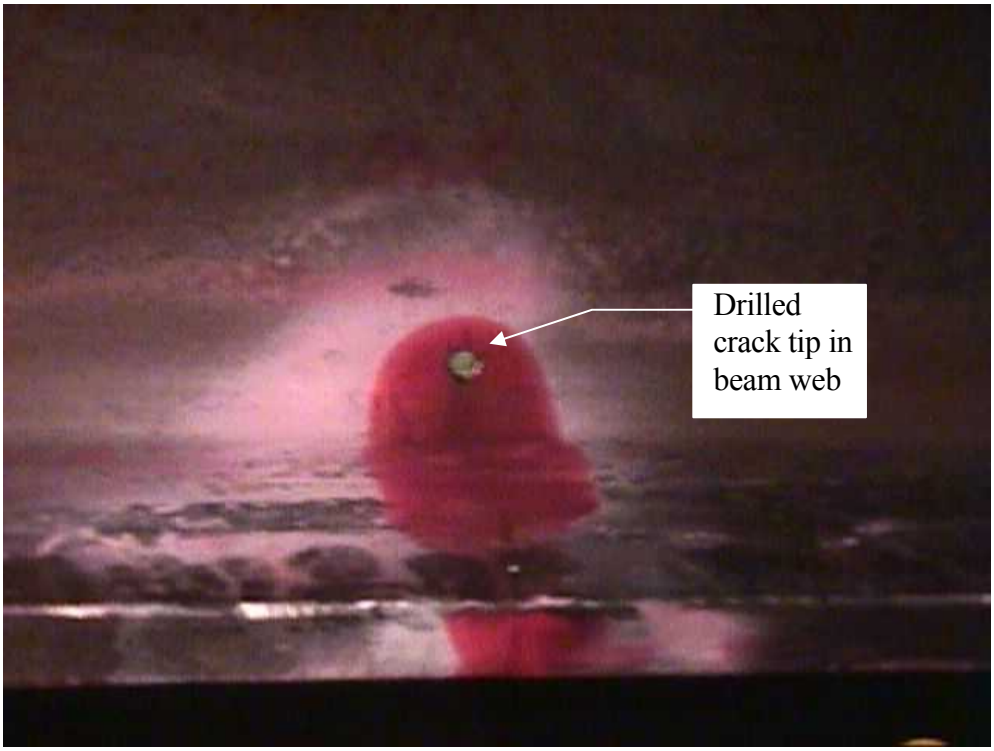

Figure 11-33: Crack tip in beam web drilled out.

To illustrate the importance of making sure the crack tip has been drilled out, Figure 11-34 shows a first attempt at drilling out the crack tip. After drilling the hole, the red dye penetrant is re-used to make sure the crack terminates in the hole that was drilled. On this occasion, the crack tip was missed by the drilled hole and a larger hole became necessary, as seen in Figure 11-35. Note that these holes are not intended to arrest the crack. They are merely placed to remove the crack tip and provide a guide on the extent of the crack faces in welding.

Figure 11-34: Initial hole drilled which missed the crack tip.

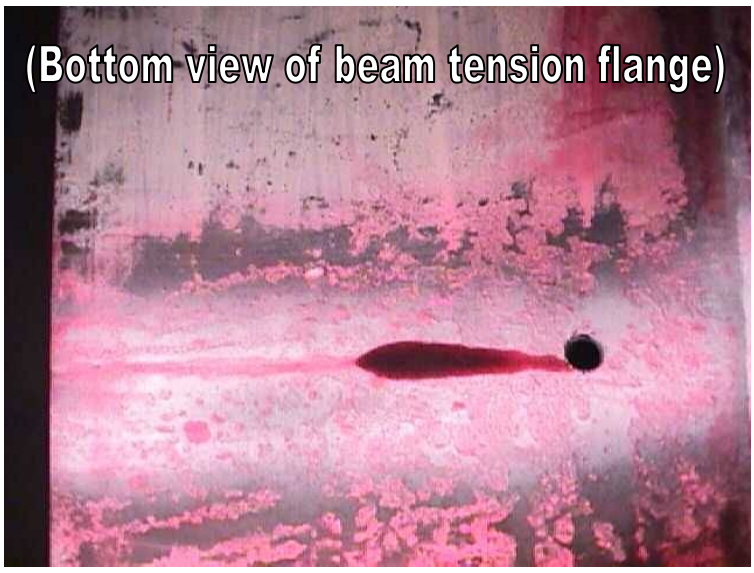

Figure 11-35: Enlarged hole captures the crack tip.

Once the crack tips had been drilled out, a one-sided butt weld was made with a backing bar in place (See Figure 11-36). The completed butt weld was then ground smooth to allow for redundant bolted plates to be used. The ground butt weld and bolting pattern may be seen in Figure 11-37. The bolted plates were included as an additional precaution as this location was a critical region of the support structure. Although the bolted plates were designed as a slip-critical assembly, it was projected that slip-critical connection should only be relied upon as a safety measure in the event of full flange cracking. In other words, the slip-critical connection was projected to not be effective in preventing future crack initiation.

Figure 11-36: Completed butt weld with backing bar in place.

Figure 11-37: Ground butt weld with bolt pattern drilled for adding redundant plates.

The full repair is shown in Figure 11-38. The redundant plates have been placed above and below the previously cracked flange. A spacer plate was required on the lower side of the beam to provide a level surface with the specimen. Eight A490 bolts having a 22-mm diameter were used on either side of the former crack location. In the other three corners of the support structure, only small cracks were found (< 19-mm). Drilling a hole through the crack tips successfully stopped these cracks for the remainder of the testing.

Figure 11-38: Final repair of cracked beam tension flange.

11.8 FINAL COMMENTS ON HOLE DRILLING SUCCESSES

Drilling out the crack tip has been repeatedly shown to be successful in stopping a crack. Figure 11-39 is shown as a final illustration of the exceptional success common to this repair technique. The photo shows a location where a fatigue crack had grown to a through-thickness crack in the beam tension flange. This crack had propagated to within 50-mm of the flange edge prior to hole drilling, and a large 29-mm hole was necessary to capture the crack tip and arrest the crack. To quantify the stress in the remaining tension strip, a strain gage was mounted mid-way between the hole edge and the free edge of the flange. Strain gage readings indicated large stress ranges of 108 MPa were present. Furthermore, a noticeable dip at this location was observed during testing, indicating the area was tolerated a significant amount of stress fluctuations throughout testing. Surprisingly, after eight million cycles at this stress range no further cracking was observed. For this reason, the practice of hole drilling is highly advocated as an effective fatigue repair.

Figure 11-39: Several cracks arrested by hole drilling.

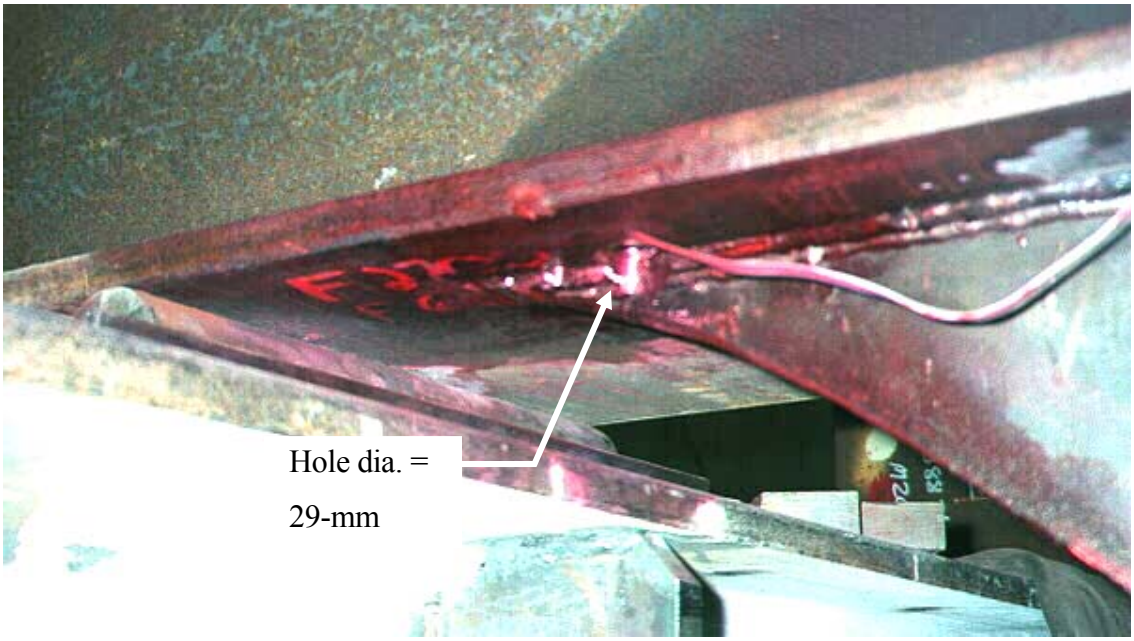

Figure 11-40: Large hole used in arresting crack at fatigue sensitive location.

12 Appendix B: Flowchart for Analytical Program

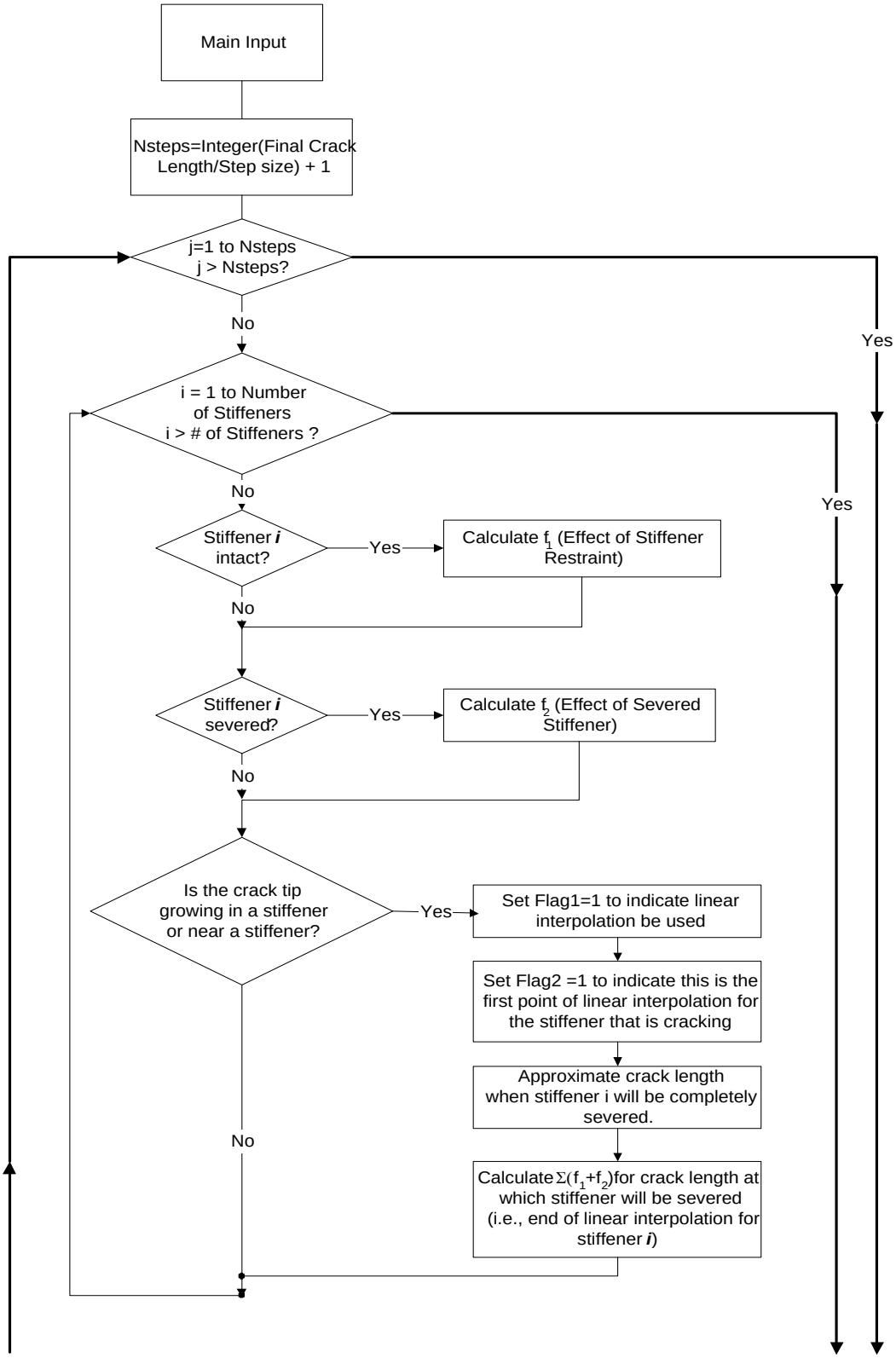

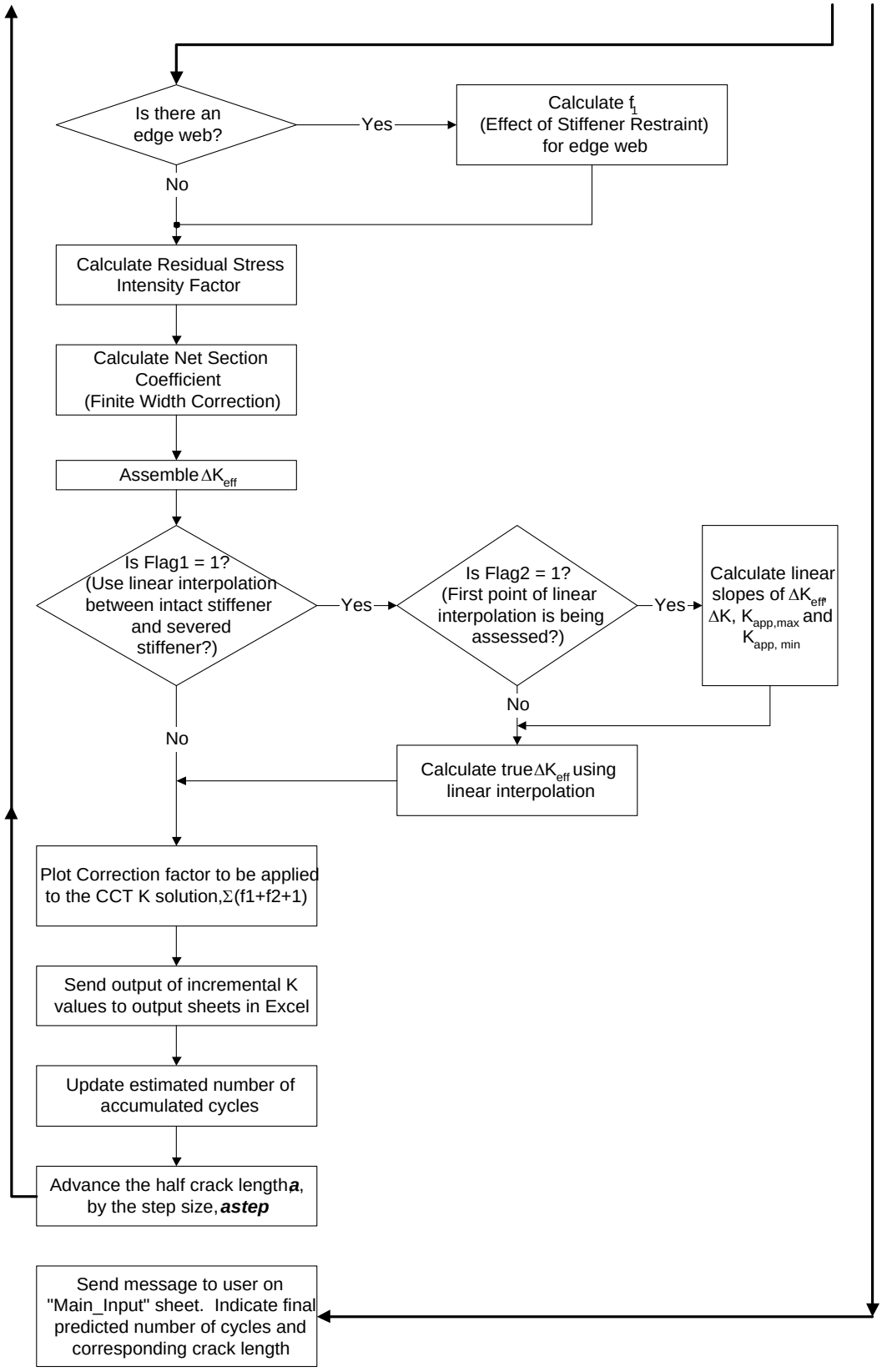
Is there an edge web?
Yes
Calculate f_1 (Effect of Stiffener Restraint) for edge web
No
Calculate Residual Stress Intensity Factor
Calculate Net Section Coefficient (Finite Width Correction)
Assemble ΔK_{eff}
Is Flag1 = 1? (Use linear interpolation between intact stiffener and severed stiffener?)
Yes
Is Flag2 = 1? (First point of linear interpolation is being assessed?)
Yes
Calculate linear slopes of ΔK_{eff}, ΔK, $K_{app,max}$ and $K_{app,\ min}$
No
No
Calculate true ΔK_{eff} using linear interpolation
Plot Correction factor to be applied to the CCT K solution, Σ(f1+f2+1)
Send output of incremental K values to output sheets in Excel
Update estimated number of accumulated cycles
Advance the half crack length ***a***, by the step size, ***astep***
Send message to user on "Main_Input" sheet. Indicate final predicted number of cycles and corresponding crack length

13 Appendix C: Arbitrary Point Force in Infinite Medium

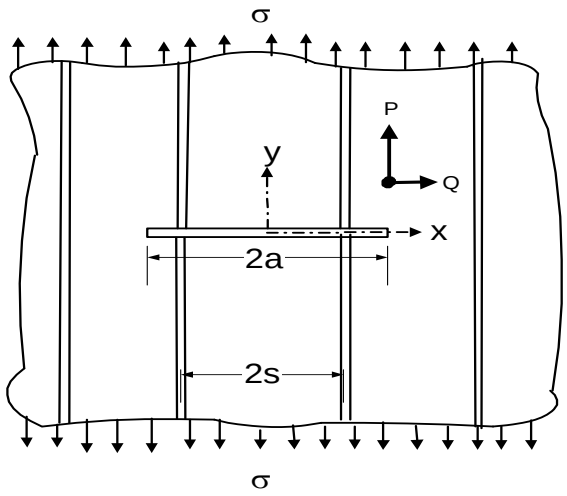

Two complex functions necessary for arbitrary force stress intensity factor:

(See Compendium of Stress Intensity Factors , Ref. 131 page 1.1.12)

Equation 1

$$H(z)=\frac{a\cdot(zhat-z)}{(zhat-a)\cdot\left(\sqrt{zhat^2-a^2}\right)}$$

Equation 2

$$G(z)=\frac{a+z}{\sqrt{z^2-a^2}}$$

where : $zhat=x-i\cdot y$ $z=x+i\cdot y$

The resulting stress intensity factor requires these functions to be broken into four parts:

$G1=1+Re(G(z))$ $H1=Re(H(z))$

$G2=Im(G(z))$ $H2=-Im(H(z))$

Note: There was an error found in the handbook solution for G1 and G2. Originally, the handbook incorrectly stated: G1 = 1 - Re(G(z)) and G2 = -Im(G(z))

Equation 1: Manipulation into seperate real and complex parts:

$$H(z)=\frac{a\cdot(zhat-z)}{(zhat-a)\cdot\left(\sqrt{zhat^2-a^2}\right)}$$

Let $\frac{zhat-z}{zhat-a}$ be part 1,

and $\sqrt{zhat^2-a^2}$ be part 2

Part one:

$$\frac{zhat - z}{zhat - a} = \frac{x - i\cdot y - (x + i\cdot y)}{x - i\cdot y - a}$$

$$\frac{zhat - z}{zhat - a} = \frac{x - i\cdot y - (x + i\cdot y)}{x - i\cdot y - a}$$

$$\frac{zhat - z}{zhat - a} = \left[2\cdot i\cdot \frac{y}{(-x + i\cdot y + a)}\right]\cdot \frac{(-x - i\cdot y + a)}{(-x - i\cdot y + a)} = \frac{-2\cdot i\cdot y\cdot x - 2\cdot i^2\cdot y^2 + 2\cdot i\cdot y\cdot a}{x^2 - 2\cdot x\cdot a - i^2\cdot y^2 + a^2} = \frac{2\cdot y^2 + 2\cdot y\cdot i\cdot (a - x)}{(x - a)^2 + y^2}$$

Part 2 (denominator):

$$\sqrt{zhat^2 - a^2} = \sqrt{(x - i\cdot y)^2 - a^2}$$

$$\sqrt{zhat^2 - a^2} = \sqrt{x^2 - 2\cdot i\cdot y\cdot x + i^2\cdot y^2 - a^2} = \sqrt{\left(x^2 - y^2 - a^2\right) - 2\cdot i\cdot y\cdot x}$$

let:

$$q = x^2 - y^2 - a^2 \qquad r = 2\cdot y\cdot x$$

then

$$\sqrt{\left(x^2 - y^2 - a^2\right) - 2\cdot i\cdot y\cdot x} = \sqrt{q - i\cdot r}$$

Assembling this denominator portion of the fraction:

$$\frac{1}{\sqrt{\left(x^2 - y^2 - a^2\right) - 2\cdot i\cdot y\cdot x}} = \frac{1}{\sqrt{q - i\cdot r}}\cdot \frac{\sqrt{q + i\cdot r}}{\sqrt{q + i\cdot r}} = \frac{\sqrt{denom}\cdot\left(\cos\left(\frac{\phi}{2}\right) + i\cdot\sin\left(\frac{\phi}{2}\right)\right)}{\sqrt{q^2 + r^2}}$$

where

$$denom = \sqrt{q^2 + r^2} = \sqrt{\left(x^2 - y^2 - a^2\right)^2 + (2\cdot y\cdot x)^2} \qquad \tan(\phi) = \frac{r}{q} = \frac{2\cdot y\cdot x}{x^2 - y^2 - a^2}$$

Assembly:

$$H(z) = \frac{a\cdot(zhat - z)}{(zhat - a)\cdot\left(\sqrt{zhat^2 - a^2}\right)} = \frac{a\cdot\sqrt{denom}}{denom}\cdot\left(\cos\left(\frac{\phi}{2}\right) + i\cdot\sin\left(\frac{\phi}{2}\right)\right)\cdot\frac{2\cdot y^2 + 2\cdot y\cdot i\cdot(a - x)}{(x - a)^2 + y^2}$$

$$H(z)=\frac{a\cdot\sqrt{denom}}{denom}\cdot\left(\cos\left(\frac{\phi}{2}\right)+i\cdot\sin\left(\frac{\phi}{2}\right)\right)\cdot\frac{2\cdot y^2+2\cdot y\cdot i\cdot(a-x)}{(x-a)^2+y^2}$$

$$H(z)=\frac{2\cdot a\cdot y\cdot\sqrt{denom}}{denom\cdot\left[(x-a)^2+y^2\right]}\cdot\left[\begin{array}{l} y\cdot\cos\left(\frac{\phi}{2}\right)+\sin\left(\frac{\phi}{2}\right)\cdot(x-a)\ \ldots \\ +i\cdot\left[y\cdot\sin\left(\frac{\phi}{2}\right)+(a-x)\cdot\cos\left(\frac{\phi}{2}\right)\right]\end{array}\right]$$

Resulting Values:

$$H_1=Re(H(z))=\frac{2\cdot y\cdot a\cdot\sqrt{denom}}{denom\cdot\left[(x-a)^2+y^2\right]}\cdot\left[y\cdot\cos\left(\frac{\phi}{2}\right)-\sin\left(\frac{\phi}{2}\right)\cdot(a-x)\right]$$

$$H_2=-Im(H(z))=\frac{-2\cdot a\cdot y\cdot\sqrt{denom}}{denom\cdot\left[(x-a)^2+y^2\right]}\cdot\left[y\cdot\sin\left(\frac{\phi}{2}\right)+(a-x)\cdot\cos\left(\frac{\phi}{2}\right)\right]$$

Now seperate real and imaginary parts of Equation 2:

Equation 2: $$G(z)=\frac{a+z}{\sqrt{z^2-a^2}}$$

$$G(z)=\frac{a+z}{\sqrt{z^2-a^2}}=\frac{a+x+i\cdot y}{\sqrt{(x+i\cdot y)^2-a^2}}=\frac{a+x+i\cdot y}{\sqrt{\left(x^2-a^2-y^2\right)+i\cdot 2\cdot y\cdot x}}\cdot\frac{\sqrt{q-i\cdot r}}{\sqrt{q-i\cdot r}}$$

where

$$q=x^2-a^2-y^2 \qquad r=2\cdot y\cdot x$$

$$\tan(\theta)=\frac{-r}{q}=\frac{-2\cdot y\cdot x}{x^2-y^2-a^2}$$

Substitution of q and r:

$$G(z)=\frac{a+x+i\cdot y}{\sqrt{q+i\cdot r}}\cdot\frac{\sqrt{q-i\cdot r}}{\sqrt{q-i\cdot r}}=\frac{(a+x+i\cdot y)}{\sqrt{q^2+r^2}}\cdot\left(\sqrt{q^2+r^2}\right)^{0.5}\cdot\left(\cos\left(\frac{\theta}{2}\right)+i\cdot\sin\left(\frac{\theta}{2}\right)\right)$$

substitute for q and r with: $\text{denom} = \sqrt{q^2 + r^2}$

$$G(x) = \frac{(a + x + i \cdot y)}{\text{denom}} \cdot \sqrt{\text{denom}} \cdot \left(\cos\left(\frac{\theta}{2}\right) + i \cdot \sin\left(\frac{\theta}{2}\right) \right)$$

$$G(x) = \frac{\sqrt{\text{denom}}}{\text{denom}} \cdot \left[\begin{array}{l} \left[(a + x) \cdot \cos\left(\frac{\theta}{2}\right) - y \cdot \sin\left(\frac{\theta}{2}\right) \right] \ldots \\ + i \cdot \left[y \cdot \cos\left(\frac{\theta}{2}\right) + (a + x) \cdot \sin\left(\frac{\theta}{2}\right) \right] \end{array} \right]$$

Therefore:

$$G1 = 1 + \text{Re}(G(z)) = 1 + \frac{\sqrt{\text{denom}}}{\text{denom}} \cdot \left[(a + x) \cdot \cos\left(\frac{\theta}{2}\right) - y \cdot \sin\left(\frac{\theta}{2}\right) \right]$$

$$G2 = \text{Im}(G(z)) = \frac{\sqrt{\text{denom}}}{\text{denom}} \cdot \left[y \cdot \cos\left(\frac{\theta}{2}\right) + (a + x) \cdot \sin\left(\frac{\theta}{2}\right) \right]$$

and

$$H1 = \text{Re}(H(z)) = \frac{2 \cdot y \cdot a \cdot \sqrt{\text{denom}}}{\text{denom} \cdot \left[(x - a)^2 + y^2 \right]} \cdot \left[y \cdot \cos\left(\frac{\phi}{2}\right) - \sin\left(\frac{\phi}{2}\right) \cdot (a - x) \right]$$

$$H2 = -\text{Im}(H(z)) = \frac{-2 \cdot a \cdot y \cdot \sqrt{\text{denom}}}{\text{denom} \cdot \left[(x - a)^2 + y^2 \right]} \cdot \left[y \cdot \sin\left(\frac{\phi}{2}\right) + (a - x) \cdot \cos\left(\frac{\phi}{2}\right) \right]$$

These resulting expressions are used to formulate K for a variety of cracks:

For a vertical force P, as shown in Figure 13-1:

$$\frac{K_I}{K_0} = G_2 - \left(\frac{1}{\kappa + 1}\right) \cdot H_2 \quad \text{with} \quad K_0 = \frac{P}{2\sqrt{\pi\ a}}$$

where K_I indicates an opening mode crack

$$\frac{K_{II}}{K_0} = G_1 - \left(\frac{1}{\kappa - 1}\right) \cdot H_1 \quad \text{with} \quad K_0 = \frac{-P}{2\sqrt{\pi\ a}} \cdot \left(\frac{\kappa - 1}{\kappa + 1}\right)$$

where K_{II} indicates an sliding mode crack

Alternatively, if an arbitrary horizontal force Q was applied, the following relations would result:

$$\frac{K_I}{K_0} = G_1 + \left(\frac{1}{\kappa - 1}\right) \cdot H_1 \quad \text{with} \quad K_0 = \frac{Q}{2\sqrt{\pi\ a}} \cdot \left(\frac{\kappa - 1}{\kappa + 1}\right)$$

where K_I indicates an opening mode crack

$$\frac{K_{II}}{K_0} = G_2 + \left(\frac{1}{\kappa + 1}\right) \cdot H_2 \quad \text{with} \quad K_0 = \frac{Q}{2\sqrt{\pi\ a}}$$

where K_{II} indicates an sliding mode crack